SPECIAL PUBLICATION SJ2004-SP33

CEDAR/ORTEGA RIVER BASIN, FLORIDA, RESTORATION: AN ASSESSMENT OF SEDIMENT TRAPPING IN THE CEDAR RIVER

PHASE 2 FINAL REPORT

UFL/COEL-2004/001

CEDAR/ORTEGA RIVER BASIN, FLORIDA, RESTORATION: AN ASSESSMENT OF SEDIMENT TRAPPING IN THE CEDAR RIVER

PHASE 2 FINAL REPORT

By

Ashish J. Mehta

And

Earl J. Hayter

Submitted to:
St. Johns River Water Management District
Palatka, FL 32178-1429

Coastal and Oceanographic Engineering Program
Department of Civil and Coastal Engineering
University of Florida, Gainesville, FL 32611

February, 2004

SYNOPSIS

This report includes the findings of the study, "Remediation/Restoration of Cedar/Ortega Rivers. Phase 2: Scope of Work to Assess Fine Sediment Deposition, Erosion and Transport Rates and Evaluate Dredge Scenarios", carried out by the University of Florida (UF) for the St. Johns River Water Management District (SJRWMD), Palatka, Florida. The project objective was to predict the rates of deposition, erosion and transport of fine sediment, to evaluate proposed remedial dredging works (e.g., sediment trap/channel dredging, computation of dredge volumes), and to develop management strategies in the lower Cedar/Ortega Rivers. This objective was met by carrying out physical measurements, modeling hydrodynamics and sediment transport, and evaluate present and future rates of sediment deposition, erosion and transport under selected remediation scenarios provided by SJRWMD.

We have examined both on-line and off-line sediment removal approaches, specifically off-line Wet Detention Systems and on-line dredged pits, as well as dredging and sand capping in the Cedar/Ortega River confluence area. Three assessment criteria have been used qualitatively to rank the 11 options; these criteria being – removal of contaminated sediment from its source in upstream Cedar River, improved navigability in the confluence area and water quality.

We find that if the capture of contaminated sediment from upstream sources in Cedar River is the only or the main goal, one of the two off-line sites proposed by SJRWMD, preferably the one closer to the source of sediment, would be the preferred choice, *provided the facility operates at very high, i.e, 80% removal efficiency.* If improvement is navigation coupled with reduced resuspension of *in situ* material is additionally desired, selective dredging and sand capping in the Cedar/Ortega confluence area should be considered. If capping proves

to be costly, removal of the top layer of very soft mud from areas where boats regularly ply the waters may be further evaluated.

We would like to acknowledge the cooperation and assistance provided by Dr. Chandy John and Dr. Fred Morris of SJRWMD throughout the study. Principal contributors to the appendices of this report, Dr. Earl Hayter, Dr. Robert Kirby and Dr. John Land, and UF graduate students Vladimir Paramygin, Jason Gowland and Dan Stoddard are recognized. A noteworthy contribution independent of the present study was also made by visiting researcher Fernando Marván. Prior contribution by graduate student Jianhua Jiang to Phase 1 of this study formed the basis for the design of the present Phase 2.

TABLE OF CONTENTS

LIST OF FIGURES

LIST OF TABLES

1 INTRODUCTION

1.1 Preamble

This report is the final technical report to be submitted to the St. Johns River Water Management District (SJRWMD) by the University of Florida (UF). It includes work carried out on the contract entitled "Remediation/Restoration of Cedar/Ortega Rivers. Phase 2: Scope of Work to Assess Fine Sediment Deposition, Erosion and Transport Rates and Evaluate Dredge Scenarios".

The Cedar/Ortega River basin is located west of the St. Johns River in south-central Duval County in northern Florida, and is an important tributary of the St. Johns River (Figs. 1.1 and 1.2). The Ortega River is the main tributary of the system, discharging approximately half of the total system's volume to the St. Johns River. The Cedar River is the second most important tributary, and there are three other secondary tributaries of the system (Fishing Creek, Butcher Pen Creek and Williamson Creek). The upstream portion of the Ortega River is known as McGirt's Creek. The creek lies within the Duval uplands physiographic province and flows generally north to south. The Ortega River continues this course until it reaches the Eastern Valley physiographic province, where the river gradually turns 180 degrees to a north-northeasterly course before reaching the St. John's River north of the Jacksonville Naval Air Station. A tributary, Big Fishweir Creek, joins the Ortega near its mouth (Figure 1.2).

The Cedar River is actually a major system itself. From its headwaters north of Interstate-10 and west of Interstate-295, this river flows southeast to its confluence with the Ortega River. Major tributaries to the Cedar River are Willis Branch, Williamson Creek, Butcher Pen Creek, and Fishing Creek. The tidal interface for the Ortega River is at Collins Road, while the tidal interface for the Cedar River is near Lane Ave. (These two and other road

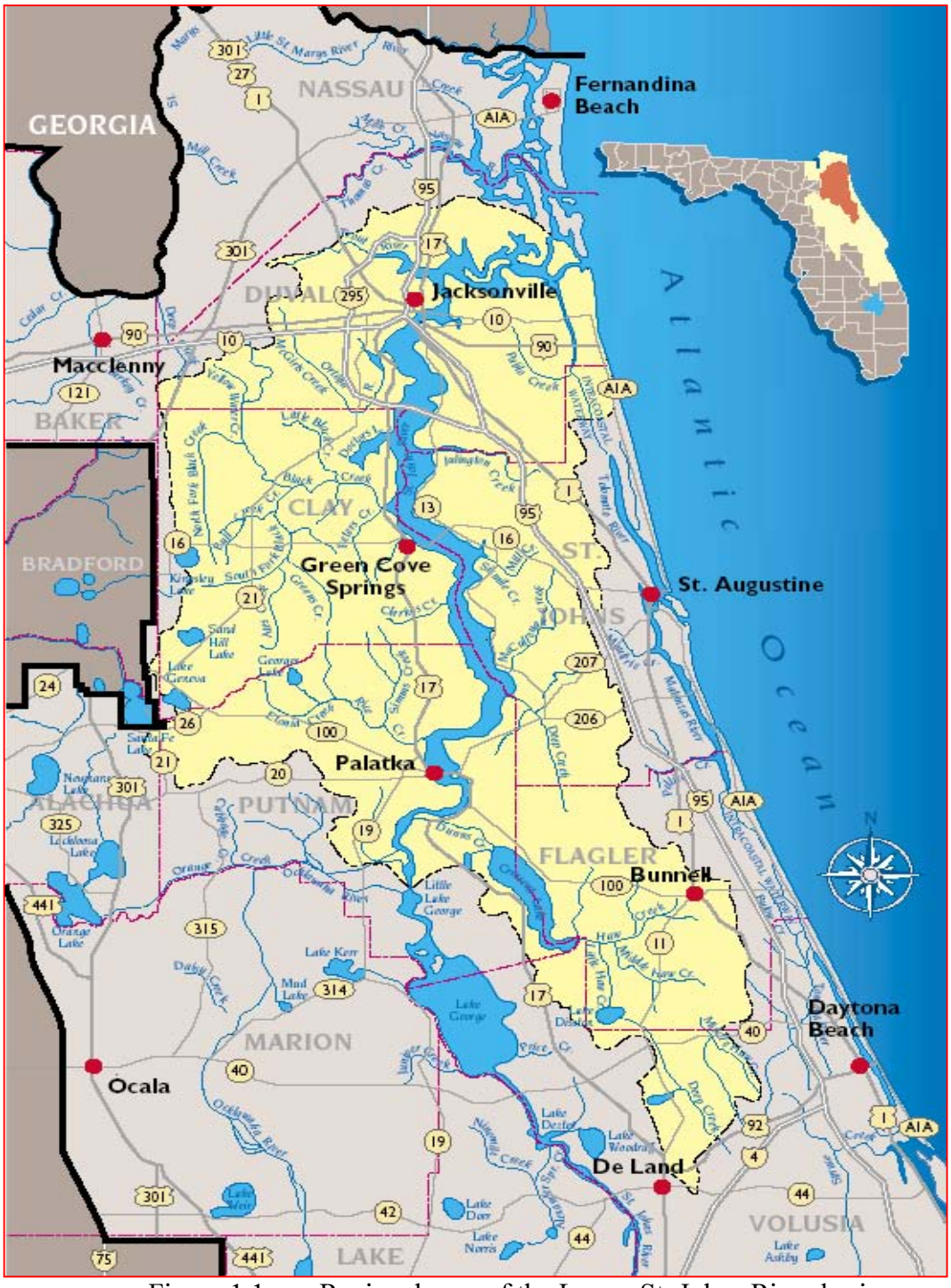

Figure 1.1 Regional map of the Lower St. Johns River basin.

locations are not highlighted in any drawings herein; they are found in road maps of the Jacksonville area.)

In the early 1990's, approximately one-third of the Cedar/Ortega River basin was residential, with commercial/industrial and vacant land comprising the other major land uses. Since then, vacant land has decreased significantly. The average annual rainfall in the Ortega/Cedar basin is approximately 132 cm and the major portion of it falls between June and September (Campbell et al., 1993). Water depths in the Ortega/Cedar basin study area range between 1 and 7 m, with the range in the Cedar River between 0.7 m and 4.3 m (NGVD). At the mouth of the Ortega River with St. Johns River, the semi-diurnal (M_2) tide ranges from 0.14 m (neap tide) to 0.28 m (spring tide), having a mean of 0.19 m. The bottom and suspended sediment is mostly a mixture of clay, silt and organic matter, with occasional intrusions of sand. Typical suspended sediment concentration is approximately 15 mg/l; however, during storm runoff events it rises to as much as 105 mg/l**.** The dominant range of organic content was found to be 20-30%.

Remediation of contaminated sediment in the Cedar River has become a critical issue due to elevated concentration of PCBs (polychlorinated biphenyls) in the water system due to leeching of sediments and runoff from a fire at a chemical company in January 1984. The site was located approximately 0.6 km east of the Cedar River near the headwaters north of Interstate route I-10 and adjacent to municipal storm drains and drainage ditches. The fire destroyed several tanks storing high concentrations (4,425 ppm) of PCB-laden oils and other materials. It is believed that a combination of damage to the storage tanks and the fire-fighting effort created a vehicle for the PCB to enter the Cedar River basin. (Environmental Protection Board, 1985). The surrounding groundwater and soil were sampled extensively in 1989 and the concentrations were still significantly above the regulated amount of 50 ppm.

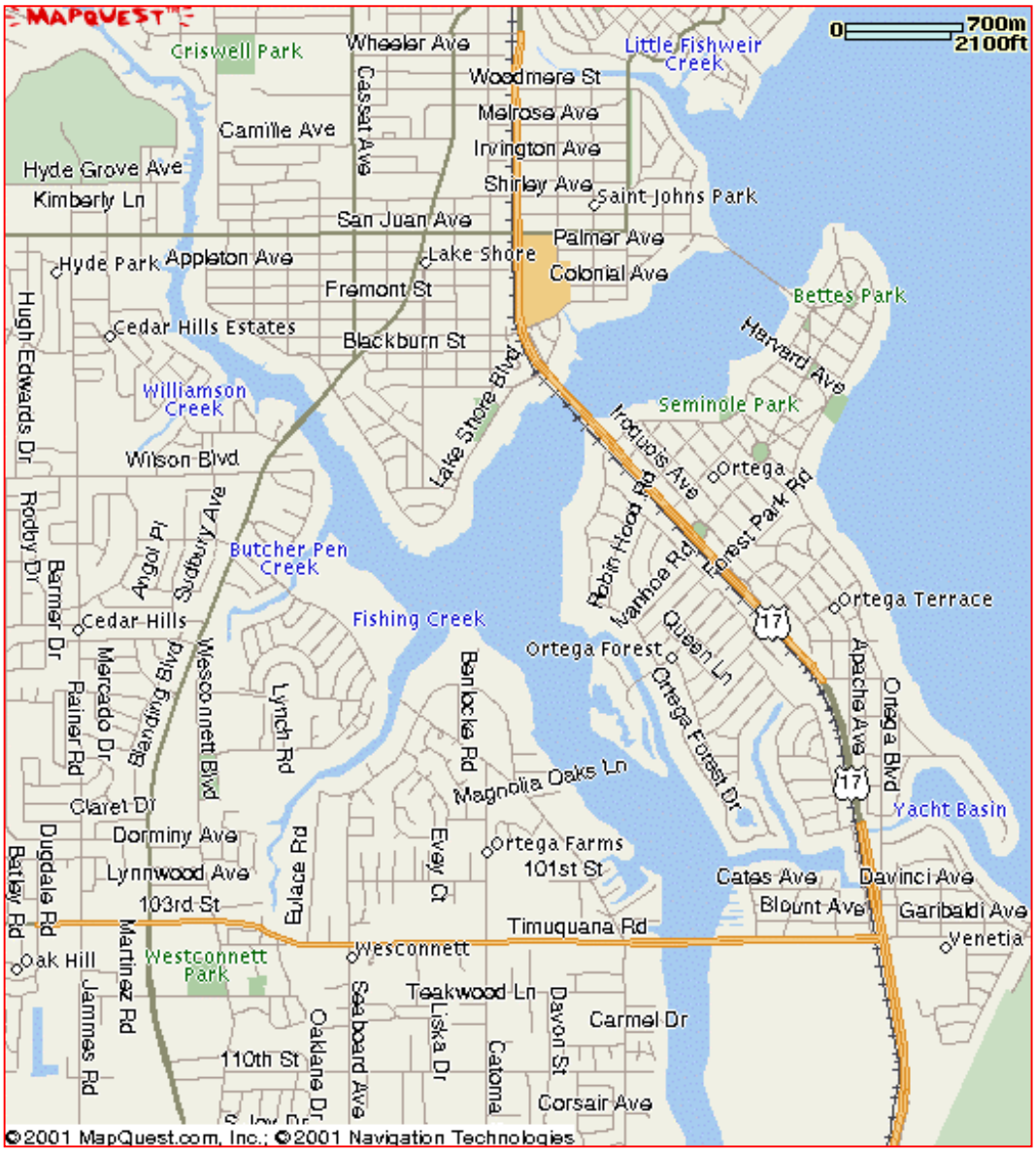

Figure 1.2 Cedar/Ortega River system and tributaries.

1.2 Objective

As stated in the contract, the objective of this project was to predict the rates of deposition, erosion and transport of fine sediment, to evaluate proposed remedial dredging works (e.g., sediment trap/channel dredging, computation of dredge volumes), and to develop management strategies in the lower Cedar/Ortega Rivers. It was required to conduct physical measurements, set up and apply a numerical model, the Environmental Fluid Dynamics Code

(EFDC), to simulate hydrodynamics and sediment transport, and evaluate present and future rates of sediment deposition, erosion and transport under selected remediation scenarios provided by SJRWMD. Core and any related data already collected by SJRWMD were to be used for sediment model calibration and validation and quantification of sediment fluxes to from the lower Cedar/Ortega Rivers, and accumulation/depletion of sediment within this area.

Specific objectives of the contract were listed below.

1. To collect and analyze bottom sediment grab samples from 10 sites, including Fishweir Creek, and to analyze these samples for erosion potential, settling rates and consolidation in the Coastal Engineering Laboratory of the University of Florida UF).

2. To obtain continuous measurement of the water level (tide and waves), conductivity and temperature (hence salinity) at three sites – one in upstream Cedar River, the second in upstream Ortega River and the third at the mouth of the Ortega River where it joins with the main stem. In addition, continuous data on the current velocity are to be obtained at the Ortega River mouth using a moored Endeco current meter. These measurements are to be carried out over a period of one lunar month, and are to be used to calibrate the circulation model.

3. To obtain current velocity and suspended solids concentration data at selected cross-sections within the lower Cedar/Ortega Rivers using an Acoustic Doppler Current Profiler (ADCP) and synchronous bottle-sampling of water at these cross-sections. The ADCP measurements are to be carried out twice, each time over a 13-hour duration covering the semi-diurnal tide. One 13-hour run should obtain "normal" values of the current velocity and suspended solids concentration and the second shall be run under "storm" conditions.

4. To carry out model calibration with one set of data, and to use a second set of data for model validation.

5. To conduct model simulations to study circulation and sediment transport in the Cedar and Ortega Rivers using EFDC to evaluate past, present and likely future rates of sediment deposition, erosion and transport and depth-shoaling patterns.

6. To run model scenarios for dredging and provide results to be evaluated by the District Project team.

7. To develop short and long term goals for dredging and sediment removal management, and criteria for environmental enhancement (e.g., due to sedimentation traps/basins).

8. To provide a critical evaluation of selected sediment remediation alternatives to be provided by the District including the "no-action" alternative and suggest recommended option(s).

1.3 Tasks

Seven tasks were assigned to accomplish the eight objectives given above. In what follows, these tasks and locations (Appendices A through H and other citations) in which they are reported are described.

1.3.1 Task 1: Assembly of Existing Data

In order to assemble the data required for the sediment transport modeling, a review of all available data related to the sedimentological regime of the rivers and their tributaries will be conducted.

The sedimentological regime of the rivers and tributaries is reviewed in Appendices A and E, and in Mehta et al. (2000).

1.3.2 Task 2: Samples for Engineering Characterization of Sediments

Ten surficial sediment samples will be collected to describe the present spatial distribution of sediment types. Selected fine-grained samples will be tested at UF's Coastal Engineering Laboratory to determine the erosion, deposition and consolidation properties of these sediments.

The erosion, deposition and consolidation properties of the river sediment are reported in Appendix B, and also in Appendix H.

1.3.3 Task 3: ADCP, Water Level and Salinity Measurements

Current velocities and suspended solids concentrations will be measured at selected cross-sections in the confluence of the Cedar/Ortega Rivers. Water and suspended sediment fluxes at these cross-sections will be calculated using the measured data.

ADCP and suspended sediment measurements as well sediment flux calculations are presented in Appendices C, D and E. Water level and conductivity/temperature data utilized for modeling are provided in Appendix E.

1.3.4 Task 4: Sediment Load Rating Curves

TSS-discharge rating curves will be developed, to the extent possible, at these cross-sections. These rating curves should be used to determine sediment flux time series over the period of record.

The rating curves are presented in Mehta et al. (2000) and Appendix H, and revised in Appendix F. It is shown that both the original and the revise curves yield reasonable values of suspended sediment fluxes and deposition rates within the Cedar/Ortega River area, although the paucity of data leaves a degree of uncertainty that is difficult to quantify. Subsequently, SJRWMD supplied and required the use of rating relations at the heads of Cedar River and its tributaries (Williamson Creek, Butcher Pen Creek and Fishing Creek), derived from applications of the SWMM model. Predicted sediment concentrations based on these appear to be lower than those derived from the rating curve, as noted in Appendix E.

1.3.5 Task 5: Model Setup, Simulations and Results

S*etup, calibrate, validate and run EFDC using measured tides, currents, river and tributary discharges and suspended solids concentrations for boundary conditions.*

Exploratory modeling work related to sediment entrapment in the Cedar River and using EFDC is reported in Appendix E and expanded in Appendix G. Appendix E also summarizes the modeling framework including equations, grid development, boundary conditions and output.

1.3.6 Task 6: Run Model Scenarios

Run model scenarios to "assess likely short term (e.g., 1-3 years) and long term (e.g., a decade or longer) sedimentation rates based on historical trends and likely future scenarios with respect to the hydrologic/hydrodynamic regime of the rivers".

The above statement was further quantified during the study to include the examination of the impact of placing sediment traps at selected locations with three different removal efficiencies (i.e., 40%, 60%, 80%) on the net sediment flux out of the Cedar River. Exploratory work in this regard is described in Appendix E. Further work is reported in Appendix G.

1.3.7 Task 7: Dredging Alternatives Evaluation

Evaluate potential dredging alternatives for basin restoration.

Dredging alternatives of two types are considered – off-line and on-line. Exploratory work related to off-line sediment entrapment systems prescribed by SJRWMD is carried out in Appendix E, and expanded in Appendix G. On-line entrapment was not initially prescribed; nevertheless, in Appendices E and F, the role of on-line trapping of sediment is examined as a remediation option, and five scenarios that involve the placement of at least one on-line (i.e., in-channel) sediment trap were simulated, the results of which are described in Appendix G.

2 OBSERVATIONS FROM FIELD INFORMATION

2.1 Preamble

In what follows, noteworthy findings from the analyses of (collected and procured) field data are provided. See also Appendices A, C, D and E.

2.2 Bottom Sediment Sampling

Figure 2.1 shows core-sampling sites for a 1998 survey (SJRWMD) of physical and chemical attributes of bed sediments in the Cedar/Ortega River system. The system can be separated aerially into four identifiable regions. Figure 2.2 gives distributions of clay, silt, sand and organic content (loss on ignition). Figures 2.3 and 2.4 respectively give distributions of moisture content and total solids. Figure 2.5 shows the distribution of total organic carbon and, finally, Figure 2.6 gives annual sedimentation rates (Appendix A).

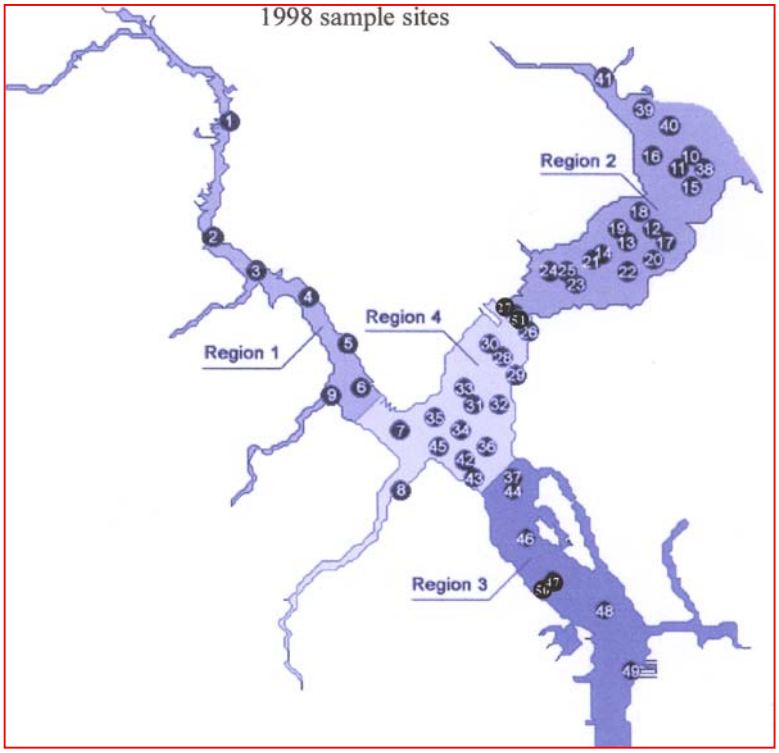

Figure 2.1 Bottom sediment-sampling sites in 1998. The region is conveniently divided into four regions (from Appendix A).

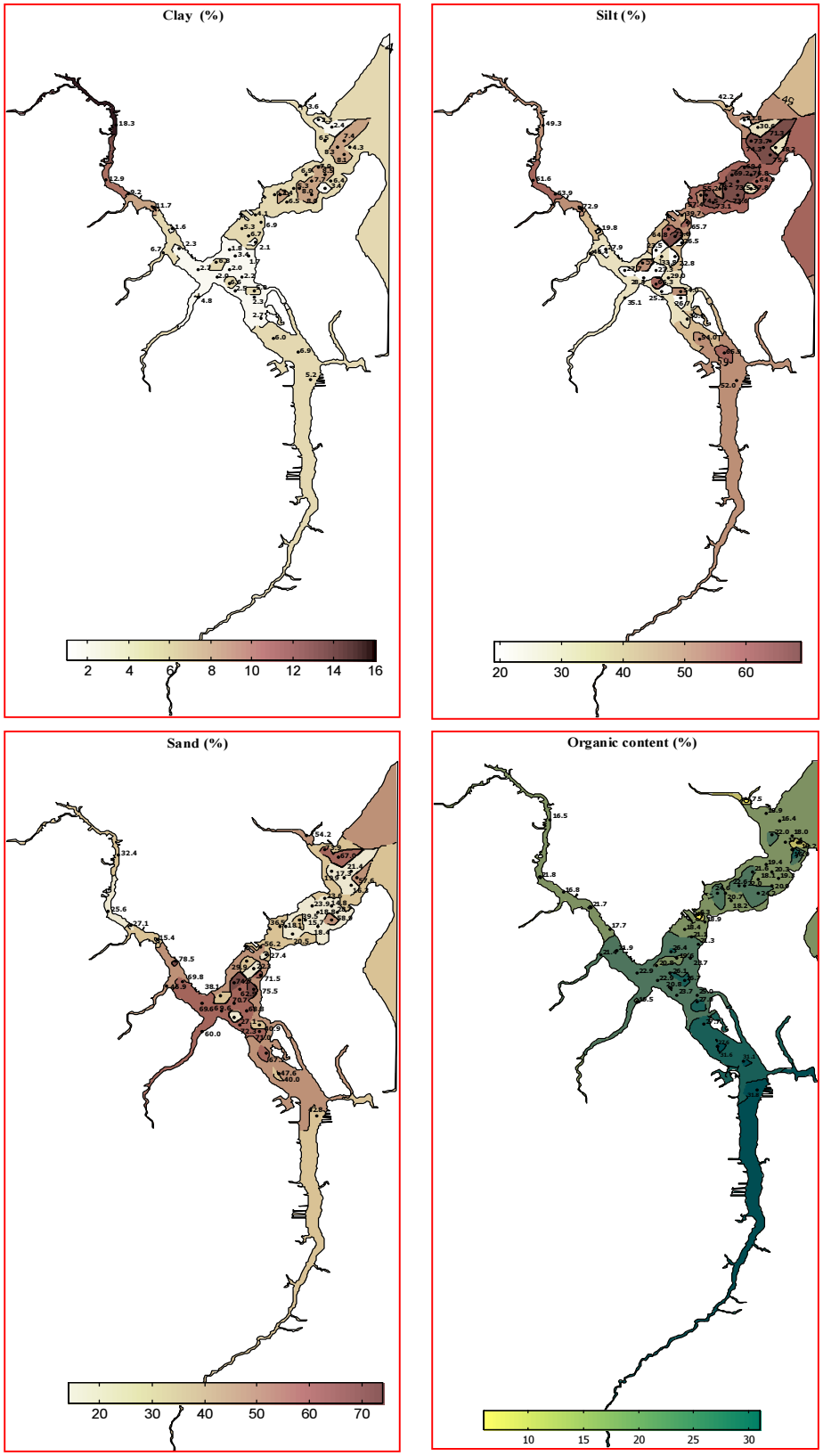

Figure 2.2 Composition of area bottom sediment (from Appendix A).

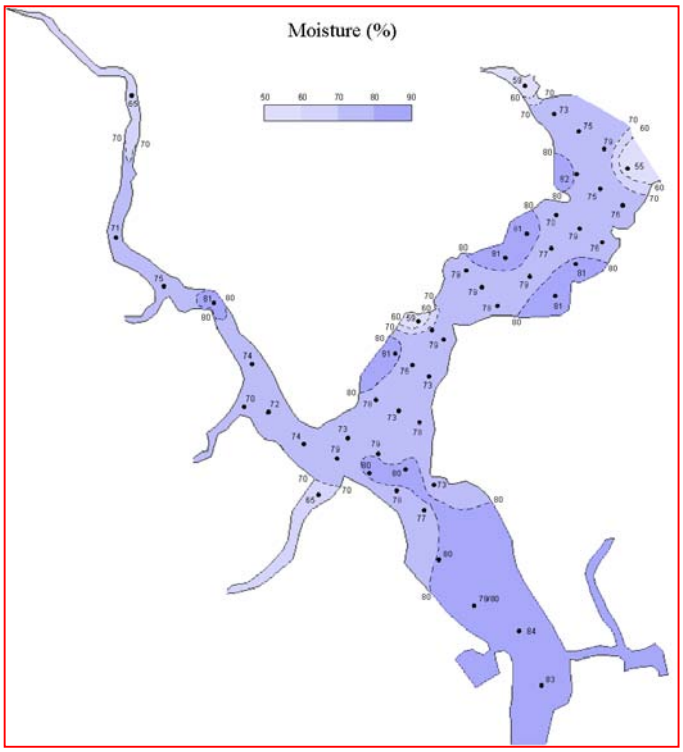

Figure 2.3 Moisture content distribution (from Appendix A).

Figure 2.4 Total solids distribution (from Appendix A).

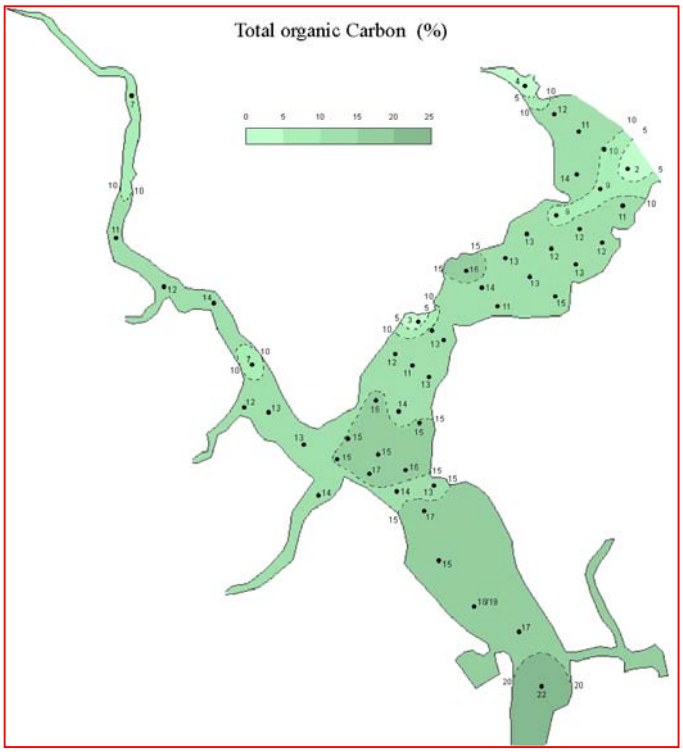

Figure 2.5 Total organic carbon distribution (from Appendix A).

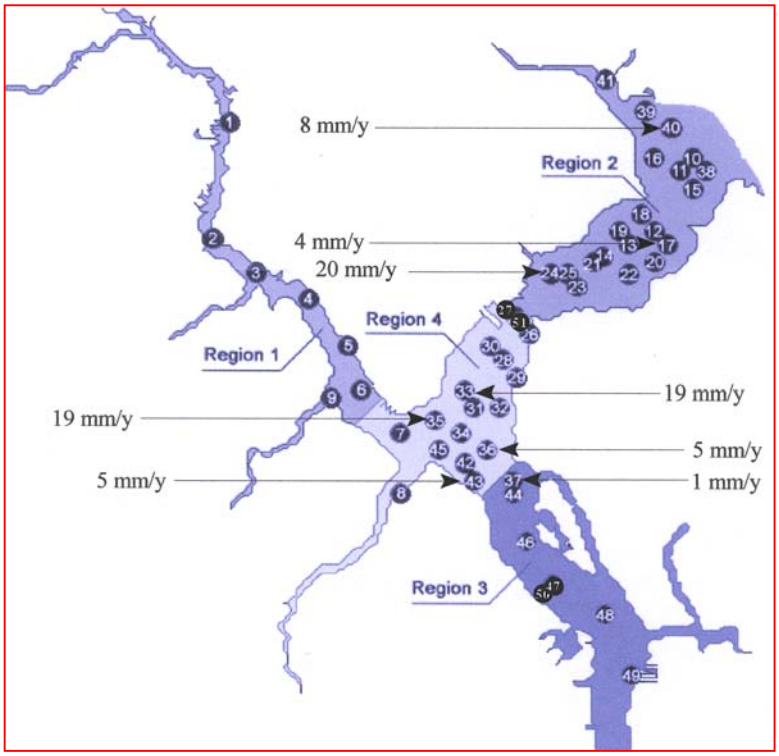

Figure 2.6 Sedimentation rates (based on Donoghue, 1999).

Data examination indicates that there is a limited input of inorganic sediment from the main-stem, although this has only penetrated into the outer confluent region. No clear evidence has emerged as to the extent of autochthonous, plankton sediment production or the breakdown products of *in situ* sea grass in the system. Human settlement within the last century has had a major impact on the types of sediment being input to the estuary and on the sedimentation rate.

2.2.1 Cedar River

With respect to the more minor, inorganic fraction of the sediment, the Cedar River (Region 1, Figure 2.1) deposits show the highest clay content in the entire system (18%). There is also a pronounced down-estuary decrease. This is consistent with a fluvial clay input. The silt content of the inorganic fraction is higher than the clay with a comparable down-estuary reduction, implying a similar detrital fluvial input. The sand fraction, in contrast, is low at the landward end and increases down-estuary. As far as the sediment as a whole is concerned, there is a much higher solids percentage, coupled with relatively low moisture content, again consistent with a significant detrital input from the watershed. The solids percentage decreases down-estuary and the moisture content rises. This implies a rising organic fraction in the down-estuary direction. Consistent with these trends, the organic content of the upper Cedar River samples is amongst the lowest in the entire system and increases down-estuary. This is the reverse of the situation in the Ortega River, and may reflect the urbanization of the Cedar River watershed. In core samples sand layers occur only very occasionally, and when they do they are present as thin laminae. This confirms that, in spite of the level of urbanization, detrital sand is not a significant input. This is equally the case for Williamson and Butcher Pen Creeks. In contrast, there is a significant detrital sand input, represented as thick and multiple layers, being transported down Fishing Creek, and doubtless accounting for what is otherwise an anomalous-looking “high” in the sand fraction in the inner confluent region. The input must be terrestrial,

arising from recent deforestation, and it cannot be relict marine sand as it lies mainly in the shallowest parts of the sediment succession.

A further prominent anthropogenic input is that of wood chips. The level of wood chips in the cores from the upper reaches of the Cedar River is low. This probably reflects the fact that deforestation and urbanization of the Cedar River watershed is a relatively old feature. To complement this, the largest quantities of wood chips emanate from Williamson, Butcher Pen and Fishing Creeks and are abundant in the sediments of the lower reaches of the Cedar River, i.e., down-estuary of these three tributary creeks. A further anthropogenic input confined to the Cedar River is oil. Oily muck is interbedded with the wood chips and with the less common sand horizons. It is not possible to comment on whether there has been a single relatively large spill, or whether frequent or maybe semi-continuous low level hydrocarbon inputs occur. Finally, to complement the large-scale sand and wood chip inputs from Fishing Creek, blue-green inorganic detrital clays were sampled at shallow depths in recent sediment material at the entrance to Fishing Creek. A tentative suggestion arising from this might be that in recent decades, deforestation and urbanization has focused not in the Cedar, but in it tributaries - Williamson, Butcher Pen and Fishing Creeks. Fishing Creek seems to have some affinities in this respect with Big Fishweir Creek in the outer confluent region (as discussed later).

2.2.2 Ortega River

The sediments of this river (Region 3) show some distinctive features and pronounced contrasts with the Cedar and other zones within the study area. It is predominantly a detrital, organic-dominated sub-estuary at a less-developed stage of urbanization than the Cedar River. With regard to its inorganic fraction, it has very low clay and sand inputs and a mid-level silt input, with a strong down-estuary decrease. The sand content rises in the down-estuary direction. With respect to sediment as a whole, the Ortega has by far the highest moisture and

lowest total solids of anywhere in the system, again reflecting the major terrestrial organic input to the watershed basin. The total solids percentages show a down-estuary decrease. Consistent with this, the organic content is at a system-maximum and also decreases down-estuary. Examination of core logs confirms the relative paucity of sand laminae. Where these are present they tend to occur deep in the sediment column. Wood chips are also less common than in the lower reaches of the Cedar and the inner confluent region. Where present they can be interbedded with the black finely divided mucks and the sand layers. These multiple-layered wood chip horizons are detectable in all sampled reaches of the Ortega and are presumed to reflect the onset of deforestation in this watershed as well.

2.2.3 Inner Confluence Region

The inorganic fraction in Region 4 shows an apparently anomalous, exceptionally low clay content, although the recent blue-green clays being input from Fishing Creek seem not to be represented in this suite of samples. In contrast, the silt content is extremely variable, although still generally low in level. There is no obvious reason for the high variability. The sand content is relatively high and variable (22-75%, but mainly 60-70%). The sand cannot originate down-estuary, as concentrations decrease into the outer confluent region, and it must be either relict marine sand or a detrital input from the tributary creeks. The high elevation of the sand layers in cores suggests a fluvial source due to recent anthropogenic changes. With respect to the "whole sediment" analyses, and in contrast with the high sand content, these sediments also have high moisture and low solids contents. They can best be described as predominantly sandy mucks. There is a suggestion of an association between the high moisture/low solids rich sediments and the left bank in the inner confluent region. This is very likely induced by the presence of the flow impediment provided by the large commercial marinas along this coast. A tongue of high organic-rich sediment is issuing from the Ortega and

is strongly evident in this region. It possibly indicates that the signature of Ortega type sediments is locally stronger than either that of Cedar or St. Johns River sediments. In vertical sections from the core logs, multiple sand layering is found to be well developed and widespread, but there are never more than 10 sand layers. The sand must be contributed from Fishing Creek during occasional high discharge events. Wood chips are frequently interbedded with the sand layers in these reaches. These are very likely input from Williamson, Butcher Pen and Fishing Creeks. The distribution of wood chips and the variability in the silt content might be consistent with the presence of a large stable eddy in this region (Mehta et al., 2000).

Measurements of sedimentation rate show a strong lateral variation, with relatively low values on the right bank, but high rates up to 20 mm/yr on the left bank amongst the marina developments. Mehta et al. (2000) show that this is consistent with the Ortega's potential to erode bottom sediment opposite to the marinas during high river discharge events.

2.2.4 Outer Confluence Region

The inorganic fraction of sediments in this area (Region 2) is elevated compared to values in the up-estuary direction back into the Cedar and Ortega, and probably reflects inputs from the main-stem. The silt content is elevated and relatively constant in this area, with a small degree of axial increase. Sand contents are generally low. Whole sediment analyses show levels and distributions very similar to the inner confluent region, i.e., the sediments have a high moisture concentration (>70%) and a low solids percentage. The maximum moisture and minimum solids contents are again found along the left bank, and probably linked with the marina developments. Lateral partitioning is further evident in the presence of a tongue of low moisture, high solids detrital sediments penetrating the right bank of this region from the main-stem. In cores, the pronounced lateral segregation is again detectable with multiple sand layering involving up to 15-20 sand horizons towards the right bank. The most seaward of these

cores is all sand. In contrast, there are commonly no sand layers along the left bank, and the maximum number of layers found is seven.

There is an unambiguous sand input from Big Fishweir Creek on the left bank at the confluence with the main-stem. In general, few wood chip horizons are to be found in outer confluent region core samples, consistent with input from the river watershed up-estuary. Core logs at sites in the entrance to Big Fishweir Creek consistently identify one of the components of the sediments as "woody". In spite of this consistency in description, it is not possible to confidently associate this non-specific term with the "wood chips" described from up-estuary sites, and thus, the provenance of this material must remain unknown.

Sedimentation rate measurements show the same lateral partitioning, with values in the range of 4-8 mm/yr along the right bank, rising to 20 mm/yr along the left. Whether these are linear sedimentation rates or, instead, whether surficial rates of sedimentation might be even higher, are also unknown.

2.2.5 Data Statistics

Table 2.1 summarizes the overall statistics of moisture content, organic content and solids content for the study area. We make particular reference to the organic content, which is high in the mean, and characteristically influences fine sediment transport in a complex manner. This complexity is especially due to the adhesive effect of mucopolysaccharides, and the binding effect of long-chain polymers (Mehta and Parchure, 2000).

Table 2.1 Statistical values associated with bed sediment distribution (from Appendix E)

Statistic	Moisture content (%)	Organic content (%)	Solids content (%)
Minimum	54	6	16
Maximum	84	51	46
Mean	76	21	24

2.3 Hydrographic Measurements

Sites at which data were collected during the study are shown in Figure 2.2. Tide, salinity, and temperature data were obtained at TG1, TG2 and TG3, and tide, waves and current measurements were made at WGC. At the three transects shown, ADCP (RDI 1200 kHz Broadband Workhorse Acoustic Doppler Current Profiler, together with an on-line DGPS system) data on current velocity were obtained along with water samples and (Seapoint) optical backscatter sensor data for suspended solids. These three transects were traversed on May 17, 2001. Additional transects were traversed at other dates, as described later.

Depths (NGVD) within the area varied from 0.5 to 3 m with an average depth of just over 1 m. Depths in the Cedar River varied from 0.3 m to 1.5 m with an average of 0.5 m. From data collected during 09/29/00-10/18/01 using Infinities USA Inc. ultrasonic recorders, (semi-diurnal) tide statistics given in Table 2.2 were obtained.

Table 2.2 Tide statistics for the study area (based on Appendix E)

Gage location	Cumulative percentile range (m)			
	25	50	95	98
TG1	0.27	0.44	0.70	0.90
TG2	0.04	0.10	0.45	0.62
TG3	0.08	0.18	0.45	0.53

The observed variation of ranges reflects gage distances from the mouth of the Ortega. In general it is evident that the system is very much micro-tidal (< 2 m), and that the upstream reaches covered by the study are only weakly tidal. Such weakly tidal systems are substantially influenced by episodic runoff. Elsewhere (Mehta et al., 2000) it is shown that when the runoff is very high, as during the February 1998 El Nino event, flow in the entire system was directed downstream at all stages of tide (See Figures 2.8 and 2.9).

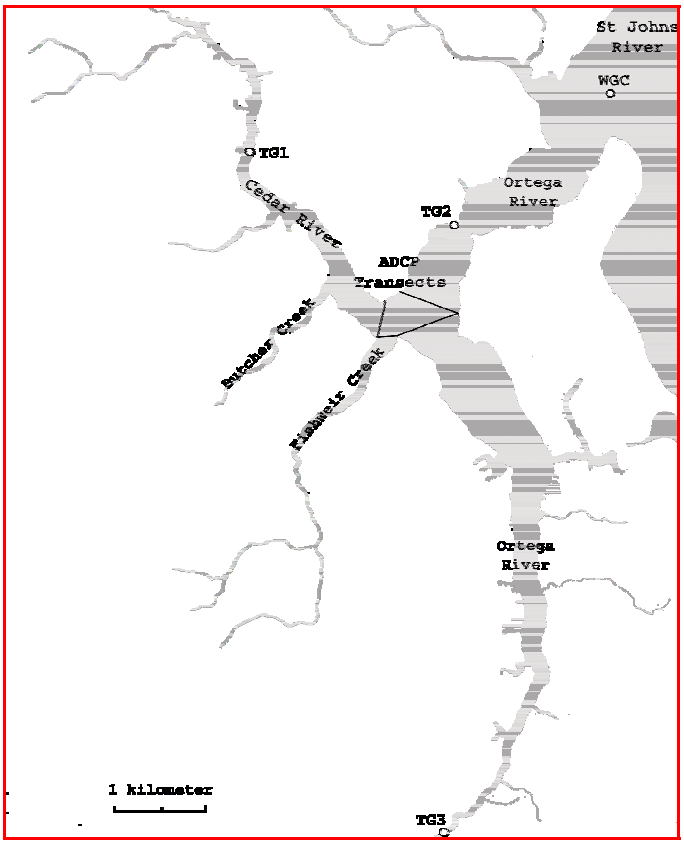

Figure 2.7 Cedar/Ortega River data collection sites (from Appendix E).

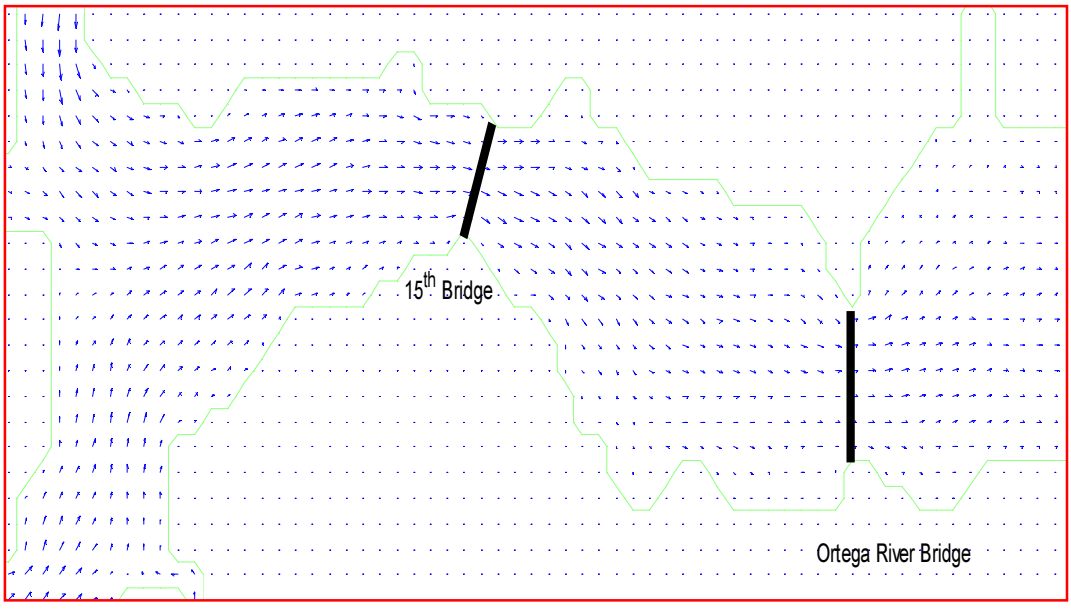

Figure 2.8 Simulated flood flow (depth-mean) velocity field during El Nino discharges in the Cedar/Ortega system (after Marván, 2001).

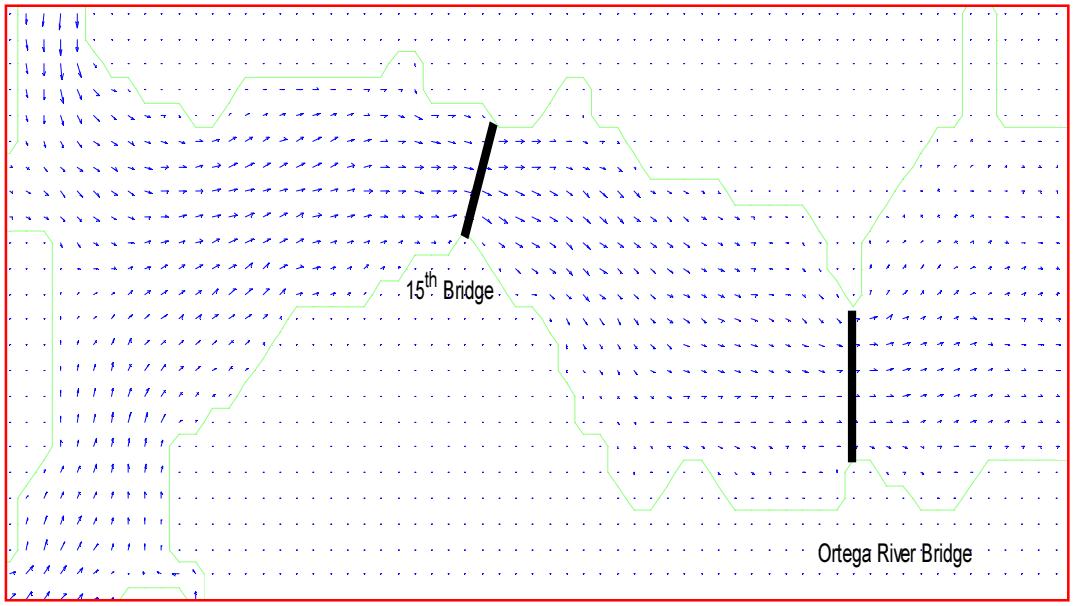

Figure 2.9 Simulated ebb flow (depth-mean) velocity field during El Nino discharges in the Cedar/Ortega system (after Marván, 2001).

Tidal current measurements were made initially with an Endeco tethered meter, and later using UF's P-U-V gage employing a Marsch-McBirney electromagnetic transducer. Statistics derived from the Endeco for the 02/05/01-03/08/01 period are given in Table 2.3. Magnitude-wise the 98 percentile value of 0.30 m/s is consistent with the tidal range at the mouth (Table 2.2). As a rule of thumb, when the current speed is less than ~0.30 m/s, sediment resuspension is weak and the suspended load low. As shown elsewhere (Mehta et al., 2000), resuspension and transport of sediment is noteworthy only when runoff is high enough to generate velocities on the order of 0.5-1.0 m/s.

Statistics for the salinity values calculated from conductivity and temperature measurements (using Greenspan VEC-250 transducers) for the period 10/27/00-11/26/00 are given in Table 2.4. During the period of measurement the system was brackish, with very low salinities in the upper reach of the Ortega. Nevertheless, inasmuch as critical salinities for flocculation of clay minerals in water are quite low, on the order of 0.5-2 psu, it is evident, and

confirmed by observation, that the clayey material in suspension is flocculated, even as the floc properties are substantially modulated by organic matter.

Table 2.3 Current statistics at the mouth of the Ortega River (based on Appendix E)

Cumulative percentile	Speed (m/s)
98	0.30
95	0.25
50	0.08
25	0.04

Table 2.4 Salinity statistics for the study area (based on Appendix E)

Location	Cumulative percentile value (psu)			
	25	50	95	98
TG1	6.3	6.9	8.8	9.5
TG2	6.9	7.6	10.1	11.0
TG3	0.3	0.7	2.6	3.2

River discharge data from Cedar River for the period 03/01/97 to 10/22/98 are plotted on a cumulative basis in Figure 2.10. These imply typically very low values (< 5 m^3/s 94% of the time and > 45 m^3/s for only 0.16% of the time). The mean and maximum discharges are found to be 1.4 m^3/s and 112 m^3/s, respectively.

Tidal discharge measurements carried out using an ADCP on 05/17/01 (along the transects shown in Figure 2.2) revealed that due to the shallow nature of the estuary and the marginal performance of the ADCP in shallow waters, the data were found to have a somewhat qualitative significance. Nevertheless, Table 2.5 presents the analyzed data for the Cedar River transect; see Figure 2.7, in which this transect is located at the confluence of the Cedar and Ortega Rivers. Positive discharge is directed west, and negative is directed east. As shown later, these discharges are consistent with tidal forcing at the site.

Sediment samples collected during the 05/17/01 ADCP study (Table 2.5) indicated that with the exception of one “anomalous” value of 101 mg/l (sample no. 73), possibly due to its

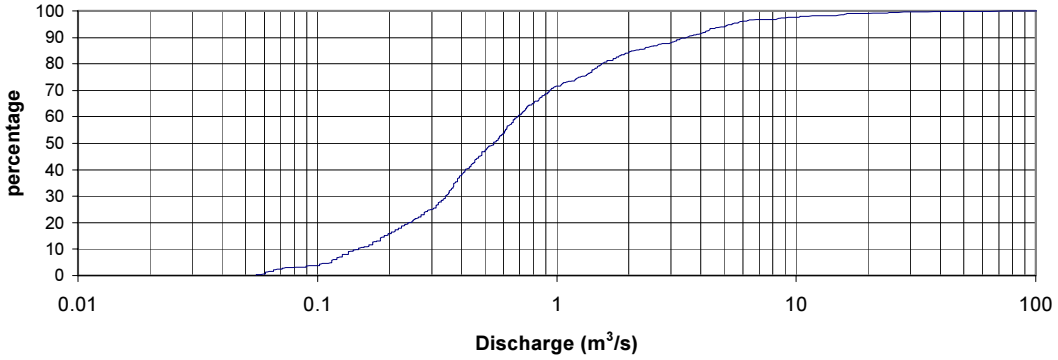

Figure 2.10 Cumulative frequency distribution of Cedar River discharge.

proximity to the bed, the sample range was 8 to 57 mg/l and the mean 20 mg/l, indicating a characteristically very low suspended sediment concentration regime. These values are comparable to those in Table 2.6 obtained by SJRWMD over a four-year period at Ortega Bridge.

Table 2.5 Confluence region concentrations on May 17, 2001 (from Appendix E)

Sample no.	Conc. (mg/l)	Sample no	Conc. (mg/l)	Sample no	Conc. (mg/l)	Sample no	Conc. (mg/l)
1	14	21	33	41	15	61	16
2	17	22	17	42	14	62	15
3	16	23	19	43	18	63	16
4	17	24	16	44	12	64	20
5	8	25	14	45	19	65	15
6	22	26	16	46	37	66	15
7	14	27	17	47	13	67	14
8	13	28	17	48	17	68	16
9	35	29	16	49	16	69	16
10	23	30	13	50	19	70	26
11	15	31	14	51	17	71	15
12	15	32	14	52	21	72	14
13	20	33	13	53	16	73	101
14	15	34	17	54	18	74	19
15	14	35	18	55	13	75	17
16	15	36	17	56	13	76	16
17	19	37	17	57	16	77	15
18	16	38	15	58	15	78	57
19	13	39	11	59	16		
20	27	40	11	60	16		

Table 2.6 Statistics based on measured TSS by SJRWMD during 01/09/94-02/11/95

Station	Maximum (mg/l)	Minimum (mg/l)	Mean (mg/l)
Ortega Bridge	50	3	14
Ortega mouth	22	1	9
Timaquana Bridge (Ortega)	25	6	14
San Juan Bridge (Cedar)	105	4	21

The long term (01/9/94-02/11/95) data from Cedar River also reveal the significance of the episodic nature of sediment transport in this river, as seen from Figure 2.11, in which the measured time-series is plotted. Note that the TSS is typically less than 20 mg/l. During El Nino, however, it exceeded 100 mg/l. Any sediment remediation technique for this area must recognize this significant non-steadiness of sediment transport in the area.

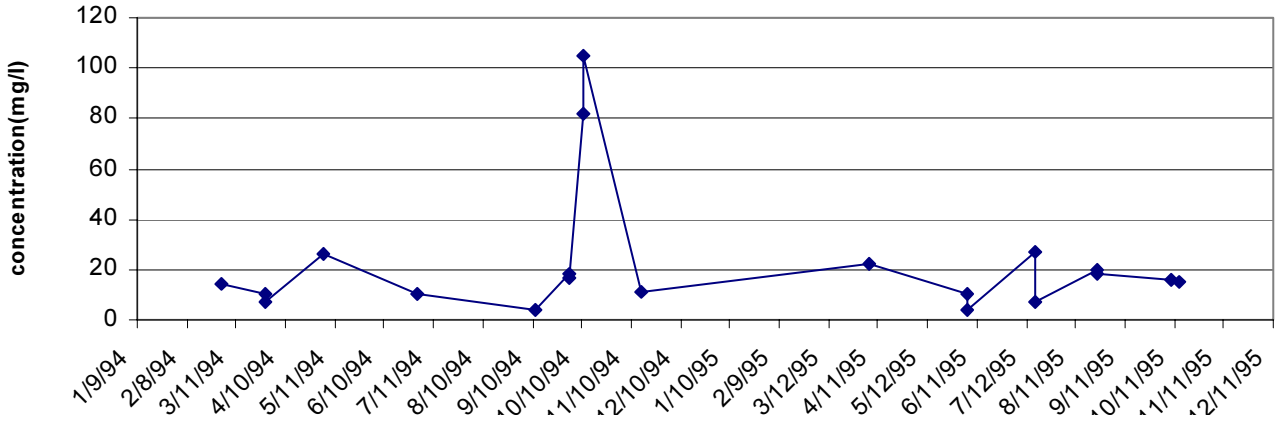

Figure 2.11 Measured suspended sediment time-series at San Juan Rd. Bridge, Cedar River, 01/09/94-02/11/95.

Wind record from the nearby Jacksonville Naval Air Station for the 01/01/95 - 12/31/98 period indicate that speeds of 3-5 m/s are common (61.7% of time). Significant directions are the 48^{o}-72^{o} (10.3%) and 168^{o}-192^{o} (15.2%) sectors. During that period the highest speed recorded was 15 m/s from the 72^{o}-96^{o} sector. These data, taken along the main stem, must be interpreted with care when applying to the study area, especially because portions of the waterway reaches are flanked by trees, while others have been cleared and developed (see Appendix E).

Wave data obtained using a Transmetrics Inc. pressure transducer at the mouth of the Ortega showed generally mild wave action. For example, during the 02/10/01 to 04/25/01 period, the wave modal period was found to be 2.0 s and the significant wave height only rarely exceeded 0.2 m (Figure 2.12).

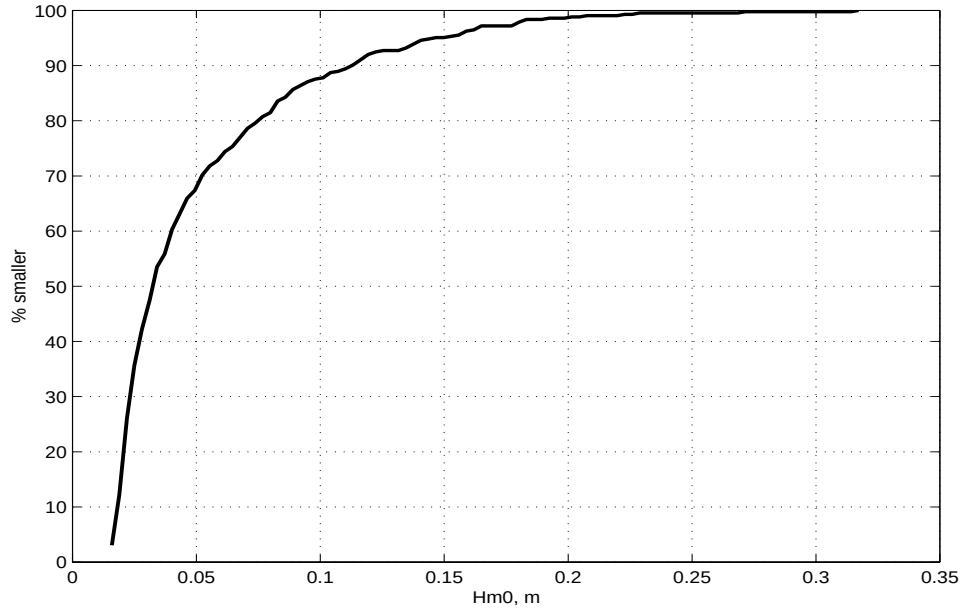

Figure 2.12 Cumulative distribution of significant wave height (H_{mo}) at the mouth of the Ortega during 02/10/01 to 04/25/01 (from Appendix E).

This mild climate is due to the limited wind fetches in the St. Johns River. Wave action in the Cedar River is believed to be even milder, and is unlikely to contribute much to sediment transport except possibly under severe conditions when comparatively large waves may break along the banks.

2.4 Suspended Solids Content from Acoustic Profiling

In addition to the May 17, 2001 survey, detailed acoustic profiling using the ADCP was carried out during October 2-3, 2000. The nine transects covered are shown in the inset of Figure 2.13. The ADCP was also to be run with the "Sediview" software, which permits simultaneous suspended solids data to be obtained without any alteration to the manufacturer's (RDI) hardware.

On the advice of RDI the ADCP came equipped to operate in "Mode 8", said by the manufacturer to be ideally suited to working in conditions of very weak currents in shallow water. Sediview is a DOS program and works with Transect software supplied by the equipment manufacturer. To calibrate the ADCP, the survey vessel was also equipped with salinity and temperature measuring instruments and a calibrated optical backscatter sensor for measuring suspended sediment concentration. These instruments were mounted on a water-sampling bottle.

For the nine transects, estimates of suspended solids concentration are plotted in Figure 2.13. Very shallow water at transect 2 (Big Fishweir Creek) and transect 7 (Butcher Pen Creek) precluded data collection. In Figures 2.14 and 2.15, the corresponding estimates of discharge and solids flux, respectively, are plotted.

Observe that whereas tidal discharges during October 2-3, 2000 (Figure 2.4) were comparable to those on May 17, 2001 (Table 2.3), concentrations were generally higher on May 17, 2001 (mean 20 mg/l) than during October 2-3, 2000 (Figure 2.15, with a mean of ~8 mg/l). This variability may result from the corresponding variation of river discharge, as seen from the concentration (C) versus discharge Q rating function in Figure 2.16. The data points are derived from long-term measurements at San Juan Bridge on Cedar River. Despite the evident data scatter, Stoddard (Appendix F) attempted to derive a plausible mean relationship. Marván's (2001) relationship (Appendix H) is based on a different analysis of the same data.

In general, the Cedar and Ortega Rivers are a challenging environment in which to measure suspended solids because of the consistently low solids concentrations. This makes calibration of both turbidity meters and ADCPs difficult because calibrations must be based on comparisons with water sample data that are inherently subject to errors at low concentrations. In addition, the unavoidable temporal and (particularly) spatial mismatching of three different

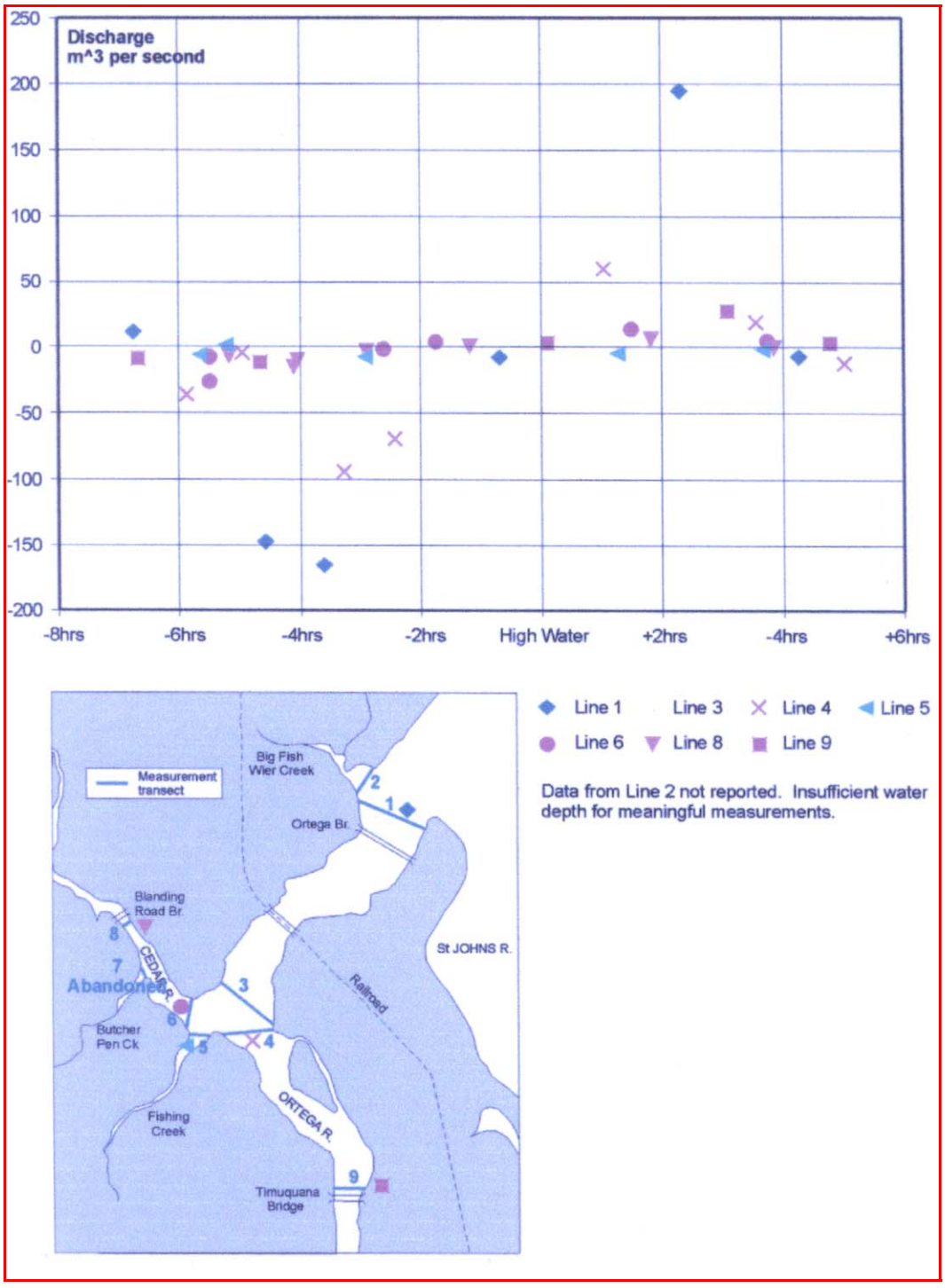

Figure 2.13 Discharge relative to high water level at Ortega Main bridge (from Appendix C).

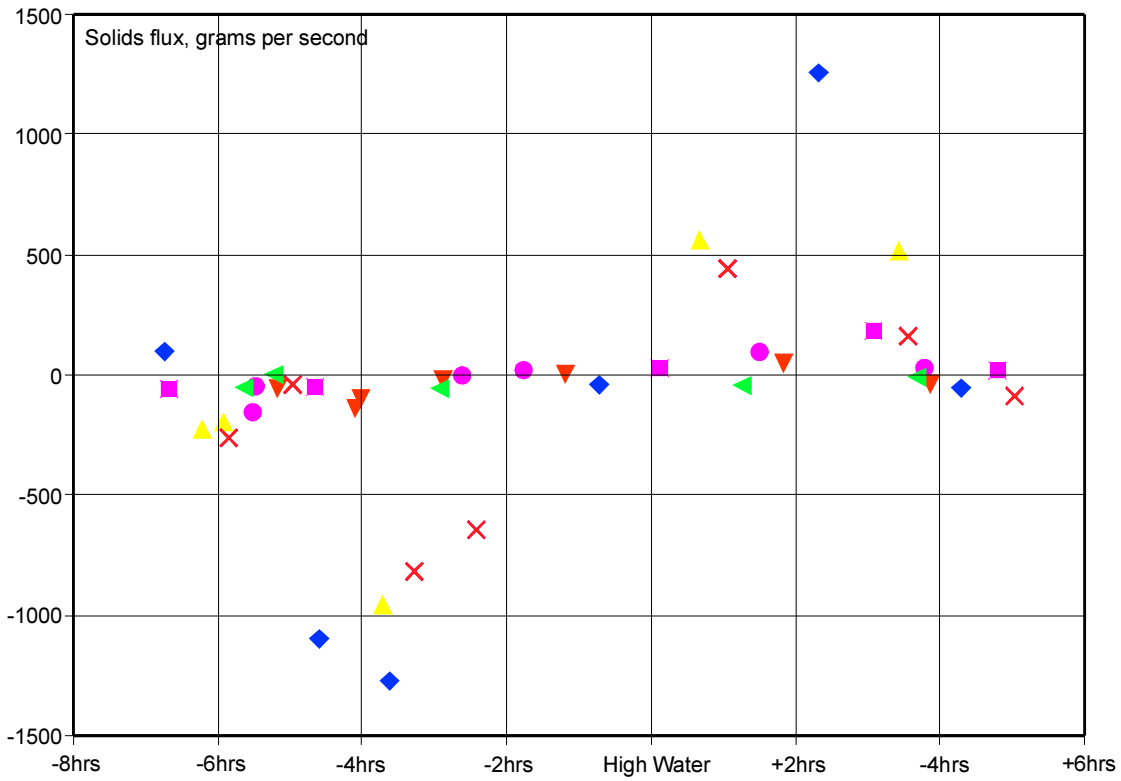

Figure 2.14 Solids flux estimates corresponding to Figure 2.13 (from Appendix C).

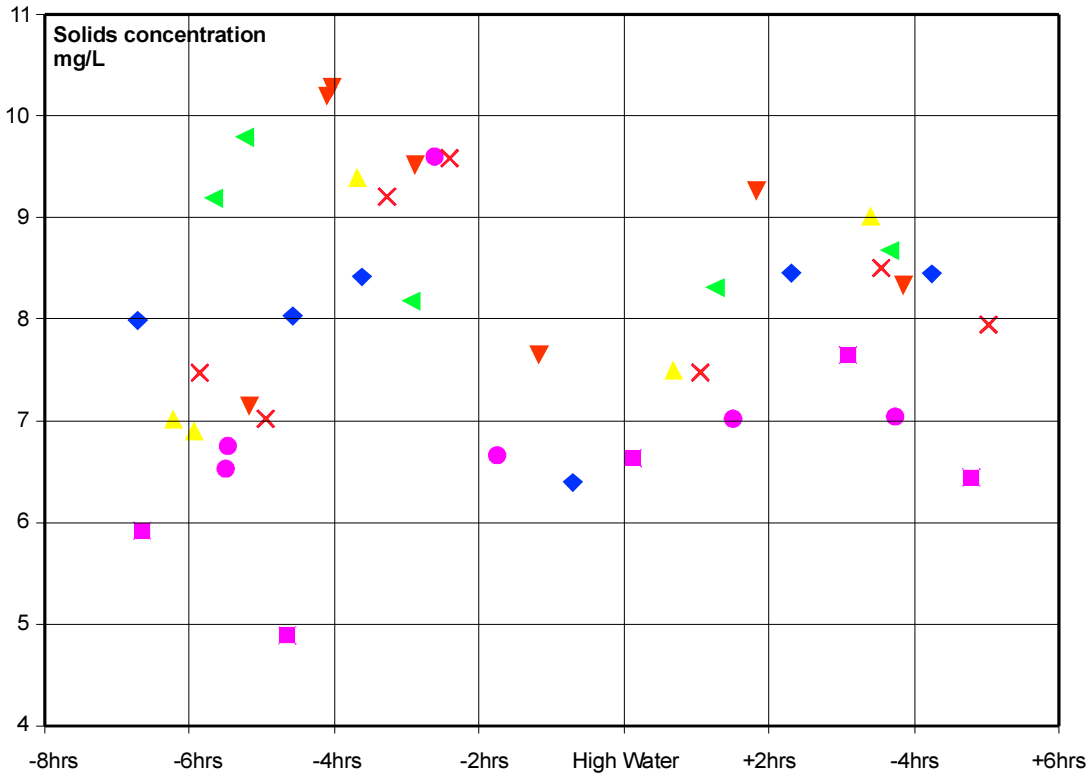

Figure 2.15 Solids concentration estimates corresponding to Figures 2.13 and 2.14 (from Appendix C).

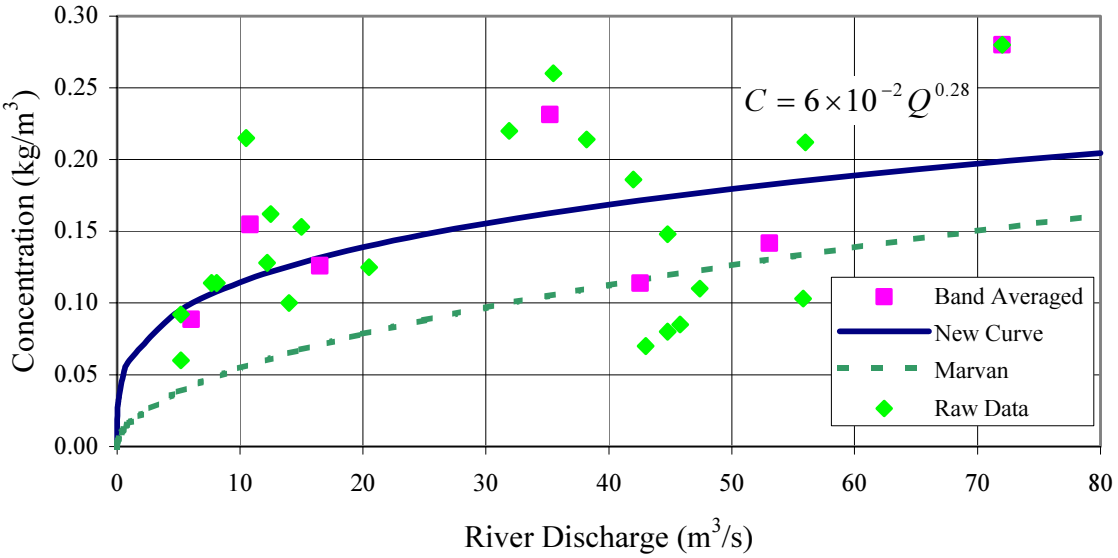

Figure 2.16 Rating curve of Stoddard compared with that of Marván (from Appendix F).

types of measurements (i.e., ADCP backscatter intensity, infrared backscatter intensity of the optical sensors, and gravimetric analysis of bottle samples) leads inevitably to scatter in comparisons between the results. Despite these difficulties, a satisfactory calibration has been achieved. Although scatter is evident in the comparison between Sediview concentration estimates and the water sample data, there is a high degree of correlation and the scattering lies within the expected range.

Measurements of discharge and solids flux were hampered by the shallow water and the presence of extensive fields of sea grass. The sea grass resulted in frequent loss of bottom track which meant that current data had to be referenced to GPS, rather than bottom track, using compass corrections determined for each line by comparing bottom track data with GPS data. A considerable amount of bed level editing was required in order to correct the bed levels and ensure that all valid measurement data were included in the estimates. There was clearly nothing that could be done about the shallow water, which resulted in significant proportions of the total discharge and flux estimates being based on estimated data. However, in future

surveys, the magnitude of this problem might be reduced by using the recently introduced ZeeHead ADCPs. Also, shorter time intervals between successive transects and sailing at a slower speed might provide more reliable data in future surveys.

3 LABORATORY TESTING FOR SEDIMENT TRANSPORT

3.1 Preamble

Noteworthy findings from the analysis of (collected and procured) laboratory data are provided here. See also Appendices B and E.

3.2 Erosion and Settling Tests

Laboratory tests were carried out on 20 grab samples obtained from locations identified in Figure 3.1 (Appendix B). Figure 3.2 shows the erosion plot. It was found that, with the exception of two samples, which mainly consisted of sand, the remaining 18 samples had organic content ranging from 16 to 74%. For the organic-rich samples the erosion rate equation was prescribed as:

$$\varepsilon = \varepsilon_N(\tau - \tau_{ce}) \tag{3.1}$$

in which ε is the erosion rate and ϑ is the applied shear stress. Relative to this equation, the condition for the onset of significant erosion was characterized by the critical shear stress τ_{ce} = 0.17 Pa. The corresponding erosion rate constant was ε_N = 3.5x10^{-4} kg/m^{2}s Pa. These coefficients apply to beds with bulk densities ranging between 1,021 and 1,274 kg/m^3, which are within the range of surficial sediment densities found in the study area.

Under quiescent conditions, the settling velocity, W_s of fine-grained sediment is related to suspension concentration, C, according to:

$$W_s = \frac{aC^n}{(b^2 + C^2)^m} \tag{3.2}$$

In the present study (see Appendices B and E), a = 0.035, b = 2.0, n = 3.5 and m =2.75 were obtained, given settling velocity W_s in m/s and suspension concentration C in kg/m^3. The characteristic peak settling velocity was found to be 1.5x10^{-2} m/s (see Figure 3.3).

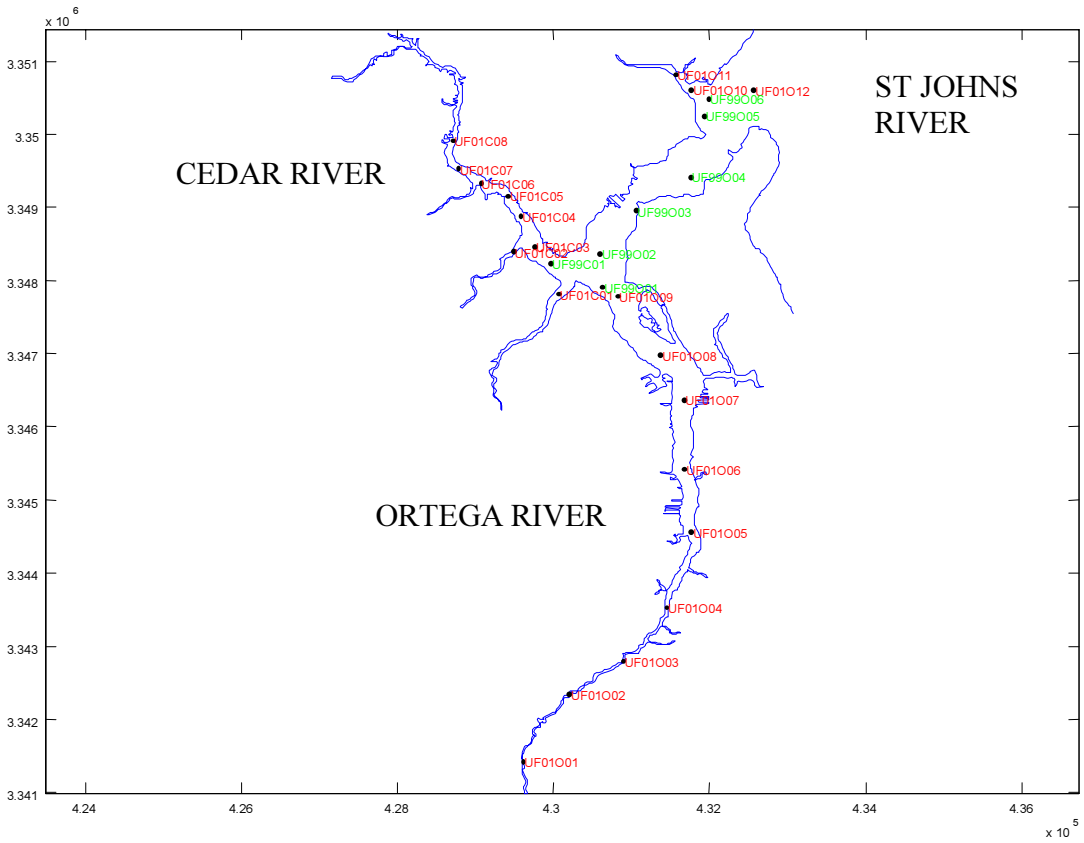

Figure 3.1 Map of Cedar and Ortega River sampling sites. Sites UF01 are for the present study; UF99 are from a previous sampling study (Mehta et al. 2000).

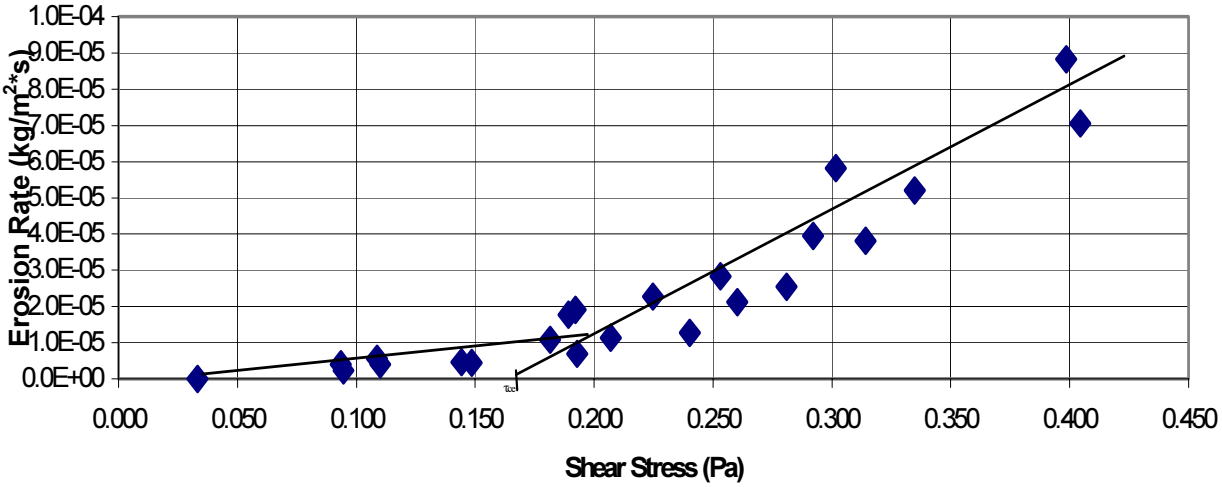

Figure 3.2 Composite plot of bed erosion rate versus bed shear stress (from Appendix B). Note that for computational purposes, the first line, representing minor "floc entrainment" is ignored.

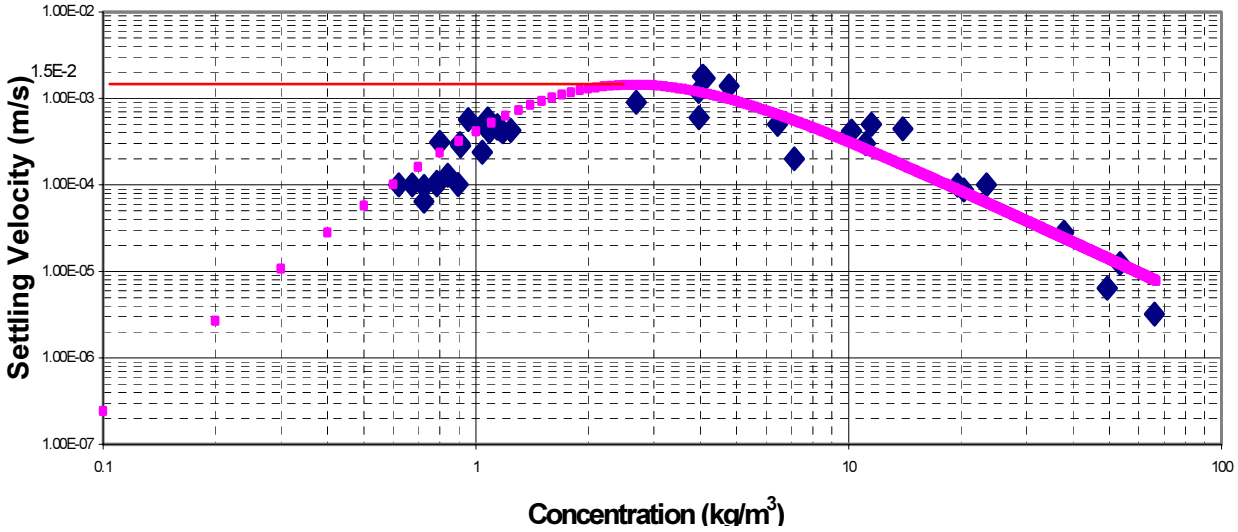

Figure 3.3 Settling velocity variation with concentration – data and best-fit of Eq. 3.2. Peak velocity is 1.5×10^{-2} m/s (from Appendix B).

3.3 Settling Velocity Algorithm

A settling velocity algorithm was developed for incorporation in the Environmental Fluid Dynamics Code (EFDC) used herein for examining sediment remediation scenarios. This code for estuarine flows contains a three-dimensional, hydrostatic flow model, as well as a compatible sediment model. It uses either a Cartesian or curvilinear - orthogonal coordinate system in the horizontal plane, and a stretched or sigma vertical coordinate that enables it to follow the bottom topography and free surface displacement. A level 2.5 turbulence closure scheme in the hydrodynamic model relates the turbulent viscosity and diffusivity to the turbulence intensity and a turbulence length scale. An equation of state relates density to pressure, salinity, temperature and suspended sediment concentration (Hamrick 1992; 1996).

The settling velocity algorithm calculates the settling velocity of the particles by accounting for the floc growth and breakup processes that occur for fine-grained sediment in estuarine and coastal waters due to different mechanisms. As a result, instead of using the settling velocity derived from measurements in a laboratory settling column in still water (Eq.

3.2) directly, the model is merely calibrated using laboratory data. This enabled the settling velocity to be not only dependent on suspended sediment concentration, but also on flow turbulence, as characterized by the energy dissipation parameter *G*.

The model was validated against the floc size data of Winterwerp (1998) from two settling column tests using fine sediment from the Ems-Dollard River area in The Netherlands. Comparisons between simulations and data are shown in Figure 3.4. Values of concentration *C* and dissipation parameter used are given in Table 3.1. Floc size is seen to grow with time until it reaches an equilibrium value (there is an equilibrium particle size for given concentration and dissipation parameter) and remains the same beyond that point. For Cedar River the dissipation parameter was estimated to range from 0.5 to 10 Hz (Appendix E).

Table 3.1 Data from settling column tests with Ems-Dollard fine sediment (from Appendix E)

Test Number	*C* (kg/m^3)	*G* (Hz)
T-73	1.21	81.7
T-69	1.17	28.9

Wolanski et al. (1992) measured the settling of sediment obtained from Townsville Harbor, Australia in a Plexiglas cylinder of 10 cm internal diameter and 140 cm height. Turbulence could be generated in this column by oscillating 1 cm wide rings along the walls, spaced 2 cm apart. Two sets of data were obtained: in quiescent water, and with rings oscillating. Quiescent water can be characterized by very low values of dissipation parameter G. These data are compared in Figure 3.3 with model output. The simulated curve based on measurement in oscillating water indicates a reasonably good match with data points. However, measurements in quiescent water are not predicted as well. This is believed to be due to the fact that, the model does not perform well for low values of dissipation parameter G (i.e., in the absence of turbulence).

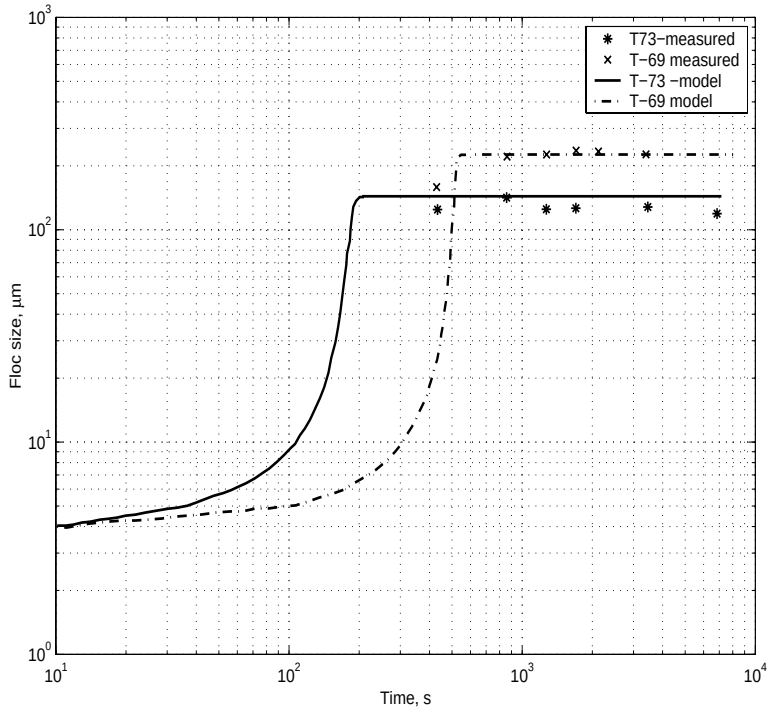

Figure 3.4 Floc growth with time measured and predicted for River Ems-Dollard fine sediment (Winterwerp, 1998) (from Appendix E).

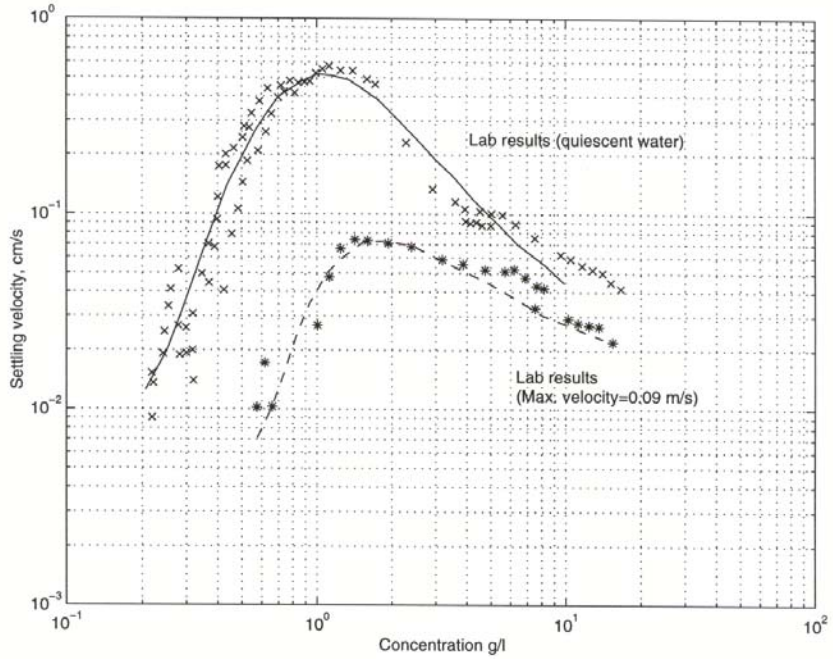

Figure 3.5 Settling velocity calculation test results, and comparison with data of Wolanski et al. (1992) using sediment from Townsville Harbor, Australia (from Appendix E).

3.4 Consolidation

Two tests on the self-weight consolidation of bottom material from the study area were carried out (Marván, 2001). In Figures 3.6 and 3.7, hindered, or collective settling can be observed during the first 10 to 15 (t^{-1} = 6-4 h^{-1}) minutes, respectively. Note that h_o is the initial height of suspension and h(t) is the instantaneous height. At this point, a transition to consolidation occurs which is related to the change from the first consolidating mode to the second mode. This transition point does not necessarily have to be the same in each case since it is expected to be a function of the initial concentration. Within the consolidation phase, three trend lines can be observed, which can result from a rearrangement of particles due to self-weight consolidation at discrete time intervals. As observed in Figure 3.7, the transition point for every phase occurs sooner than the corresponding times for the sample shown in Figure 3.6. This could be due to the higher self-weight at higher concentrations.

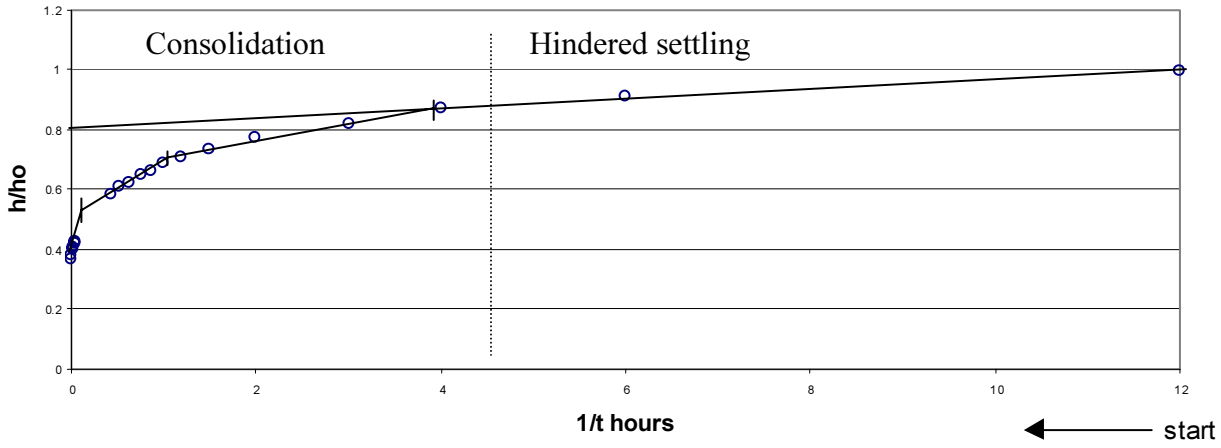

Figure 3.6 Consolidation for initial concentration of 13.7 g/l (from Marván, 2000).

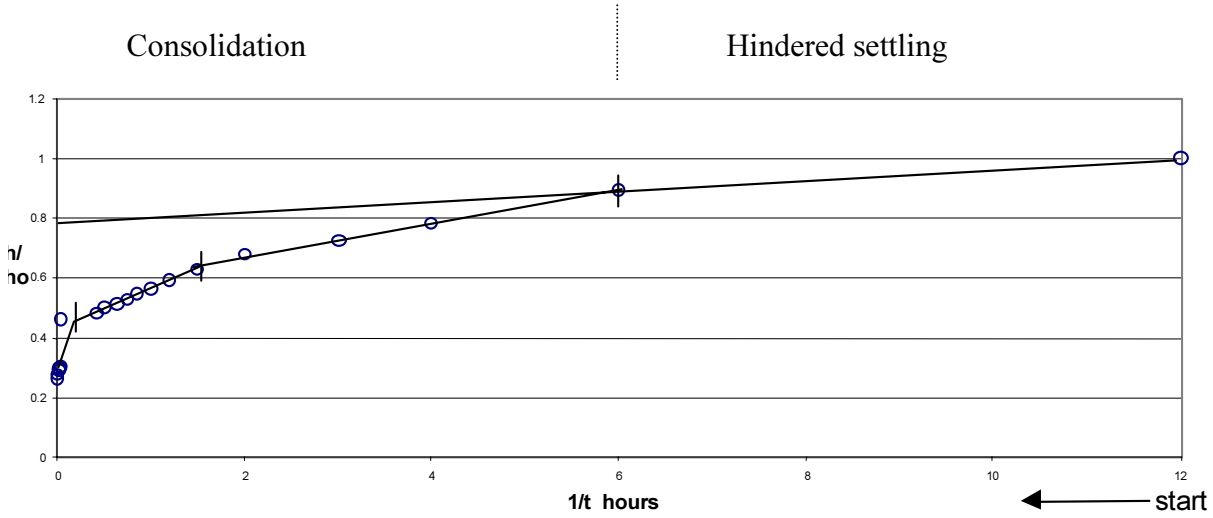

Figure 3.7 Consolidation for initial concentration of 24.3 g/l (from Marván, 2000).

4 SEDIMENT REMEDIATION

4.1 Sediment Treatment Scenarios

Referring to Figure 4.1, the two off-line sediment treatment alternatives (OFL-1 and OFL-2) proposed by SJRWMD are seen to be in the upstream reach of the Cedar River. At the better of the two sites, a Wet Detention Systems (WDS) would be constructed with the objective to entrap contaminated sediment, off-line and especially during high flood events, from sources upstream of these facilities, thus intercepting the material well before it reaches the confluence area, where in has accumulated over the years.

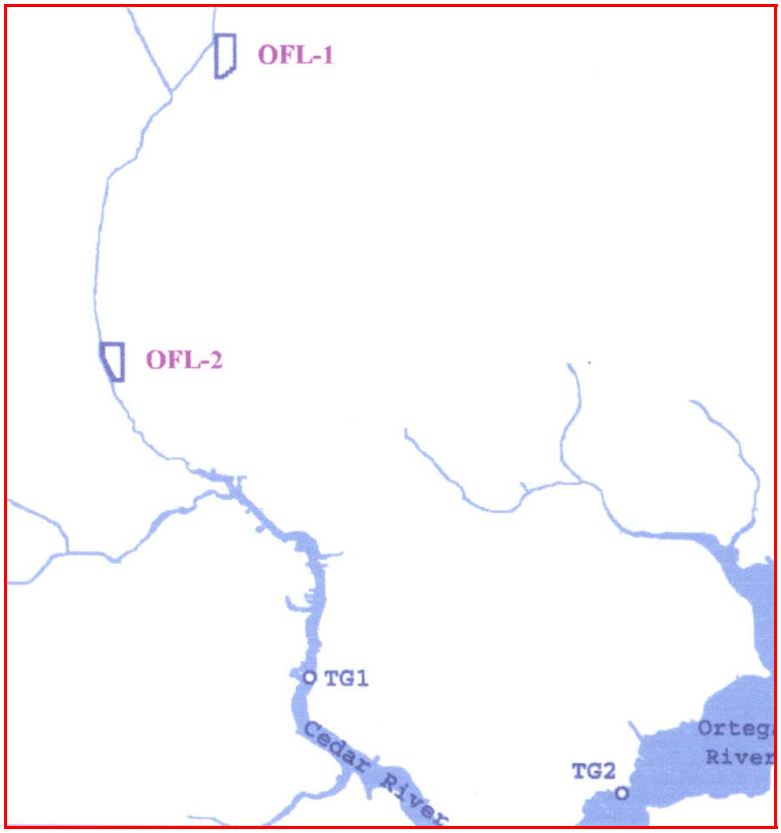

Figure 4.1 Cedar/Ortega Rivers data collection and sediment off-line treatment (Wet Detention System) alternative sites OFL-1 and OFL-2 proposed by SJRWMD.

Further alternatives investigated in this study are shown in Figure 4.2, and for reference purposes, the bathymetry of the study area is shown in Figures 4.3 and 4.4. The latter figure especially highlights the shallow waters in the confluence area. Note that OFL-1 is located

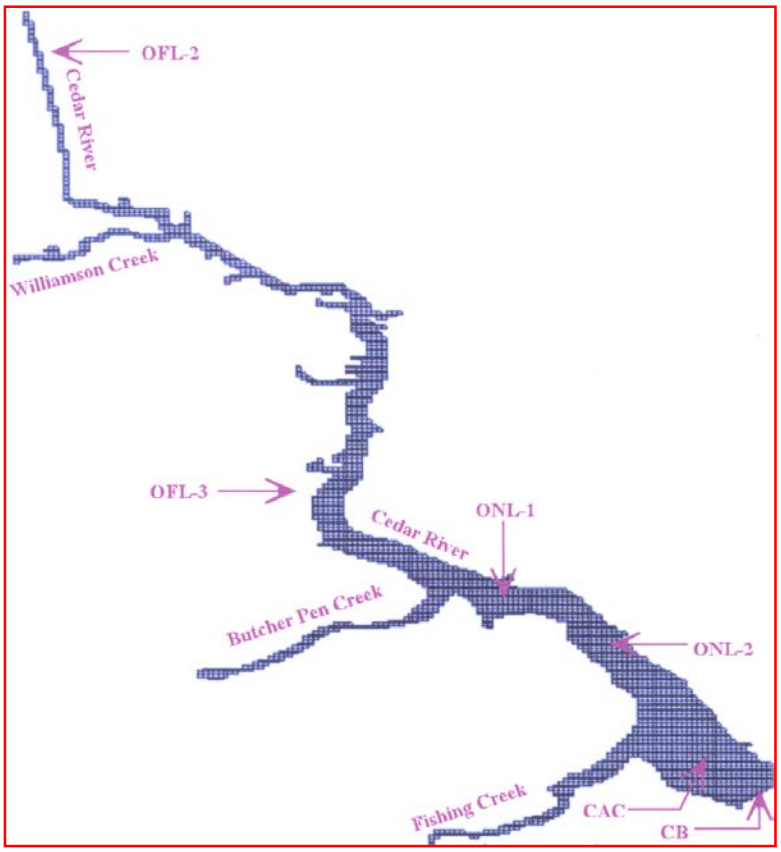

Figure 4.2 Sediment treatment facility alternatives in addition to those proposed by SJRWMD.

north of OFL-2, beyond the sketch boundary (see Figure 4.2). Assuming the feasibility of its construction, a third off-line treatment site, OFL-3, is conveniently chosen to be downstream of Williamson Creek, which debouches sediment into Cedar River. Two on-line (i.e., in channel) sites, ONL-1 and ONL-2, located at sites (see Figure 4.2) where it may not be feasible to design WDS due to land requirements, are on-line sediment traps or pits into which sediment would be captured due to enhancement of settling as the flow velocity over the depressed bottom is reduced relative to the velocity away from the pit (Parchure et al., 2000). They are chosen to be downstream of Butcher Pen Creek, which also empties water and sediment into Cedar River. In Figure 4.2, CAC refers to sediment accumulation in the confluence area, and CB is the reference downstream flow boundary for the Cedar River at the confluence.

In what follows each of the above options will be examined separately. To that end, the following four general criteria may be selected as a basis for the examination: 1) A significant

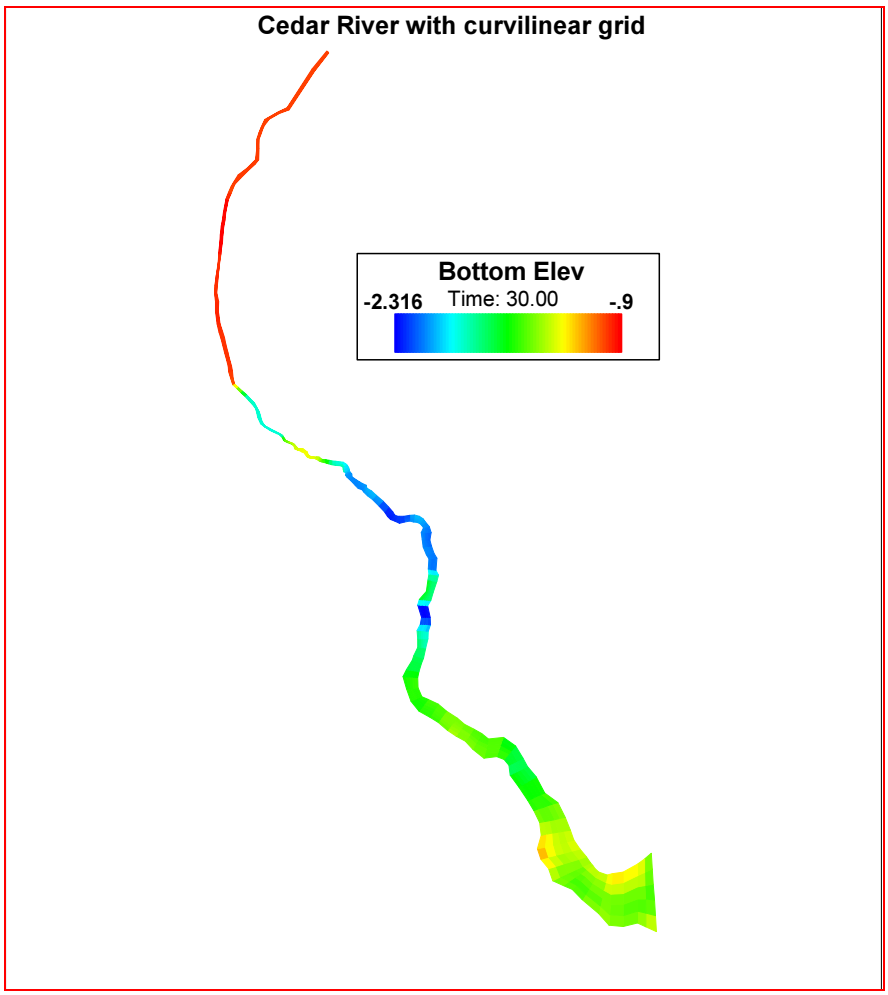

Figure 4.3 Cedar River bathymetry. Bottom elevations are in meters with reference to NGVD.

reduction in sediment flux out of CB, 2) removal of accumulated sediment from critical sites in the confluence area, 3) sequestration of accumulated sediment at critical sites in the confluence area, and 4) improvement in navigation. The choice of the first three criteria is rationalized by the need to enhance water quality. Two water quality indices are commonly used in Florida's estuaries, both associated in part with water column turbidity via Secchi disc reading.

The Florida Water Quality Index (WQI) is used to quantify the quality of water. A higher WQI number indicates poorer water quality. This index is comprised of six categories

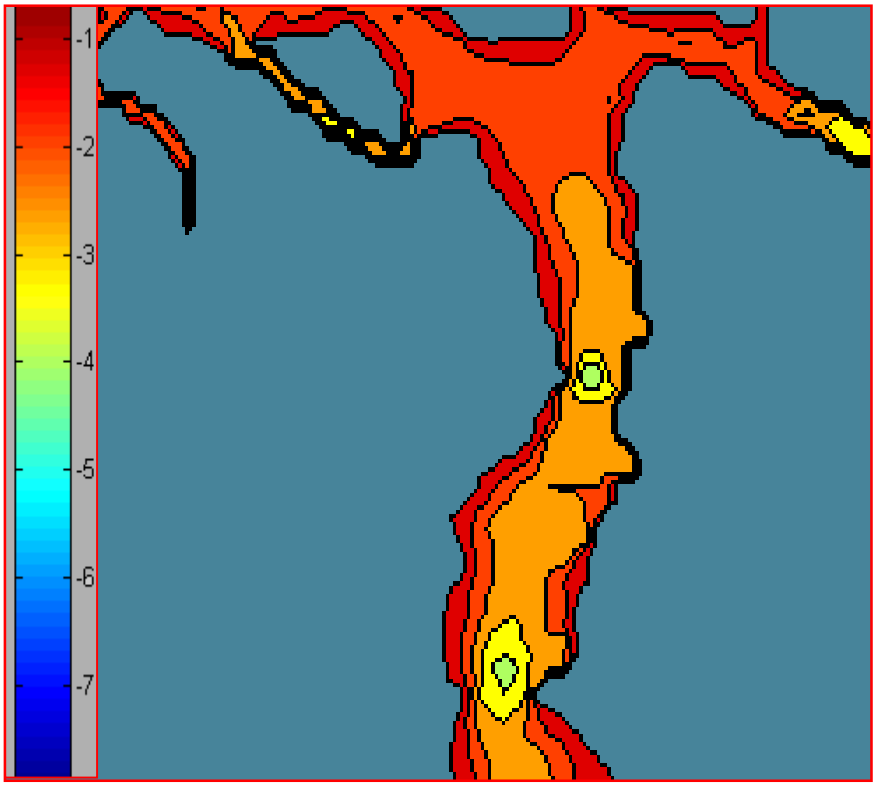

Figure 4.4 Bathymetry of the Ortega River (running north-south) at its confluence with the Cedar River (to left). Depths are in meters. Note the change in map orientation with respect to Figure 4.3.

that include: (1) biological integrity including species diversity, (2) clarity of the water which can be tested through light penetration tests, turbidity analysis, total suspended solids tests, color determination, and Secchi disc depth tests, (3) dissolved oxygen in the water, (4) organic wastes which, for example, in the Loxahatchee River tend to accumulate in deep holes in the riverbed and become resuspended during a storm event or periods of heavy rain, (5) nutrients including nitrates, and (6) bacteria and specifically fecal coliform. Note that besides the Secchi disc value, WQI also depends on organic content.

The Florida Trophic State Index (TSI) includes four components in its attempt to quantify the water quality in a sample (Wanielista, 1978). The four indices include: (1) total nitrogen concentration, (2) total phosphorous concentration, (3) mean Secchi disc depth, and (4) Chlorophyll A concentration. Increasing TSI implies poorer water quality.

Thus we note that both indices are contingent upon Secchi disc readings, hence to a degree on the suspended sediment load. We must note, however, that whereas these indices are meant for surface water quality, accumulation of contaminated sediment and associated pore water influence surface water quality in an indirect way. In other words, for the present analysis WQI and TSI can only be considered as indicators of the environmental state of the river system in a qualitative way.

The choice of navigation too must be considered in a qualitative sense, inasmuch as specific channel depth requirements have not been integral to the problem statement specified by SJRWMD.

4.2 Wet Detention Systems

In a WDS, by diverting river flow into a pond where flow velocities are small, a major portion of suspended sediments can be expected to settle out. Such systems can also be effective for storm water treatment when the bulk of the solids are carried with the first flush, as they can be intercepted and given a sufficient residence time to allow them to deposit. The concern for the Cedar River WDS is to provide as much treatment as possible; hence the effectiveness of the facility has been defined by the area available for constructing the facility. As we shall see later, this requirement also limits sites for its construction, hence sediment remediation based on this technique.

In its simplest form, WDS is a settling pond with weir inflow and outflow (Bedient and Huber, 2002) into which sediment is shunted out of the main stem river, as shown schematically in Figure 4.5. The length of the pond is determined by the depth of water and the sediment settling velocity (Sarikaya, 1977). Naturally, the peak flow velocity (or, better, associated bed shear stress) in the pond must be less than the critical velocity (or critical stress) for resuspension. Referring to Figure 3.2, for design purposes and for fine sediment, this stress

is equal to 0.17 Pa. For an assumed depth of 2 m and Manning's n = 0.020, the critical velocity would be about 0.5 m/s.

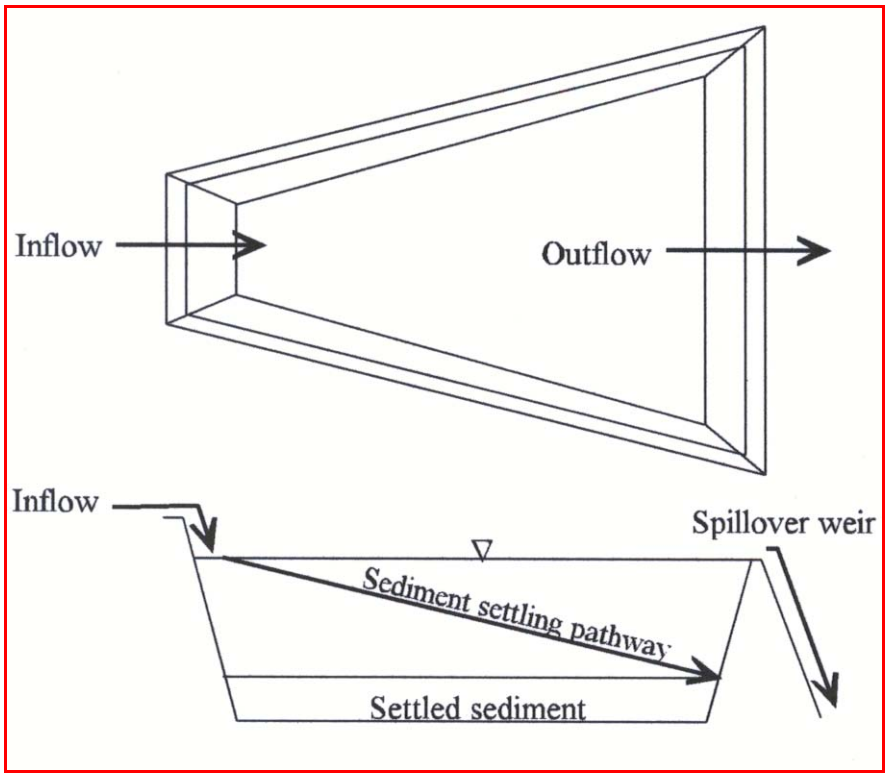

Figure 4.5 Schematic drawing of a Wet Detention System

4.3 Cedar River Sediment Trapping Modeling Results

4.3.1 Cartesian Grid Modeling Results

The results from Cedar River modeling performed by Paramygin (2002) using EFDC with a Cartesian grid are presented in Appendix E and summarized in this section. Model runs were carried out without and with the off-line sites in place for the selected efficiencies of 0%, 30%, 60% and 90%, in order to cover a wider range than the prescribed 40%, 60% and 80%. The model was run for three days, during May 16-18, 2001. Three output-control points (OFL-2, OFL-3 and CB) were selected. OFL-2 and OFL-3, corresponding to the off-line sites, were placed just upstream of a site to measure sediment flux into the site, and CB was the control

point just upstream of the downstream boundary, for monitoring trapping influence at the downstream end.

As discussed in Appendix E, it was found that the two sites (OFL-2 and OFL-3) would have a low effect on sediment transport at the lower end of the Cedar River individually and together, especially if removal efficiencies at the traps are not found to be high. The primary reason for this finding is that the majority of sediment load is derived from Williamson and Butcher Pen Creeks, rather than the Cedar River. However, this does not mean that either OFL-2 or OFL-3 would be ineffective in capturing contaminated sediment from sources upstream of OFL-2, especially if these off-line sites can be operated at, say, 80% efficiency. An advantage both sites have is that the Cedar River sediment load is typically low (Appendix E and Table 4.2); hence it should be feasible to operate an effective containment system for a longer period without renewal in comparison with systems further downstream.

4.3.2 Curvilinear-Orthogonal Modeling Results

The results from the EFDC modeling using Curvilinear-Orthogonal grids, described in Appendix G, are summarized in this section. Using the boundary conditions generated by the Cedar-Ortega-St. Johns River (COSJR) model (see Appendix G), the 21 trapping scenarios defined in Tables 4.1 and 4.2 were run using the Cedar River (CR) model. The purpose of running these 21 scenarios was to allow for relative comparisons of the proposed remediation measures under varying hydrodynamic and sediment loading conditions. The 18 scenarios given in Table 4.1 involve simulation of the three off-line (i.e., sedimentation ponds) sediment traps, whereas the three scenarios given in Table 4.2 involve simulation of up to three on-line (i.e., in-channel) sediment traps. Each of the 21 scenarios was run for seven days during the COSJR model validation period.

Table 4.1 Cedar River off-line sediment trapping scenarios (from Appendix G)

Scenario No.	Off Channel Trap efficiencies (%)			Hydrodynamic/Sediment Conditions			
	OFL1	OFL2	OFL3	Wind	CR inflow	CR TSS	Downstream tide BC
1	0	0	0	None	1	1	1
2	0	0	0	measured	1	1	1
3	40	0	0	None	1	1	1
4	60	0	0	None	1	1	1
5	80	0	0	None	1	1	1
6	40	40	0	None	1	1	1
7	80	80	0	None	1	1	1
8	40	40	40	None	1	1	1
9	80	80	80	None	1	1	1
10	40	40	40	measured	1	1	1
11	40	40	ONL3	measured	1	1	1
12	40	40	40	30 mph S	1	1	1
13	40	40	40	30 mph N	1	1	1
14	40	40	40	measured	1	1	1.5
15	40	40	40	measured	2.5	2.5	1
16	40	40	40	measured	5	5	1
17	40	40	40	measured	10	10	1
18	40	40	ONL3	measured	10	10	1

Table 4.2 Cedar River on-line sediment trapping scenarios (from Appendix G)

Scenario No.	In Channel Trap			Hydrodynamic/Sediment Conditions			
	ONL3	ONL1	ONL2	Wind	CR inflow	CR TSS	Downstream tide BC
19	yes	0	0	None	1	1	1
20	yes	yes	0	None	1	1	1
21	yes	yes	yes	None	1	1	1

The bathymetry of the CR modeling domain is shown in Figure 4.6. The horizontal grid was curvilinear-orthogonal, and was five cells wide to represent the lateral variability in flow and transported constituents, i.e., dissolved salt and sediment. To simulate the partially stratified estuarine flow in the lower reach of the Cedar River, six vertical layers were used in every computational cell. Also shown in Figure 4.6 are the locations of the six open water boundaries (BC1 – BC6) where boundary conditions were applied. The stage, salinity and suspended sediment concentration boundary conditions at the downstream boundary (BC6)

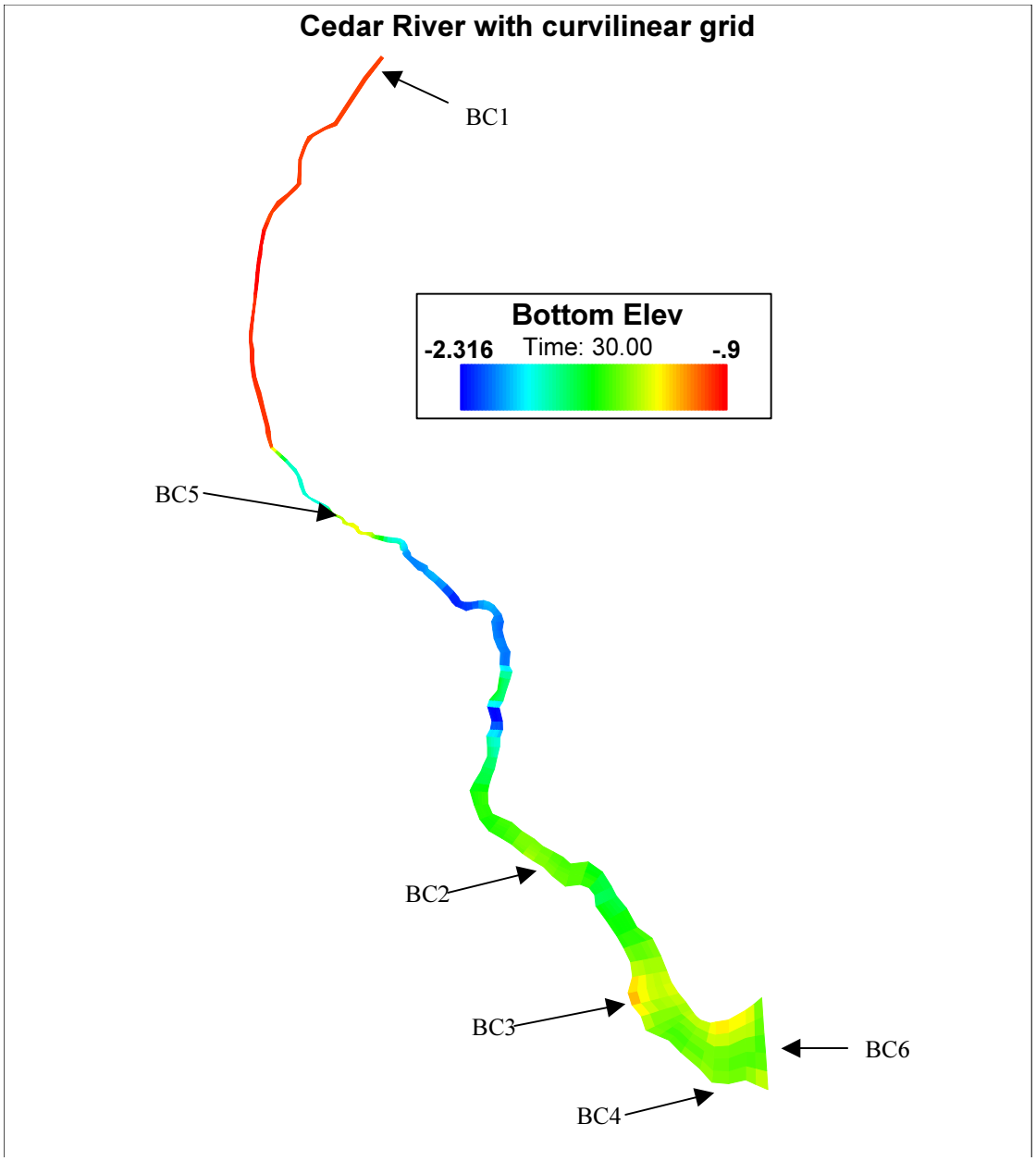

Figure 4.6 Location of open water boundaries in the Cedar River modeling domain (from Appendix G).

were generated by the COSJR model. Time-variable freshwater inflows and suspended cohesive sediment concentrations were applied at the following locations: BC1 – Cedar River; BC2 – Williamson Creek; BC3 – Butcher Pen Creek; BC4 – Fishing Creek; BC5 – Willis Branch. These time series were generated using the SWMM (Freeman 2001).

4.3.2.1 Off-line Sediment Traps

As seen in Table 4.1, each of the three off-line sites was tested with four assumed trapping efficiencies of 0% (no trapping), 40%, 60% and 80%. The last three were prescribed by the SJRWMD. The maximum efficiency (80%) is in part based on the estimated 85% for TSS (Total Suspended Solids) removal by WDS in Florida (see Table 4.3). For each scenario, the assumed sediment trapping (or removal) efficiency (0, 40, 60 or 80%) is given for each of the three proposed remediation sites. For scenarios 1 and 2, no sediment traps were simulated. These are considered the low-flow baseline cases. As seen in Table 4.1, the difference between these two scenarios is that in Scenario 1 wind was not included as a driving force, whereas in Scenario 2 the measured wind velocity at the NAS_Jax weather station was used to calculate the (assumed) spatially constant wind-induced surface shear stress over the modeling domain.

Table 4.3 TSS removal efficiencies of treatment systems in Florida (after Harper, 1997)

Treatment system	Estimated TSS removal efficiency (%)
Dry Retention	60-98
Off-Line Retention/Detention	90
Wet Retention	85
Wet Detention	85
Wet Detention with Filtration	98
Dry Detention	70
Dry Detention with Filtration	60-70
Alum Treatment	90

The numbers in the “CR Inflow”, “CR TSS” and “Downstream tide BC” columns in Table 4.1 indicate the factors the corresponding time series are multiplied by during the model run. For example, in Scenario 15, both the CR inflow time series and the CR TSS time series are multiplied by a factor of 2.5 to simulate a higher flow (and corresponding higher TSS) than that predicted by the SWMM. In Scenario 14, the downstream water surface elevation time

series (predicted by the COSJR model) is multiplied by a factor of 1.5 to simulate a tide with a 50% larger tidal range.

In Scenarios 3 – 9, the number of sediment traps and their efficiencies were systematically varied. The difference between Scenarios 8 and 10 is that wind was included as a driving force in Scenario 10, whereas it was not in Scenario 8. In Scenarios 12 – 17, in which three off-line traps with 40% sediment trapping efficiencies were represented, one or more of the driving forces were varied. The hydrodynamic/sediment boundary conditions changed in Scenarios 14 and 15 were described above. In Scenarios 16 and 17, the CR inflow and TSS time series were multiplied by factors of 5 and 10, respectively, to represent increasing flows and sediment loads from the watershed upstream of the upstream CR boundary. In Scenarios 11 and 18, the two upstream most off-line traps were represented along with the upstream most on-line trap (ONL-3). The latter is located at the same location as OFL-3. These two scenarios were run (with the difference between them indicated in Table 4.1) to investigate the use of both off-line and on-line traps.

Due to modeling related complications in representing the off-line sites as water bodies with channelized flow diverted into them, the representation of off-line treatment sites in the model was simplified. Accordingly, a function was implemented in EFDC that decreased the sediment flux bypassing the grid cell by a pre-defined percentage. The channel cross-section, where the treatment site would be located, was represented by model grid cells having such a sediment removal function, in terms of the percentage by which the effluent sediment load leaving the site is reduced with respect to the influent load entering the site.

4.3.2.2 On-line Sediment Traps

As an alternative to off-line treatment sites, it is instructive to examine the effects of on-line traps (see Figure 4.7 which shows a dredged pit). This is because along portions of the

Cedar River land is believed to be unavailable for an off-line facility. The general principle of such a trap have been examined in Appendix F based on the use of a depth-averaged model setup for the Cedar/Ortega River system in an independent study summarized in Appendix H.

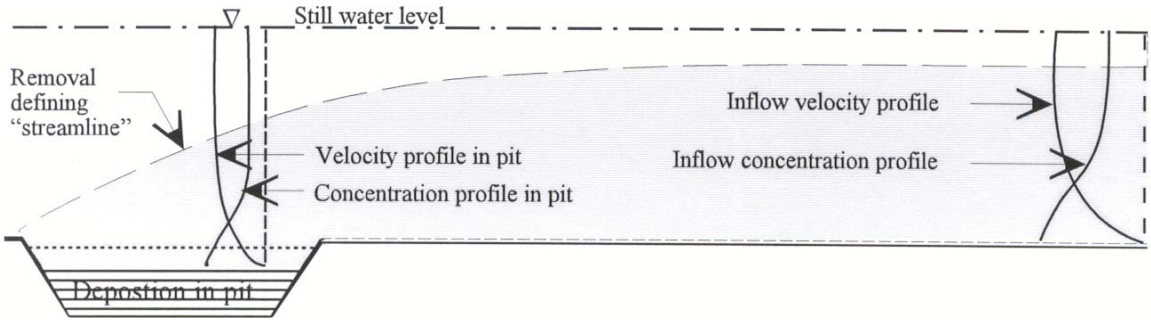

Figure 4.7 Sediment pit or trap and, on the tide-mean basis, a removal defining "streamline" separating material that deposits from that carried past the trap (after Ganju, 2001).

Formalizing the trap efficiency basis already introduced, we note that in the tidal situation the seaward edge of the trap will be the influent side during flood tide, and the effluent side during ebb tide, and vice versa for the landward edge. The sediment load q is calculated as:

$$q = UCH\Delta x \tag{4.1}$$

where U is the local flow velocity and Δx is the cell width. The sediment load on each side of the trap yields sediment removal ratio R:

$$R = \frac{q_i - q_e}{q_i} \tag{4.2}$$

where q_i is the influent sediment load, and q_e is the effluent sediment load. The removal ratio is averaged over a tidal cycle.

The locations of two of the on-line traps (ONL-1 and ONL-2) are shown in Figure 4.2. Both traps are selected 60 m (1 grid cell) wide by 300 m (5 grid cells) long with a surface area of 18,000 m^2 and a (dredged) volume of 36,000 m^3. The traps have an initial dredged depth of 2 m (below the ambient bed depth of 1.2 m at ONL-1 and 1.8 m at ONL-2). The traps have an

initial dredged depth of 2 m (below the ambient bed depth of 1.2 m at ONL-1 and ONL-3 and 1.8 m at ONL-2). These are considered sufficient to reduce the velocity in the river to allow measurable sediment to deposit. For example, at a river discharge of 3 m^3/s and M_2 tidal forcing, the mean velocity over ONL-1 would be 0.13 m/s with the trap and 0.24 m/s without it, i.e., a 49% reduction in velocity over the trap.

Removal ratios were calculated only during periods of ebb tide flow through the ONL-1 trap and are plotted against Cedar River discharge in Figure 4.8. These simulations, which assume a constant (time-independent) dredged depth for each trap, show that the removal ratio is maximum at a discharge of approximately 16.4 m^3/s. It can be shown that as the discharge increases above its characteristic value, the flow increasingly becomes unidirectional, and *R* varies inversely with it (Baker et al., 1999). In contrast, as the discharge decreases below the characteristic value, the tidal influence increases and *R* decreases as the oscillating flow inhibits deposition in the pit (Appendix F).

The poorer performance by ONL-2 observed in Figure 4.8 can be partly attributed to the increased tidal action closer to the confluence of the Cedar and Ortega Rivers. ONL-1 performed more effectively due to more consistent flow direction and velocity since the location is well within the Cedar River.

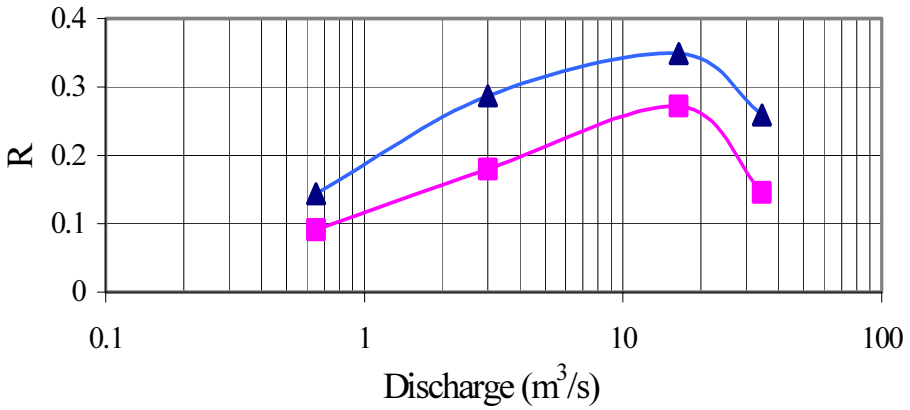

Figure 4.8 Removal ratios for ONL-1 (upper curve) and ONL-2 (lower curve) as functions of Cedar River discharge (from Appendix F).

The trapping efficiencies of ONL-1 and ONL-2, in accordance with Figure 4.8, are an artifact of the chosen dimensions of the traps. Also, the trap efficiency will decrease, rapidly at first and more slowly with time, as a first order rate function (Vincente, 1992). It can be accordingly shown that, for instance, considering the pit shoaling thickness equal to 90% of the initial pit depth, filling of the pit would occur in time $t_{90\%} = 2.3/K$, where K is a site-specific time-constant. In that connection, the above R-values merely indicate initial trap performance.

As an alternative approach, the EFDC application of Section 4.3 was extended (as described in Appendix G) to include the three on-line traps ONL-1, ONL-2 and ONL-3. The middle of the latter trap is located at OFL-3 (see Figure 4.2). As seen in Figure G.26, each on-line trap was three cells wide and had an initial bottom elevation 2 m lower than that of the surrounding cells. The lengths of ONL-1, ONL-2 and ONL-3 were 298 m, 287 m, and 319 m, respectively. Scenarios 11 and 18 in Table 4.1 and Scenarios 19 – 21 in Table 4.2 were run using one of more of these on-line traps.

In Table 4.5 the impact of treatment (load reduction) in the confluence area corresponds to 30% trapping efficiency at OFL-2 and OFL-3 (considering it to be realizable). It is evident that, from the point of view of intercepting sediment arriving in the confluence area: 1) OFL-2 is too far upstream to be effective, 2) OFL-3 is a better choice, and 3) OFL-3 coupled with ONL-1 is the most appropriate treatment scenario.

4.3.2.3 Results from Sediment Trap Simulations

For each of the 21 scenarios, net sediment fluxes, in units of grams per second (g/s), over the seven-day simulation at five transects along the CR were computed. The results are presented in the second through the sixth columns in Tables 4.4 and 4.5. The five transects, identified as T1 – T5 in Tables 4.4 and 4.5 and showed in Figure G.27, were located as follows: T1: immediately downstream of OFL-1; T2: immediately downstream of OFL-2; T3:

immediately downstream of OFL-3, which is located in the middle of ONL-3; T4: immediately downstream of ONL-1; and T5: immediately downstream of ONL-2. The last four columns in Tables 4.4 and 4.5 give the percentage decrease in the net downstream sediment flux at transects T1 – T4 relative to that for each of these transects calculated for Scenario 1 (the dashes in the first row of these last four columns indicate that the percentages were not calculated for these transects since the relative differences are meaningless for Scenario 1). The dashes in the last four columns in Table 4.4 for Scenarios 15 – 18 were not calculated since the changes in the boundary conditions for these scenarios nullified comparisons in terms of the relative net sediment fluxes. The negative sediment fluxes given under T1 and T4 in Table 4.5 indicate that the net flux increases at these transects relative to Scenario 1.

Percentage changes (relative to Scenario 1) in reach average bed elevation change for six reaches over the seven-day simulations are shown in Table 4.6. A positive percentage in this table indicates that there was more erosion in that reach than that which occurred in Scenario 1. The first reach, designated u/s – T1, extends from the upstream (u/s) boundary to T1, reach T1 – T2 extends from T1 to T2, reach T2 – T3 extends from T2 to T3, reach T3 – T4 extends from T3 to T4, reach T4 – T5 extends from T4 to T5, and reach T5 – d/s extends from T5 to the downstream (d/s) boundary. The actual reach average erosion (not the percentage change in reach average erosion) is given in Table 4.6 for reach T4 – T5 since the reach average erosion for reach T4 – T5 for Scenario 1 was zero, thus not allowing the percentage change to be calculated.

As seen by comparing the results for Scenarios 1 and 2 in Tables 4.4 – 4.6, the measured wind had no impact on net sediment fluxes or reach average erosion. The impact of adding OFL-1 is seen for Scenarios 3 – 5 in Table 4.4. With increasing trap efficiency, the net sediment flux decreases at T1 – T3. As expected, the largest decreased occurred at T1 as this

Table 4.4 Results from off-line sediment trapping scenarios (from Appendix G)

Scenario No.	Net sediment flux (g/s) at indicated transects					Decrease in net sediment flux (%)			
	T1	T2	T3	T4	T5	T1	T2	T3	T4
1	4.91	19.47	2.00	4.26	2.85	-	-	-	-
2	4.91	19.47	2.00	4.26	2.85	0	0	0	0
3	3.54	17.81	1.98	4.25	2.85	28	9	1	0.2
4	3.11	17.28	1.97	4.25	2.85	37	11	1.5	0.2
5	2.78	16.86	1.96	4.25	2.85	43	13	2	0.2
6	3.54	11.00	1.92	4.23	2.85	28	44	4	0.7
7	2.78	7.54	1.88	4.22	2.84	43	61	6	0.9
8	3.54	11.00	1.03	3.63	2.77	28	44	49	15
9	2.78	7.54	0.742	3.43	2.74	43	61	63	19
10	3.54	11.00	1.03	3.63	2.77	28	44	49	15
11	3.64	10.06	1.53	4.26	2.84	26	48	24	0.9
12	3.54	11.00	1.03	3.63	2.77	28	44	49	15
13	3.54	11.00	1.53	4.05	2.83	28	44	24	5
14	3.56	11.21	1.01	4.12	1.45	27	42	50	3
15	20.76	68.39	8.42	12.87	4.66	-	-	-	-
16	75.88	215.5	64.46	111.5	30.10	-	-	-	-
17	286.9	659.9	394.9	870.1	271.8	-	-	-	-
18	278.8	638.7	382.1	1024	327.9	-	-	-	-

Table 4.5 Results from on-line sediment trapping scenarios (from Appendix G)

Scenario No.	Net sediment flux (g/s) at indicated transects					Decrease in net sediment flux (%)			
	T1	T2	T3	T4	T5	T1	T2	T3	T4
19	5.05	18.46	1.57	4.28	2.84	-3	5	22	-0.5
20	5.04	18.54	1.59	4.02	2.95	-3	5	21	6
21	5.04	18.63	1.60	4.15	2.14	-3	4	20	3

transect was located immediately downstream of OFL-1. Essentially no reduction in net sediment flux occurred at T4. The results in Table 4.6 for these same three scenarios show that the reach average net erosion increased with increasing trap efficiency for the three upstream-most reaches. The increase in the net erosion for these three reaches, possibly explained by the decreasing suspended sediment concentrations (due to the increasing trap efficiencies) partially counters the decrease in the net sediment flux noted above.

The impact of adding OFL-2 (in addition to OFL-1) is seen in Table 4.4 for Scenarios 6 and 7. The percentage decrease in the relative net sediment flux at T2 increases from 9% to 44% for Scenario 6 and from 13% to 61% for Scenario 7. Similar, though smaller, increases are

Table 4.6 Percentage change in reach average net erosion (from Appendix G)

Scenario No.	Change in Reach Average Net Erosion (%)					
	u/s–T1	T1–T2	T2–T3	T3–T4	T4–T5 *	T5–d/s
1	-	-	-	-	-	-
2	0	0	0	0	0	0
3	0.6	8.4	9.8	0	0	0
4	0.9	10.8	13.0	0	0	0
5	1.2	12.7	15.4	0	0	0
6	0.6	14.0	53.1	0	0	0
7	1.2	19.9	75.3	0	0	0
8	0.6	14.0	53.2	0	0	0
9	1.2	19.9	75.5	0	0	0
10	0.6	14.0	53.2	0	0	0
11	17.0	21.9	16.8	-76.6	0	21.2
12	0.6	14.0	53.2	0	0	0
13	0.6	13.9	70.3	0	0	0
14	2.2	17.7	57.2	19.6	8.77×10^{-5}	4.03×10^{5}
15	374	402	178	-1.85×10^{3}	5.79×10^{-5}	823
16	1.03×10^{3}	1.20×10^{3}	695	-2.09×10^{4}	2.16×10^{-3}	-9.52×10^{3}
17	2.41×10^{3}	2.88×10^{3}	2.07×10^{3}	-7.08×10^{4}	1.51×10^{-2}	-9.69×10^{4}
18	2.55×10^{3}	3.00×10^{3}	2.33×10^{3}	-8.52×10^{4}	1.73×10^{-2}	-1.17×10^{5}
19	16.1	6.9	-43.4	-76.6	0	21.2
20	16.1	7.6	-41.9	-29.8	0	37.4
21	15.9	8.4	-39.7	16.6	0	79.9

* the numbers in this column are the reach average bed elevation change (m)

noted at both T3 and T4 for both Scenarios. These results show that OFL-2 has a larger impact on reducing the net sediment flux to the lower portion of the Cedar River than OFL-1 by itself. Also note that increasing the trapping efficiencies of both OFL-1 and OFL-2 from 40% to 80% results in only a 17% decrease in the relative net sediment flux at T2, though the relative decrease at T3 is 50%. Also as seen in Table 4.4, the net sediment flux at T4 decreases from 0.2% for Scenario 5 to 0.9% for Scenario 7. The additional increase in the reach average net erosion is noted in Table 4.6 for Scenarios 6 and 7.

The impact of adding OFL-3 (in addition to OFL-1 and OFL-2) is seen in Table 4.4 for Scenarios 8 and 9. The percentage decrease in the net sediment flux at T3 increases from 4% to 49% for Scenario 8 and from 6% to 63% for Scenario 9. The percentage decrease in the net sediment flux at T4 increases from 0.7% to 15% for Scenario 8 and from 0.9% to 19% for Scenario 9. Thus, adding OFL-3 has a large impact in reducing the net sediment flux at both T3

and T4. Also note that increasing the trapping efficiencies for all three off-line traps from 40% to 80% results in a moderate 14% decrease in the net sediment flux at T3 and a minimal 4% decrease at T4. The reach average net erosion is essentially the same for Scenario 8 (in comparison to Scenario 6) and for Scenario 9 (in comparison to Scenario 7). Similar to the comparison between Scenarios 1 and 2, no change due to the measured wind is noted in Tables 4.4 or 4.6 between Scenarios 8 and 10.

In Scenario 11, the addition of ONL-3 instead of OFL-3 results in a 49% higher net sediment flux at T3 than that in Scenario 8, a 17% higher flux at T4, and a 3% higher flux at T5. The -76.6% change in net erosion given in Table 4.6 for Scenario 11 at reach T3 – T4 is attributable to the deposition that occurs in ONL-3. Thus, using three off-line traps is more efficient at reducing the net sediment flux in the Cedar River than the use of two off-line traps and one on-line trap. Comparison of Scenarios 6 and 11 shows that the relative net sediment flux at T3 is reduced from 4% to 24% by the addition of ONL-3. The difference in the net fluxes at T4 is negligible.

Next, Scenarios 12 and 13 were compared with Scenario 8. As seen in Table 4.4, the results obtained for Scenario 8 (no wind) and Scenario 12 (constant 13.4 m/s (30 mph) Southerly wind over the seven-day simulation) were surprisingly identical. The constant 13.4 m/s Northerly wind simulated in Scenario 13 resulted in a 25% less relative decrease in the net sediment flux at T3, and a 10% less relative decrease in the net sediment flux at T4. Taken together, these three scenarios show that low to moderate winds (i.e., less than that during tropical storms) have an insignificant impact on the sedimentary regime in the relatively narrow and winding Cedar River.

Scenario 14 shows the impact that a 50% higher tidal range at the downstream boundary has on the net sediment flux in the Cedar River. A smaller decrease in net sediment flux occurs

at T4 in Scenario 14 (3%) than that in Scenario 8 (15%). Insignificant differences occur at the upstream transects. The biggest differences between these two scenarios are seen in Table 4.6, in which the higher tidal range at the downstream boundary results in reach average net erosion for the three downstream-most reaches, i.e., reaches T3 – T4, T4 – T5, and T5 – d/s. The latter is particularly significant in reach T5 – d/s.

Scenarios 15 – 17 simulate the impact of increasing both the flow and TSS boundary conditions at the upstream boundary of the Cedar River by factors of 2.5, 5 and 10, respectively. These three scenarios are compared to Scenario 8. As seen in Table 4.4, the net sediment fluxes at all five transects increase in proportion to the increase of inflow and TSS loads at the upstream boundary. Scenario 18 is identical to Scenario 17 except that an on-line trap is used at the location of OFL-3 instead of the off-line trap. The ONL-3 on-line trap results in higher net sediment fluxes at T4 and T5 than those obtained with the OFL-3 off-line trap. This same finding was obtained by comparing Scenarios 10 and 11.

The results for Scenarios 19 – 21 seen in Table 4.5 show that the only transect at which a significant reduction in the net sediment flux occurs is T3, which is located immediately downstream of ONL-3. Scenarios 11 and 19 show that the reductions in the net sediment flux at T3 is essentially the same. This indicates that OFL-1 and OFL-2 have minimal impact at T3.

To summarize the significant findings from the Cedar River modeling reported in Appendix G, more than one order of magnitude reductions in the net sediment fluxes at T3 and T4 were obtained using three off-line sediment traps as opposed to using just the two upstream-most off-line traps. The largest reduction (25%) in the net sediment flux at T5 was found using three on-line traps (Scenario 21). The largest reduction in the net sediment flux at T5 using on-line traps was seen to be only 4%.

4.4 On-Line Alternative: Dredging in the Confluence Area

Dredging soft sediment accumulated in the confluence area is an option that must be considered, inasmuch as it is this material that is contaminated, and has led to concern for water quality and accumulation of high levels of toxicity in local biota.

A measure of the thickness of the material in question can be estimated from the lengths of the bottom cores collected from the area, assuming that they were pushed down to the hard substrate below. If so, consider the soft sediment thickness isopleths in Figure 4.9.

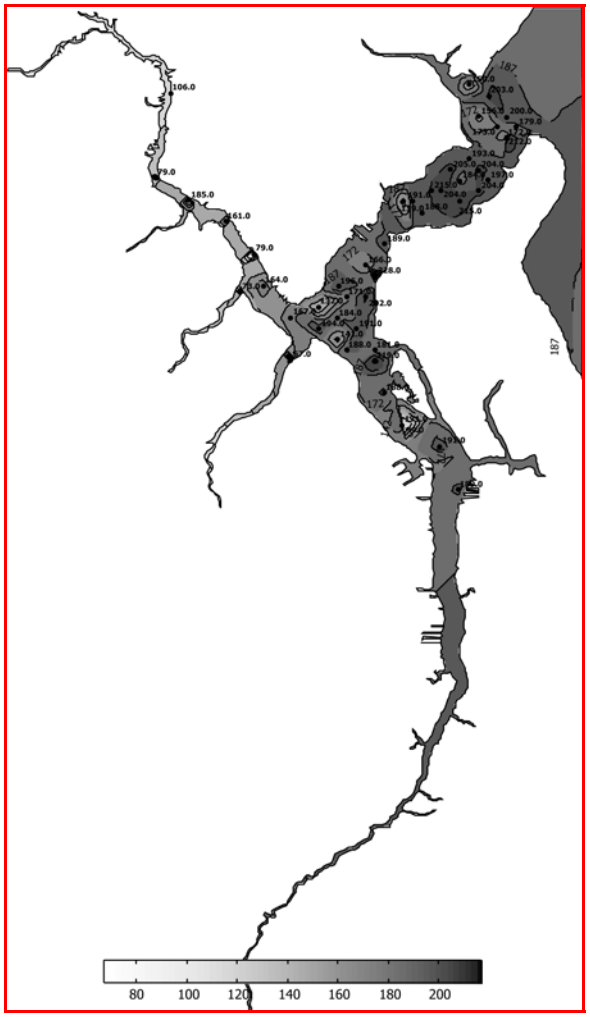

Figure 4.9 Core thickness isopleths based on 1998 data (from Appendix E).

In Figure 4.10, the confluence region is enclosed within conveniently marked dashed lines. The mean thickness of the deposit here is about 1.85 m. Consequently, the volume of deposit in the area (~0.95 km^2) is approximately $1.76x10^6$ m^3. Assuming a mean wet bulk density of 1,200 kg/m^3, corresponding to 21% organic matter (Table 2.1 and Appendix F), the total mass (solids + pore water) would be $2.11x10^6$ metric tons, a very large value. Using the corresponding dry density of 300 kg/m^3 (Appendix F), the (dry) solids mass would be $0.53x10^6$ metric tons. Now if we consider, for the sake of a practical illustration, that it may be feasible to identify critical areas for sediment removal by leaving out one-half the total area, the dredged mass would be $1x10^6$ metric tons, which is still large. It may therefore be necessary to look at dredging in the confluence area on a more selective basis.

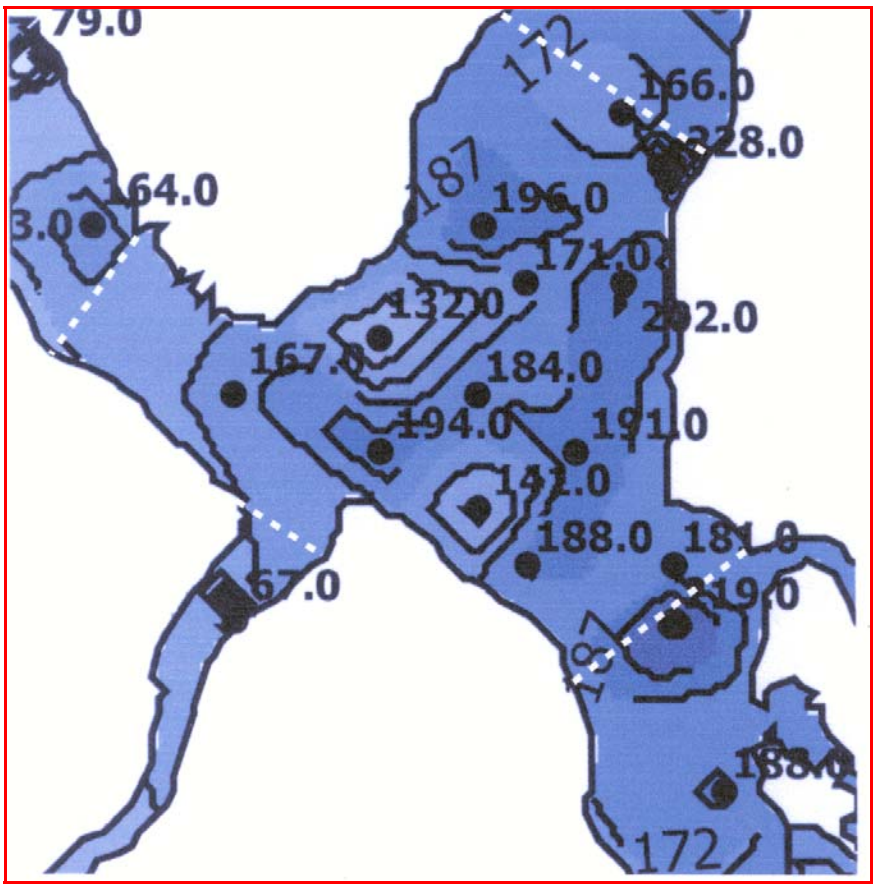

Figure 4.10 Isopleths in the confluence area (bounded by dashed lines). Dark circles are 1998 core sites.

4.5 Selective Dredging

This process will be explored here on a qualitative basis with reference to Figure 4.11, which represents, in a general way, the bed structure in the confluence area. Under very high runoff conditions, such as occurred during El Nino in February of 1998, a few (up to ~ 10 cm in selected locations, but generally 1-5 cm) centimeters of the very soft bottom mud may erode (Mehta et al., 2000). Since mud of this type cannot bear overburden unless the bed density is on the order of 1,300 kg/m^3 (Mehta, 1991), from the point of view of navigation and stability of bottom mud, it appears reasonable to remove the ~0.5 m thick top layer down to ~1,300 kg/m^3 density. If once again we assume that half the total area of 0.95 km^2 needs to be dredged, we get a volume of 2.38x10^5 m^3, or assuming the mean layer density to be 1,075 kg/m^3, the mass would be 2.55x10^5 metric tons, which is more reasonable than the previous 1x10^6 metric tons.

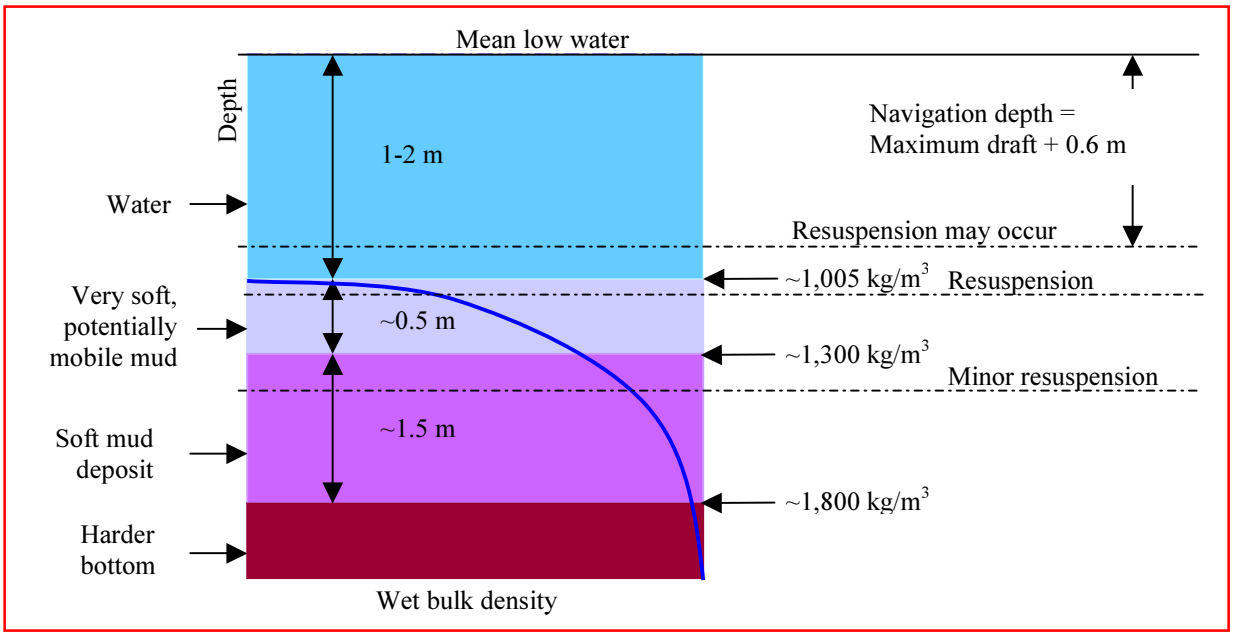

Figure 4.11 Illustrative plot of bed density stratification in the confluence area.

The rationale for selective dredging can be for maintaining navigable depths for small craft. Assuming the maximum vessel draft to be 1.5 m, the depth can be 1.5 m + 0.6 m

(underkeel clearance) + 0.3 m (wave allowance) = 2.4 m, which would mean down to the hard bottom in the confluence area. ADCP based measurements in the confluence area and downstream (see Appendices C and D) suggest that bottom sediment resuspension due to boat traffic in the shallow zones is not minor. Thus, even for very shallow draft vessels, dredging to remove the top (~0.50 m; Fig. 4.11) soft layer down to a bulk density of 1,300 kg/m^3 can be arguably important from the point of view of navigation and minimization of resuspension of very soft contaminated mud.

4.6 Selective Dredging and Capping

Sand capping of the bed after removal of the top ~0.50 m should be considered, since it would have three advantages over the no-capping scenario:

1. It would prevent the freshly exposed surface of soft mud deposits (Figure 4.11) from softening by wave induced liquefaction and by bioturbation, which may mean that the top ~10 cm of the surface would eventually become potentially mobile.
2. It would sequester the contaminated mud on a more or less permanent basis.
3. It would increase the depth of navigation due to consolidation by overburden. Considering a 0.50 m thick cap and the mean density of the soft mud deposit underneath to increase from, say, 1,500 kg/m^3 to 1,650 kg/m^3, would decrease the thickness of the ~1.5 m thick soft deposit to ~1.4 m. In other words the bed level would lower by ~10 cm at the end of the consolidation process. Considering the mean deposition rate in the area to be ~1 cm/year, this would mean a 10 year advantage in terms of navigation.

5 ASSESSMENT OF REMEDIATION ALTERNATIVES

5.1 Selected Alternatives/Options

The alternatives/options considered in Section 4 are summarized in Table 5.1. An assessment of the remedial measures for the Cedar River are summarized in Table 5.2. Their advantages/disadvantages are summarized in Table 5.3. In Table 5.2, the listed removal efficiency at the specified transect is calculated as the reduction in the net sediment flux at that transect over the seven-day simulation.

5.2 Qualitative Assessment

The following three criteria are considered for each remedial option on a qualitative basis:

1. Optimization of capture of contaminated sediment in transport;
2. Minimization of accumulation and navigability; and
3. Water quality (in terms of contamination of surface water).

In Table 5.3 the options have been ranked (1 = good, 0 = moderate, -1 = poor) according to each criterion, and the net values for all options are calculated.

Based on the evaluation in Table 5.3 it is noted that if the capture of contaminated sediment from upstream sources in Cedar River is the only or main goal, one of the two off-line sites proposed by SJRWMD, preferably the one closer to the source of sediment, i.e., OFL-1, would be the first choice, *provided the facility operates at very high, e.g., ~80% removal efficiency.* If improvement in navigation coupled with reduced resuspension of *in situ* material is additionally desired, selective dredging and sand capping in the confluence area should be considered. If capping proves to be too costly, removal of the top layer of very soft mud from areas where boats regularly ply the waters may be further evaluated.

Table 5.1 Selected alternatives/options

No.	Approach	Description
1	No-action	Maintain the system as is, with continued arrival of contaminated sediment from Cedar River and its accumulation downstream, especially in the confluence area, at the rate of ~10 mm/yr.
2	Off-line treatment: up-reach at OFL-1	SJRWMD proposed Wet Detention System in the u/s reach of Cedar River meant to capture a significant fraction of the contaminated material at its source.
3	Off-line treatment: up-reach at OFL-2	SJRWMD proposed Wet Detention System in the u/s reach of Cedar River meant to capture a significant fraction of the contaminated material close to its source. This facility would be d/s of OFL-1, but u/s of Williamson Creek.
4	Off-line treatment: mid-reach at OFL-3	Treatment (e.g., Wet Detention System) between Williamson Creek and Butcher Pen Creek.
5	Off-line treatments: up-reach at OFL-1 & OFL-2	Treatments (Wet Detention Systems) in the u/s reach of Cedar River.
6	Off-line treatments: up-reach at OFL-1 & OFL-2, and mid-reach at OFL-3	Treatments (Wet Detention Systems) in the u/s reach of Cedar River, and mid-reach between Williamson Creek and Butcher Pen Creek.
7	On-line entrapment: mid-reach at ONL-1	Treatment (dredged pit) between Butcher Pen creek and Fishing Creek.
8	On-line entrapment: down-reach at ONL-2	Treatment (dredged pit) between Butcher Pen Creek and Fishing Creek, downstream of ONL-1.
9	Off-line treatments up-reach at OFL-1 & OFL-2 and on-line treatment at ONL-3	Treatments (Wet Detention Systems) u/s of Williamson Creek combined with a dredged pit) between Williamson Creek and Butcher Pen Creek.
10	Selective dredging at confluence	Dredging for navigation within the shallowest zone of the confluence.
11	Selective dredging and capping at confluence	Dredging for navigation within the shallowest zone of the confluence coupled with sand capping.

Table 5.2 A summary assessment of remediation options for Cedar River sediment

Opt.	Approach	Advantages	Disadvantages
1	No-action	System remains undisturbed	Sediment accumulation at confluence likely continue at present rate (~10 mm/yr)
2	Off-line treatment: upreach at OFL-1	Capture contaminated sediment close to its source; removal efficiency at T3 is 2%	No impact on accumulation at confluence; removal efficiency at T4 is 0%
3	Off-line treatment: upreach at OFL-2	Advantage over #2 in capturing sediment due to d/s location; removal efficiency at T3 is 4%	No impact on accumulation at confluence; removal efficiency at T4 is 1%
4	Off-line treatment: mid-reach at OFL-3	Entrapment of sediment load is significant; removal efficiency at T3 is 57% and at T4 is 18%	Off-line site location may be difficult
5	Off-line treatments: up-reach at OFL-1 & OFL-2	Entrapment of sediment load could be significant, provided both facilities operate at high efficiencies; removal efficiency at T3 is 6% and at T4 is 1%	Construction and maintenance of two facilities may be untenable
6	Off-line treatments: at OFL-1, OFL-2 and OFL-3	Entrapment of sediment load could be very significant, provided both facilities operate at high efficiencies; removal efficiency at T3 is 63% and at T4 is 19%	Construction and maintenance of three facilities may be untenable
7	On-line entrapment: mid-reach at ONL-1	Entrapment of sediment load could be significant depending on pit design	Capital and maintenance dredging of on-line trap containing contaminated sediment could be problematic
8	On-line entrapment: down-reach at ONL-2	Due to proximity to confluence, considerable advantage in intercepting sediment load, if the removal ratio can be optimized	Capital and maintenance dredging of on-line trap containing contaminated sediment could be problematic
9	Off-line treatments at OFL-1 & OFL-2 and on-line at ONL-3	Entrapment of sediment load could be significant, depending on pit design and provided both off-line facilities operate at high efficiencies	Capital and maintenance dredging of on-line trap containing contaminated sediment could be problematic
10	Selective dredging at confluence	Reduce *in situ*, mobile contaminated sediment and improve navigation	Dredging of contaminated hot-spots could be environmentally problematic
11	Selective dredging and capping at confluence	Reduce *in situ*, mobile contaminated sediment and improve navigation; cap would sequester contaminated material	Dredging of hot-spots could be environmentally problematic; cost will be higher than dredging alone

Table 5.3 Ranking of options based on selected criteria

Option	Criterion			
	Capture of contaminated sediment	Improvement in navigation	Water quality	Net
1. No-action	-1	-1	-1	-3
2. OFL-1	1	-1	1	1
3. OFL-2	1	-1	1	1
4. OFL-3	1	-1	1	1
5. OFL-1 + OFL-2	1	-1	1	1[a]
6. OFL-1 + OFL-2 + OFL-3	1	-1	1	1[a]
7. ONL-1	1	0	0	1
8. ONL-2	1	0	0	1
9. OFL-1 + OFL-2 + ONL-3	1	0	1	2[a]
10. CAC dredging	-1	1	0	0
11. CAC dredging + capping	0	1	0	1

[a] The cost of operating multiple facilities may negate part of the advantage.

BIBLIOGRAPHY

Baker, E. T., Milburn, H. B., and Tannant, D. A., 1999. Field assessment of sediment trap efficiency under varying flow conditions. *Journal of Marine Research*, 46, 573-592.

Bedient, P. B., and Huber, W. C., 2002. *Hydrology and Floodplain Analysis*. 3rd ed., Prentice-Hall, Upper Saddle River, NJ.

Campbell, D., Bergman, M., Brody, R., Keller, A., Livingston-Way, P., Morris, F., and Watkins, B., 1993. *Lower St. Johns river basin SWIM plan*. St. Johns River Water Management District, Palatka, FL.

Donohue, J. F., 1999. Investigation of historic sedimentation rates in the lower St. Johns River. *Technical Report*, St. Johns River Water Management District, Palatka, FL.

Environmental Protection Board, 1985. *Annual Environmental Status Report: Year Ending September 30, 1985*. Jacksonville, FL.

Freeman, R.J. 2001. Simulation of Total Suspended Solids Loads into the Cedar/Ortega River, Duval County, Florida Using SWMM. St. Johns River Water Management District, Palatka, Florida. *Department of Water Resources Technical Memorandum No. 46*.

Ganju, N. K., 2001. Trapping organic-rich fine sediment in an estuary. *M.S. Thesis,* University of Florida, Gainesville, FL.

Harper, H. H., 1997. Pollutant removal efficiencies for typical stormwater management systems in Florida. *Proceedings of the Biennial Stormwater Research Conference*, Southwest Florida Water Management District, Tampa, FL, 6-19.

Hamrick, J. M., 1992. A three dimensional environmental fluid dynamics computer code: Theoretical and computational aspects. *Special Report No 317*, Applied Marine Science and Ocean Engineering, Virginia Institute of Marine Science, Gloucester Point, VA.

Hamrick, J. M., 1996. User's manual for environmental fluid dynamics computer code. *Special Report Special Report No 331*, Applied Marine Science and Ocean Engineering, Virginia Institute of Marine Science, Gloucester Point, VA.

Marván, F. G., 2001. A two-dimensional numerical transport model for organic-rich cohesive sediments in estuarine waters. *Ph.D. Thesis*, Heriot-Watt University, Edinburgh, UK.

Mehta A. J., 1991. Understanding fluid mud in a dynamic environment. *Geo-Marine Letters*, 11, 113-118.

Mehta, A. J., Kirby, R., and Hayter, E. J., 2000. Ortega/Cedar River basin, Florida, restoration: work plan to assess sediment-contaminant dynamics, *Report UFL/COEL-99/019*, Coastal and Oceanographic Engineering Department, University of Florida, Gainesville.

Mehta, A. J., and Parchure, T. M., 2000. Surface erosion of fine-grained sediment revisited. In: *Muddy Coast Dynamics and Resource Management*, B. W. Flemming, M. T. Delafontaine, and G. Liebezeit eds., Elsevier, Amsterdam, 55-74.

Paramygin, V., 2002. Sediment Trapping in a microtidal estuarine system. *MS Thesis*, University of Florida, Department of Civil and Coastal Engineering.

Parchure, T. M., Brown, B., and McAdory, R. T., 2000. Design of sediment trap at Rollover Pass, Texas. *Report ERDC/CHL TR-00-23*, U.S. Army Engineer Research and Development Center, Vicksburg, MS.

Sarikaya, H. Z., 1977. Numerical modeling of discrete settling. *Journal of the Hydraulics Division of ASCE,* 103(8), 866-876.

Vincente, C. M., 1992. Experimental dredged pit of Ka-Ho. Analysis of shoaling rates. *Proceedings of the International Conference on the Pearl River Estuary in the Surrounding Area of Macao,* Vol. 2, Civil Engineering laboratory of Macao, Macao, paper P6.4, 11p.

Winterwerp, J. C., 1998. A simple model for turbulence induced flocculation of cohesive sediment. *Journal of Hydraulic Research*, 36(3), 309-326.

Wanielista, M. P., 1978. *Stormwater Management*. Ann Arbor Science, Ann Arbor, MI.

Wolanski, E., Gibbs, R., Ridd, P., Mehta A., 1992. Settling of ocean-dumped dredged material, Townsville, Australia. *Estuarine, Coastal and Shelf Science*, 35, 473-489.

Appendix A

Sedimentary Regime of the Lower Cedar/Ortega River System and its Environs, Florida, Report

Ravensrodd Consultants Ltd.
6 Queen's Drive, Taunton
Somerset TA1 4XW UK
February 2002

Contents

List of Figures

List of Tables

A1. The Lower St. Johns River

A1.1 Sedimentary Regime

A good perspective on the sedimentary regime in tidal reaches of the Cedar and Ortega River System can be obtained from comparison with studies in adjacent reaches of the main stem of the St. Johns River (Cooper and Donoghue 1999). These authors applied a range of geochemical techniques—mainly ^{210}Lead, ^{137}Caesium, Carbon:Nitrogen Ratios, ^{13}Carbon:^{12}Carbon Ratios, ^{13}Carbon Solid-state, Natural Magnetic Remnance (NMR) Spectroscopy, and so-called "Biomarkers", distinctive organic molecules synthesised by plants or animals and incorporated into sediments. Cooper and Donoghue undertook multiple analyses on eight cores from the lower tidal reaches of the St. Johns River. The three most down-estuary cores, situated in the reaches to the south of and above of the confluence of the combined Cedar/Ortega River system, at Christopher Cove/Beauclerc Point, Mandarin Point and Doctors Lake, are especially relevant here.

The report is remarkably light in its overall description of the bulk sediment type, but it is presumed to be the dark colloidal, highly organic-rich mud, locally called "Muck". In the report the sediments are described as "overwhelmingly fine-grained, averaging 80% fines, unusually high in moisture content, averaging 79%, and in organic material, averaging 29% by weight", all leading to extremely low dry bulk densities, averaging 0.24g cm^{-3}. This work, and another by Alexander et al. (1993), do, nevertheless, give some estimates of siltation rate, which may lead to an expectation for the Cedar/Ortega River system. Similarly, these same authors have investigated sediment sources in the St. Johns River.

A1.2 Linear Sedimentation Rate

In Table A1, siltation rates for the lower St. Johns River and Cedar River derived from Cooper and Donoghue (1999) and Alexander et al. (1993) here below summarized.

A1.3 Sediment Sources

The fractional contribution of marine and fluvially derived ^{137}Cs in estuarine sediment are claimed by Mulholland and Olson (1972) to be distinguishable if marine and riverine ^{137}Cs input concentrations are known. Applying the Mulholland and Olsen equation obtained for the Savannah River to these Cedar/Ortega samples leads to an estimate of 29% for the marine-derived portion in core Cs^{-127}, compared to 20% in core 039. The precise sampling localities of neither core is known.

Further evidence for sediment sources in the St. Johns main stem may be taken from C:N ratios of cores from the 3 sites immediately up-estuary from the Cedar/Ortega Rivers. Elemental carbon should represent roughly 40% of the sedimentary organic fraction based on a chemical formula approximation for biomass of methanal (CH_2O)(CH_2O Methanal/ Formaldehyde, a compound produced by the oxidation of methanol or by oxidation of ethane in the presence of a catalyst), although this number is usually significantly lower in sedimentary organic matter due to the complexity of biologically derived molecules. The

Table A1. Measurements of siltation rate for lower St. Johns River and for Cedar River mouth

Locality	Excess ^{210}Lead		^{137}Caesium	
	Core Sample No.	Amount (mm/yr)	Core Sample No.	Amount (mm/yr)
Christopher Cove	1	6.2	NA	NA
	2	9.3	NA	NA
Mandarin Point	1	38.8	NA	NA
	2	25.0	NA	NA
	3	15.1	NA	NA
Doctors Lake	1	10.3	NA	NA
	2	10.8	NA	NA
	3	13.5	NA	NA
also Alexander et al. (1993)	1	11.0	1	9.0
Cedar River Mouth Alexander et al. (1993)	"039"	11.0	"039" Cs^{-127} "039"	~ 9.0/~12.0 2.13 dpm/g* 2.4 dpm/g*

Source: (Cooper and Donoghue 1999; Alexander et al. 1993).
Note: NA = not applicable
*average surface concentration.

elemental carbon values at Christopher Cove, 6%, parallel lower combustible organic matter at the same site, 25–30%, (they reach about 40% at the most up-estuary sample sites in the St. Johns River). Mandarin Point values are intermediate between the down- and up-estuary extremes, lying at ~8% elemental carbon and 30–35% combustible organic matter. C:N ratios for most of the cores were found to lie in the range 10–14:1 and do not vary significantly with depth. Such values are consistent with values in terrestrial soils and the surface sediments of lakes. The suggestion from this is of a mainly terrestrial source for the organics in these suites of cores.

Organic matter in sediments known to originate from higher terrestrial plants exhibit a functional grouping of stable Carbon isotopes, approximately 30–40% aliphatic (Aliphatic Compounds: methane derivatives of fatty compounds; open chain or ring carbon compounds not having aromatic properties), 20–30% aromatic (Aromatic Compounds. Compounds related to benzene. Ring compounds containing conjugated double bonds) and 20–30% heteroaliphatic. (Heteroaliphatic. Hetero—a prefix meaning other or different).

This contrasts with the typical distribution of carbon isotopes in brackish water-derived organics, which are reflected in the sedimentary biomass as 40–50% aliphatic, 15–20% aromatic and 20–30% heteroaliphatic. The values detected in the St. Johns River cores are consistent with derivation from degraded higher plant (terrestrial) sources. Only at Mandarin Point and Christopher Cove did sediments with higher (marine/aquatic) stable carbon ratios make any contribution to the overall ^{13}C isotope ratio pool.

When geochemical "biomarkers" were investigated in the suite of cores, the over-whelming feature in each is the predominance of higher molecular weight hydrocarbons, i.e., those containing 22–24 or more carbon atoms. This also reflects a strong terrestrial input

signal, since the alkanes and alcohols in plant waxes, the most prominent sources of hydrocarbons in terrestrially-derived sedimentary organic matter, are primarily in the 25–33 range (Tissot and Welte 1984). In contrast, hydrocarbons derived directly from planktonic algae are dominated by shorter alkanes in the 15–17 range. This is further evidence that organics in the St. Johns River sediments are mainly allochthonous and terrestrial, being derived from the catchment. Cooper and Donoghue further report … "In spite of the overwhelming dominance of higher-molecular weight hydrocarbons, there are measurable quantities of hydrocarbons in the C_{16}–C_{20} range. These most likely originate from planktonic algae". The presence of these shorter chain alkanes is consistent with a small contribution to the organic content of these sediments (~10–20%) from authigenic, aquatic sources. The ratios of the various fractions presented can be taken as reflecting their sources and it is suggested these ratios have not been significantly affected by diagenetic post-depositional changes.

The summary of important attributes of these main stem sediments is that their sedimentary regime is a net and rapid depositional one, with a mean long-term average linear sedimentation rate for the 8 sites of 10.7 mm/yr. At all 8 sites the mass accumulation rate can be observed to have increased during the latter half of the Twentieth Century in some cases by a factor of 3 or more. Sand laminae are relatively common in the upper 40 cm sections of many cores, possibly as a result of deforestation followed by storms or floods in recent years. All 4 approaches adopted by Cooper and Donoghue for characterising sources and transformations of organic matter in sediments from the lower St. Johns River indicate that allochthonous, terrestrially-derived material from the watershed is the primary carbon source in these organic-rich sediments. There does not appear to be any significant historical change in sources or qualitative variation.

A2. Sedimentary Regime of the Lower Cedar and Ortega Rivers

A2.1 Data Sets and Background

Two data sets are available for appraisal. One was a set of 172 cores obtained between 1993 and 1995 and subsequently analyzed and reported by Morgan & Eklund, Inc., in 1995. The history of deposition within the study area has been interpreted herein from core descriptions made at that time. A second set of 51 surface grab samples was obtained and a preliminary report submitted in 1998 by Battelle Ocean Sciences. Both grain size and geochemical analyses were performed on this suite of samples. The geochemical analyses were variously subcontracted to Mote Marine Laboratory, Savannah Laboratories, etc.

The bed materials involved are locally referred to as "muck". Muck is defined as "black, fine-grained sediment with a high water content, composed of partly decomposed organic matter with a considerable amount of admixed silt and clay material".

The St. Johns River system, which the Cedar/Ortega are part of, has an unusually low gradient, dropping less than 10m from head to mouth (approx. 480 km). It also has a low tidal range (about 30 cm at the Cedar/Ortega River mouth) and a channel often 6m below

mean sea level. Normal river flows and the perturbation of these by the tides give rise to a gentle flow regime which is depositional/retentive for sediment during most normal circumstances. This largely explains the relative paucity of detrital mineral inputs. The system is, nevertheless, susceptible to wave stirring during windy spells, such as storms and the exceptional hurricane. Such disturbance might be expected to have a noticeable impact on bed sediments due to the unusually shallow nature of much of the system. Winnowing and segregation of sediment might be anticipated. Similarly, occasional high rainfall and run-off events occur, the consequences of which might also be detectable in the sediments. The physical properties of both surface sediment samples and cores have been investigated and plotted, leading to a comprehension of the bed sediment regime both areally and with depth.

It turns out that the sediments of the Cedar/Ortega River system fall very readily into four quite distinct zones and they are best described in these. The zones are: the Cedar River, the Ortega River, the inner confluent region between Fishing Creek and Roosevelt Boulevard Narrows and finally the outer confluent region between Roosevelt Boulevard Narrows and the junction with the St. Johns River itself. The minor tributary creeks, Big Fishweir Creek, Fishing Creek, Butcher Pen Creek and Williamson Creek, are considered within these zones (Figure A1).

A2.2 Grain Size Variations

The areal variation of grain size of the inorganic fraction has been plotted from the 1998 data. These appear here as three maps based on % Clay, % Silt, % Sand (Figures A2, A3 and A4).

A2.2.1 Clay (< 2 µm*)*

There is very little clay in the system (Figure A2). The highest clay percentage in the entire data set, 18%, occurs at the innermost station in the Cedar River and there is a pronounced decreasing down-estuary gradient in the clay fraction. The Ortega has a uniform and low clay content, whereas the inner reach of the confluent region is an anomalous-looking zone of exceptionally low (mainly 1–2%) clay content. The outer confluent region is wholly separated from the elevated clay contents of the Cedar River, but clay contents are again slightly elevated (> 7.0%).

A2.2.2 Silt (> 2 µm < 62.5 µm)

The silt content of bed sediments also shows distinctive area groupings (Figure A3). Both the Cedar and Ortega show values in the mid-levels (50–60%) and both show a pronounced decreasing down-estuary gradient to the inner confluent region. This, latter, zone is again apparently anomalous having both variable silt contents (25–71%) but an extensive region of values significantly lower than elsewhere in the system (23–35%). Both the variability and the unusually low silt fraction in these reaches needs to be explained. The most pronounced feature of the silt distribution is the elevated and fairly constant quantities

Figure A1. Grab sampling sites for 1998 survey of physical and chemical attributes of bed sediments in the Cedar & Ortega Rivers system (after Battelle, Mote Marine, Savannah, etc.). The system can be separated areally into four distinctive regions

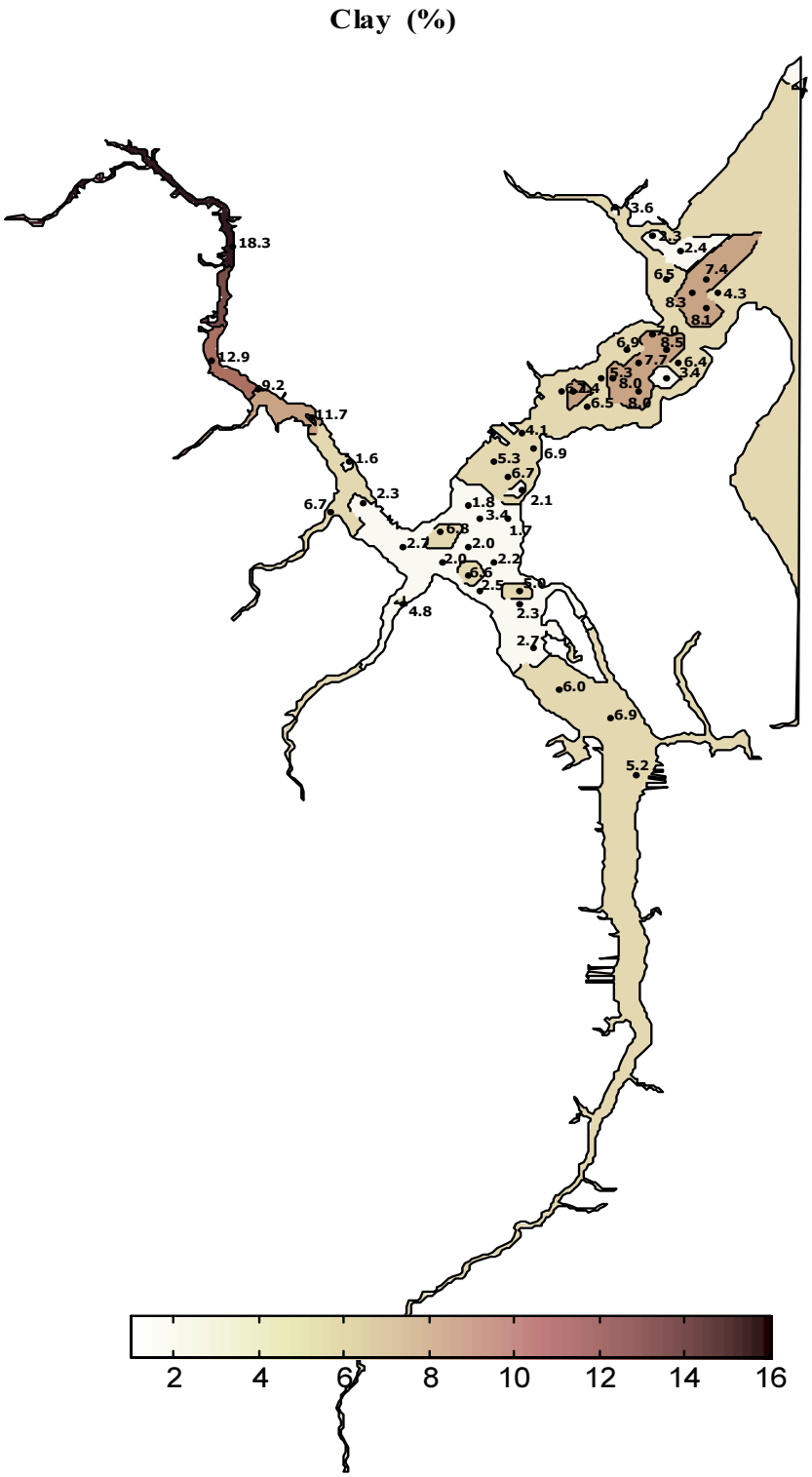

Figure A2. Areal variation in percent clay in the 1998 suite of grab samples. A detrital input from the Cedar River catchment and especially low values in the Cedar/Ortega confluence are evident

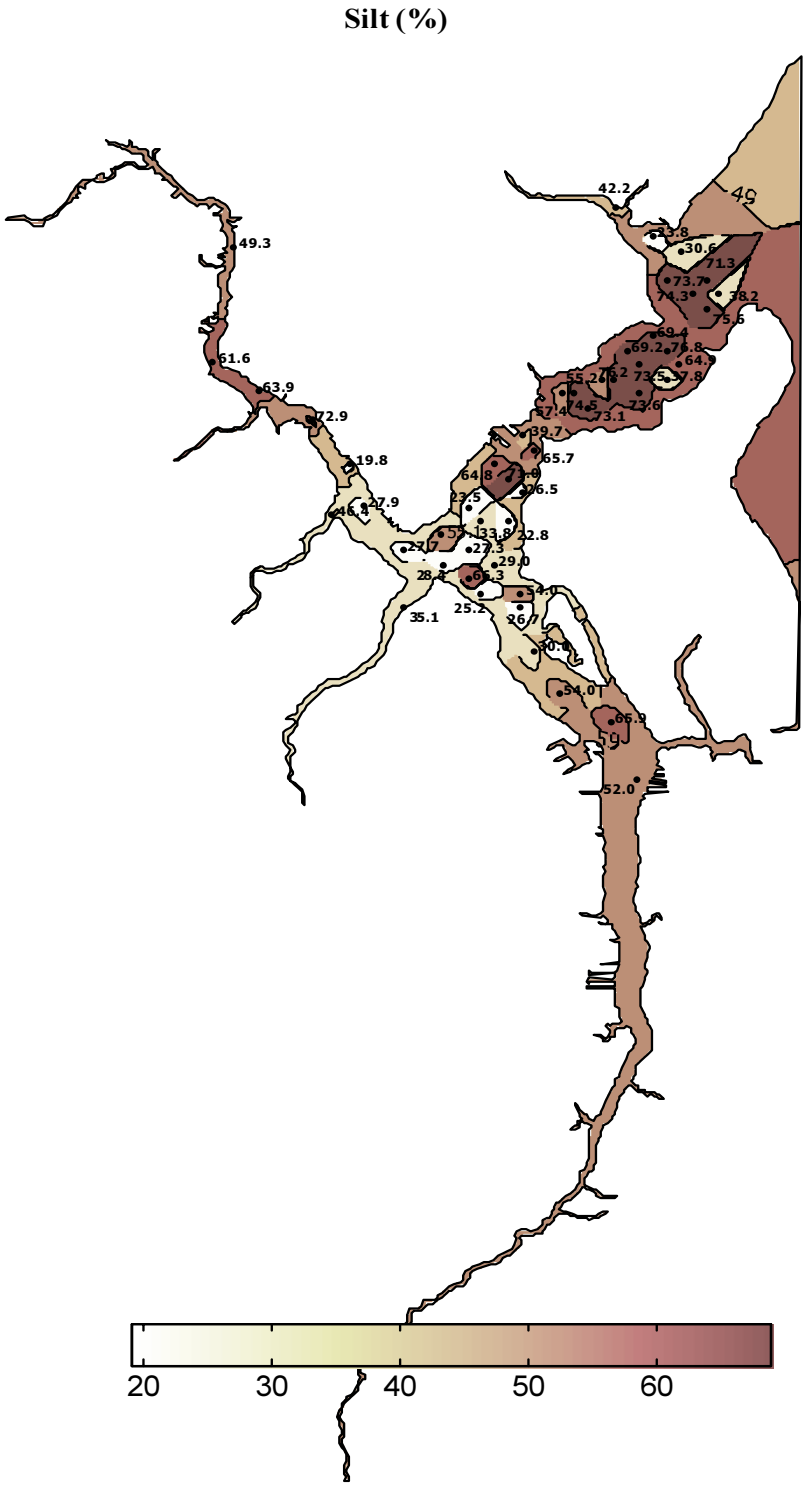

Figure A3. Areal variation in percent silt in the 1998 suite of grab samples. There are elevated values, signifying inputs, from the Cedar River and the main stem. Silt is the main detrital inorganic input into the Ortega. There is a zone of variable and often very low values in the Cedar/Ortega confluence region

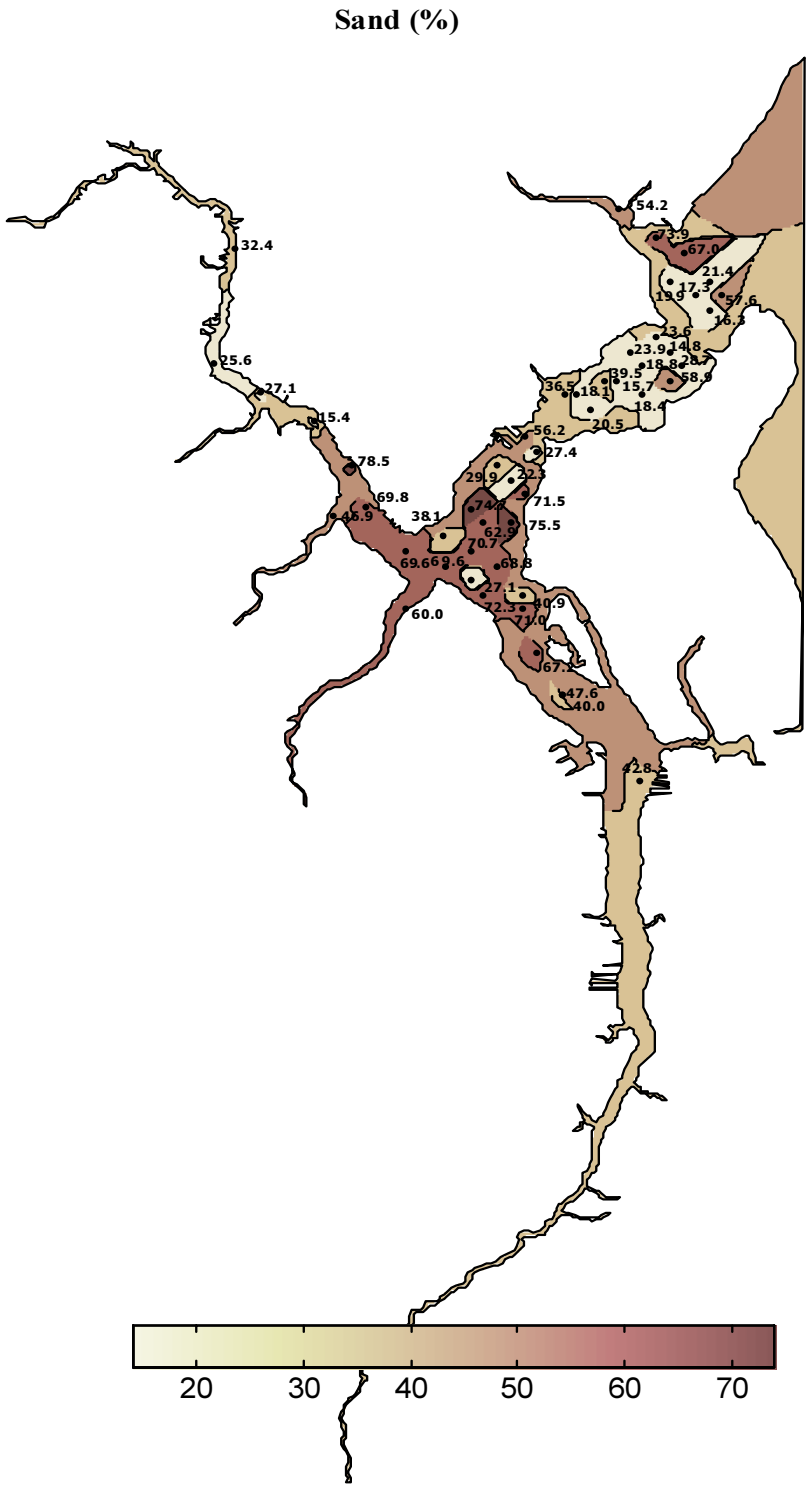

Figure A4. Areal variation in percent sand in the 1998 suite of grab samples. There are minor inputs from both the Cedar and Ortega but high inputs from Butcher Pen and Fishing Creek which are spread into the inner confluent reaches. Some sand also enters from the main stem

in the outer confluent reaches extending from the main stem, (> 70–< 80%). There is some tendency for these zones of elevated silt content to be associated with the axial zone of the estuary.

A2.2.3 Sand (> 62.5 μm < 1000 μm)

The sand fractions of the inorganic portion of bed samples, naturally, mirrors the clay and silt fraction distribution (Figure A4). Unlike the fines, which show a down-estuary decrease in amount, the sand fraction increases down-estuary in both the Cedar and Ortega Rivers to reach a system maximum in the inner confluent region. This latter zone also shows the greatest area variability (22–75%). The sand content of the inorganic portion of much of this zone lies in the range 60–70%.

The sand content of the outer confluent region is the lowest anywhere in the system, generally ranging between 15 and 25%. Extreme values span 16–74%, with no obvious pattern.

A2.3 Other Physical and Chemical Properties of Bed Sediments

The 1998 grab samples have been subjected to further analyses. Samples have been analyzed for physical properties, such as moisture content, quoted in percentages, and for total % solids. (Obviously solids and moisture are reciprocals of each other). The samples have also been subjected to chemical analysis for total organic carbon and for organic content (%). In the plots the data has mainly been contoured by hand. In areas of great topographic complexity and with relatively few sample points to describe a distribution, hand contouring avoids the anomalies a computer is unable to cater for.

A2.3.1 Moisture and Total Solids Content

Within the system the four regions described above are distinguishable. In respect of the related moisture and total solids percentages, there is a strong contrast between the sediments in the Ortega, coming in from the south, and those of the Cedar entering the confluent region from the north. The Ortega bed sediments have by far the highest moisture contents (Figure A5) and by the same token, the lowest total solids input (Figure A6). There appears to be an axial "tongue" of high moisture content sediments projecting from the Ortega River and into the inner confluent region off Fishing Creek. Unfortunately, there are only six axially placed samples in the Ortega such that any lateral and more extended longitudinal gradients cannot be determined. In contrast, the Cedar has much higher detrital solids percentage values in its inner reaches, as well as a pronounced down-estuary decrease. Similarly, the moisture content of the sediments of the inner reaches of the Cedar is virtually the lowest in the entire system.

The inner confluent region shows a broad zone of bed sediments with 73–79% moisture and 20–27% solids. This contrasts markedly with the peak in sand content in bed sediments of this zone (Figure A4). Although the sample grid is wanting in this respect, there is a possible focussing of high moisture, low solids bed sediments on the left bank,

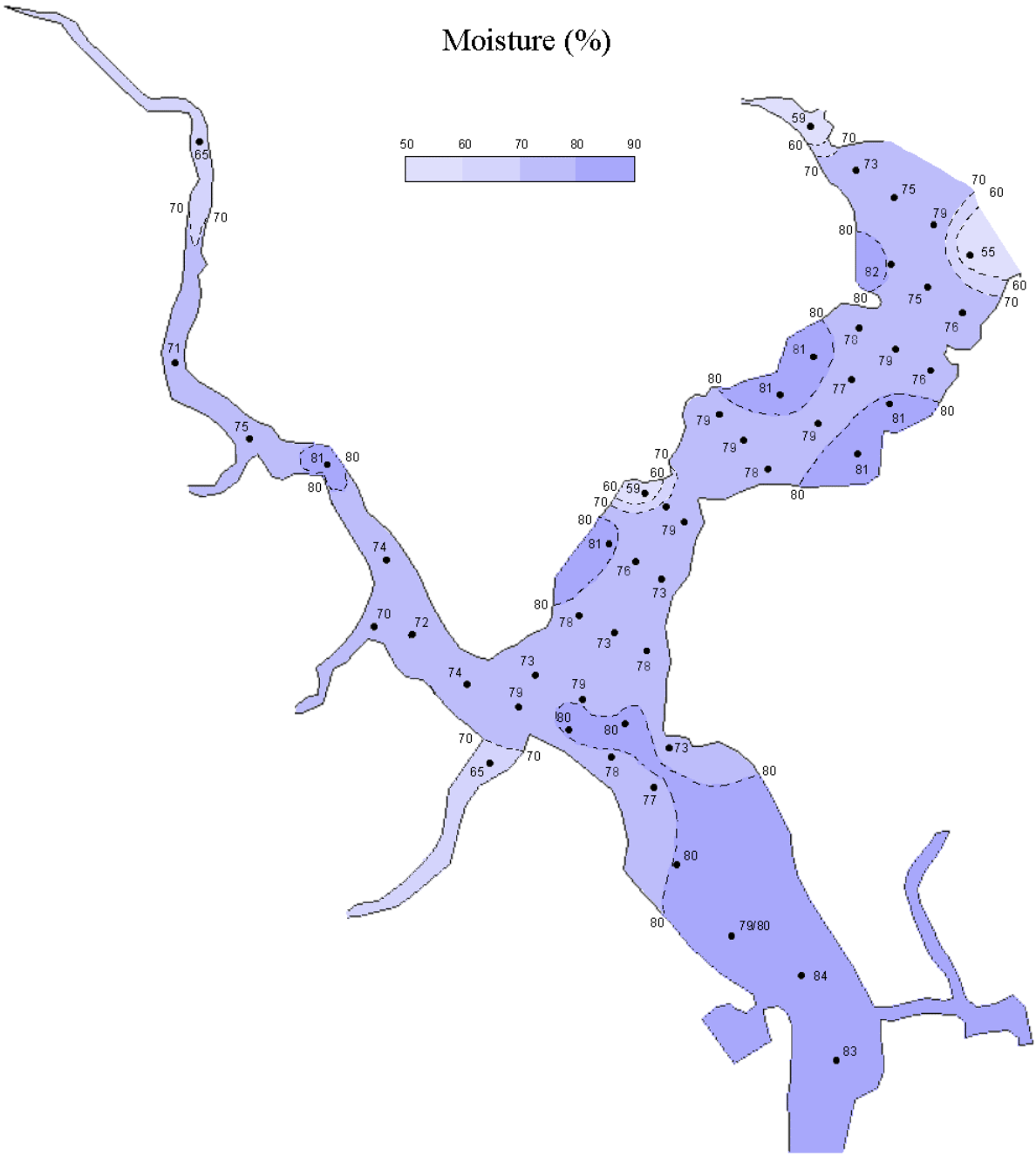

Figure A5. Areal variation in percent moisture content of bed sediments from 1998 grab sampling survey. The distinctive and high moisture content of Ortega River samples and at marginal sites often coincident with marina developments in the inner and outer confluent region is evident

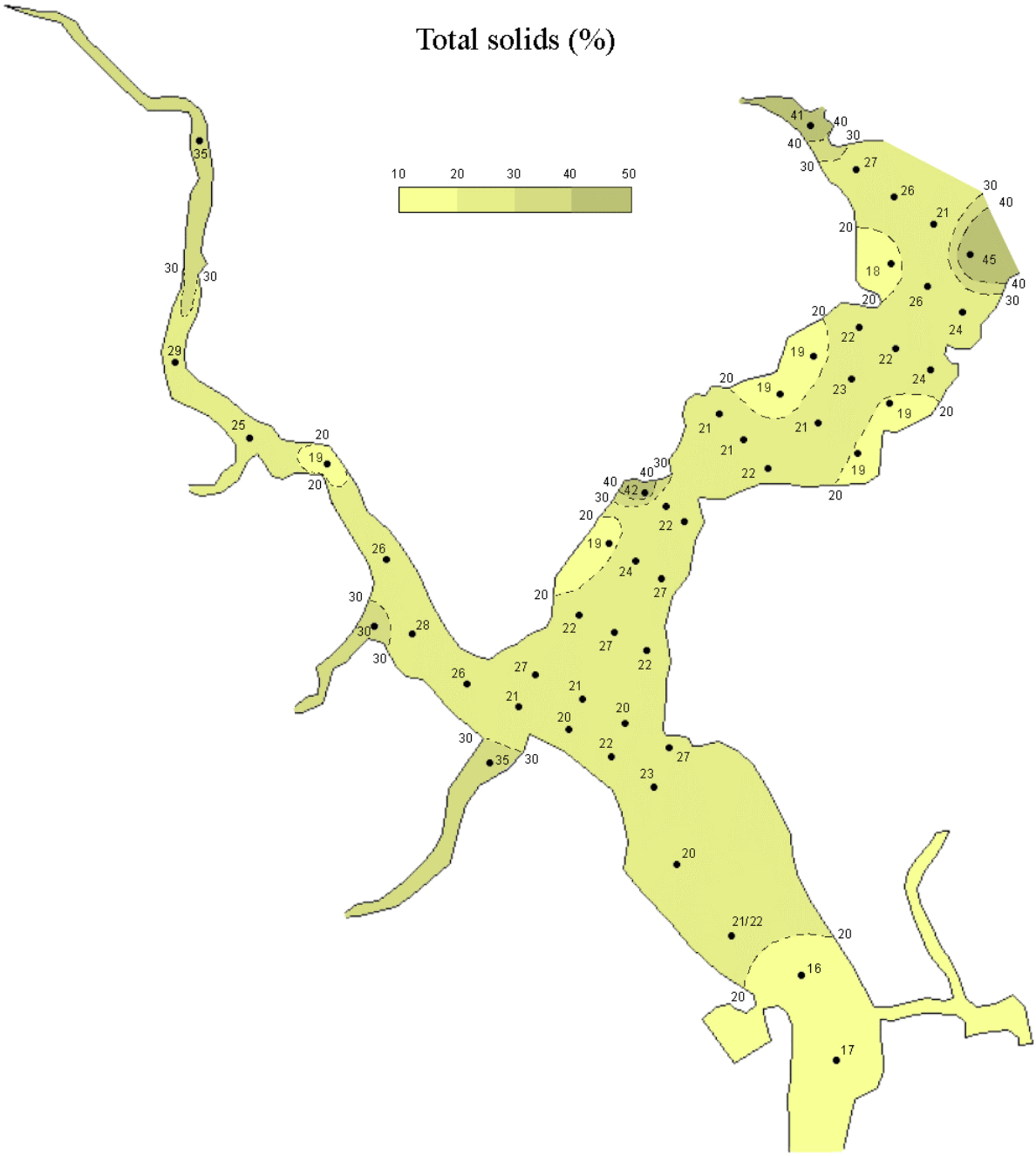

Figure A6. Areal variation in percent solids content of bed sediments from 1998 grab sampling survey. The highest solids contents occur in the Cedar River, Butcher Pen and Fishing Creeks and at the meeting point with the main stem. The Ortega River input is especially low in solids

coincident with the flow impediment provided by commercial marina development in these reaches. The outer confluent region is not dissimilar to the inner region in respect of % moisture and solids. There is a broad zone where sediments show % moisture in the high 70s, low 80s in 1995. Particular features of this outer confluent zone are the high moisture/low total solids zones, again on the left bank co-extensive with marina developments. A separate and strong feature is an apparent tongue of low moisture %, high solids sediments apparently penetrating the system from the main stem direction.

A2.3.2 Total Organic Carbon/Organic %

As with % moisture and % solids, these analyses reflect directly the organic content of bed samples, as opposed to the inorganic fraction revealed in the grain size measurements. The results show some pronounced contrasts from the inorganic bed sediment plots and also some distinctive features. The Ortega River sediments have a significantly higher organic content than any others in the system (Figures A7 and A8), as well as a pronounced down-estuary decrease.

There is also a tongue of relatively elevated organics fraction sediment, possibly emerging from the Ortega and enriching sediments in the inner confluent region. This region thus exhibits the combination of unusually sandy bed sediments, which are also unusually organics-rich. In contrast, the innermost sediments in the Cedar River are amongst the lowest in the system in organics content and the analyses show a steady rise in organics in a down-estuary direction, the reverse of that in the Ortega.

The outer confluent region shows TOC % background values mainly in the 11–14% range. Organic content (%) shows a little more variability and a higher range, 16–24%. There is possibly some tendency for elevated organic values in more marginal sediments, especially along the left (northerly) bank coincident with the marinas. A tongue of low organic-rich sediments appears to be penetrating the system from the main stem along the outermost (down-estuary) line of samples.

A2.4 Core Descriptions from the 1995 Campaign (plus measurements of sedimentation rate)

The Morgan & Eklund, Inc., report from 1995 gives detailed and useful core logs and their positions. More recent, and still preliminary, determinations of sedimentation rate have been made available for 8 samples (Higman, pers com). The evaluation of the sedimentary regime has also benefited from advice from Dr. J. Higman, especially in respect of biological issues. The core logs and mapped distributions permit additional understandings of the area and depth variation of sediment characteristics.

In respect of sedimentation rate measurements using ^{210}Pb and ^{137}Cs, at the three closest sampling localities of Cooper and Donoghue in the St. Johns River, rates normally in the range 9–12 mm/yr but rising at exceptional localities to 25–40 mm/yr have been determined. The measurement of core 0-39 from the Cedar River mouth gave 11.0 mm/yr.

Figure A7. Areal variation in percent total organic carbon (TOC) of bed sediments from 1998 grab sampling survey. The especially high TOC of Ortega River samples, spreading into the inner confluent region, as well as the low TOC at the confluence with the main stem, is evident

Figure A8. Computer-contoured plot of areal variation in percent organic content of bed sediments from 1998 grab sampling survey. The most distinctive features are the high organic content of the Ortega River input together with low organics content of Roosevelt Narrows and the main stem confluence

Figure A9 shows the sedimentation rate for these 8 latest cores, which are all more or less confined to the inner and outer confluent regions of the two rivers. It is evident that cores from the right bank and main stem confluence show accumulation rates ranging between 4 and 8 mm/yr—almost half the value of the "normal" range of the few analyses available from the St. Johns River. There are three samples from the left bank of the confluent region, amongst or in close proximity to the commercial marinas. These have high and consistent sedimentation rates of about 20 mm/yr, though these are still half the maximum rates determined in adjacent sites in the main stem.

A2.4.1 Clean Sand Distribution in Cores

Detailed descriptions of 172 cores taken from the system in 1995 and extruded for examination have been studied. Sand admixed with silt, clay or the large organic muck fraction cannot be distinguished in laboratory descriptions, but clean sand laminae in mud cores are quite distinctive. Review of these core logs reveals that there is no sand in cores from the Ortega in the section immediately down-estuary of Collins Road Bridge, and virtually no sand in the lower reaches of the Ortega. Such sand layers as are occasionally recognized are invariably very thin and present at deep horizons in the core. A similar situation applies to the Cedar River. Sand layers are present only occasionally, often singly in cores, and are thin.

Two cores from Williamson Creek show virtually no sand. Down-estuary from the Blanding Boulevard Bridge, multiple sand layers are common in Cedar River cores and in cores from Butcher Pen Creek. Fishing Creek appears to be exceptional, having either thick or multiple sand layers in all cores taken from it and in its entrance. Sand layers 0.5 and 2.0 cm thick are noted, for example. Several cores in the approaches to this creek have thick sand layers at their surface or in one case are all sand to 46 cm below the estuary bed.

In the lower Cedar River below the Blanding Boulevard Bridge, as mentioned above, not in the Ortega, but also in the inner confluent and outer confluent region of the estuaries, the cores show multiple sand layering. For the most part there are never more than 10 sand layers in cores up-estuary of Roosevelt Boulevard Bridge and they tend to be very thin. A local area with thicker sand layers is coincident with Roosevelt Boulevard Narrows.

The situation in the outer confluent region is developed to a greater degree. There is also a pronounced lateral variation in this zone. On the right bank the stratigraphic column in the mucks is characterized by multiple thin clean sand layers, generally exceeding 10. The most down-estuary sample on the right bank is entirely sand to 98 cm. In contrast, on the left bank, sand layers may be absent entirely, or present in low digit numbers 4, 2, 6, 7, etc. Big Fishweir Creek also has sand-rich sediments, the innermost core has all sand down to 13 cm, whereas others have multiple and thick clean sand layers. Muck sediments lying immediately off Big Fishweir Creek tend to have more sand layers, despite being on the left bank.

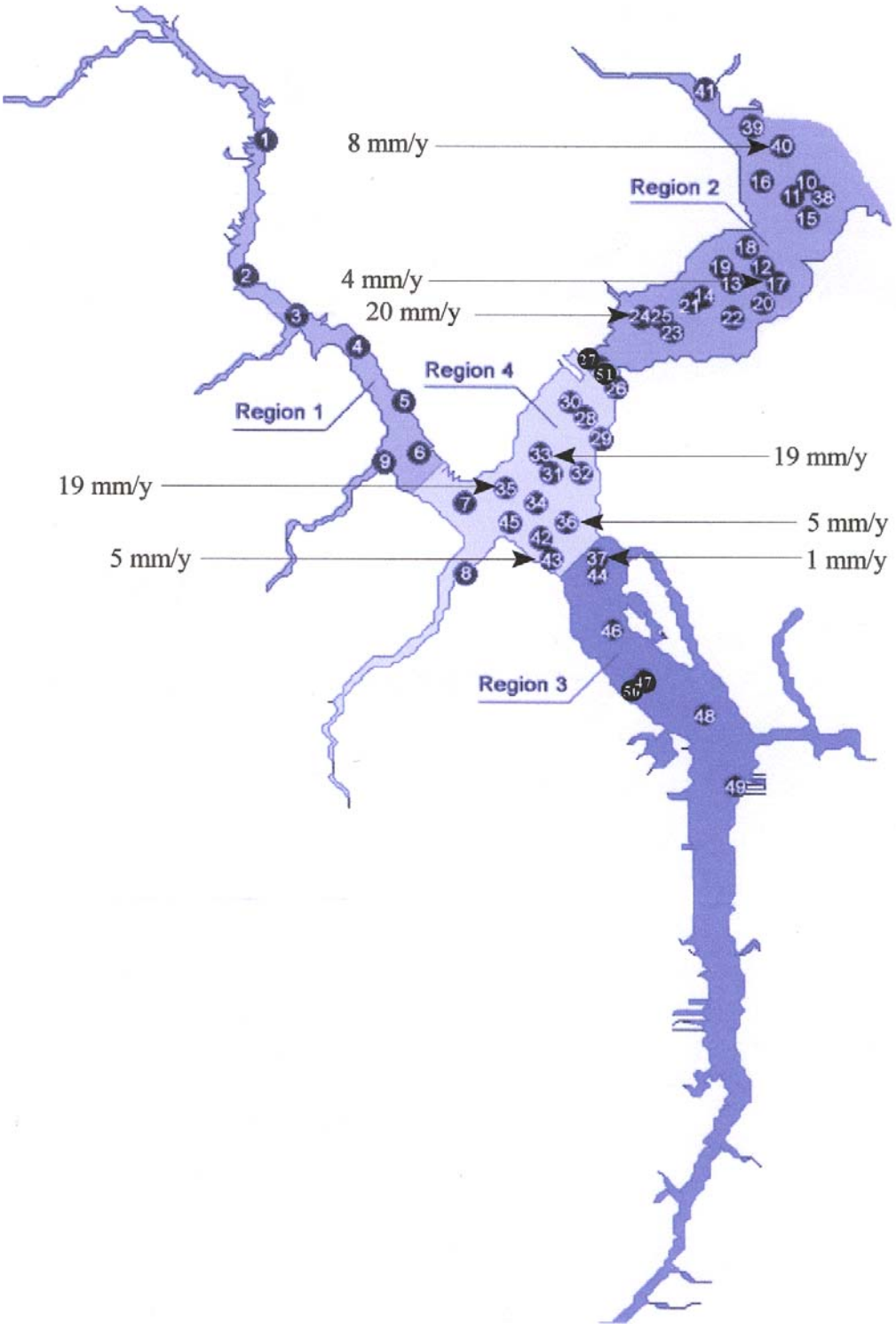

Figure A9. Sedimentation rate measurements for eight recent cores from the inner and outer confluent regions of the Cedar/Ortega River system. The siltation rate progressing at about four times the rate on the left compared to the right bank seems not entirely explained by the flow impediments created by marinas

A2.4.2 Core Stratigraphy

Study of the 172 detailed core logs permits further interpretation of the bed sediment regime in the Cedar/Ortega going back over perhaps 50 or 100 years or so. There has been a profound change in the sedimentary regime, which is evident in every core examined. It is difficult to envisage a natural regime change of such widespread extent in this benign system.

The lower horizons of most cores comprise material termed soupy muck, muddy muck, etc. Frequently these muck sediments have had or still have living bivalves in them. The bivalves can never have been dense faunal communities as the mucks remain largely unbioturbated. The two most common species are the clam *Rangia* and the Dark False Mussel *Mytolupis*. The former is a filter-feeding organism which initially colonizes the bed surface, often as a result of massive "sets" of spat during occasional high salinity events. These can then survive a return to low salinity conditions. The *Rangia* individuals eventually burrow into the bed, reaching up to 15 cm below the bed/water interface. *Mytolupis*, on the other hand, is a filter-feeding, surface dwelling organism attaching itself to any available "hard ground" on the bottom. The shells of these organisms are recorded in cores as articulated pairs, as single individuals, as layers in life position or as reworked, disarticulated groups or zones. The existence of these disarticulated layers indicates occasional exceptional events in the past when the weak and soupy mucks were swept away and shelly material was left on the surface as a kind of "lag" deposit. A good example is to be found in Core Sample No 39D from the Cedar River, although such features are doubtless present throughout the system.

There is always a strong disconformity in the successions above which distinctly contrasted sediments occur. These upper deposits still involve mainly the finely divided black muck sediments, often with tree leaves swept in from the catchment, but these are inter-bedded with the sandy intercolations described above, and with other materials. The most widespread additional material is wood chippings or in some cases bark chippings. These can only arise due to tree felling or pruning operations. Wood chips and sand layers are frequently inter-bedded with the muck layers in cores, hinting at a penecontemporaneous input or source. The next most common material, widely evident but confined to the Cedar River is oil. The oil-rich sediments are sometimes buried under more recent uncontaminated mucks and at other times occur at or close to the surface of the riverbed. Presumably there must have been a spill at some time, or instead successive series of spills.

One sample close to the northern coastline in the outer confluent region contained an abundance of grass-cuttings, described as "yard grass" in the core descriptions. Another, close to the Blanding Road Bridge in the Cedar River, contained asphalt and rubble attributed to construction or destruction of a car park. Finally, two samples immediately of Fishing Creek are described as a blue-green sandy clay, in this case with associated leaf litter and roots, but seemingly attributed by the logger of the cores as derived from ancient Hawthorne Formation deposits. In both cases these occur at the top of the succession and are the most recent input material.

Wood chips are present in cores right up towards the headwaters of the Ortega River and in places occur as multiple layers, indicative of repeated or intensive activity, but they are relatively uncommon compared to in the Cedar River. Wood chips are again relatively uncommon towards the headwaters of the Cedar River, but become very common in deposits in the lower Cedar River and at times with multiple layers from the reaches off Williamson Creek, Butcher Pen Creek and Fishing Creek, down-estuary. Wood chips are present in cores from the outer reaches of all three of these tributaries as well. Wood chips are also relatively common in the inner confluent region east of Roosevelt Boulevard Bridge. They are also present, but infrequently, in the sediments of the outer confluent region.

Sediments at the entrance to Big Fishweir Creek have layers within them, consistently with the enigmatic description "woody". It is unclear whether such materials should be regarded as having a natural or instead an anthropogenic input.

A2.5 Interpretation

The presentation of the results, above, shows that a pronounced and consistent areal and vertical variation in the sediment types is present.

The organic and inorganic sediments of the Cedar/Ortega River system are allochthonous and originate very largely in their own catchment system. There is a limited input of inorganic sediment from the main stem, although this only penetrated into the outer confluent region. No clear evidence has emerged as to the extent of autochthonous, plankton sediment production or the breakdown products of in situ sea grass in the system. Human settlement within the last 100 years has had a major impact on the types of sediment being input and on the sedimentation rate.

A2.5.1 Cedar River

In respect of the more minor, inorganic fraction of the sediments, the Cedar River deposits show the highest clay content in the entire system (18%). There is also a pronounced down-estuary decrease. This is consistent with a fluvial clay input. The silt content of the inorganic fraction is higher than the clay with a comparable down-estuary reduction, implying a similar detrital fluvial input. The sand fraction, in contrast, is low at the landward end and rises down-estuary. As far as the whole sediment is concerned, there is a much higher solids percentage, coupled with a relatively low moisture content, again consistent with a significant detrital input from the catchment. The solids percentage decreases down-estuary and the moisture content rises. This implies a rising organic fraction in the down-estuary direction. Consistent with these trends, the organic content of the innermost Cedar River samples is amongst the lowest in the entire system and rises down-estuary. This is the reverse of the situation in the Ortega River. It is suggested to reflect the urbanisation of the catchment. In core samples sand layers occur only very occasionally and when they do they are present as thin laminae. This confirms that, in spite of the level of urbanisation, detrital sand is not a significant input. This is, equally, the case for Williamson and Butcher Pen Creeks. In contrast, there is a significant detrital sand input, represented as thick and multiple layers, being discharged down Fishing Creek and doubtless accounting for

what is otherwise an anomalous-looking "high" in the sand fraction in the inner confluent region. The input must be terrestrial, must arise from recent deforestation and it cannot be relict marine sand as it lies mainly in the shallowest parts of the sediment succession. A further prominent anthropogenic input is that of wood chips. The levels of wood chips in the cores from innermost reaches of the Cedar River is low. This probably reflects the fact that deforestation and urbanisation of the Cedar River catchment is a relatively old feature. To complement this the largest quantities of wood chips emanate from Williamson, Butcher Pen and Fishing Creeks and are abundant in the sediments of the lower reaches of the Cedar River, down-estuary of these three tributary creeks. A further anthropogenic input confined to the Cedar River is oil. Oily muck is interbedded with the wood chips and with the less common sand horizons. It is not possible to comment on whether there has been a single relatively large spill or instead whether frequent or maybe semi-continuous low level hydrocarbon inputs occur. Finally, to complement the large scale sand and wood chip inputs from Fishing Creek, blue-green inorganic, detrital clays were sampled at shallow depth in recent sediment material in the entrance to Fishing Creek. A tentative suggestion arising from this might be that in recent decades, deforestation and urbanisation has focussed not in the Cedar but in it tributaries—Williamson, Butcher Pen and Fishing Creeks. Fishing Creek seems to have some affinities in this respect with Big Fishweir Creek in the outer confluent region (see later).

A2.5.2 Ortega River

The sediments of this river show some highly distinctive features and pronounced contrasts with the Cedar and other zones within the study area. It is predominantly a detrital, organic-dominated sub-estuary at a less-developed stage of urbanisation than the Cedar River. In respect of its inorganic fraction, it has a very low clay and sand input and a mid-level silt input, with a strong down-estuary decrease. The sand content rises in a down-estuary direction. In respect of whole sediment physical and chemical analyses, the Ortega has by far the highest moisture and lowest total solids of anywhere in the system, again reflecting the major terrestrial organic input to the catchment basin. The total solids percentages show a down-estuary decrease. Consistent with this, the organic content is at a system-maximum and also decreases down-estuary. Examination of core logs confirms the relative paucity of sand laminae. Where these are present they tend to occur deep in the sediment column. Wood chips are also less common than in the lower reaches of the Cedar and the inner confluent region. Where present they can be interbedded with the black finely divided mucks and the sand layers. These multiple-layered wood chip horizons are detectable in all sampled reaches of the Ortega and are presumed to reflect the onset of deforestation in this catchment, too.

A2.5.3 Inner Confluent Region

The inorganic fraction shows an apparently anomalous, exceptionally low clay content, although the recent blue-green clays being input from Fishing Creek seem not to be represented in this suite of samples. In contrast, the silt content is extremely variable, although still generally low in level. There is no obvious reason for the high variability. The sand content is relatively high and variable, (22–75%, but mainly 60–70%). The sand cannot

originate down-estuary, as concentrations decrease into the outer confluent region, and it must be either relict marine sand or a detrital input from the tributary creeks. The high elevation of the sand layers in cores suggests a fluvial source due to recent anthropogenic changes. In respect of the "whole sediment" analyses, and in contrast with the high sand content, these sediments also have a high moisture and low solids content. They can best be described as predominantly sandy mucks. There is a suggestion of an association between the high moisture/low solids rich sediments and the left bank in the inner confluent region. Very likely this is induced by the presence of the flow impediment provided by the large commercial marinas along this coast. A tongue of high organic-rich sediment is issuing from the Ortega and is strongly evident in this region. Possibly it indicates that the signature of Ortega type sediments is locally stronger than either Cedar or St. Johns River sediments? In vertical sections from the core logs multiple sand layering is well developed and widespread but there are never more than 10 sand layers. The sand must be contributed from Fishing Creek during occasional high discharge events. Wood chips are frequently interbedded with the sand layers in these reaches. These are very likely input from Williamson, Butcher Pen and Fishing Creeks. The distribution of wood chips and the variability in the silt content might be consistent with the presence of a large stable eddy in this region, but this must be a speculation.

Measurements of sedimentation rate are available and show a strong lateral variation, with relatively low values on the right bank, but high rates up to 20 mm/yr on the left bank amongst the marina developments.

A2.5.4 Outer Confluent Region

The inorganic fraction of sediments in this region are elevated compared to values in the up-estuary direction back into the Cedar and Ortega and probably reflect inputs from the main stem of the St. Johns River. The silt content is elevated and relatively constant in area, with a small degree of axial increase. Sand contents are generally low. Whole sediment analyses show levels and distributions very similar to the inner confluent region, i.e., the sediments have a high moisture concentration (>70%) and a low solids percentage. The maximum moisture and minimum solids contents are again found on the left bank, linked with the marina developments. Lateral partitioning is further evident in the presence of a tongue of low moisture, high solids detrital sediments penetrating the right bank of this region from the main stem. In cores, the pronounced lateral segregation is again detectable with multiple sand layering involving up to 15–20 sand horizons towards the right bank. The most seawards of these cores is all sand. In contrast, on the left bank, there are commonly no sand layers and the maximum number found is 7.

There is an unambiguous sand input from Big Fishweir Creek on the left bank at the confluence with the main stem. In general, few wood chip horizons are to be found in outer confluent region core samples, consistent with input from the river catchment up-estuary. Core logs at sites in the entrance to Big Fishweir Creek consistently identify one of the components of the sediments as "woody". In spite of this consistency in description, it is not possible to confidently associate this non-specific term with the "wood chips" described from up-estuary sites and the provenance of this material must remain unknown.

Sedimentation rate measurements show the same lateral partitioning, with values in the range 4–8 mm/yr on the right bank, rising to 20 mm/yr on the left. Whether these are linear sedimentation rates or, instead, whether surficial rates of siltation might be even higher, is also unknown.

A3. Implications of Sediment Regime for PCB Remediation and System Restoration

Establishing the areal and vertical extent and the severity of PCB contamination of sediments has not been part of these contracted investigations. Nevertheless, a few guiding comments are possible. We are not aware of how widespread and severe the initial distribution of PCB contamination has been, nor whether significant amounts are still held up within the urban drainage system to be flushed into the Ortega River in the future. Neither are we aware of whether episodic events capable of entraining and further redistributing the PCB contaminated sediment have occurred since the spill. However, from recent Acoustic Doppler Current Profilers (ADCP) work, which is a component of this investigation, it is now well-established that recreation vessel propeller scour of the shallow and weak bed sediment throughout the system is a perpetual feature. Sediment flux calculations have proved a challenge, not least on grounds that, where boat tracks cross an ADCP traverse line, a large percentage of the sediment flux is that contained within the boat wake. These sediment-laden wakes are also very persistent. There is possible evidence that high-speed racing-type motorboats may be particularly effective in stirring sediments. An implication of this finding is likely to be that the PCB contaminated sediment has spread more widely in the system due to this unanticipated anthropogenic effect than would otherwise be the case. We have not investigated the extent to which PCB contaminated sediment may have become capped by more recent, hopefully less-severely contaminated sediment in the years since the spill. The extreme shallowness of the system and the frequency of traversing of broad swathes of the estuaries by recreational vessels suggests that PCB contaminated sediment may still be accessible or may even have been reworked from the most actively trafficked zones into quiet water areas. The ADCP work indicates that in the low flow situations which exist for the bulk of the time, axially-directed currents are weak, whereas the two-dimensional internal medium and small scale turbulent eddying is by comparison strong. Over a prolonged period this may have provided a mechanism for lateral mixing. It might be anticipated from this that the PCB contaminated sediment will be more widely distributed in the Cedar River, inner and outer confluent regions than might otherwise have been anticipated.

On the other hand, this investigation of the fabric of core samples indicates a sedimentary system dominated by primary depositional structures. There are relatively few living organisms and winnowed shell layers are relatively uncommon. There is little evidence that soft-bodied invertebrates are any more successful than the shelly invertebrates in colonizing the bed deposits. This relative lack of bioturbation evidenced from the scarcity of the fauna and the apparent lack of secondary, biogenic structures in the sediments strongly suggests an inability to mix the PCB contaminated sediment deep into the underlying uncontaminated deposits.

Such knowledge as we have, consequently, leads to an expectation of a relatively widespread and increasingly distant spread of PCB contaminated sediment away from the source but of only a shallow penetration of the contaminated material into the bed. This indicates the wisdom of rather urgent intervention with a technique capable of thin layer dredging in order to remove the worst of the contamination and minimize future spread.

Presumably it can be anticipated from this that the level of environmental damage arising from thin-layer dredging will be relatively minor compared to the longer term environmental benefit of removal of a large fraction of PCB contaminated sediment. The invertebrate fauna is sparse and suggested to be recruited, at least in part, arising from exceptional events and from outside the area. It seems likely that some removal of sea grass beds will be necessary. The removal is taken to be local as opposed to being system-wide. It is a matter for speculation how long recolonization will require. Some entrainment of the weak bed deposits by the dredging process is inevitable but in this sheltered and benign environment containment using silt curtains will be straightforward. Some impact on the dissolved oxygen levels in the water column is assumed to be inevitable. The system has weak currents and poor flushing capabilities but this can be anticipated to be a local effect compared to the postulated large scale entrainment of bed deposits occurring during storms and hurricanes.

Subsequent to removal of the PCB contaminated upper layer, it can be anticipated that input of detrital clay and especially silt from the catchment of the Cedar River will continue. The main component of organic sediment input will continue to be allocthanous, highly degraded terrestrial plant debris, with a more minor autochthonous organic contribution arising from things like sea grass growth and decay, possibly allied to a small planktonic micro-organism input. The siltation rate in the remediated zone can be anticipated to continue in the immediate future at about 1.0 cm/yr in the lower Cedar River. In these lower reaches Williamson, Butcher Pen and Fishing Creek might, depending on the degree of urbanisation they have achieved, be expected to continue to input wood chips on an episodic basis. Fishing Creek will certainly continue to input fluvial sand and blue-green Hawthorn Formation (detrital) clays. The Jacksonville urban catchment will continue to input a broad range of contaminants, most noticeably oil, but in reality the full spectrum of wastes typical of a conurbation of its size.

References

Alexander, C. R., R. G. Smith, R. D. Calder, S. J. Schropp, and H. L. Windom. 1993. The history of metal enrichment in two Florida estuaries. *Estuaries* 16(3B):627–637.

Cooper, W.T., and J. F. Donoghue. 1999. *Investigation of historic sedimentation rates in the lower St. Johns River*. Report to St. Johns River Water Management District. Florida State University, Tallahassee (includes analysis of a core from the Cedar River mouth).

Higman, J. N.d. Personal communication. Ortega River cores. Preliminary sedimentation rate data as supplied to A. J. Mehta.

Morgan & Eklund Inc. 1995. *Ortega River and Cedar Creek, Duval County, Florida: Investigations of water depth* and *sediment characteristics*. Report for St. Johns River Water Management District. (Also core logs as an appendix to this report).

Mote Marine Laboratory. 1998. Analysis of sediment samples for St. Johns River Water Management District: Methodology and seventh data report. *Technical Report No 610*. Submitted through Battelle Ocean Sciences.

Mulholland, P. J., and C. R. Olsen. 1992. Marine origin of Savannah River estuary sediments: Evidence from radioactive and stable isotope tracers. *Estuarine, Coastal & Shelf Science* 34: 95–107.

Tissot, B. P., and D. H. Welte. 1984. *Petroleum Formation & Occurrence*. New York: Springer Verlag, 699 pp.

(Page intentionally blank)

Appendix B

Laboratory Experiments on the Erosional and Settling Properties of Sediment from the Cedar/Ortega River System

Jason E. Gowland
UFL/COEL/CR-2002/01
Department of Civil and Coastal Engineering
University of Florida

February 2002

Contents

Acknowledgment

Thanks are due to staff in the Coastal Engineering Laboratory for helping collect samples and in the laboratory during the experiments. Also, acknowledgment is due to Prof. Clay L. Montague of the Department of Environmental Science and Engineering for furnishing a furnace for determination of the organic content of the samples. Funds for field data collection were obtained through the St. Johns River Water Management District, Palatka, Florida.

List of Figures

List of Tables

B1. Introduction

The Florida Legislature (1999) finds that the quality of many of the surface waters of the state has degraded, or is in danger of becoming degraded, and that the natural system associated with many surface waters have been altered so that they no longer perform the important functions they once did. These functions include: (a) providing aesthetic and recreational pleasure for the people of the state, (b) providing habitat for native plants, fish and wildlife including endangered and threatened species, (c) providing safe drinking water to the growing population of the state, and (d) attracting visitors and accruing other economic benefits. Factors contributing to the decline in the ecological, aesthetic, recreational, and economic value of the states surface waters include point and non-point source pollution, and destruction of the natural systems that purify these waters and provide habitat.

The St. Johns River Water Management District has identified the Cedar and Ortega Rivers (Figure B1) in North Florida to be heavily contaminated with polychlorinated byphenyls (PCBs) and polycyclic aromatic hydrocarbons (PAHs), along with heavy metals such as mercury, cadmium and lead as well as pesticides and bacteriological wastewater. Heavy industrialization and urbanization are suspected sources. A significant fraction of the material transported through the river system is decaying organic matter, with larger particles

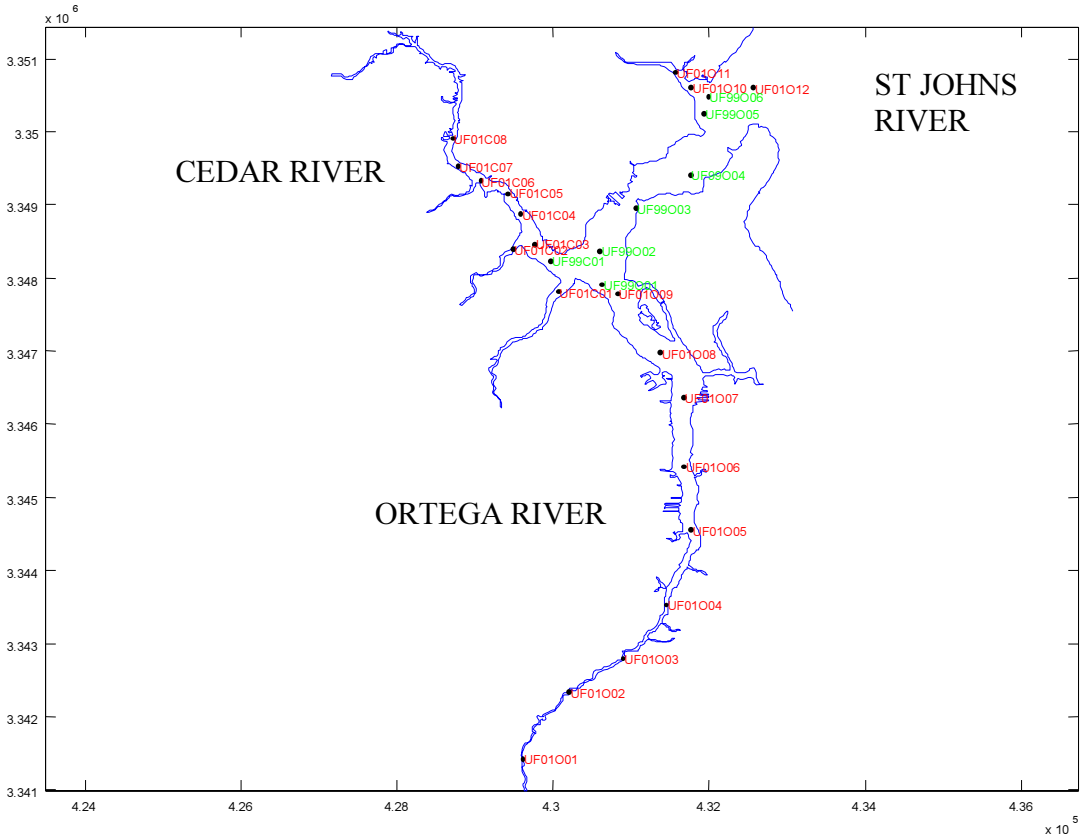

Figure B1. Map of Cedar and Ortega River sampling sites. Sites UF01 are for the present study; UF99 are from a previous sampling study (Mehta et al. 2000)

being present in the Ortega River due in part to the natural ecosystem and marshland that comprise the riparian environment. Cedar River, however, is more developed and environmentally impacted with a high accumulation of organic-rich, fine, cohesive sediment and associated turbidity.

Organic-rich sediment tends to be light-weight compared to inorganic material in water, and therefore low fluid stresses can cause its resuspension. Cohesion is electrochemical in nature, is important when the particles are less than 63 μm in size, and tends to cause such particles to aggregate. As a result they become larger and more massive and settle faster than the individual particles. This behavior results in the aggregate settling velocity increasing with sediment concentration in suspension. At very higher concentrations hindered settling occurs, i.e., the settling velocity decreases even as concentration increases.

B2. Scope of Work

It was desired to characterize the erosional and depositional properties of the bottom sediment from the study area. Because these properties of fine sediment are site-specific, it is necessary to determine the coefficients in generalized formulas for the erosion rate and the settling velocity. In this study these coefficients were determined through laboratory tests on selected bottom samples from the study area.

B3. Method

Twenty bottom grab-samples were taken from the two rivers at sites shown in Figure B1. The samples were then tested for the organic content and percent fines (Table B1). Wet-sieving for that purpose was done in order to determine percent finer than #200 sieve (or 74 μm size). A furnace was used to ignite organic material at 400°C. For details on the methods used for determining the organic content and sediment size see, for example, Rodriguez et al. (1997).

A vertical grid-oscillator (Particle Erosion Simulator) was used for erosion testing. Settling velocity was determined from tests in a 2-m tall plexiglass settling column. A numerical code was used to calculate and graphically display the settling velocity results. Rodriguez et al. (1997) provide relevant details.

Cedar River had more material below 74 μm and consistently high organic content in comparison with the Ortega (Figure B2 shows bridge over the Ortega near its mouth with the St. Johns River), which had larger “chunks” of organic matter greater than the #50 sieve, presumably due to the natural wetland habitat that surrounds it (see Figures B3 and B4). A sample (O-02) from the Ortega was mostly sand and was retained on the #200 sieve; see Figure B5. A noteworthy property of the material from the Cedar was the seeming strength it developed after being placed in the oven. The samples had an almost ceramic-like appearance and strength, after they were cooled and a mortar and pestle was used to attempt to grind them. Once taken from the furnace the Ortega sediment was mostly ash, while the Cedar samples where hard and strong.

Table B1. Percent fines and organic content in samples

Sample No.	Percent finer than #200 (%)	Organic content (%)
O-01	9	36
O-02	2	1
O-03	3	22
O-04	4	16
O-05	7	57
O-06	15	55
O-07	8	74
O-08	15	36
O-09	12	36
O-10	12	18
O-11	4	4
O-12	60	37
C-01	33	50
C-02	19	31
C-03	61	46
C-04	53	35
C-05	60	31
C-06	34	30
C-07	56	33
C-08	29	26

*O = Ortega sites
C = Cedar sites

Figure B2. Bridge across the mouth of the Ortega River at St. Johns River

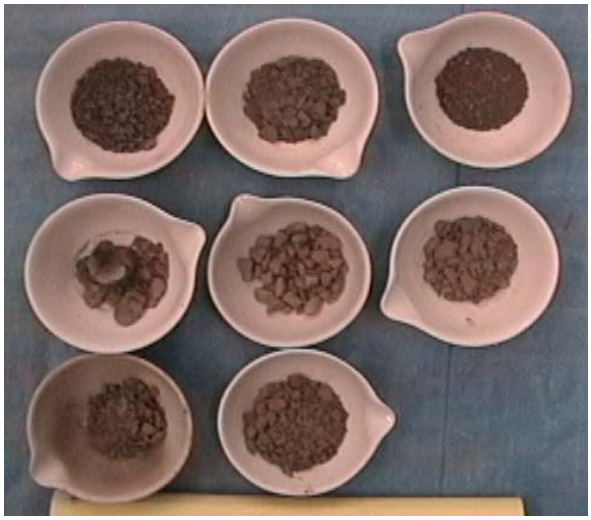

Figure B3. Cedar River sample residues after ignition

Figure B4. Ortega River sample residues after ignition

Figure B5. Ortega River sample O-02 (sand collected on #200 sieve)

B4. Erosion Tests

The grid-oscillator consists of a cylindrical chamber made of cast acrylic tubing and a grid element or perforated disk. The sample is stirred into the cylinder an allowed to settle and consolidate (in the present tests for up to 96 hours). After consolidation, the disk is oscillated at a given rpm, which effectively applies a shear stress along the fluid-bed plane. The concentration above the bed is recorded using a gravimetric method. In the present case four different shear stresses (of increasing magnitudes) were applied (for 1 hour each) to each sample. An example of the data (concentration-time plot) is shown in Figure B6, and results are given in Table B2 for the Cedar samples tested. Note that the organic matter from both rivers appeared to be similar.

The erosion rate (or erosion flux) for each applied shear stress is obtained by converting the measured time-variation of the suspension concentration, dC/dt:

$$\varepsilon = \frac{dm}{dt} = h\frac{dC}{dt} = \varepsilon_N(\tau - \tau_{ce}) \qquad \text{(B.1)}$$

where ε is the erosion rate, m is the eroded sediment mass per unit bed area, t denotes time, C is the suspended sediment concentration and h is the water depth. Determination of the erosion critical shear stress, τ_{ce}, is done by finding the intersection of the best-fit line of the plot of erosion rate versus applied shear stress on the abscissa. The slope of the same line yields the erosion rate constant, ε_N. These data are evaluated from the C-t plot such as the one in Figure B6.

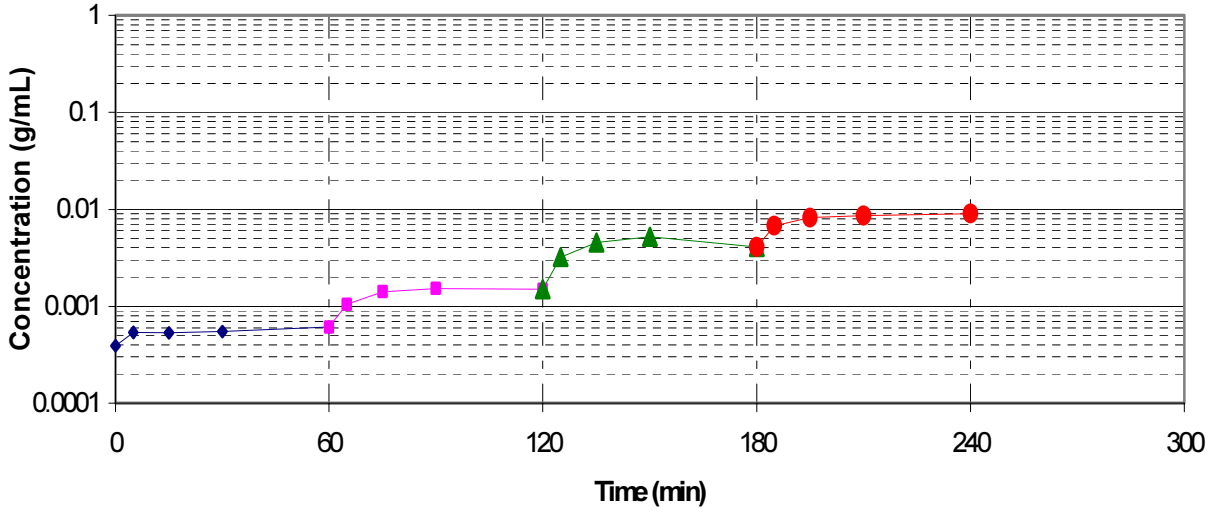

Figure B6. Time-variation of suspended sediment concentration during erosion of sample C-06 after 96 hours of bed consolidation. The four steps correspond to four applied shear stresses, 0.11 Pa, 0.19 Pa, 0.30 Pa and 0.40 Pa, in that order

Table B2. Bed shear stress, erosion rate and bed density

Station no. consolidation time	Shear stress (Pa)	Erosion rate (kg/m^2s)	Density* (kg/m^3)
C-01 96 h	0.095 0.207 0.281 0.405	2.33×10^{-6} 1.14×10^{-5} 2.54×10^{-5} 7.06×10^{-5}	1274
C-03 72 h	0.093 0.148 0.225 0.292	4.07×10^{-6} 4.40×10^{-6} 2.28×10^{-5} 3.94×10^{-5}	1092
C-04 96 h	0.189 0.260 0.314	1.76×10^{-5} 2.12×10^{-5} 3.81×10^{-5}	1031
C-05 72 h	0.033 0.144 0.193 0.240	0.00 4.66×10^{-6} 6.99×10^{-6} 1.27×10^{-5}	1101
C-06 96 h	0.109 0.192 0.302 0.399	5.64×10^{-6} 1.91×10^{-5} 5.82×10^{-5} 8.82×10^{-5}	1098
C-08 48 h	0.110 0.182 0.253 0.335	4.06×10^{-6} 1.09×10^{-5} 2.84×10^{-5} 5.19×10^{-5}	1021

*after consolidation

Based on samples in Table B1 from the Cedar River, where much of the contaminated sediment, characteristically associated with high organic content bed material, is believed to lie, erosion tests yielded the composite (of all tests) plot of Figure B7 for the rate of erosion as a function of bed shear stress (see Table B2). The data trend can be approximated by two lines of different slopes. Of these, the intersection of the flatter line with the shear stress axis corresponds to the condition for incipient motion, in this case characterized by the critical shear stress of 0.035 Pa. The intersection of the steeper line yields the characteristic "design" critical shear stress τ_{ce} = 0.17 Pa relative to Equation B.1. The slope of the same plot yields $\varepsilon_N = 3.5 \times 10^{-4}$ kg/m^2s Pa.

B5. Settling Tests

For fine-grained sediment, the settling velocity W_s varies with suspension concentration, C. This variation is divided into three regimes, as shown in Figure B8: free settling ($C \# C_1$), flocculation settling ($C_1 < C \# C_2$), and hindered settling ($C_2 < C \# C_3$). Note that the settling velocity as well as concentration are in log scale and cover wide ranges of values.

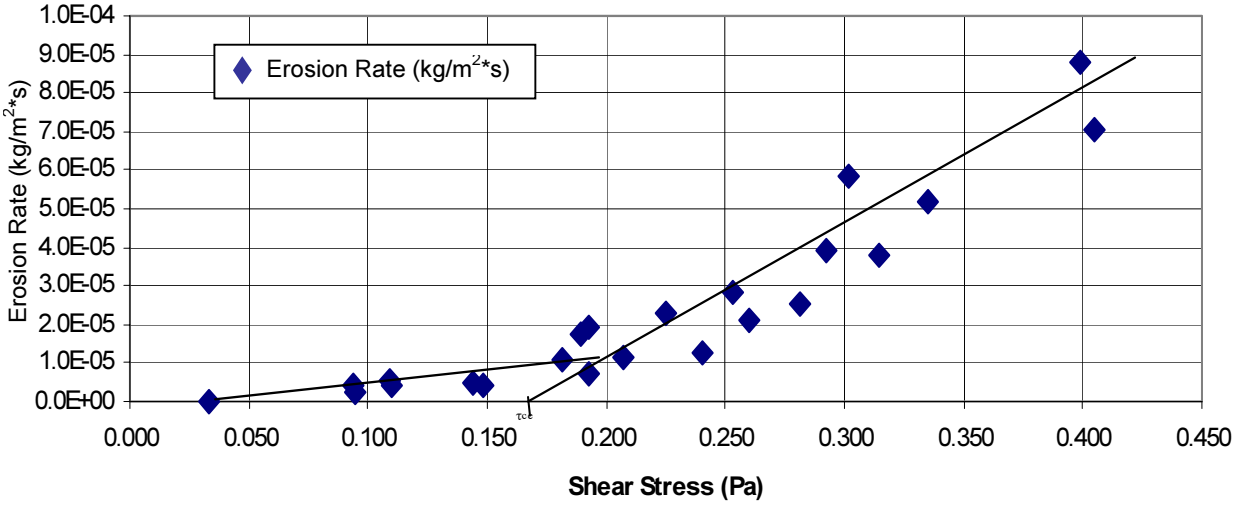

Figure B7. Composite plot of erosion rate versus bed shear stress

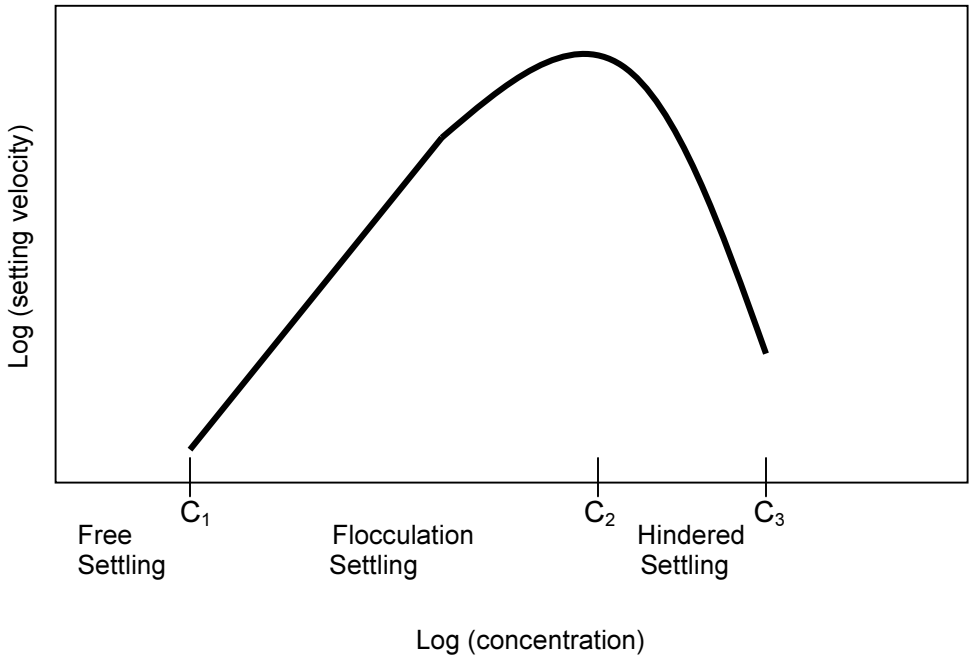

Figure B8. Schematic plot of settling velocity variation with suspension concentration

The general equation for the settling velocity in the flocculation settling and hindered settling ranges is (Hwang 1989):

$$W_s = \frac{aC^n}{(b^2 + C^2)^m} \tag{B.2}$$

The settling column test yields concentration versus elevation plots at different times after settling commences, as shown by the examples in Figure B9. By applying mass balance to the settling sediment and using such profiles the settling velocities and the best-fit coefficients in Equation B.2 can be determined. For the settling velocity data in Figure B10 for sediment of Table B2, estimates of a, b, n and m were determined to be 0.035, 2.0, 3.5 and 2.75, respectively.

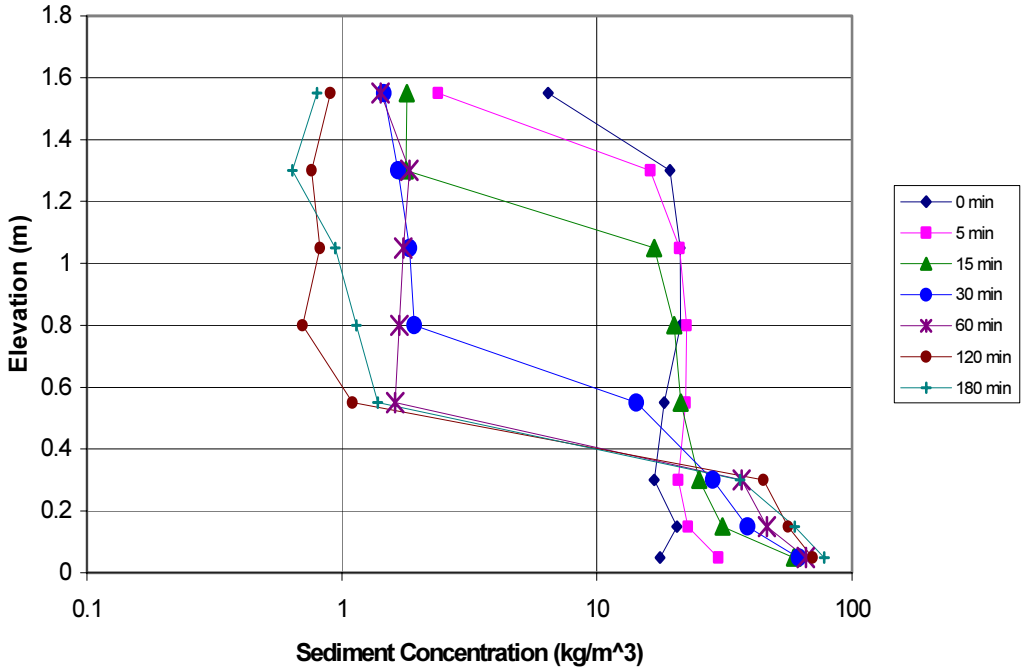

Figure B9. Examples of measured vertical profiles of concentration at different times in the settling column

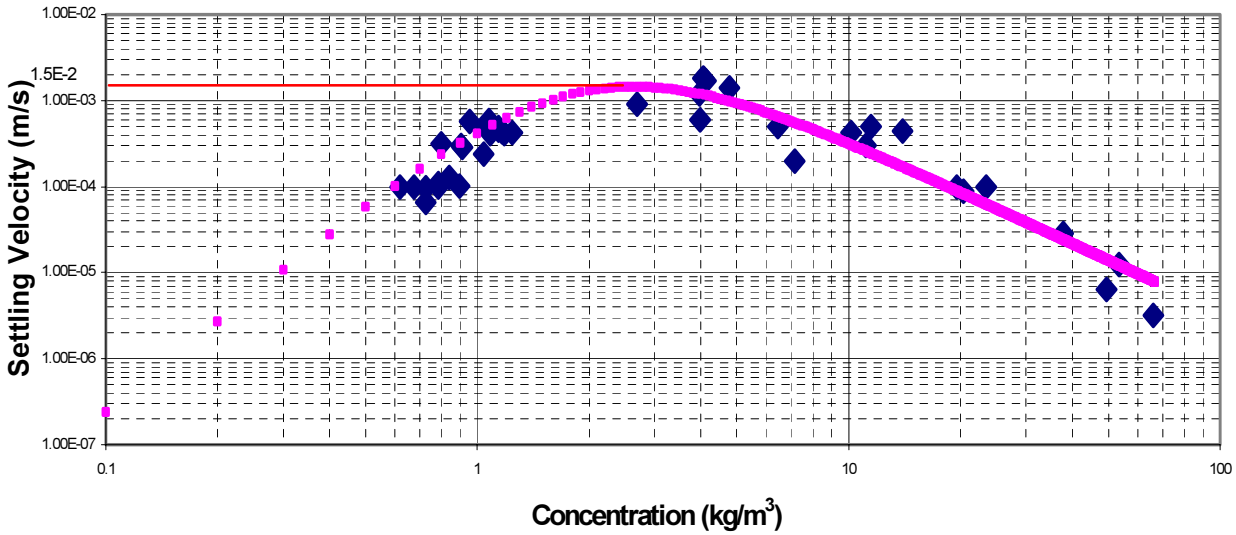

Figure B10. Settling velocity variation with concentration–data and best-fit of Equation B.2. Peak velocity is 1.5×10^{-2} m/s

B6. Conclusions

The following findings should be noted:

1. With the exception of two samples (O-02 and O-11), which mainly consisted of sand, the remaining 18 samples had organic content ranging from 16 to 74%.

2. For the erosion rate Equation B.1, the following coefficients were obtained: characteristic critical shear stress $\tau_{ce} = 0.17$ Pa and the corresponding erosion rate constant $\varepsilon_N = 3.5 \times 10^{-4}$ kg/m^{2}s Pa. These coefficients apply to beds of density ranging between 1,021 and 1,274 kg/m^3.

3. The characteristic peak velocity was 1.510^{-2} m/s. For the settling velocity Equation B.2, $a = 0.035$, $b = 2$, $n = 3.5$ and $m = 2.75$ (with W_s in m/s and C in kg/m^3) were obtained.

References

Florida Legislature. 1999. Surface water improvement and management act. *Sections 373.451 to 373.4595*. Tallahassee, Fla.

Hwang, K.-N. 1989. Erodibility of fine sediment in wave dominated environments. *Master's thesis*, University of Florida, Gainesville.

Mehta, A. J., R. Kirby, and E.J. Hayter. 2000. Ortega/Cedar River basin, Florida, restoration: work plan to assess sediment-contaminant dynamics. *Report UFL/COEL-99/019.* Department of Civil and Coastal Engineering, University of Florida, Gainesville.

Rodriguez, H. N., J. Jiang, and A. J. Mehta. 1997. Determination of selected sediment properties and erodibility of bottom sediments from the lower Kissimmee River and Taylor Creek-Nubin Slough Basins, Florida. *Report UFL/COEL-97/09*, Coastal and Oceanographic Engineering Department, University of Florida, Gainesville.

Appendix C

Sediview Survey in the Cedar and Ortega Rivers, Jacksonville, Florida

Dredging Research Ltd.
Bargate House, Catteshall Lane
Godalming, Surrey GU7 1LG, UK

and

Ravensrodd Consultants Ltd.
6 Queen's Drive, Taunton
Somerset TA1 4XW UK

DRL Report No. 253.US.0101-1

January 2002

Contents

List of Figures

List of Tables

C1. Introduction

This report describes the results of a Sediview survey undertaken during November 2000 in the Ortega and Cedar rivers by Dredging Research Ltd. (DRL) and Ravensrodd Consultants Ltd. for the Civil and Coastal Engineering Department of the University of Florida (UFL), Gainesville. The Sediview Method was developed by DRL to obtain measurements of suspended solids concentrations from the acoustic backscatter intensity recorded by Acoustic Doppler Current Profilers (ADCPs) manufactured by RD Instruments, Inc. of San Diego, California. When used in combination with the water current data obtained using the ADCP, the measurements can be used to provide detailed estimates of sediment flux in rivers and estuaries.

UFL require discharge and sediment flux data to calibrate a numerical model of the Cedar and Ortega rivers. The rivers are shallow, slow-flowing and characterised by low and relatively uniform suspended solids concentrations. The concentrations observed during the survey lay typically in the range 5–10 mg/L. Under such conditions, it is difficult, using any method, to accurately and confidently define variations of solids concentration. However, the quality of the ADCP calibration has exceeded our expectations. The main limitations of the survey results presented here concern the current measurements and the very limited water depths. Recommendations for improving the quality of future measurements are provided in Section C5.

C2. Field Methods

Measurements were attempted along the eight cross-river transects shown in Figure C1. After trial runs, Transect 7 (Butcher Pen Creek) was abandoned because the water was too shallow to obtain any data.

The remaining seven transects were surveyed repeatedly on November 2 and 3. After each transect had been sailed (with only a few exceptions), the survey boat was moved into the middle of the river, close to the transect, and two or three water samples were obtained for the Sediview calibration. Details of the calibration are presented in Section C3.

Siltmeter (turbidity meter) data were also obtained but the data set is incomplete due to instrument malfunction. Water temperature and salinity data were collected at each sampling location. These are used by Sediview to compute the profile of water absorption coefficient.

In all, 46 cross-river transects were obtained. The data from Transect 2 are meaningless and are not presented here because of the limited water depth and the short length of the transect.

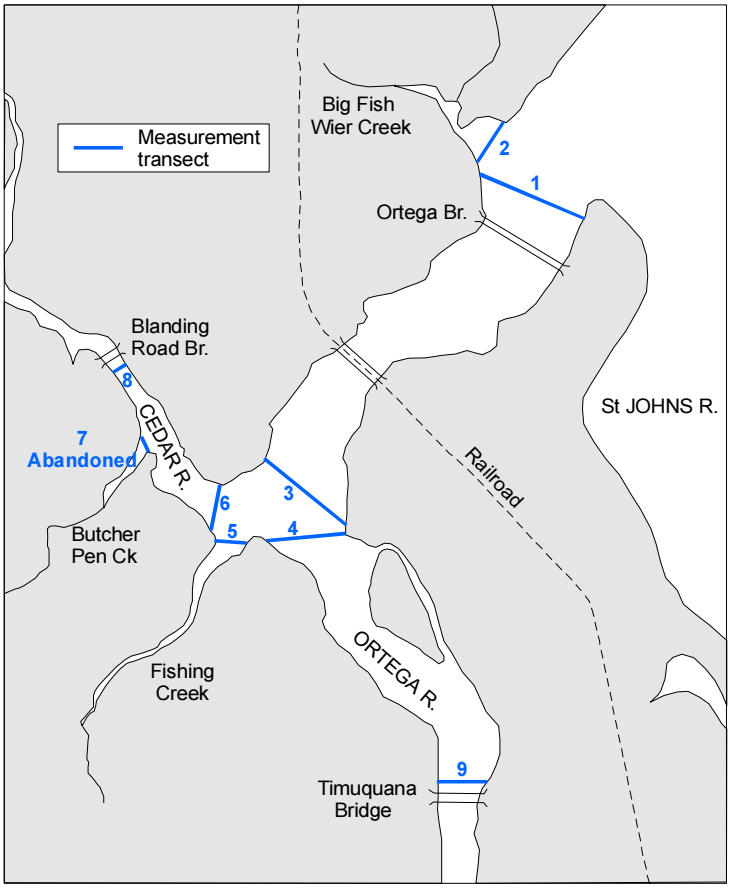

Figure C1. Locations of measurement transects

C3. The Sediview Calibration

C3.1 General Approach to Calibration and Data Processing

The conversion from backscatter intensity to solids concentration requires knowledge of several parameters that describe the performance of the ADCP used to collect the data and the environment in which the data are obtained. In summary, these are:

1. conversion factor from instrument 'counts' (i.e., the unprocessed output of the Received Signal Strength Indicator) to decibels for each of the four ADCP transducers;
2. internal noise levels of each of the four transducer / RSSI assemblies;
3. temperature of the ADCP's electronics chassis (which affects items 1 and 2 above);
4. profile of water absorption coefficient throughout the water column;
5. profile of speed of sound throughout the water column;
6. profile of kinematic viscosity throughout the water column;

7. acoustic attenuation coefficient of the sediment (dB/m/mg/L, the unit attenuation due to scattering and absorption by the sediment); and
8. site-specific relationship between solids concentration and backscatter intensity.

The water absorption coefficient, speed of sound and kinematic viscosity are derived using measurements of water temperature and salinity that are obtained at appropriate time intervals during each deployment. The ADCP transducer and RSSI performance characteristics can either be measured in the laboratory or, as in this case, established within the Sediview software calibration module using an iterative approach to beam normalisation and error elimination. The temperature of the ADCP electronics chassis is recorded during data collection and is used by Sediview during data processing.

The acoustic absorption coefficient and the site-specific backscatter relationship are derived within the Sediview calibration module on an iterative basis. Contrary to popular opinion, is it not necessary to know the particle size of the suspended sediment. Although the backscatter intensity is in part dependent on particle size (and some other properties), each Sediview calibration is necessarily undertaken on a site-specific basis and, unless the particle size varies with time or location during the deployment, the calibration therefore incorporates and allows for all of the various characteristics of the sediment that affect backscatter intensity. In those situations where particle size varies during a deployment, it is readily apparent from the calibration data. The calibration can therefore be adjusted to accommodate such change. This often occurs, for example, in estuaries where significant shifts of the calibration may be observed in response to the state of the tide. Two types of tidal effect are common:

- sediment particle size progressively shifts as the tidal cycle proceeds and may be distinctly different during the ebb and flood components; and
- fine sediment may flocculate over slack water periods in response to reduced turbulent energy.

There was no indication of any temporal or spatial variation of sediment quality that affected the calibration of the ADCP during the November 2000 survey. A single, uniform calibration has therefore been adopted. The results of the calibration are presented below.

It should be noted that the data processing has been undertaken using Version 3 of DRL-Sediview. This incorporates a near-field adjustment to the correction for spherical spreading of the acoustic beams, based on the work of Downing et al. (1995). The correction offsets the error inherent in the assumption that beam spreading is spherical in the near field; this assumption yields anomalously low backscatter intensities in the one or two measurement intervals closest to the ADCP transducers leading, in turn, to underestimation of solids concentration. The incorporation in Sediview of a two-stage spreading algorithm is important in the context of this work because the Ortega and Cedar rivers are very shallow and at least half of the cross sectional areas of the rivers lie within the near-field beam-spreading regime of the ADCP. Substantial errors in the estimates of solids flux would therefore arise if simple spherical spreading of the beams was assumed.

C3.2 Calibration Data

During the survey, the boat was stopped at frequent intervals (usually each time a line was surveyed) and one or two water samples were obtained for calibration purposes. In addition, turbidity meter data were obtained although, for a large part of the survey, the turbidity meter was not functioning. A total of 65 water samples were obtained. Of these, 38 samples have matching turbidity meter data collected using low- and high-range settings (25 JTU and 175 JTU, respectively). Water temperature and salinity data were obtained each time a water sample was taken. The laboratory-determined total solids concentrations of the water samples averaged 7.62 mg/L with a standard deviation of 2.48 mg/L. The range of concentrations was 3.24–18.11 mg/L. The distribution of measured concentrations is shown in Figure C2 from which it can be seen that the highest reported value (18.11 mg/L) is somewhat isolated and may therefore be suspect.

The water sample data were used to develop linear calibrations for the low and high range turbidity meter outputs. The solids concentrations estimated using the turbidity meter calibrations are compared with the water sample data in Figure C3. Although there is a definite correlation between the two types of observation, there is a high degree of scatter and some apparently outlying data. However, in view of the very low concentrations, and their limited range, such scatter is to be expected. It will be due partly to the fact that the turbidity meter measures a different volume of water and partly because the errors inherent in the laboratory determination of solids content become significant at such low concentrations.

C3.3 Sediview Calibration Results

Figure C4 shows the comparison between the Sediview concentration estimates and the reported water sample concentrations. In each case, the Sediview estimate is expressed

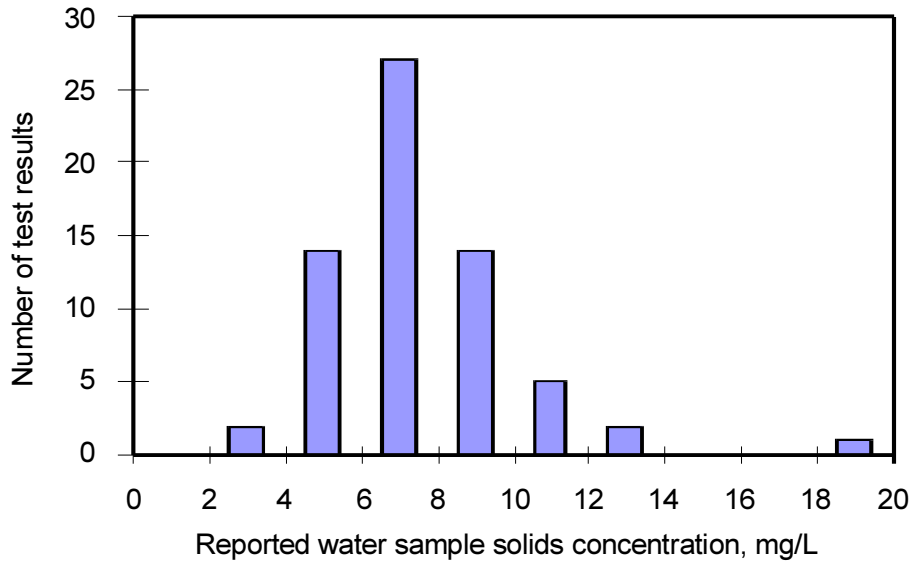

Figure C2. Distribution of results of gravimetric analyses of water samples

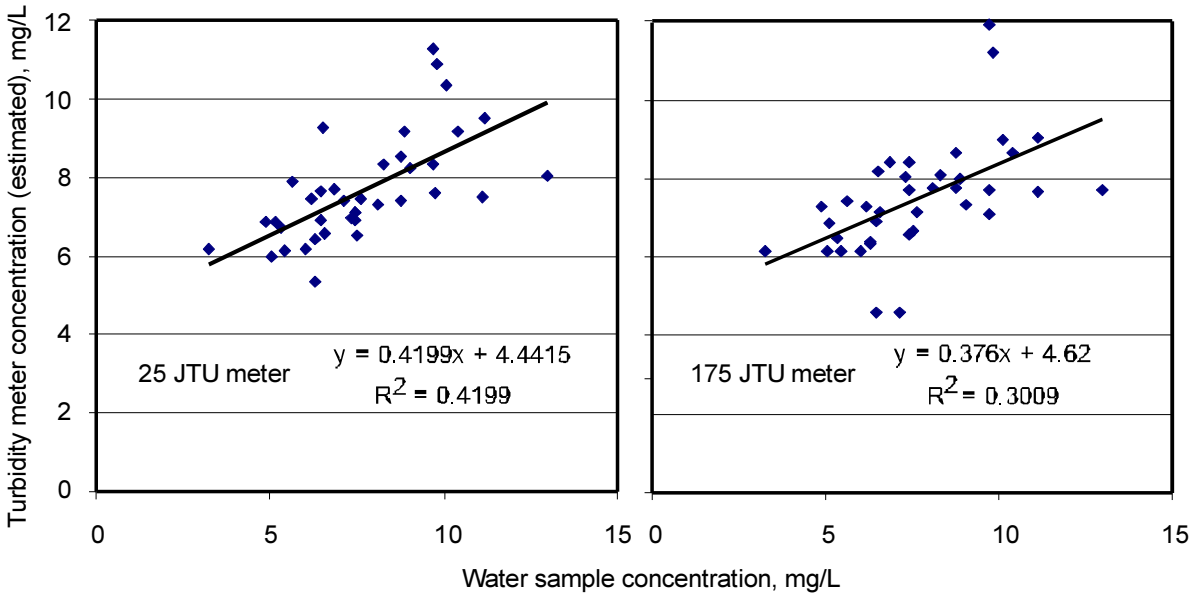

Figure C3. Solids concentrations derived from turbidity meter data, compared with gravimetric analyses on water samples

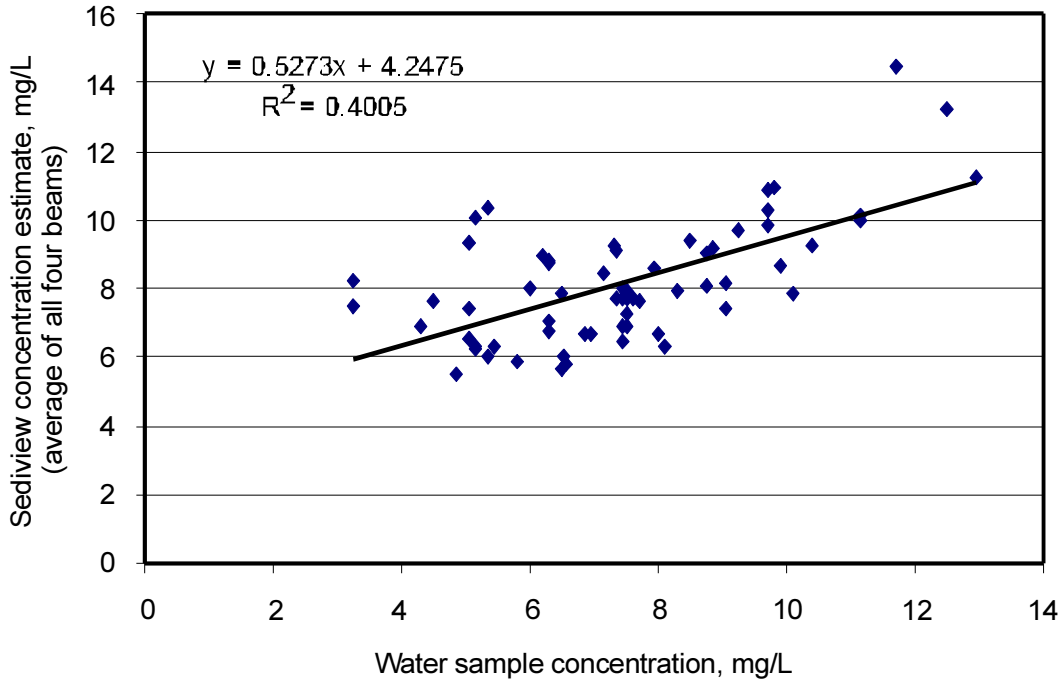

Figure C4. Sediview concentration estimates (4-beam average) compared with results of gravimetric analyses of water samples.

as the average of the four concentration estimates derived for each measurement depth interval (one for each of the four ADCP beams).

All of the observed data are presented with the following exceptions and qualifications:

1. data corresponding to the water sample from which the concentration of 18.11 mg/L was obtained have been excluded (the water sample appears to be an outlier and the ADCP data do not provide any indication of such high concentrations in the area where the sample was obtained—unfortunately, no turbidity meter data are available to compare with this sample);
2. in three cases, the water sample was obtained from within fields of sea grass (the acoustic reflection from the sea grass has corrupted the ADCP data—in these cases, the ADCP concentration estimates have been derived from the measurement interval immediately above the water sample depth); and
3. in one case, the water sample was taken too close to the bed, in the zone where the ADCP backscatter data are corrupted by side lobe echoes (as above, the ADCP concentration estimates have been taken from the measurement interval immediately above the water sample depth).

At each measurement depth, the four concentrations derived from the ADCP data were observed to vary over an average range of about 20–25% of the mean value. This is entirely expected and is typical of natural sediment suspensions. The average depth at which the samples were collected was 1.5 m at which depth the four ADCP beams are separated by about 1.1 m over which distance solids concentrations will inevitably vary.

Figure C5 shows the same data as Figure C4 except that, from each set of four Sediview concentration estimates corresponding to a water sample, the estimate closest to the reported water sample concentration has been used.

The degree of correlation is considerably better than when the average concentration is used (and is much better than that obtained using data from the siltmeter that was attached to the water sampler). However, there remains a degree of scatter, particularly at the lower end of the concentration range. There are a number of possible explanations for the scatter:

1. some of the ADCP backscatter data appear to have been corrupted by air bubbles generated as the boat drifted through the water when samples were being obtained (these data have not been excluded from the data as corruption appears to be slight—however, even a few air bubbles can ‘inflate’ concentration estimates when working in very low concentrations);
2. errors inherent in the testing of the water samples may contribute to much of the scatter. AAPH (1995) noted that the coefficient of variation of measurements of the solids concentration of water samples increases rapidly at low concentrations (at 242 mg/L they report a coefficient of variation of 10% while at 15 mg/L this increases to 33% which is equivalent to 5 mg/L or approximately 66% of the average water sample solids concentration used to derive the calibration presented here); and

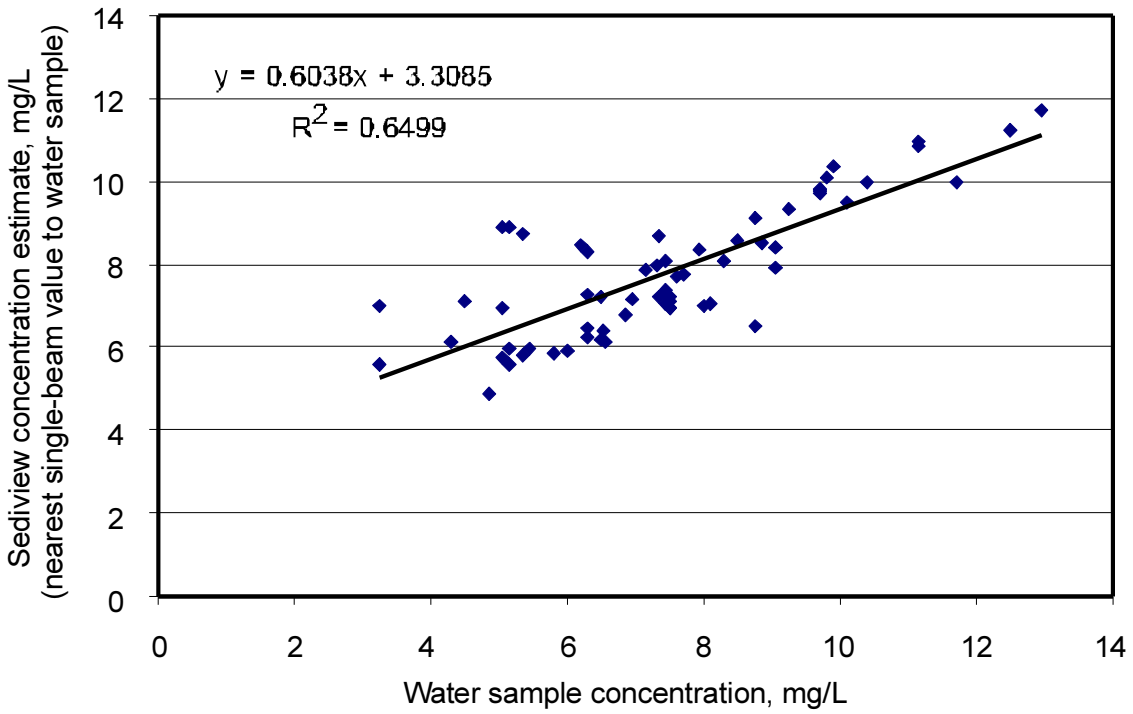

Figure C5. Sediview concentration estimates (1-beam, closest estimate) compared with results of gravimetric analyses of water samples

3. the approximately 2-metre spatial separation of the water sampler and the ADCP results in sampling/measurement of different volumes of water and, thus, to inevitable differences between the measurements.

The scatter below water sample concentrations of about 7 mg/L has the effect of yielding a large constant in the regression analysis. It is likely that this is in fact spurious. Visual examination of Figure C5 suggests that the constant should be very small and it is probable that the isolated data points that lie well above the regression line at low concentrations are an artefact of air contamination of some of the ADCP data and/or errors in the determination of water sample concentrations.

Figure C6 shows a quasi-time series comparison of the ADCP and water sample (i.e., presented in the order in which they were obtained). Good correlation is evident but five very low concentration water samples are not reflected by the ADCP data. A broadly similar trend can be seen in the turbidity meter data (i.e., the turbidity meter often did not register concentrations of less than 5 mg/L where the water samples suggested such concentrations, see Figure C3), thus reinforcing the sense that these data may represent laboratory under-measurement of the sample concentrations (i.e., the results lie at the low end of AAPH's +/-5 mg/L variance for low concentration samples).

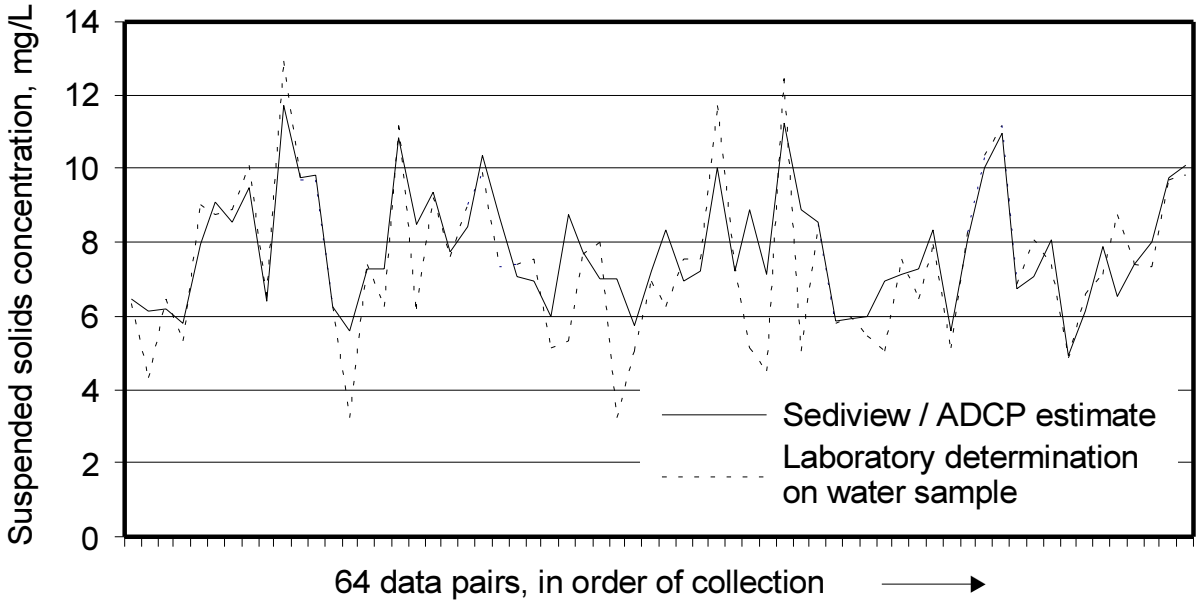

Figure C6. Quasi-time series comparison of ADCP estimates and reported water sample concentrations

C3.4 Summary Calibration Statistics

The summary statistics of the ADCP calibration, based on 64 data sets, are given in Table C1 below. Table C2 sets out the statistics for the siltmeter data, based on a reduced data set of 38 water samples.

Table C1. Summary statistics, water samples and Sediview/ADCP

Parameter	Water Samples	Sediview	
		4-Beam Average	Closest Beam
Range	3.24–12.95	5.47–13.24	4.88–11.21
Average	7.62	8.18	7.81
Median	7.43	7.91	7.33
Mode	7.43	7.67	6.12
Standard deviation	2.48	1.77	1.59
Linear regression *vs.* water samples:	Constant	4.2475	3.3085
	Coefficient	0.5273	0.6038
	R^2	0.4005	0.6499

Note: Water sample data exclude the apparent outlier at 18.11 mg/L
Sediview data include some data which are slightly air-corrupted

Table C2. Summary statistics, water samples and turbidity meter

Parameter	Water Samples	Turbidity Meter	
		25 JTU Range	175 JTU Range
Range	3.24–12.95	5.36–11.26	4.59–11.94
Average	7.65	7.65	7.50
Median	7.43	7.41	7.38
Mode	7.43	6.90	6.16
Standard deviation	2.08	1.35	1.42
Linear regression *vs.* water samples:	Constant	4.415	4.62
	Coefficient	0.4199	0.376
	R^2	0.4199	0.3009

C3.5 Data Processing

Discharge computations are normally based on current data that are derived by reference to the ADCP's bottom-tracking facility. This is because any compass errors effect equally both the apparent direction of movement of the survey vessel and the measurement of currents relative to the instrument and thus offset each other. The reported current direction may be erroneous (because it incorporates the ADCP's compass errors), but the estimates of discharge and flux will be accurate.

However, during this survey, the ADCP frequently lost bottom track due to the presence of extensive fields of sea grass. For some transects, up to about 30% of the data were so effected. Depending on the nature of the bottom track signal, the depth recorded in the binary raw data files was either higher or lower than the true depth to the bed. In addition, the data collection software extrapolates good bottom-track data through areas where bottom-track has been lost. Unless the vessel speed and direction are perfectly uniform (which is unlikely to be the case), this approach can give rise to errors of current measurement and estimation of the dimensions of each measurement cell.

In order to overcome these problems, it is necessary to reference the current data to the GPS position data and to establish accurately for each line the compass offset. The compass offset was established by careful comparison of valid ADCP bottom track data and the GPS data. Individual offsets were computed for each transect sailed during the survey. In addition, it is necessary to correct the river bed levels for all of those ensembles that are effected by loss of bottom-track so that all data are included in the estimates of discharge and solids flux. These adjustments were carried out using Sediview's on-screen editing facilities. An example, from Line 1, is shown in Figure C7.

In addition to the difficulties presented by loss of bottom-track, some records were effected by anomalously high backscatter caused by air bubbles in the wakes of passing boats. These data, and any 'bad' current data, were also rectified using Sediview's editing facilities. These permit data to be copied from 'good' measurement cells into adjacent (or

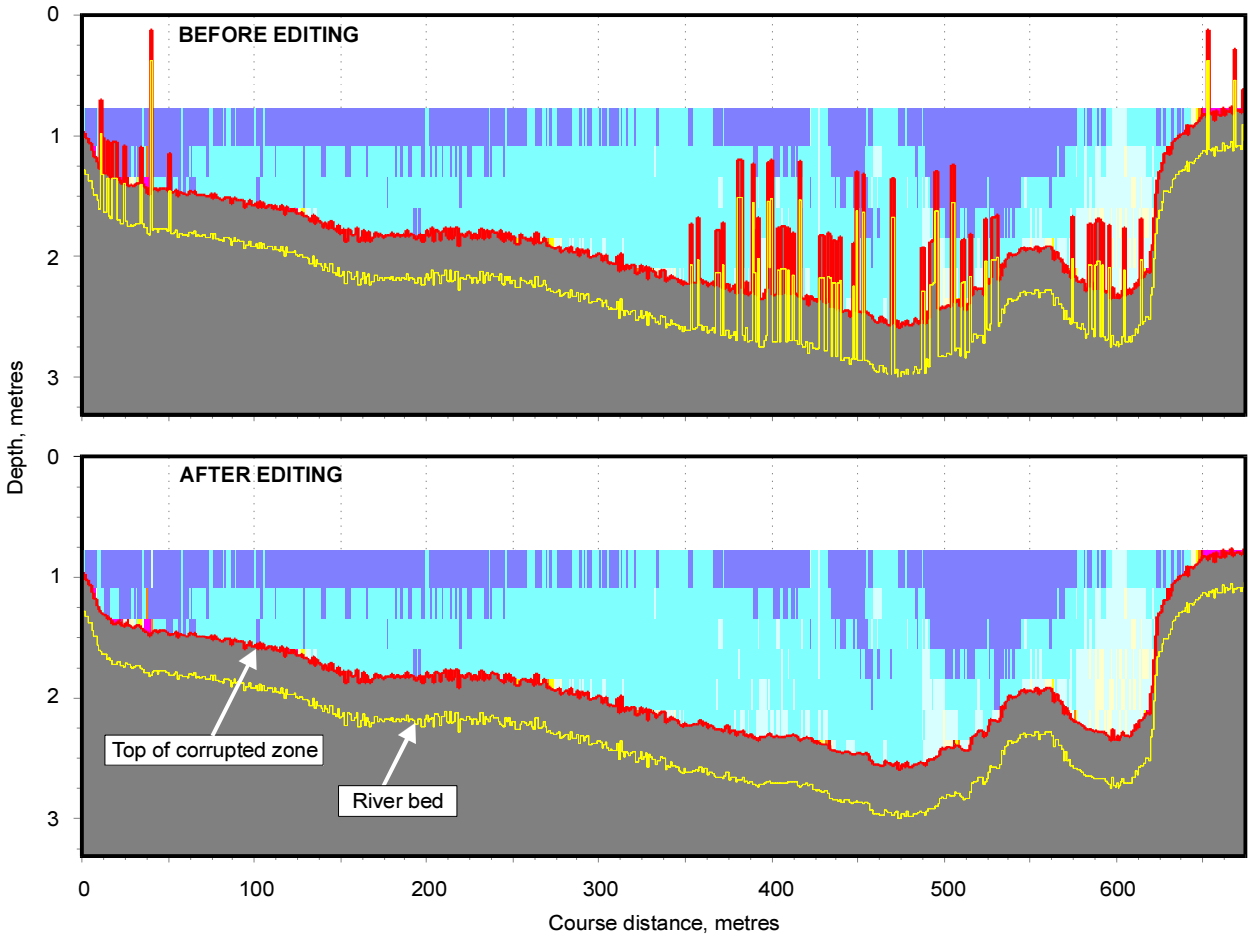

Figure C7. Example of results of seabed editing to restore data effected by loss of bottom-tracking

nearby) 'bad' data cells. Using these facilities, even badly corrupted records can be 'repaired'. However, there are obvious limitations to this approach and estimates based on transects with more than about 20% corrupted and repaired data must be viewed with some caution.

Another problem encountered during this survey was caused by the limited water depths. When the survey was undertaken, the minimum vertical measurement interval with the instrument that was used was 0.25 m. The instrument must be immersed in the water and there is a 'blank-after-transmit' distance between the transducers and the first valid measurement data. In the case of this survey, the first measurement bin was centered at a nominal depth of 0.97 m. The depth above the bed to which data are corrupted by side lobe echoes depends on the distance between the transducers and the bed. When working in the maximum water depth encountered during this survey, the corrupted zone extended to a nominal altitude above the bed of about 0.15m but, because of the measurement cell size, the actual amount of lost data was always at least 0.25 m. Thus, typically, about 1.2 metres of the water column could not be measured due to instrument limitations. Water depths along the transects varied between almost nil and about 3 m. This meant that for almost the full

length of all transects, a significant proportion of the water column was not measured. The example record shown in Figure C7 illustrates the extent of the problem.

Data in the upper and lower 'blank' zones is normally estimated by extrapolation from the measurement interval. In the upper zone, it is usually assumed (as was the case here) that both the current is the same as that in the highest measurement bin. In the near-bed zone, the current is usually estimated using a power curve derived from the data in the measured interval. If that interval comprises only one, two or three measurement bins, there exists the potential for the use of 'anomalous' power functions and thus the derivation of significantly erroneous current (and discharge estimates). In this case, a simplistic approach was adopted in which the current in the near-bed zone was simply assumed to be half the current in the lowest valid measurement bin.

The solids concentration in the upper blank zone was assumed to be 90% of that measured in the highest valid bin while that in the lower 'blank' zone was assumed to be 110% of the concentration observed in the lowest valid bin.

The blank zones typically accounted for about 50% of the total cross-sectional area of the transects, sometimes more (e.g., line 3) sometimes a little less (e.g., line 5). The difficulties of working in such shallow water have largely been overcome by the recent introduction of RDI's ZedHead ADCPs. These are discussed in Section C5 of this report.

The main data processing details are summarised below.

1. A single calibration, Sediview calibration, was applied to all data in order to derive the measured solids concentrations.
2. All current and discharge computations were referenced to GPS data with compass corrections computed separately for each line by comparing satellite and bottom track data.
3. Erroneous river bed levels caused by loss of bottom-track were corrected using Sediview's editing functions.
4. Bad concentration and current data (caused mainly by wakes from passing vessels) were excised and replaced with good data from adjacent cells.
5. Currents in the upper blank zone (approx. 0.8 m) were assumed to be the same as those measured in the highest valid ADCP bin (centered at 0.93 m).
6. Currents in lower (side lobe) blank zone were assumed to be 50% of current measured in lowest valid ADCP bin.
7. Solids concentration in upper blank zone (approx. 0.8 m) were assumed to be 90% of concentration in the highest valid ADCP bin (centered at 0.93 m).
8. Solids concentration in lower (side lobe) blank zone were assumed to be 110% of concentration measured in lowest valid ADCP bin.

C4. Measurement Data

C4.1 Discharge and Solids Flux Estimates

The estimates of discharge and solids flux are plotted in Figures C8 and C9, respectively, 7 against time before and after high water at Ortega main bridge.

C4.1.1 Line 1—Downstream of Ortega Main Bridge

The discharge and solids flux data for Line 1 are summarised below Table C3. Due to the extended time periods between successive transects it is difficult to estimate the peak values of discharge but a 4th-order polynomial function suggests that it is of the order of +/- 200 cumecs with a peak solids flux of +/- 1300 gs^{-1}.

Table C3. Discharge and solids flux data for Line 1

Record	Date	Time	Discharge, m^3s^{-1}			Solids flux, gs^{-1}		
			Measured	Estimated	Total	Measured	Estimated	Total
20	2 Oct 00	11:25	-74.0	-73.3	-147.3	-594.3	-510.7	-1105.0
43	2 Oct 00	15:18	-11.0	2.9	-8.1	-60.2	22.1	-38.1
72	2 Oct 00	18:19	71.2	123.6	194.3	621.6	630.9	1252.5
83	2 Oct 00	20:16	3.1	-9.4	-6.3	14.0	-74.2	-60.3
87	3 Oct 00	09:46	9.9	1.7	11.6	87.6	13.4	101.0
117	3 Oct 00	12:53	-83.9	-81.1	-165.0	-697.2	-582.9	-1280.1

Record 83 appears to be anomalous as it yields a negative value during late stages of ebb tide but the data suggest that tide is flooding at western end of line while still ebbing at eastern end.

C4.1.2 Line 2—Big Fish Weir Creek

Extremely shallow water precluded any sensible estimates of discharge or flux.

C4.1.3 Line 3—Exit of Combined Cedar & Ortega Rivers from Confluence Area

This was the best line in terms of the relative proportions of measured and estimated data (see Table C4). There appear to be no major anomalies but, as with Line 1, it is difficult to identify the peak discharge and solids flux. The data suggest that the peak discharge is about +/- 175 cumecs and the peak solids flux about +/- 1200 gs^{-1}.

Table C4. Discharge and solids flux data for Line 3

Record	Date	Time	Discharge, m^3s^{-1}			Solids flux, gs^{-1}		
			Measured	Estimated	Total	Measured	Estimated	Total
6	2 Oct 00	09:48	-21.1	-15.7	-36.8	-134.3	-104.2	-238.5
27	2 Oct 00	12:19	-68.1	-43.4	-111.5	-567.7	-395.8	-963.5
54	2 Oct 00	16:42	43.2	26.8	70.0	340.5	210.6	551.0
78	2 Oct 00	19:26	40.0	20.4	60.4	328.2	176.0	504.1
94	3 Oct 00	10:35	-21.5	-9.1	-30.6	-138.1	-64.2	-202.3

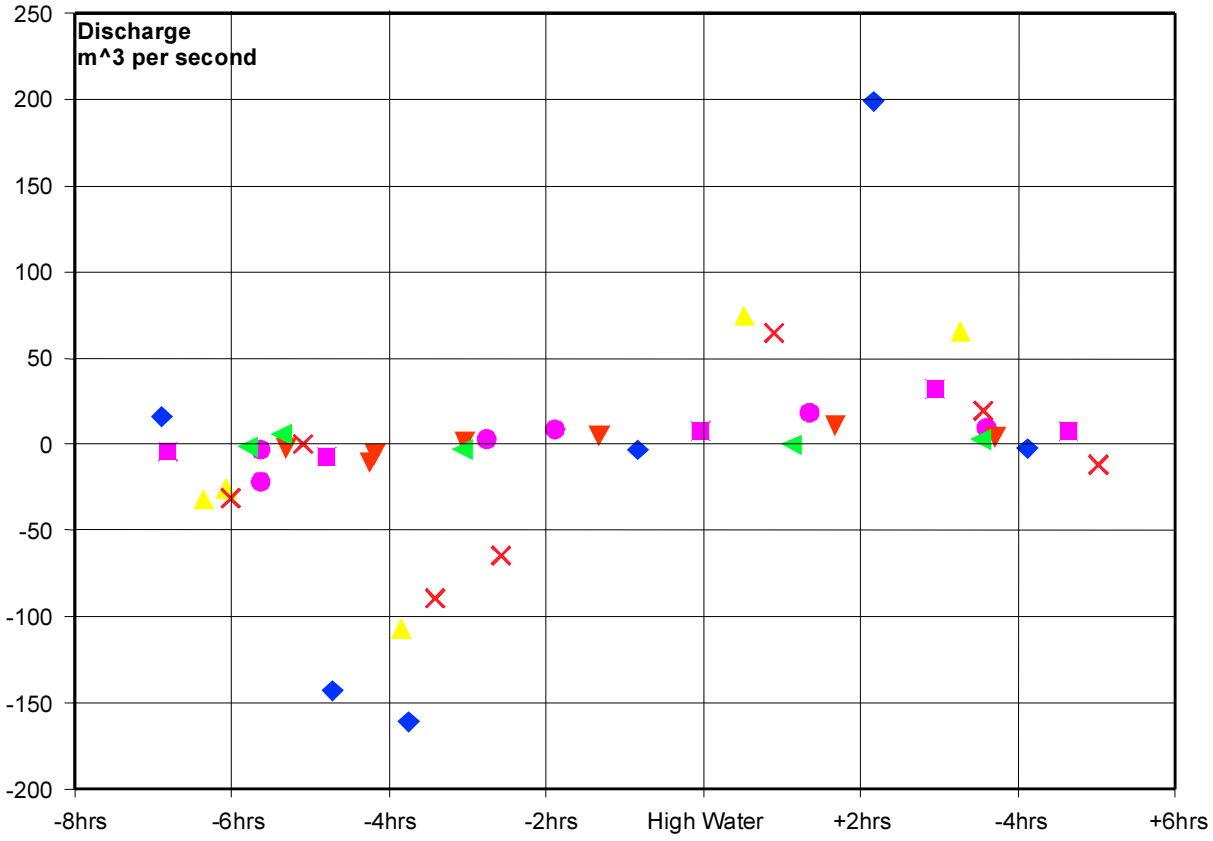

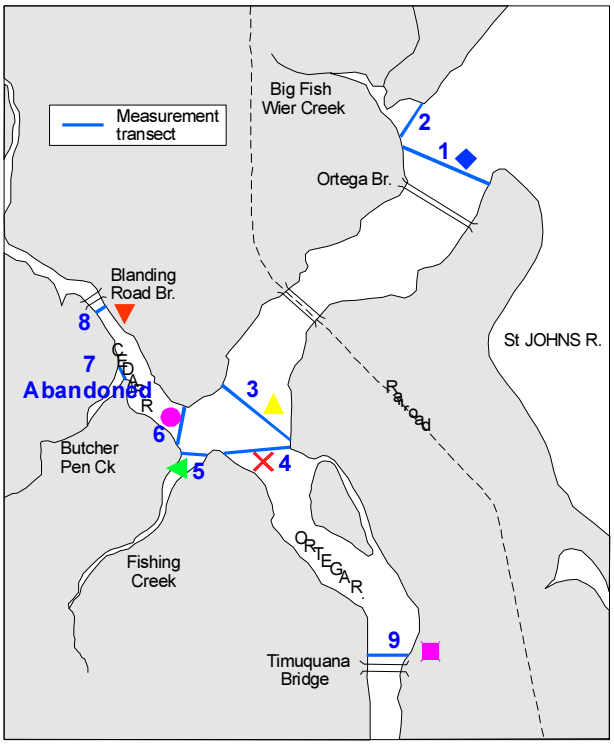

Line 1 Line 3 Line 4 Line 5
Line 6 Line 8 Line 9

Data from Line 2 not reported. Insufficient water depth for meaningful measurements.

Figure C8. Discharge relative to high water level at Ortega main bridge

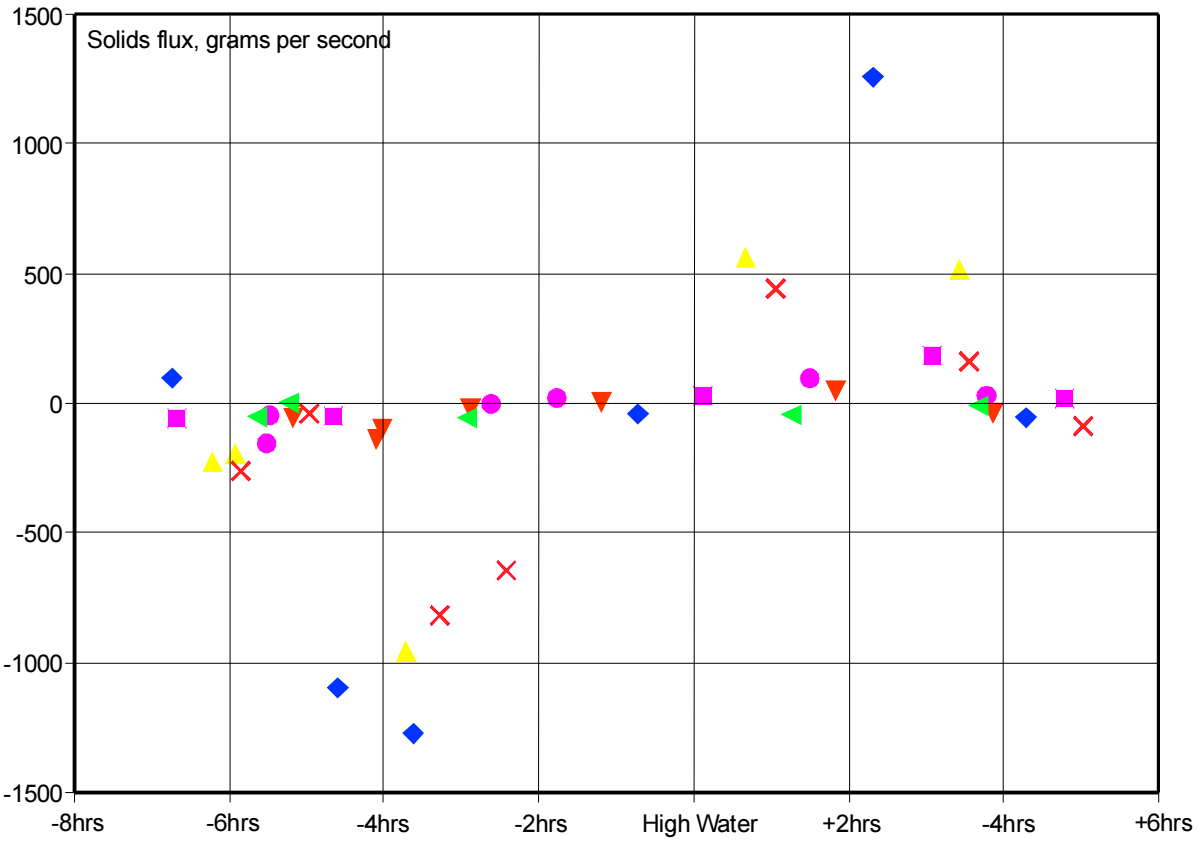

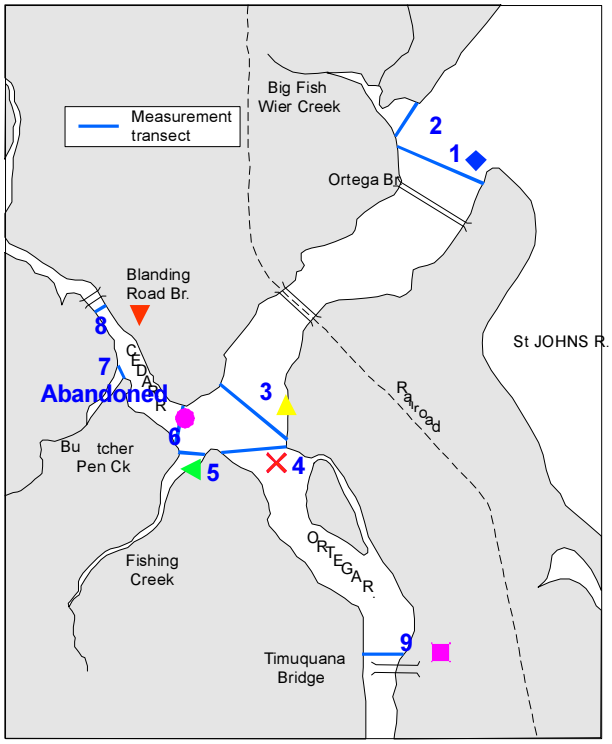

Line 1 Line 3 Line 4 Line 5
Line 6 Line 8 Line 9

Data from Line 2 not reported. Insufficient water depth for meaningful measurements.

Figure C9. Solids flux relative to high water level at Ortega main bridge

C4.1.4 Line 4—Ortega River, Entry into Confluence Area

The estimated component of discharge/flux is far greater than measured component but, with the possible exception of record 106, the results appear reasonable (see Table C5). Peak discharge probably exceeds +/- 130 cumecs and the peak solids flux may be as much as +/- 1000 gs^{-1}, i.e., about 85% of flux through Line 3 across combined rivers).

Table C5. Discharge and solids flux data for Line 4

Record	Date	Time	Discharge, m^3s^{-1}			Solids flux, gs^{-1}		
			Measured	Estimated	Total	Measured	Estimated	Total
9	2 Oct 00	10:09	-10.5	-24.9	-35.4	-79.2	-180.5	-259.6
31	2 Oct 00	12:44	-34.5	-58.8	-93.3	-316.9	505.5	-822.3
58	2 Oct 00	17:04	20.8	40.0	60.8	159.6	292.3	451.8
79	2 Oct 00	19:34	8.2	11.1	19.2	71..	93.0	164.3
86	2 Oct 00	21:02	-1.4	7.1	-8.4	-12.0	-55.8	-67.8
106	3 Oct 00	11:33	-0.7	-3.6	-4.3	-6.8	-29.1	-35.8
128	3 Oct 00	14:05	-26.2	-42.5	-68.7	-249.0	-392.5	-641.4

C4.1.5 Line 5—Fishing Creek, Entry into Confluence Area

The measurements are summarised overleaf. The current data are very poor due to the combination of weak currents and limited water depth / line length (see Table C6). The concentration data were often corrupted by boat wakes; these were edited out of the records but the short line length means that a large proportion of data were effected. Records 61 and 80 should yield positive values (on ebbing tide). This is indicative of the poor quality of the current data. The peak discharge and solids flux are crudely estimated to be 10 cumecs and 75–100 gs^{-1}, respectively.

Table C6. Discharge and solids flux data for Line 5

Record	Date	Time	Discharge, m^3s^{-1}			Solids flux, gs^{-1}		
			Measured	Estimated	Total	Measured	Estimated	Total
11	2 Oct 00	10:21	-1.2	-4.9	-6.1	-12.4	39.0	-51.3
35	2 Oct 00	13:04	-1.2	-4.9	-6.1	-19.0	-37.2	-56.2
61	2 Oct 00	17:16	-2.4	-5.3	-7.7	-13.6	-21.9	-35.5
80	2 Oct 00	19:41	-1.7	-3.0	-4.7	-2.3	-8.2	-10.5
102	3 Oct 00	11:17	-0.3	-1.6	-1.9	1.0	3.6	4.6

C4.1.6 Line 6—Cedar River, Entry into Confluence Area

Record 38 should yield positive values (on ebbing tide); this is indicative of poor data quality for reasons similar to those encountered at Line 5 (see Table C7). The measured component is small compared with estimated component. Record 13 data may be a little too high and should be treated with caution.. The peak discharge appears to be of the order of +/- 20–25 cumecs, with a peak solids flux of about 100-150 gs^{-1}.

Table C7. Discharge and solids flux data for Line 6

Record	Date	Time	Discharge, m^3s^{-1}			Solids flux, gs^{-1}		
			Measured	Estimated	Total	Measured	Estimated	Total
13	2 Oct 00	10:30	-2.6	-23.0	-25.6	-16.5	-139.0	-155.5
38	2 Oct 00	14:15	0.5	-0.3	0.2	0.4	-3.3	-2.9
65	2 Oct 00	17:30	3.0	11.1	14.1	21.7	76.0	97.8
81	2 Oct 00	19:45	-0.6	-5.2	4.6	-3.3	31.8	28.5
99	3 Oct 00	11:01	-1.5	-6.3	-7.8	-10.2	-39.4	-49.6
127	3 Oct 00	13:54	-0.3	-1.3	-1.6	-0.6	0.8	0.2

C4.1.7 Line 7—Butcher Pen Creek

Butcher Pen Creek was found to be too shallow to obtain any data and the line was abandoned before the main survey commenced.

C4.1.8 Line 8—Cedar River, Blanding Road Bridge

Records 115 and 116 are indicative of level of accuracy obtained on this line (and other similar short lines such as Line 5). Record 116 was obtained immediately after 115 due to boat wake contamination. Both needed much editing and there is a 30% difference between the measured discharges (Figure C8). However, the Line 8 data are broadly consistent with the downstream Line 7 if allowance is made for a small contribution from Butcher Pen Creek. The peak discharge is probably about +/- 15 cumecs and the peak solids flux about +/- 150 gs^{-1}. These measurements must be treated with caution.

Table C8. Discharge and solids flux data for Line 8

Record	Date	Time	Discharge, m^3s^{-1}			Solids flux, gs^{-1}		
			Measured	Estimated	Total	Measured	Estimated	Total
16	2 Oct 00	10:51	-2.6	-4.4	-7.1	-19.7	-35.2	-54.9
41	2 Oct 00	14:50	-0.8	-0.3	-1.0	-6.2	-6.2	-12.7
68	2 Oct 00	17:50	1.9	3.5	5.4	19.2	31.9	51.1
82	2 Oct 00	19:53	-0.8	-4.7	-5.6	-7.3	-36.3	-43.7
115	3 Oct 00	12:26	-5.5	-9.6	-15.1	-54.6	-89.6	-144.2
116	3 Oct 00	12:29	-2.9	-7.4	-10.3	-29.8	-66.4	-96.2
124	3 Oct 00	13:38	-1.2	-1.6	-2.8	-9.1	11.9	-21.0

C4.1.9 Line 9—Ortega River, Timuquana Bridge

Data for record 24 was found to be corrupted. The indicated peak discharge of about +/- 30 cumecs seems anomalously low when compared with downstream Line 4 (peak about +/- 130 cumecs) but there is a large storage volume between the two lines (see Table C9).

Table C9. Discharge and solids flux data for Line 9

Record	Date	Time	Discharge, m^3s^{-1}			Solids flux, gs^{-1}		
			Measured	Estimated	Total	Measured	Estimated	Total
2	2 Oct 00	09:20	-4.5	-3.9	-8.4	-29.2	-27.7	-56.8
24	2 Oct 00	11:58	–	–	–	–	–	–
50	2 Oct 00	16:07	0.3	3.2	3.5	0.4	29.2	29.6
77	2 Oct 00	19:05	11.0	16.3	27.3	82.0	105.9	187.8
85	2 Oct 00	20:48	-1.1	4.4	3.3	3.8	20.5	24.3
109	3 Oct 00	11:51	-3.9	7.5	-11.4	-18.5	-30.6	-49.0

Note: – = corrupted data

C4.2 Solids Concentrations

The solids concentrations observed during each individual transect were generally very consistent and exhibited modest vertical gradients but little or no lateral variation. The overall average solids concentrations for each transect are plotted against time relative to high water in Figure C10 overleaf. A clear trend is apparent with the highest concentrations occurring during the main part of the flood tide (HW - 4 hrs) and the lowest occurring at low water. Lines 6 and 9 exhibited the lowest concentrations. Of the other lines, no one stands out as having consistently the highest concentrations but Line 8 appears to be rather high. This may be due to the relatively high leisure boat traffic that was observed in this area. This could give rise to consistent sediment resuspension but would also result in some aeration of the water column, giving rise to spuriously high concentrations, even though efforts were made to avoid sailing transects immediately after the passage of other boats.

C5. Recommendations for Future Surveys

The generally very weak currents, extensive areas of sea grass and shallow water mean that the measurements reported here are subject to some uncertainty, especially in the case of Lines 5, 6, 8 and 9. The upper and lower blank zones, where the ADCP that was used cannot collect data, amounted in most cases to more than 50% of the cross sectional area of the transects. On many transects, only one or two 'bins' of valid data could be obtained and reliable power curves describing the current profiles could not be developed. The estimates of discharge and solids flux in the blank zones are therefore necessarily crude.

Since these measurements were undertaken, RD Instruments have introduced 'ZedHead' ADCPs. These are specifically designed to measure currents in very shallow water and can measure over depth increments of as little as 10mm. It is considered that the use of a ZedHead would significantly improve the quality of data obtained in future surveys in the Cedar and Ortega rivers, particularly if the data were obtained at slower sailing speeds than those adopted during this survey.

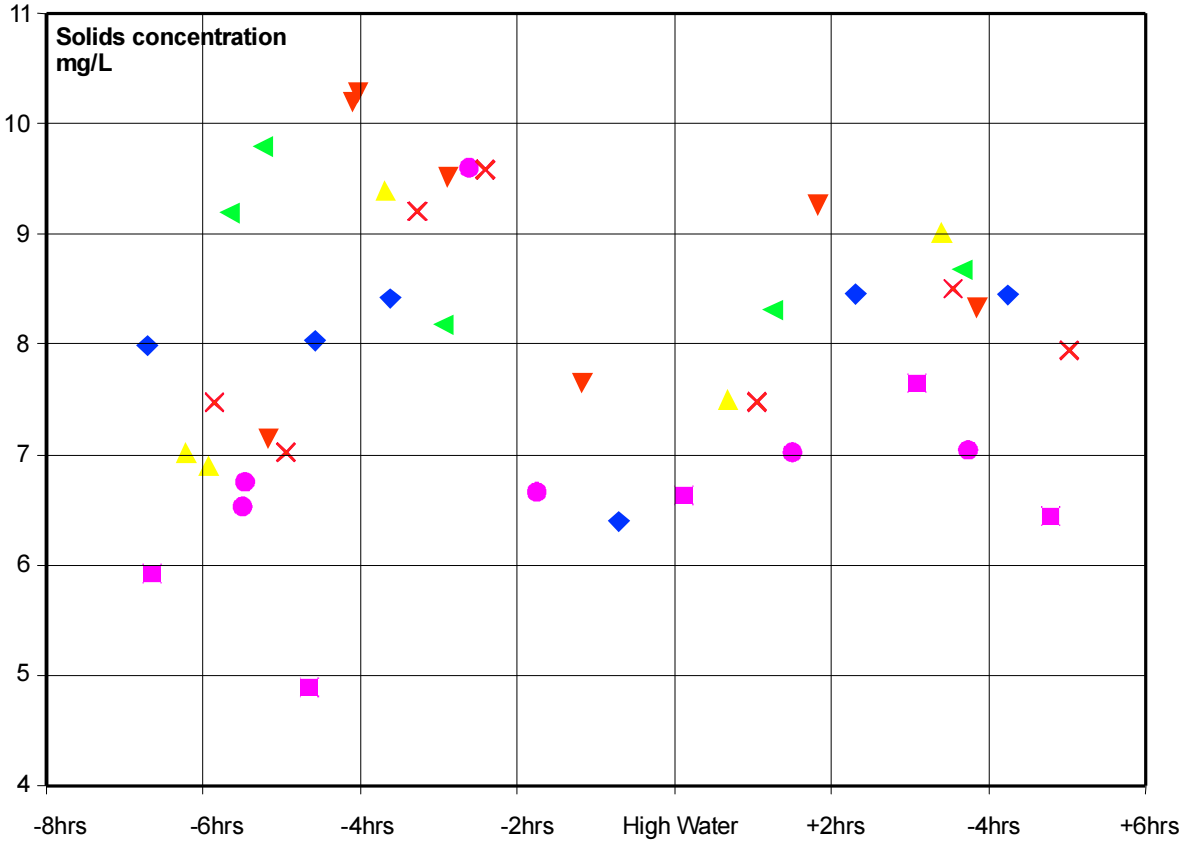

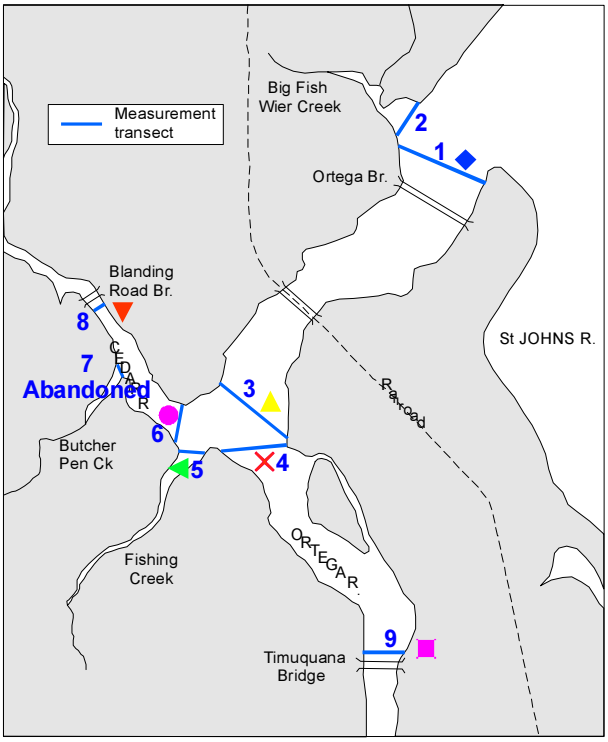

Line 1 Line 3 Line 4 Line 5
Line 6 Line 8 Line 9

Data from Line 2 not reported. Insufficient water depth for meaningful measurements.

Figure C10. Average solids concentration relative to high water level at Ortega main bridge

Bottom-tracking problems due to the presence of sea grass would not be overcome by the use of a ZedHead but the editing facilities in Sediview can easily be used to overcome this problem. It is strongly recommended that the Department investigate the ZedHead instruments as they have significant advantages over conventional ADCPs in environments such as the Cedar and Ortega Rivers.

It is clear from the data that, although the general trends are obvious, the time intervals between repeat transects on individual lines was too great to confidently construct continuous curves of discharge and solids flux. Some uncertainty is thus inherent in the estimates of maximum discharge and flux. More frequent transects would provide a more detailed picture and would facilitate identification of data that have been corrupted by decaying boat wakes (very old wakes are sometimes difficult to distinguish from localised concentration elevations). In order to reduce the time between transects, two boats would be required.

Our recommendations for future surveys are thus:

- use RDI's new ZedHead ADCPs;
- sail transects more slowly to improve current measurements without loss of resolution; and
- sail transects more frequently to improve definition of the discharge and solids flux curves.

C6. Conclusions

The Cedar and Ortega rivers are a challenging environment in which to measure suspended solids because of the consistently low solids concentrations. This makes calibration of both turbidity meters and ADCPs difficult because calibrations must be based on comparisons with water sample data that are inherently subject to errors at low concentrations. In addition, the unavoidable temporal and (particularly) spatial mismatching of three different types of measurement leads inevitably to scatter in comparisons between the results.

Despite these difficulties, a satisfactory calibration has been achieved. Although scatter is evident in the comparison between Sediview concentration estimates and the water sample data, there is a high degree of correlation and the scattering lies within the expected range.

Measurements of discharge and solids flux were hampered by the shallow water and the presence of extensive fields of sea grass. The sea grass resulted in frequent loss of bottom track which meant that current data had to be referenced to GPS, rather than bottom track, using compass corrections determined for each line by comparing bottom track data with GPS data. A considerable amount of bed level editing was required in order to correct the bed levels and ensure that all valid measurement data were included in the estimates. There was clearly nothing that could be done about the shallow water which resulted in significant proportions of the total discharge and flux estimates being based on estimated

data. However, in future surveys, the magnitude of this problem might be reduced by using the recently-introduced ZedHead ADCPs.

In the light of these problems, the estimates of discharge and solids flux must be viewed with some caution, particularly for the short transects (e.g., Lines 5 and 8) where the peak discharges and fluxes can only be crudely estimated from the data. Shorter time intervals between successive transects and sailing at a slower speed might provide more reliable data in future surveys.

References

AAPH. 1995. *Standard Methods for the Examination of Water and Wastewater.* USA.

Downing, A., P. D. Thorne, and C.E. Vincent. 1995. Backscattering from a suspension in the near field of a piston transducer. *J. Acoust. Soc. Am*. 97(3), March.

Appendix D

Survey Report on ADCP With Sediview for Ortega and Cedar Rivers

(Also Appendix to Report: Sediview Survey in the Cedar and Ortega Rivers, Jacksonville, Florida, November 2000)

Dredging Research Ltd.
Bargate House, Catteshall Lane
Godalming, Surrey GU7 1LG, UK

and

Ravensrodd Consultants Ltd.
6 Queen's Drive, Taunton
Somerset TA1 4XW UK

DRL Report No. 253.US.0101-1

January 2002

Contents

List of Figures

List of Tables

D1. Introduction

This field survey had a number of objectives. One was to gather high quality data on river discharge and sediment flux on tidal timescales in the lower reaches of the Ortega and Cedar Rivers. These data were to be used to calibrate a mathematical model. A second objective was to evaluate a new technology not previously applied in the St. Johns River watershed. Evaluation was necessary on the grounds of the exceptional shallowness and unusually low turbidity of these systems. These characteristics provide a challenge to any measurement system, but in this case, the instrumentation measures whole water depth and whole cross-section profiles. It is currently limited by an inability to measure close to the surface and to the bed. In extremely shallow waters, the intervening mid-water zone is narrow and may become non-existent.

D2. Equipment

The principal tools used were an RDI 1200 kHz Broadband Workhorse Acoustic Doppler Current Profiler (ADCP), together with an on-line DGPS system. The ADCP was also to be run with the "Sediview" software, which permits simultaneous suspended solids data to be obtained without any alteration to the RDI hardware. On the advice of RDI, the ADCP came equipped to operate in "Mode 8", said by the manufacturer to be ideally suited to working in conditions of very weak currents in shallow water. Sediview is a DOS program and works with Transect software supplied by the equipment manufacturer.

To calibrate the ADCP the survey vessel was also equipped with a salinity and temperature measuring instrument and a calibrated siltmeter. These instruments were mounted on a water sampling bottle. In use, the array was lowered to a predetermined depth from a location close to, but not in, the ADCP beam. Measurements and samples closely correlated in space and time with the ADCP reading were obtained (within 3 ensembles).

D3. Program

Monday, 10/30/00—Pack and load all equipment in Gainesville.

Tuesday, 10/31/00—Drive to launch site at Fishing Creek. Stream out into river to set up and test all equipment. Problem found and overcome in waking up the ADCP. At the end of the afternoon, a dummy run made around the nine survey lines established in the Ortega and Cedar Rivers using Mode 8. Line 7 at Butcher Pen Creek found not to be viable. Repeated attempts within the creek, at its entrance and offshore, failed to find more than 1 m of water.

In fact, none of the eight remaining survey lines produced Sediview data comparable with that obtained elsewhere and previously. Investigation continued during the evening to

assess whether this was real data or some artifact of either the RDI Workhorse or the untried Mode 8 system.

Wednesday, 11/1/00—Set aside planned tidal cycle measurement in order to further evaluate ADCP with Sediview and the problem outputs. Identical cross-sectional traverses run with Mode 8 and Mode 1 settings. The two were very dissimilar and Mode 8 obviously spurious. Among other things noise level outputs below the seabed were "frozen". Decided to commence and run survey with the familiar Mode 1 system.

Before tidal cycle measurement program could commence, the survey computer failed and could not be repaired. This was the only computer available to capture and merge ADCP and DGPS data simultaneously.

Only course of action was to obtain another computer but to reconfigure the survey to run in "WinRiver" not in "Transect". (Transect is an RDI DOS program used to run Sediview2, WinRiver is an RDI Windows program and will be used in future for Sediview3, which is due to be in operation in January, 2001.)

Reconfiguring files to run ADCP in Win River and to accept DGPS until 0100 on 11/2/00.

Thursday, 11/2/00—Complete tidal cycle run, repeatedly visiting the eight standard lines. The only practical operating difficulty encountered was that it proved necessary to operate the survey computer shaded from the sun under a coat in order that the screen could be seen. Arising from the calmness of the waters it proved possible to operate with the top of the ADCP transducer only just covered by water (37 cm). At a survey speed of about 2.5 knots cavitation beneath the transducer was not encountered. Bottom track was lost at the inner, shallow ends of all sections even at high tide, the distance off the bank when surveying was no longer possible was recorded on each occasion. The shallowest valid readings were obtained from about 80 cm below the water surface, implying a loss of about 40 cm below the transducer.

In the course of surveying it proved possible to come to terms with boat wakes. Regrettably, it turned out that a significant number of boat operators did not follow the rules concerning speed and its consequences for wake creation or for manatees. A number of users operated high-speed twin-hulled racing speed boats and these were the worst offenders. However, these did not give rise to any significant degradation to the ADCP signals in wide reaches of the system. The wakes were no more than 10-m wide in cross-sections 600-700 m across. Furthermore, there is now a capability within Sediview during the interpretation phase to eliminate a boat wake and replace it with immediately adjacent valid data. Boat wakes were, nevertheless, a problem from time to time in the narrower reaches, especially at Line 9, the Timuquana Bridge in the Ortega River and at Line 8, the Blanding Road Bridge in the Cedar River. Such undesirable boating activities not only degrade the quality of ADCP survey data but are also dangerous to a slow-moving survey vessel running bank to bank cross-sections, often partly obscured from view by bridge piers. Fortunately, there was only limited boat traffic to disturb the mid-week survey operations.

Friday, 11/3/00: Planned decommissioning day substituted for a tidal cycle survey day to replace time lost on 11/1/00 due to computer failure. No undue problems encountered.

D4. Results

Some 61 complete cross-sections of velocity, direction and suspended solids were obtained. The 10 cross-sections obtained during trials on 10/31/00 and one additional cross-section on 11/1/00 in Mode 8 are not recoverable. Neither are the experimental profiles on Line 7 at Butcher Pen Creek, and possibly too, the profiles degraded by boat wakes at Line 8 on the Cedar River at Blanding Road Bridge. Some 46 useable sections were obtained on 11/2/00 and 11/3/00 see (Table D1). The rate of ADCP data capture was a careful compromise with parallel water sampling and salinity/temperature/siltmeter readings (for ADCP calibration). Effort was also expended in obtaining vertical siltmeter profiles to assist in the subsequent evaluation and modeling exercise. A data coverage matrix (Figure D1) reveals how the ADCP traverse data are distributed against standard survey lines and with tidal time. The traverses are well distributed against survey lines (5-7 per line) and against tidal time (2-7 traverses per hour).

In addition to the 46 cross-sectional ADCP profiles, 66 water samples with accompanying salinity, temperature and siltmeter measurements were obtained for calibration (see Table D2 for partial list). Similarly, five (generally 6" sampling interval) vertical siltmeter profiles starting at 6" below the water surface were obtained from Lines 1, 2, 3, 6 and 9 (see Tables D3 through D7). The gravimetric analysis of the water samples and all other calibration data are appended to this report.

Table D1. Cross section lines: Distance to bank from SOL/EOL

Line	Time	Date	SOL	EOL	Line	Time	Date	SOL	EOL
9	0914	11/2/00	15m Eside	30m Wside	9	1901	11/2/00	10m Wside	12m Eside
3	0942	"	10m Nside	12m Sside	3	1919	"	12m Nside	15m Sside
4	1005	"	7-8m Eside	6m Wside	4	1931	"	15m Eside	7-8m Wside
5	1020	"	5m Sside	3m Nside	5	1940	"	7m Sside	3m Nside
6	1027	"	10m Wside	20m Eside	6	1943	"	6m Wside	8m Eside
8	1050	"	20m Eside	8m Wside	8	1952	"	10m Wside	15m Eside
2	1115	"	30m Eside	12m Wside	1	2010	"	10m Sside	8m Nside
1	1120	"	40m Nside	15m Sside	2	2021	"	6m Wside	15m Eside
9	1155	"	3m Eside	8m Wside	9	2045	"	4m Wside	15m Eside
3	1212	"	18-20m Nside	2m Sside	4	2057	"	8m Eside	10m Wside
4	1239	"	15m Eside	12m Wside	1	0940	11/3/00	30m Nside	45m Sside
5	1301	"	10m Sside	4m Nside	2	1002	"	50m Eside	7m Wside
6	1411	"	10m Wside	18m Eside	3	1030	"	25m Nside	10m Sside
HW	1447	"	25m Eside	6m Wside	6	1058	"	30m Eside	2m Wside
1	1508	"	8-10m Sside	12m Nside	5	1115	"	4m Nside	5m Sside
2	1535	"	7m Wside	25m Eside	4	1129	"	30m Wside	10m Eside
9	1602	"	10m Eside	6m Wside	9	1148	"	0m Wside	6m Eside
3	1636	"	15m Nside	6m Sside	(8	1224)	"	15m Eside	*
4	1659	"	4m Nside	5m Sside	(8	1227)	"	15m Eside	*
5	1715	"	3m Sside	3m Nside	1	1245	"	10m Nside	20m Sside
6	1724	"	20m Wside	15m Eside	2	1317	"	40m Eside	15m Wside
8	1750	"	7-10m Wside	15m Eside	8	1335	"	35m Eside	8m Wside
1	1812	"	12m Sside	8-10m Nside	6	1348	"	12-15m Eside	10m Wside
2	1832	"	6m Wside	12m Eside	4	1400	"	35m Wside	10m Eside

Note: SOL = start of line
EOL = end of line
*corrupted by boat wakes

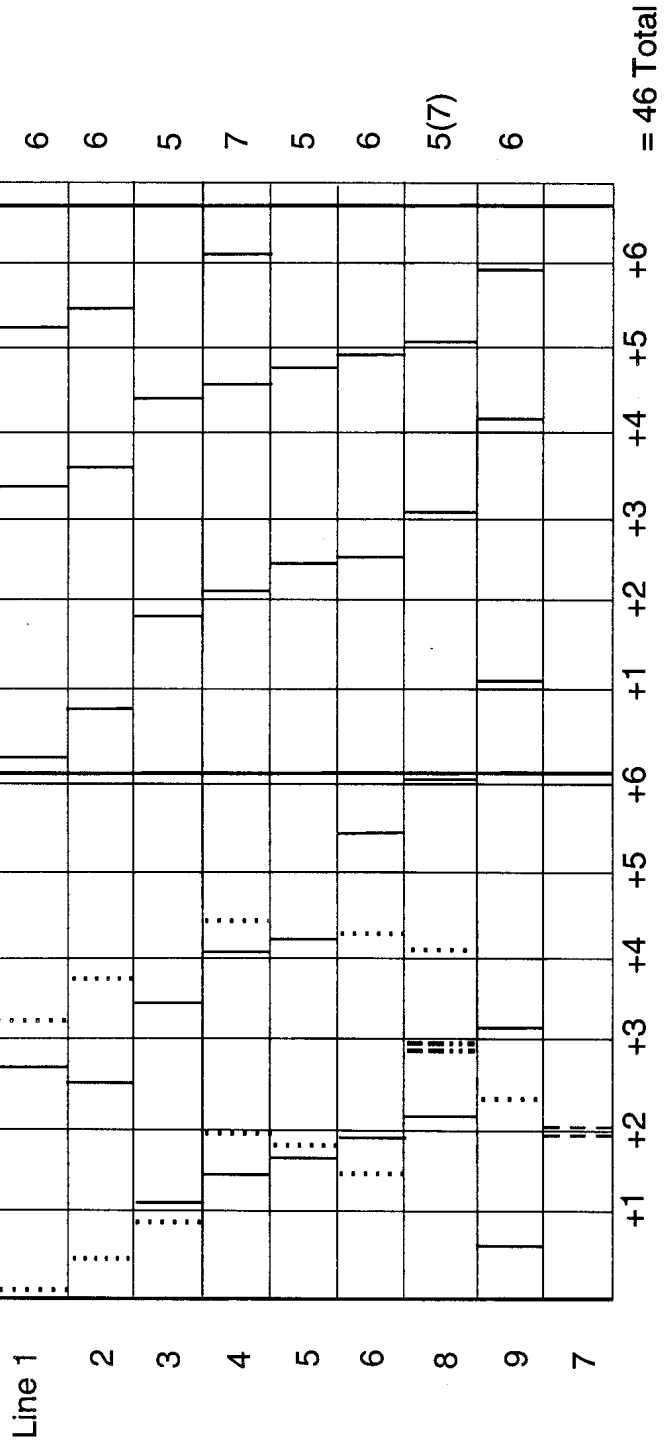

Figure D1. Data coverage matrix

Table D2. Water samples and siltmeter calibration data plus siltmeter vertical profiles, 11/2/00–11/3/00

Line	Time	Water Sample #	Bottle Sample (ppm)	Siltmeter Reading		Temperature	Salinity	Depth (feet)
				25JTU	175JTU			
Thursday, November 2, 2000								
9	0925	O/C121	6.3	-	3.5	21.46	4.1	3
9	0929	O/C122	-	-	3.8	22.16	5.0	5
9	0932	O/C122	4.29	-	3.7	21.91	5.87	5
Misfire bottle did not close								
3	0957	O/C123	6.48	4.2	5.9	22.38	5.0	3
3	1000	O/C124	5.33	3.9	4.8	22.59	5.8	5
4	1015	O/C125	9.05	6.2	7.0	22.44	5.6	4
5	1024	O/C126	8.76	6.6	8.1	22.40	5.6	4
6	1027	O/C127	8.86	7.6	8.7	22.43	5.9	4
Line 7 too shallow sampling / ADCP traverse abandoned								
8	1054	O/C128	10.10	9.3	11.2	21.80	Variable 4.1 (5.3)	5
8	1056	O/C129	6.51	7.7	9.2	21.97	5.2	3
Line 2 bad ADCP data – no sample								
1	1136	O/C130	12.95	5.9	7.9	22.46	6.4	7
1	1139	O/C131	9.71	6.3	7.9	22.96	Variable 6.5 (6.1)	6
1	1142	O/C132	9.72	5.2	6.4	22.81	6.1	4
9	1203	O/C133	6.29	3.5	4.4	22.26	5.1	5
9	1205	O/C134	3.24	3.1	4.0	21.96	3.9	3
3	1224	O/C135	7.43	4.2	5.1	22.51	6.2 South Side	4
3	1227	O/C136	Discarded bottle leaking	7.4	8.9	22.61	6.2 center of channel	4
3	1233	O/C137	6.29	1.9	4.6	23.93	5.7 North Side	4
4	1250	O/C138	11.14	5.1	7.8	22.62	5.7	4
4	1252	O/C139	6.19	5.0	6.9	24.43	6.2	5
4	1253	O/C140	9.25	No readings. Siltmeter slipped behind mounting tape		22.68	5.2	3
5	1305	O/C141	7.62	5.0	6.5	22.83	5.9	4
6	1430	O/C142	18.11	Siltmeter failed, no readings		22.62	6.0	5
6	1440	O/C143	9.05			22.49	5.7	3
8	1454	O/C144	9.91			23.15	3.7	4
1	1525	O/C145	7.33			23.88	5.5 At dock.	4
1	1528	O/C146	7.43			23.70	5.9 Red roofed	5
1	1531	O/C147	7.52			23.50	6.0 house	6
2	1543	O/C148	5.14			24.05	6.0	3
2	1545	O/C149	5.33			23.93	6.0	4
9	1611	O/C150	7.70			22.80	5.7	7
9	1613	O/C151	8.00			23.26	5.5	5
9	1615	O/C152	3.24			23.24	5.0	3
3	1650	O/C153	5.05	Siltmeter failed, no readings		22.82	4.6	4
3	1654	O/C154	6.95			23.21	5.7	5
3	1656	O/C155	6.29			23.88	5.9	3
4	1709	O/C156	7.52			23.36	5.3	3
4	1711	O/C157	7.52			23.27	6.1	4
5	1718	O/C158	11.70			23.16	5.7	4
5	1721	O/C159	7.33			23.06	Variable 5.8 (6.0)	4
6	1735	O/C160	5.14			22.61	5.2	4
6	1736	O/C161	4.48			23.32	5.7	3
8	1753	O/C162	12.48			22.26	5.3	6

Table D.2—continued

Line	Time	Water Sample #	Bottle Sample (ppm)	Siltmeter Reading		Temperature	Salinity	Depth (feet)
				25JTU	175JTU			
Thursday, November 2, 2000—continued								
8	1754	O/C163	5.05			23.63	5.2	4
1	1825	O/C164	8.48			23.11	5.6	5
1	1929	O/C165	5.81			23.63	5.9	3
Friday, November 3, 2000								
1	0954	O/C166	6.00	3.1	4.0	22.44	5.9	6
1	0955	O/C167	5.43	3.0	4.0	22.45	5.8	5
1	0956	O/C168	5.05	2.8	Variable 4.0 (3.8)	22.52	5.7	3
2	1003	O/C169	7.52	3.6	5.3	Variable 22.51(22.44)	5.8	3

Table D3. Vertical silt, temperature and salinity profile no. 1 at line 2 Big Fish Weir Creek in six-inch increments: Center channel; start 1010; finish 1015

Number	25 JTU	175 JTU	Temperature	Salinity	Depth
OBS1	2.4	3.2	22.58	5.6	6"
OBS2	2.4	3.3	22.61	5.6	12"
OBS3	2.8	3.6	22.61	5.6	18"
OBS4	2.7	3.6	22.69	5.6	2'
OBS5	2.8	3.6	22.58	5.6	2 ½'
OBS6	1.9	2.1	22.62	5.8	3'
OBS7	(2.0-2.1-2.3)	3.0	22.64	5.9	3 ½'
OBS8	2.6	3.8	22.65	5.9	4'
OBS9	3.4	4.8	22.65	5.9	4 ½'
Bottle hit bed before 5' reached			22.69	5.8	5'

Line	Time	Water Sample #	ppm	25JTU	175JTU	Temperature	Salinity	Depth (feet)
3	1043	O/C170	6.48	5.3	-	22.37	5.6	6
3	1045	O/C171	5.62	5.7	7.2	22.40	5.5	5
3	1046	O/C172	5.14	4.1	5.8	22.63	5.4	3

Table D4. Vertical silt, temperature and salinity profile no. 2 at line 3 in six-inch increments: Center channel; start 1050; finish 1054

Number	25 JTU	175 JTU	Temperature	Salinity	Depth
OBS1	4.2	5.6	23.35	5.3	6"
OBS2	4.3	5.8	23.44	5.3	12"
OBS3	4.3	5.7	23.46	5.3	18"
OBS4	4.2	5.3	22.89	5.3	2'
OBS5	4.0	5.3	22.77	5.4	2 ½'
OBS6	3.9	5.1	22.73	5.4	3'
OBS7	3.9	5.4	22.53	5.5	3 ½'
OBS8	4.1	5.6	22.41	5.5	4'
OBS9	4.8	6.5	22.29	5.6	4 ½'
OBS10	5.4	6.9	22.35	5.6	5'
OBS11	5.6	7.6	22.36	5.6	5 ½'
OBS12	5.7	7.8	22.37	5.7	6'
OBS13	Hit bottom before 6 ½“				

Line	Time	Water Sample #	ppm	25JTU	175JTU	Temperature	Salinity	Depth (feet)
6	1105	O/C173	8.29	6.3	8.9	22.37	5.6	3

Table D5. Vertical silt, temperature and salinity profile no. 3 at line 6 in six-inch increments: Center channel; start 1107; finish 1112

Number	25 JTU	175 JTU	Temperature	Salinity	Depth
OBS1	(unstable) 4.8	9.3	22.83	5.4	6"
OBS2	6.4	9.2	22.88	5.4	12"
OBS3	6.5	9.2	22.79	5.4	18"
OBS4	6.7	9.3	22.77	5.4	2'
OBS5	6.5	8.5	22.65	5.4	2 1/2'
OBS6	5.9	8.3	22.33	5.5	3'
OBS7	6.1	8.3	22.30	5.5	3 1/2'
OBS8	5.9	8.1	22.35	5.6	4'

Hit bottom before 4 ½' :

Line	Time	Water Sample #	ppm	25JTU	175JTU	Temperature	Salinity	Depth (feet)
5	1120	O/C174	10.38	variable 7.6 (8.2)	10.4	22.40	5.5	4
5	1122	O/C175	11.15	8.1	11.3	22.96	5.5	3
4	1138	O/C176	–	4.9	9.6	22.41	5.6	5
4	Repeat	O/C176	6.86	5.4	9.8	22.50	5.6	center line 5
4	1141	O/C177	8.10	4.8	8.1	22.36	5.3	3
9	1155	O/C178	7.43	4.5	(7.8) 8.0	21.82	4.6	6
9	1156	O/C179	4.86	4.1	6.9	21.81	4.3	5
9	1158	O/C180	6.57	3.7	6.5	22.37	4.2	3

Table D6. Vertical silt, temperature and salinity profile no. 5 at line 9 in six-inch increments slightly to N of mid-line close to Timuquana Bridge: start 1200; finish 1207

Number	25 JTU	175 JTU	Temperature	Salinity	Depth
OBS1	4.3 (0.2—spurious, sunlight)	7.0	23.07	4.2	6"
OBS2	4.5	7.2	23.04	4.2	12”
OBS3	4.4	7.3	22.96	4.2	18"
OBS4	4.5	7.2	22.85	4.2	2'
OBS5	4.5	7.5	22.74	4.2	2 ½'
Interference to ADCP from bridge supports, vessel moved.					
OBS5 (repeat)	3.9	6.7	22.13	4.0	2 ½'
OBS6	4.2	5.8	22.05	4.0	3'
OBS7	3.2	5.4	21.50	4.0	3 ½'
OBS8	3.2	5.5	21.51	4.1	4'
OBS9	3.3	5.8	21.55	4.3	4 ½'
OBS10	3.5	6.2	21.59	4.3	5'
OBS11	4.0	6.6	21.86	4.7	5 ½'
OBS12	3.7	6.3	22.12	5.0	6'
OBS13	4.6	7.1	22.26	5.2	6 ½'
OBS14	4.6	7.4	22.31	5.2	7'
OBS15	5.0	7.7	22.31	5.2	7 ½'
Hit bottom adjacent to bridge piile					

Line	Time	Water Sample #	ppm	25JTU	175JTU	Temperature	Salinity	Depth (feet)
1	1301	O/C181	7.14	4.9	11.4	22.84	5.7	8
1	1303	O/C182	8.75	4.9	10.4	23.15	5.5	6
1	1304	O/C183	7.43	4.5	9.8	23.44	5.5	4
1	1306	O/C184	7.31	4.3	8.8	23.38	5.5	3

Table D7. Vertical silt, temperature and salinity profile no. 6 at line 1 in foot increments: Poss towards Southside; start 1308; finish 1313

Number	25 JTU	175 JTU	Temperature	Salinity	Depth
OBS1	4.0	8.4	23.63	5.5	1
OBS2	4.0	8.5	23.52	5.5	2
OBS3	4.3	8.9	23.27	5.5	3
OBS4	4.2	9.3	23.18	5.5	4
OBS5	4.9	9.2	22.90	5.5	5
OBS6	6.5	12.2	22.84	5.6	6
OBS7	7.3	12.3	22.79	5.6	7
OBS8	7.3	12.3	22.74	5.7	7 ½
OBS9	7.4	12.4	22.73	5.7	8
OBS10	7.6	12.8	22.73	5.7	8 ½

Line	Time	Water Sample #	ppm	25JTU	175JTU	Temperature	Salinity	Depth (feet)
8	1340	O/C185	–	10.3		22.59	5.4	5
ADCP lost bottom track								
8	1340	O/C185	9.71	10.7	18.7	22.75	5.4	5
8	1343	O/C186	9.81	10.1	16.9	22.74	5.4	4

(Page intentionally blank)

Appendix E

Effect of Fine Sediment Trapping in an Estuary

by

Vladimir A. Paramygin

A thesis presented to the Graduate School of
the University of Florida in partial fulfillment
of the requirements for the degree of
Master of Science

2002

Contents

List of Figures

List of Tables

E1. Introduction

E1.1 Problem Statement

Sediment shoaling in estuarine environments can create significant problems such as degradation of water quality and concentration of organic matter and contaminants. Accumulated organic-rich sediment can increase contaminant loads in these waters, because contaminants such as polychlorinated biphenyls (PCBs) and polyaromatic hydrocarbons (PAHs) are preferentially bound to organics (National Research Council 2001).

A commonly implemented solution to reduce sedimentation is the construction of a sediment trap. Such traps can be of different types; however, all of them rely the same basic mechanism–decreasing the speed of the flow, thus allowing the larger portion of the suspended sediment load to settle out in the trap. Traps can be on-line or off-line. One example of an on-line trap is a dredged trench along the submerged bottom, which reduces the flow velocity and causes the material to settle there. An off-line trap is made by artificially diverting part of the flow into a natural/artificial pond, which would reduce flow velocity and increase deposition. Selecting the Cedar River in northern Florida as a case study, Stoddard (2001) examined the efficiency of a trap trenched at the bottom of the river. In the present study, the efficiency of a trap created by ponding along the side of the same river is explored.

For the present purposes, trap efficiency will be determined by the sediment removal ratio, i.e., the percentage by which the effluent sediment load is reduced with respect to the influent load (Ganju 2001). By creating efficient traps, much of the detrimental effects of excess sediment and unwanted contaminants entering the system can be curtailed.

E1.2 Cedar River

Cedar River estuary occurs in northeast Florida. Trapping contaminants in this river has become essential due to elevated concentrations of sediment-bound PCBs in water resulting from leaching of sediment and runoff from the site of a chemical company since January 1984. The site is located approximately 0.5 km east of the Cedar River near its headwaters, adjacent to municipal storm drains and drainage ditches. There, fire destroyed several tanks storing high concentrations (4,425 ppm) of PCB-laden oils and other materials. It is believed that a combination of damage to the storage tanks and the fire-fighting effort caused PCBs to enter the Cedar River basin. The surrounding groundwater and soils were sampled extensively in 1989, and the concentrations were still significantly above the regulated amount of 50 ppm.

Estuaries characteristically trap significant quantities of particulate matter through a wide variety of physical and biochemical processes. Fine-grained sediments play an important role in these processes. Due to relatively strong currents, fine sediments, which are mixtures of clay- and silt-sized material, are usually very mobile. In the Cedar River they are admixed with organic matter derived from local terrestrial and aquatic sources.

Fine sediment transport is mainly defined by the hydrodynamic action, which advects the suspended matter and provides the bed erosion force. Also, turbulence plays a major role in the flocculation of fine, cohesive sediments. Flocs are formed by the joining of individual particles and can greatly affect the settling velocity of particulate matter.

The St. Johns River Water Management District of Palatka, Florida is considering the possibility of establishing off-line sediment traps upstream along the Cedar River, and would like to have an estimate of the influence of this entrapment on sediment influx at the downstream end of Cedar River, at its confluence with the Ortega River, where heavy accumulation of PCB-laden, organic-rich sediment has occurred.

E1.3 Objective and Tasks

The objective of this study was to determine the effect of traps with different efficiencies at selected locations upstream in Cedar River to sediment flux at the confluence of Cedar and Ortega Rivers downstream. Several tasks were undertaken to achieve this objective including:

1. Use of data to characterize the nature of flow. Data included tidal elevations, current velocities, wind speed and direction, salinity, streamflows at the major tributaries of the Cedar River and the Cedar River itself, and suspended sediment concentrations.

2. Modeling the flow field using a numerical code to determine water velocities, water surface elevations and bed shear stresses.

3. Modeling fine sediment settling velocity as a function of the local flow conditions.

4. Use of a sediment transport model (with implemented settling velocity model) to determine suspended sediment concentrations within the modeled domain.

5. Using the calibrated flow and sediment models, modeling flow and sediment transport in the estuary with the sediment traps (with three assumed efficiencies—30%, 60% and 90%) and without the traps.

6. Comparison of the results of above modeling in terms of sediment transport at the downstream end of Cedar River to assess the effects of above traps.

E1.4 Outline of Thesis Sections

Section E2 describes the flow and sediment transport model used to evaluate trap efficiency. Section E3 contains the field data collected for this study. Section E4 describes the calibration and validation of the model using measured data. Finally, Section E5 contains the summary and conclusions, followed by bibliography.

E2. Method of Analysis

E2.1 Introduction

This section (Section E2) provides a description of the hydrodynamic and sediment models that were used to model flow and the sediment transport in the Cedar River. The section gives basic equations, numerical method used to solve these equations, and the capabilities and limitations of the models for problem analysis.

The Environmental Fluid Dynamics Code (EFDC) used herein implements a numerical algorithm for estuarine flows (Hamrick 1996). It contains a three-dimensional, hydrostatic flow model, as well as a compatible sediment model.

E2.2 Flow Field

The coordinate system of the model is curvilinear and orthogonal in the horizontal (x, y) plane. In the vertical, z, direction, which is aligned with the gravity vector, it is stretched to follow the bottom topography and free surface displacement (σ-grid). A level 2.5 turbulence closure scheme (Mellor and Yamada 1982) in the hydrodynamic model relates the turbulent viscosity and diffusivity to the turbulence intensity and a turbulence length scale. An equation of state relates density to pressure, salinity, temperature and suspended sediment concentration (Hamrick 1992).

The momentum equations in the model are

$$\begin{aligned}&\partial_t(m_x m_y Hu)+\partial_x(m_y Huu)+\partial_y(m_x Hvu)+\partial_z(m_x m_y wu)-f_e m_x m_y Hv\\&=-m_y H\partial_x(p+p_{atm}+\phi)+m_y(\partial_x z_b^*+z\partial_x H)\partial_z p+\partial_z\left(m_x m_y\frac{A_v}{H}\partial_z u\right)\\&+\partial_x\left(\frac{m_y}{m_x}HA_H\partial_x u\right)+\partial_y\left(\frac{m_x}{m_y}HA_H\partial_y u\right)-m_x m_y c_p D_p\left(u^2+v^2\right)^{1/2}u\end{aligned} \tag{E.1}$$

$$\begin{aligned}&\partial_t(m_x m_y Hv)+\partial_x(m_y Huv)+\partial_y(m_x Hvv)+\partial_z(m_x m_y wv)-f_e m_x m_y Hu\\&=-m_x H\partial_y(p+p_{atm}+\phi)+m_x(\partial_y z_b^*+z\partial_y H)\partial_z p+\partial_z\left(m_x m_y\frac{A_v}{H}\partial_z v\right)\\&+\partial_x\left(\frac{m_y}{m_x}HA_H\partial_x v\right)+\partial_y\left(\frac{m_x}{m_y}HA_H\partial_y v\right)-m_x m_y c_p D_p\left(u^2+v^2\right)^{1/2}v\end{aligned} \tag{E.2}$$

$$m_x m_y f_e = m_x m_y f - u\partial_y m_x + v\partial_x m_y \tag{E.3}$$

$$\left(\tau_{xz},\tau_{yz}\right)=A_v H^{-1}\partial_z\left(u,v\right) \tag{E.4}$$

where u and v are the horizontal velocity components in the x, y coordinate directions, respectively, and w is the vertical velocity; m_x and m_y are the scale factors of the horizontal coordinates; z_s^* and z_b^* are the vertical coordinates of the free surface and bottom bed, respectively; H is a total water column depth; $\phi = gz_s^*$ is a free surface potential; f_e is the effective Coriolis acceleration and incorporates curvature acceleration terms with the Coriolis parameter, f as in Equation E.3; A_H and A_v are the horizontal and vertical turbulent viscosities, respectively, where A_v relates the shear stresses to the vertical shear of the horizontal velocity components; the last terms in Equations E.1 and E.2 represent vegetation resistance, where c_p is a resistance coefficient and D_p is the dimensionless projected vegetation area normal to the flow per unit horizontal area; and p_{atm} is the kinematic atmospheric pressure referenced to water density. The excess hydrostatic pressure in the water column is

$$\partial_z p = -gHb = -gH\left(\rho-\rho_0\right)\rho_0^{-1} \tag{E.5}$$

where

$$\rho = \rho\left(p,S,T\right) \tag{E.6}$$

and ρ and ρ_0 are the actual and reference water densities, respectively, and b is buoyancy.

The three-dimensional continuity equation in the model is

$$\partial_t\left(m_x m_y H\right)+\partial_x\left(m_y Hu\right)+\partial_y\left(m_x Hv\right)+\partial_z\left(m_x m_y w\right)=Q_H \tag{E.7}$$

and the corresponding vertically-integrated form of the continuity equation is

$$\partial_t\left(m_x m_y H\right)+\partial_x\left(m_y H\overline{u}\right)+\partial_y\left(m_x H\overline{v}\right)=\overline{Q}_H \tag{E.8}$$

where Q_H represents volume sources and sinks including rainfall, evaporation, infiltration and lateral inflows and outflows having negligible momentum fluxes.

Transport equations for temperature and salinity are

$$\partial_t\left(mHS\right)+\partial_x\left(mHuS\right)+\partial_y\left(mHvS\right)+\partial_z\left(mwS\right)=\partial_z\left(mH^{-1}A_b\partial_z S\right)+Q_S \tag{E.9}$$

$$\partial_t\left(mHT\right)+\partial_x\left(mHuT\right)+\partial_y\left(mHvT\right)+\partial_z\left(mwT\right)=\partial_z\left(mH^{-1}A_b\partial_z T\right)+Q_T \tag{E.10}$$

where Q_T and Q_S are source and sink terms, respectively, which include sub-grid scale horizontal diffusion and thermal sources and sinks, and A_b is the vertical turbulent diffusivity.

Two transport equations determine the turbulent intensity and turbulent length scale as follows:

$$\begin{aligned}&\partial_t\left(m_x m_y H q^2\right)+\partial_x\left(m_y H u q^2\right)+\partial_y\left(m_x H v q^2\right)+\partial_z\left(m_x m_y w q^2\right)\\&=\partial_z\left(m_x m_y \frac{A_q}{H}\partial_z q^2\right)-2m_x m_y \frac{H q^3}{B_1 l}\\&+2m_x m_y\left(\frac{A_v}{H}\left(\left(\partial_z u\right)^2+\left(\partial_z v\right)^2\right)+\eta_p c_p D_p\left(u^2+v^2\right)^{\frac{3}{2}}+gK_v\partial_z b\right)+Q_q\end{aligned} \tag{E.11}$$

$$\begin{aligned}&\partial_t\left(m_x m_y H q^2 l\right)+\partial_x\left(m_y H u q_2 l\right)+\partial_y\left(m_x H v q^2 l\right)+\partial_z\left(m_x m_y w q^2 l\right)\\&=\partial_z\left(m_x m_y \frac{A_q}{H}\partial_z\left(q^2 l\right)\right)-m_x m_y \frac{H q^3}{B_1}\left(1+E_2\left(\frac{1}{kHz}\right)^2+E_3\left(\frac{1}{kH\left(1-z\right)}\right)^2\right)\\&+m_x m_y E_1 l\left(\frac{A_v}{H}\left(\left(\partial_z u\right)^2+\left(\partial_z v\right)^2\right)+gK_v\partial_z b+\eta_p c_p D_p\left(u^2+v^2\right)^{\frac{3}{2}}\right)+Q_l\end{aligned} \tag{E.12}$$

where $\left(E_1, E_2, E_3\right)=\left(1.8,1.33,0.25\right)$ are empirical constants, Q_q and Q_l represent additional source-sink terms, and the third term in the last line of both equations represents net turbulent energy production by vegetation drag with a production efficiency factor of η_p.

Equation E.4, which specifies the kinematic shear stress at the bed and free surfaces, provides the vertical boundary conditions for the solution of the momentum equations. At the free surface, the shear stress boundary conditions are given by the water surface wind stress

$$\left(\tau_{xz}, \tau_{xz}\right)=\left(\tau_{sx}, \tau_{sy}\right)=c_s\sqrt{U_w^2+V_w^2}\left(U_w, V_w\right) \tag{E.13}$$

where U_w and V_w are the x and y components of the wind velocity, respectively, 10 m above the water surface. The wind stress coefficient for the wind velocity components is

$$c_s=0.001\frac{\rho_a}{\rho_w}\left(0.8+0.065\sqrt{U_w^2+V_w^2}\right) \tag{E.14}$$

where ρ_a and ρ_w are the air and water densities. At the bed, the shear stress components are considered to be related to the near-bed or bottom layer velocity components as follows:

$$\left(\tau_{xz},\tau_{xz}\right)=\left(\tau_{bx},\tau_{by}\right)=c_s\sqrt{u_1^2+v_1^2}\left(u_1,v_1\right) \tag{E.15}$$

where u_1 and v_1 are the bottom layer velocity components and the bottom stress coefficient is

$$c_b=\left(\frac{\kappa}{\ln\left(\frac{\Delta_1}{2z_0}\right)}\right)^2 \tag{E.16}$$

which assumes that the near-bottom velocity profile is logarithmic. In Equation E.16 κ is the von Karman constant, Δ_1 is the dimensionless thickness of the bottom layer, and $z_0=\frac{z_0^*}{H}$ is the dimensionless roughness height.

The vertical boundary conditions for the turbulent kinetic energy and length scale equations are

$$q^2=B_1^{\frac{2}{3}}\left|\tau_s\right| \quad : \quad z=1 \tag{E.17}$$

$$q^2=B_1^{\frac{2}{3}}\left|\tau_b\right| \quad : \quad z=0 \tag{E.18}$$

$$l=0 \quad : \quad z=0,1 \tag{E.19}$$

The above set of equations forms a closed system that is solved by a numerical method (Hamrick 1992).

The model uses the finite volume method to bring the partial differential equation into a discrete form. The Smolarkiewicz (1983) scheme is used to solve for the 2D advection problem. An external/internal mode splitting procedure is implemented to increase the numerical efficiency of the code.

E2.3 Sediment Transport

The transport equation for a dissolved or suspended material having a mass per unit volume concentration C is

$$\begin{aligned}&\partial_t\left(m_xm_yHC\right)+\partial_x\left(m_yHuC\right)+\partial_y\left(m_xHvC\right)+\partial_z\left(m_xm_ywC\right)-\partial_z\left(m_xm_yw_{sc}C\right)\\&=\partial_x\left(\frac{m_y}{m_x}HK_H\partial_xC\right)+\partial_y\left(\frac{m_x}{m_y}HK_H\partial_yv\right)+\partial_z\left(m_xm_y\frac{K_v}{H}\partial_zC\right)+Q_C\end{aligned} \tag{E.20}$$

where K_H and K_v are the horizontal and vertical turbulent diffusion coefficients, respectively, w_{sc} is (a positive) settling velocity when C represents suspended matter, and Q_C represents external, and reactive internal, sources and sinks.

Due to a small numerical diffusion that remains inherent in the scheme used to solve the sediment transport equation, the horizontal diffusion terms are omitted from Equation E.20. This results in

$$\begin{aligned}&\partial_t\left(m_x m_y H S_j\right)+\partial_x\left(m_y H v S_j\right)+\partial_y\left(m_x H v S_j\right)+\partial_z\left(m_x m_y w S_j\right)\\&-\partial_z\left(m_x m_y w_{sj} S_j\right)=\partial_z\left(m_x m_y \frac{K_V}{H}\partial_z S_j\right)+Q_{sj}^E+Q_{sj}^I\end{aligned} \tag{E.21}$$

where S_j represents the concentration of the j-th sediment class. Source-sink are represented by two terms: an external part, which would include point and non-point source loads, and an internal part, which could include reactive decay of organic sediment, or exchange of mass between sediment classes when floc growth and breakup are simulated.

The vertical boundary conditions for Equation E.21 are

$$\begin{aligned}&-\frac{K_V}{H}\partial_z S_j - w_s S = J_0 :\ z\approx 0\\&-\frac{K_V}{H}\partial_z S_j - w_{sj} S_j = 0 :\ z\approx 1\end{aligned} \tag{E.22}$$

where J_0 is the net water column-bed exchange flux (Hamrick 1992).

E2.4 Settling Velocity Calculation

E2.4.1 Background

A settling velocity algorithm was implemented, as part of the present study, in the sediment transport code. The algorithm calculates the settling velocity of the particles by accounting for the floc growth and breakup processes that occur for fine-grained sediment in estuarine and coastal waters due to different mechanisms. As a result, instead of using the settling velocity measured in a laboratory settling column in still water directly, the model is merely calibrated using laboratory data.

There are a number of models in which the settling velocity is expressed as an analytical function of the shear rate and the sediment concentration. Also, there are some models that take a different approach in which the settling velocity only depends on the properties of the primary particles. Generally, the former use the median (or mean) size of the particles and the latter use a multi-class approach, in which particle sizes are defined by a

discrete distribution function. Both approaches have their advantages and disadvantages. The former models usually depend on empirical coefficients, about which a very little is known in most cases. The latter, however, require significant computational time and, even though they are useful in simulating simple cases, high memory and processing power requirements make them almost unusable for simulations with large grids and for significant periods of time. Accordingly, in this study an attempt has been made to implement a simple settling velocity model dependent on empirical coefficients, but which includes the basic physics of floc growth and breakup.

Floc growth/breakup can be triggered by different mechanisms—Brownian motion, turbulent motion and differential settling. The following model only accounts for the turbulence effect on growth/breakup. By analyzing theoretical results presented in the literature and carrying out their own experiments in a settling column, Stolzenbach and Elimelich (1994) concluded that the effect of the differential settling is minor and may be practically absent in many turbulent flow situations. This would be the case because the probability of the event when a particle with a large settling velocity overtakes a particle with a smaller settling velocity is small, due to the fact that the trajectories of the two particles tend to be deflected from one another. Also, the Brownian motion effect on growth/breakup can be considered to be negligible in estuaries (Winterwerp 1998).

Dyer (1989) presented a schematic description of the dependence of floc (median) diameter on both turbulence and sediment concentration, as shown in Figure E1.

At very low concentrations and shear stresses, collisions are rare and the floc growth rate is very small. Increasing fluid shear increases the number of collisions, thus forming larger particles. A further increase in shear stress, however, causes the floc breakup process to dominate over the floc growth, thus decreasing floc size. Also, increasing sediment

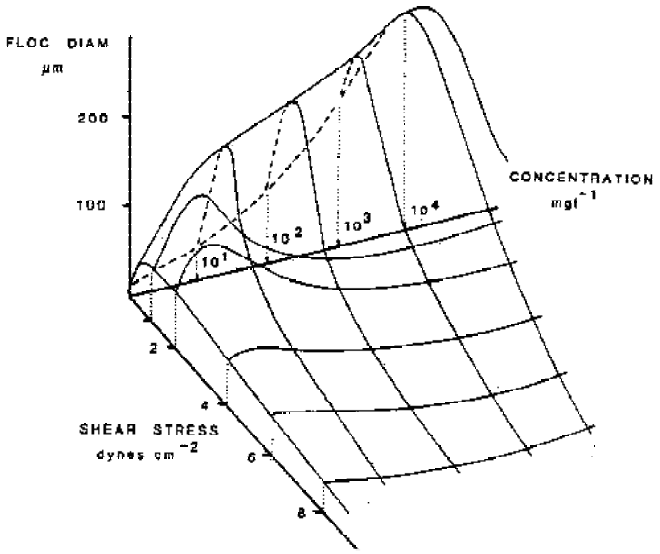

Figure E1. Effect of sediment concentration and fluid shear stress on the median floc diameter (Dyer 1989)

concentration increases the particle collision frequency, thus causing the median floc size to increase. However, above approximately 10 kg/m3, flocs start to disaggregate due to the low shear strength of the larger particles, which makes them fragile.

A study of growth/breakup of fine sediment based on multi-class grain size distribution, two- and three-body collisions, Brownian motion and differential settling was done by McAnally and Mehta (2001). They present a set of equations that characterize the growth/breakup mechanisms. These equations depend on primary particle properties, flow properties and two empirical parameters: a collision diameter function and collision efficiency. (However, collision efficiency can also be related to the collision diameter, thus the system only contains one empirical, heuristic parameter). They propose expressions for both, collision diameter and collision efficiency functions, based on dimensionless arguments, and provide fitted forms of those functions using experimental data:

Collision diameter function:

$$F_c^2 = \prod_c \left[\left(\frac{\Delta\rho_i D_i^3}{\Delta\rho_m D_m^3} \right), \frac{u_i \left(D_i + D_m \right)}{\nu}, \left(\frac{S}{S_0} \right), \left(\frac{D_g}{D_1} \right), \left(\frac{T_c}{T_0} \right), \left(\frac{CEC}{CEC_0} \right) \right] \tag{E.23}$$

Collision efficiency function:

$$\alpha' = \prod_\alpha \left[\frac{\left(\frac{D_g}{D_1} \right) \left(\frac{S}{S_0} \right) \left(1 - 0.875 \frac{T_c}{T_0} \right) \left(\frac{CEC}{CEC_0} \right) \left(\frac{\tau_m}{\tau_{im,m} + \tau_u} \right)}{\left(\frac{\Delta\rho_i D_i^3}{\Delta\rho_m D_m^3} \right) \left(\frac{u_i \left(D_i + D_m \right)}{\nu} \right)} \right] \tag{E.24}$$

where $\prod_c$ is some function of the bracketed non-dimensional terms; indices i and m denote the colliding particle size classes; D_g = diameter of primary grain; D_1 = reference particle size; S = salinity; S_0 = reference salinity; T_c = fluid temperature, deg Celsius; T_0 = reference temperature; D_i , D_m = particle diameters, $\Delta\rho_i$ and $\Delta\rho_m$ = differential densities of the particles; ν = kinematic viscosity of the fluid; u_i = velocity of particles; τ_u = maximum flow induced shear stress in a spherical particle; $\tau_{im,m}$ = shear stress experienced by the m aggregate and CEC, CEC_0 = actual and reference cation exchange capacities, respectively.

Parshukov (2002) presents a multi-class grain size settling velocity model, which implements the collision mechanisms presented in McAnally and Mehta (2001), and combines them with other turbulence related parameters and settling velocity expressions to represent growth/breakup. Testing of the model was done using laboratory data involving grid-generated turbulence and its effect on the settling of flocculated clays.

E2.4.2 Particle Density and Fractal Representation

For estuarine flocs the relation between the volumetric and mass concentrations, ϕ and c, respectively, and between ϕ and the number of particles per unit volume, n, is given by:

$$\phi = \left(\frac{\rho_s - \rho_w}{\rho_f - \rho_w} \right) \frac{c}{\rho_s} = f_s n D^3 \tag{E.25}$$

where ρ_s = is the sediment density; ρ_f = floc density; ρ_w = water density; c = sediment concentration; f_s = is a shape factor (for spherical particles $f_s = \pi/6$); and D = particle diameter.

It is has been shown elsewhere that mud flocs can be treated as fractal entities (Krone 1984, Huang 1994). Kranenburg (1994) shows that the differential density $\Delta\rho_f$ can be related to the fractal dimension of the particles using the formulation

$$\Delta\rho_f = \rho_f - \rho_w \propto \left(\rho_f - \rho_w \right) \left[\frac{D_p}{D} \right]^{3-nf} \tag{E.26}$$

where D is the particle diameter, D_p is the diameter of the primary particles and nf is the fractal dimension. The fractal dimension for strong estuarine flocs is found to be in a range of 2.1-2.3 (Winterwerp 1998).

E2.4.3 Settling Velocity

A settling velocity function including the effects of both concentration and fluid shear rate was proposed by van Leussen (1994):

$$W_s = W_{s,0} \frac{(1 + aG)}{(1 + bG^2)} \tag{E.27}$$

where W_s and $W_{s,0}$ are the actual settling velocity and reference settling velocity, respectively, G is the dissipation parameter or the rate of flow shear, and a,b are empirical constants.

Teeter (2001) proposed a more advanced functional relationship:

$$W_s = a_1 \left(\frac{C}{C_{ul}} \right)^n \left[\left(\frac{1 + a_2 G}{1 + a_3 G^2} \right) \exp\left(-a_4 \frac{C}{C_{ll}} \right) + 1 \right] \tag{E.28}$$

where C_{ul} and C_{ll} are mass-weighted average upper and lower reference concentrations, respectively; and n, a_1, a_2, a_3 and a_4 are the empirical parameters.

Using the force balance for a settling particle, one can obtain an implicit formula for the settling velocity in still water, which depends on the fractal dimension (Winterwerp 1998):

$$W_s = \frac{\alpha}{18\beta}\frac{(\rho_s - \rho_w)g}{\mu} D_p^{3-nf} \frac{D^{nf-1}}{1 + 0.15\,\mathrm{Re}^{0.687}} \tag{E.29}$$

where α, β are the coefficient that depend on particle sphericity, these coefficients will be taken as 1 (spherical particles) here; μ = dynamic viscosity and Re = settling Reynolds number, $\frac{\rho_w W_s D_p}{\mu}$.

Figure E2 shows the relationship between the floc diameter and the settling velocity in still water, as described by Equation E.29.

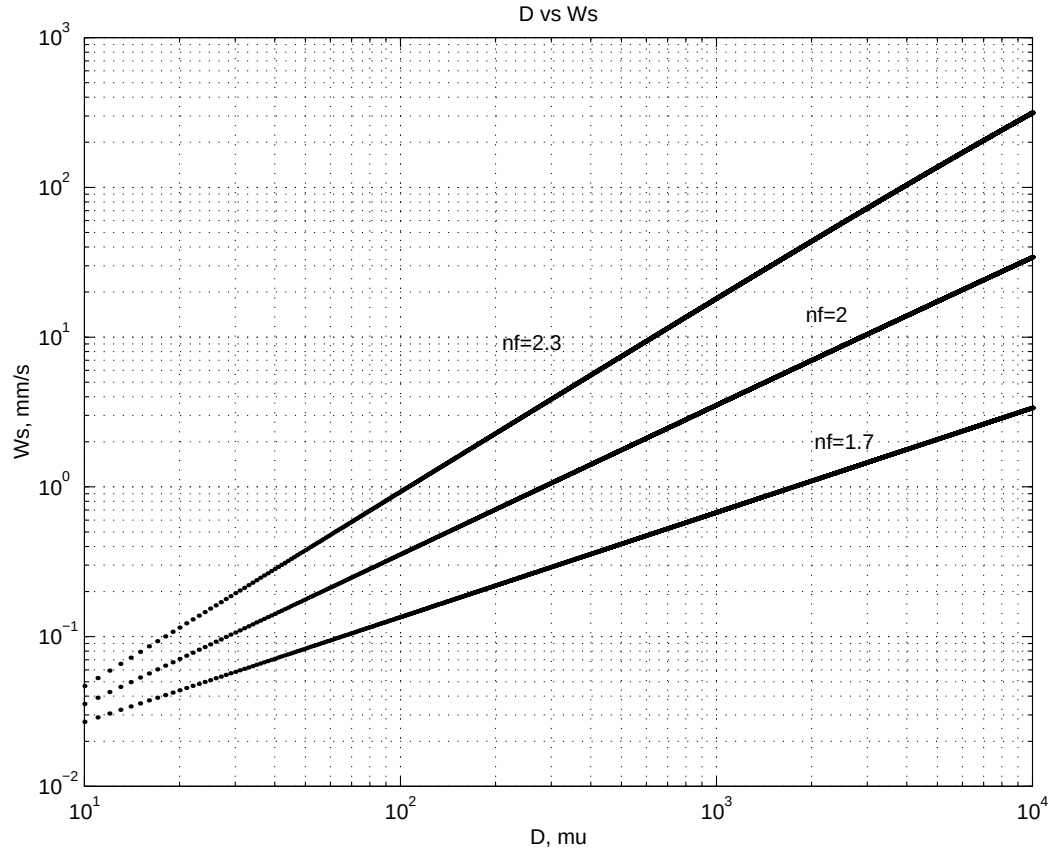

Figure E2. Relationship between settling velocity and floc diameter in still water, based on Equation E.29

E2.4.4 Floc Growth and Breakup Functions

In the following equations the effect of turbulence is expressed through the energy dissipation parameter G, defined as

$$G = \sqrt{\frac{\varepsilon}{\upsilon}} = \sqrt{\frac{\tau \frac{du}{dz}}{\mu}} \tag{E.30}$$

where ε = energy dissipation rate of flow, υ = kinematic viscosity of the fluid, μ = dynamic viscosity of the fluid, τ = fluid shear stress and u = mean flow velocity.

Levich (1962) determined the rate of coagulation of particles in a turbulent fluid by integrating the diffusion equation over a finite volume n:

$$\frac{dn}{dt} = -\frac{3}{2} e_c \pi e_d G D^3 n^2 \tag{E.31}$$

where e_c, e_d are the collision and diffusion efficiency parameters, respectively. Combining it with Equations E.25 and E.26 yields the expression for the rate of growth of particle:

$$\frac{dD}{dt} = \frac{3}{2} \frac{e_c \pi e_d}{f_s nf} \frac{c}{\rho_s} G D_p^{nf-3} D^{4-nf} = k_a c G D^{4-nf} \tag{E.32}$$

where

$$k_a = \frac{3 e_c \pi e_d}{2 f_s} \frac{D_p^{nf-3}}{nf\ \rho_s} = k_a' \frac{D_p^{nf-3}}{nf\ \rho_s} \tag{E.33}$$

The rate decay of particle due to breakup is suggested as:

$$\frac{dD}{dt} = -\frac{a e_b}{nf} D G \left(\frac{D - D_p}{D_p} \right)^p \left(\frac{\mu G}{F_y / D^2} \right)^q = -k_b G^{q+1} \left(D - D_p \right)^p D^{2q+1} \tag{E.34}$$

$$k_b = \frac{a e_b}{nf} D_p^{-p} \left(\frac{\mu}{F_y} \right)^q = \frac{k_b'}{nf} D_p^{-p} \left(\frac{\mu}{F_y} \right)^q \tag{E.35}$$

where p and q are the empirical parameters; e_b is a floc breakup efficiency parameter and F_y is the floc strength (assumed to remain constant, due to the fractal structure of flocs and determined by the number of bonds in a plane of failure) (Winterwerp 1998).

Combining the rates due to floc growth and floc breakup yields the expression for the net rate of change of rate due to turbulence:

$$\frac{dD}{dt} = \frac{k_a'}{nf}\frac{c}{\rho_s} G D_p^{nf-3} D^{4-nf} - \frac{k_b'}{nf}\left(\frac{\mu}{F_y}\right)^q G^{q+1} D_p^{-p} D^{2q+1}\left(D - D_p\right)^p \tag{E.36}$$

Winterwerp (1998) assumed that the parameters k_a' and k_b' remain constant, noting that the empirical coefficients they depend on are poorly known. In the present study, k_b' is assumed to remain constant, since it depends only on floc strength (which as noted remains unchanged due to the fractal nature of the particle). However, since the growth process is more complicated than breakup, we will allow k_a' to remain a variable, enabling a differentiation between the flocculation and hindered modes of floc settling during the calibration process. In the former mode the settling velocity increases with increasing concentration, whereas in the latter mode, which occurs at higher concentrations, the settling velocity decreases with increasing concentration. Note, however, that limitations are imposed on the choice of k_a', based on the reported ranges of $e_c = O\{10^{-2}\}$ and $e_d \approx 0.5 - 1.0$ (Levich 1962; O'Melia 1985). Winterwerp (1998) estimated $k_b' = O\{10^{-5}\}$.

E3. Cedar River Estuary

E3.1 Description of the Estuary

The Cedar River estuary is contained within Duval County in northeast Florida (see Figure E3). Both the Cedar River, and the Ortega River into which it flows, together empty into St. Johns River, which is connected to the Atlantic Ocean. Two main tributaries feed Cedar River—Butcher Pen Creek and Williamson Creek—along with several smaller tributaries. Another stream, Fishweir Creek, also flows into the Ortega (see Figure E4).

Depths within the Cedar/Ortega system vary from 0.5 to 3 m with an average depth of just over 1 m. Depths at the Cedar River vary from 0.3 m to 1.5 m with an average of 0.5 m.

E3.2 Tide, Current, Wave, Wind and Salinity Data

E3.2.1 Tide Data

Three ultrasonic recorders (Infinities USA Inc.) were installed to measure tidal elevations; data included here are for the period of November 29, 2000 through May 17, 2001.

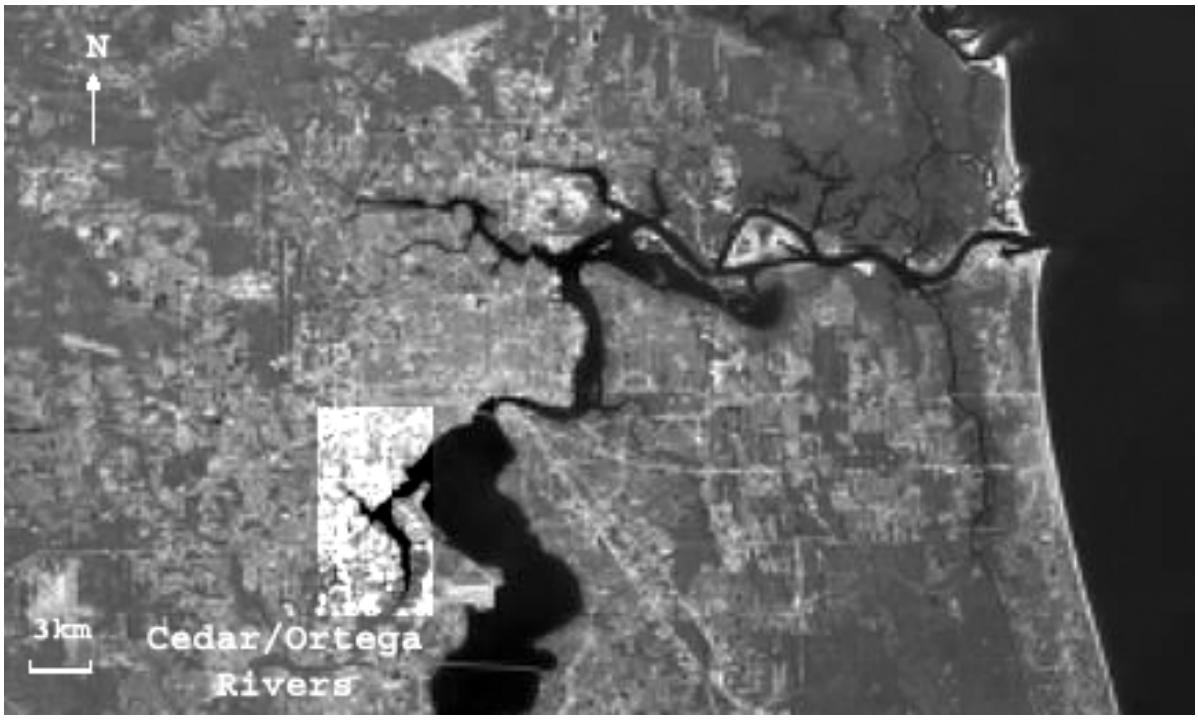

Figure E3. Cedar/Ortega Rivers estuary, (within the light rectangular area), aerial photo, May, 1998.

The locations were chosen so as to cover a relatively large area of the estuary, and also to facilitate gauge installation/removal and data retrieval. All gauges were placed against bridge piers. Gauge locations are shown in Figure E4 (TG1-TG3). Tidal elevations were measured relative to the National Geodetic Vertical Datum (NGVD). Sampling interval was set at 30 min. From the ogive curves presented in Figure E5, we note that the median range was around 30 cm. Station TG2, being the closest to the St. Johns River, in the wide portion of the Ortega River, responded to the tide the most. TG1, in Cedar River responded significantly less than the other two, possibly due to fresh water outflows from Butcher and Fishweir Creeks, which would have opposed the tide.

E3.2.2 Current Data

A tethered current meter (Endeco 174) was installed at location WGC Figure E4. The data reported here is from an approximately 1 month-long record (speed and direction) collected from February 5 through March 8, 2001, until the device malfunctioned. Data sampling interval was 15 minutes. As seen from Figure E6, the current speed was below 30 cm/s 98% percent of the time, and below 25 cm/s 95% of the time. Hence currents in the estuary are not very strong, and cannot be expected to result a high level of sediment transport under normal weather conditions.

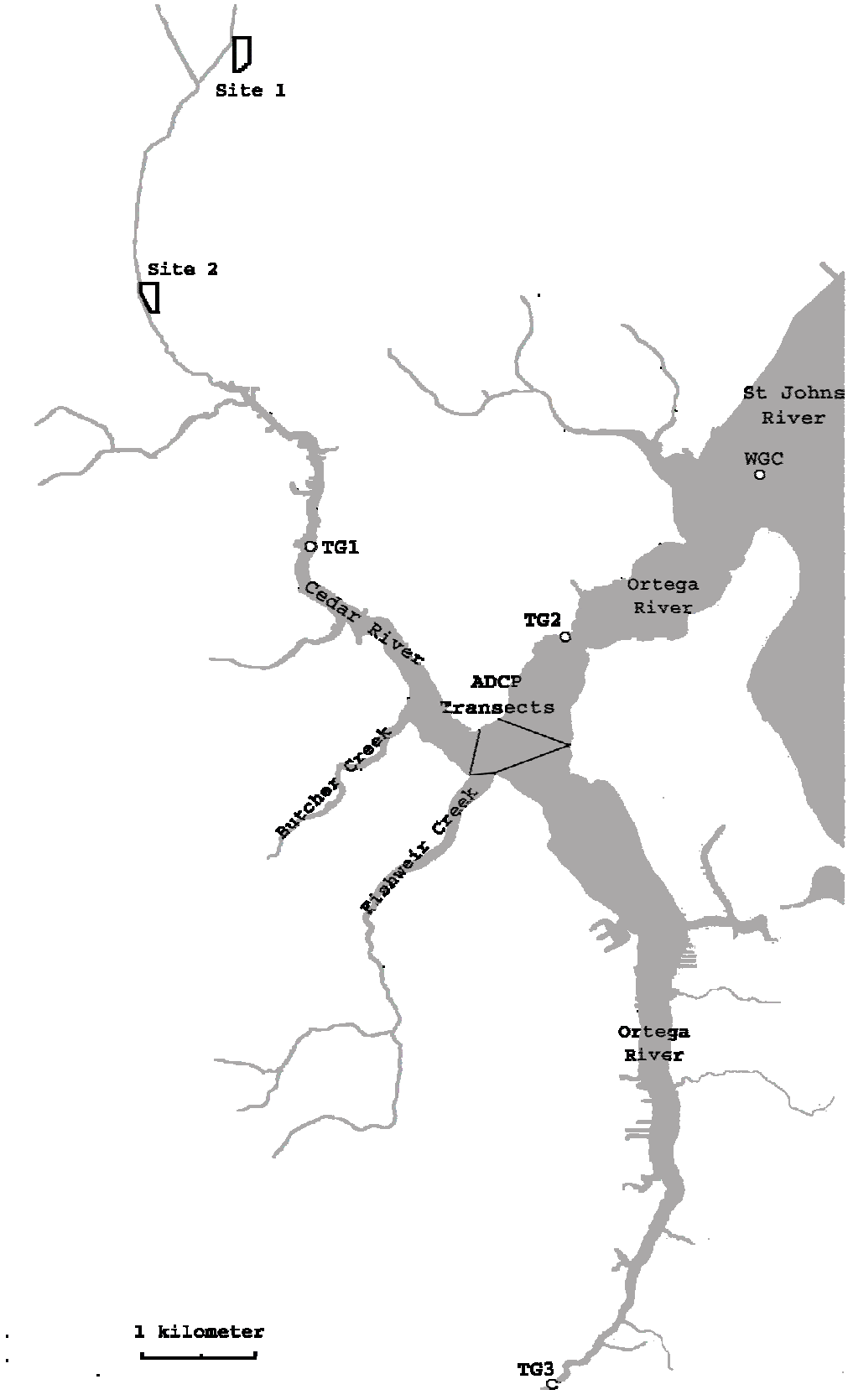

Figure E4. Cedar/Ortega Rivers data collection and sediment treatment (Wet Detention System) sites 1 and 2

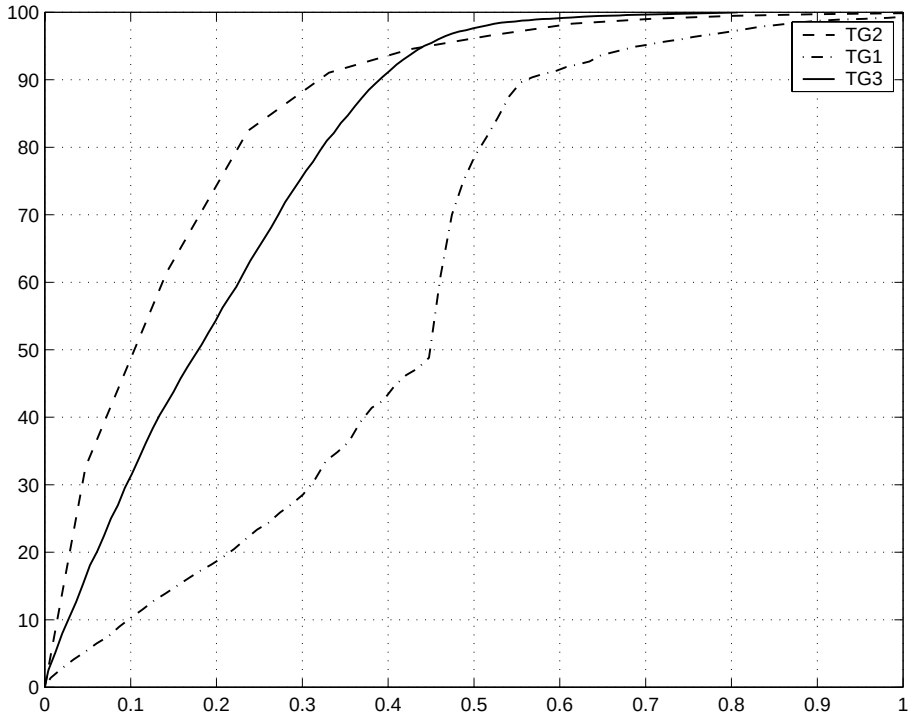

Figure E5. Tidal ranges at stations TG1-TG3. Cumulative frequency distribution based on record obtained during 09/29/00-10/18/01

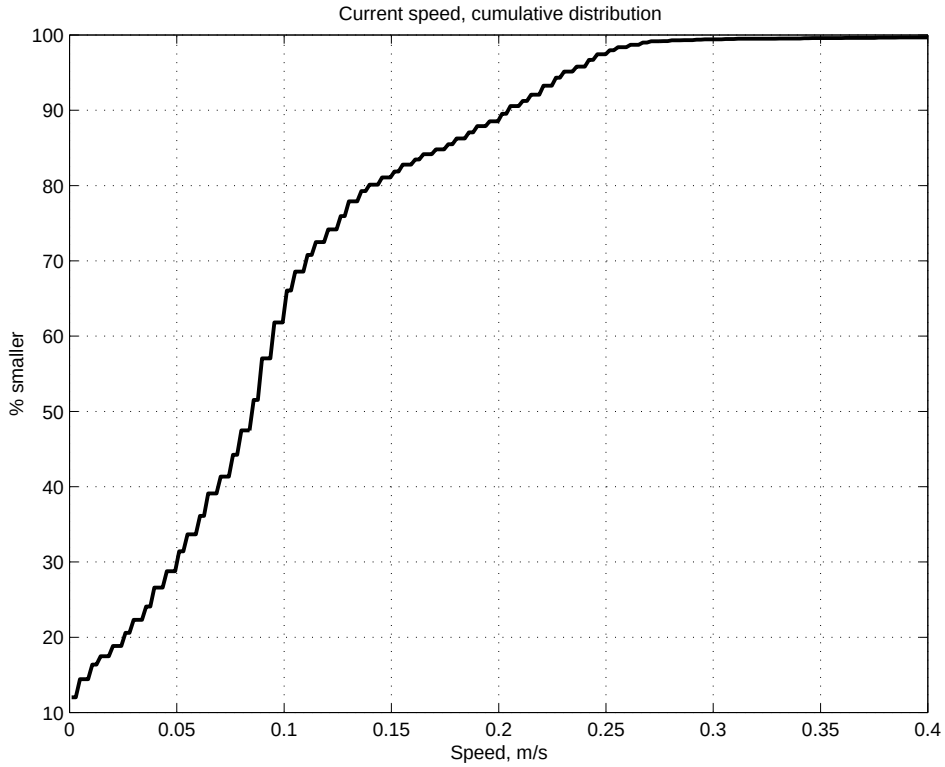

Figure E6. Current speed at station WGC (mouth of the Ortega in St. Johns River). Cumulative frequency distribution based on record obtained during 02/05/01-03/08/01

E3.2.3 Wave Data

A pressure transducer (Transmetrics Inc.) at WGC was used to obtain wave data. The sampling interval was 6 hours. Data included here are for the February 10 through April 25, 2001. The modal period was found to be 2 s. Figure E7 is a spectral representation of data. The variation of the significant wave height H_{m0} corresponding to the modal period is shown in Figure E8.

The cumulative distribution of H_{m0}, shown in Figure E9, indicates that it did not exceed ~0.2 m. This in turn implies a mild wave climate, due to the limited wind fetches in the St. Johns River. Wave action in the Cedar River is believed to be even milder, and is unlikely to contribute much to sediment transport except under severe conditions when comparatively large waves may break along the banks.

E3.2.4 Wind Data

Wind record was obtained from the Jacksonville Naval Air Station for the period January 1, 1995 through December 31, 1998 (sampling was every 3 hours). Wind statistics derived from this record (Table E1) provide information on the dominant wind speeds and directions. These data indicate a potentially complex dependence of wind on wind-driven currents in the estuary, especially because portions of the waterway reaches are lined by trees, while others have been cleared and developed.

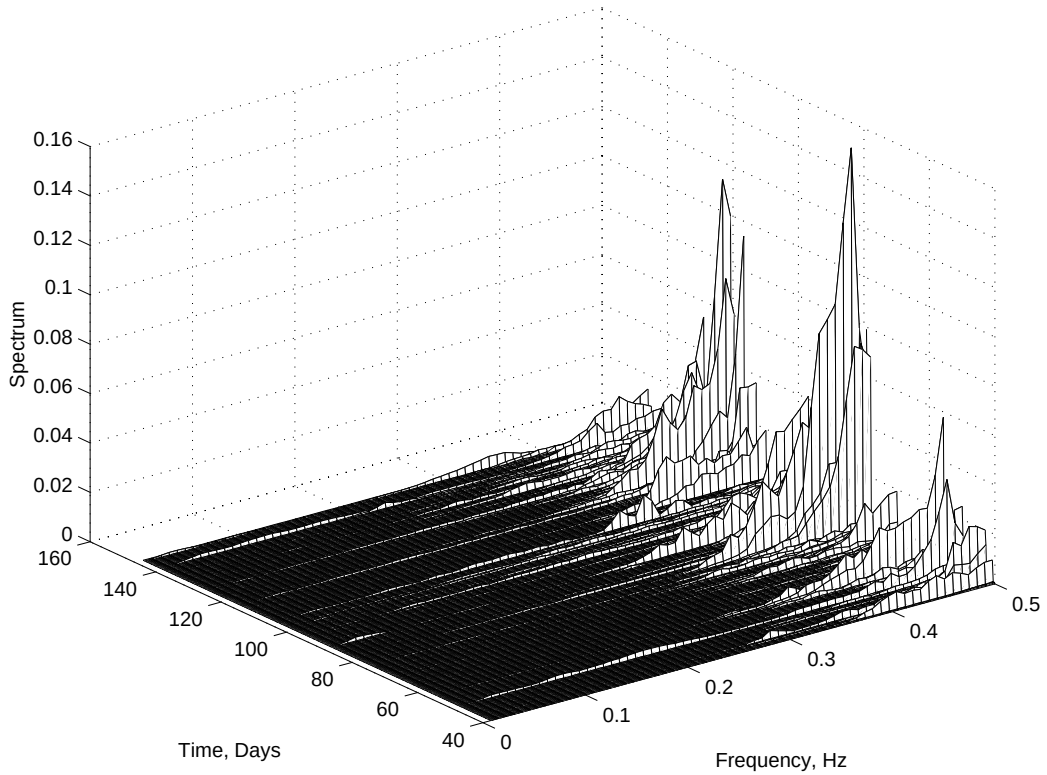

Figure E7. Wave spectrum based on 02/10/01–04/25/01 record at WGC

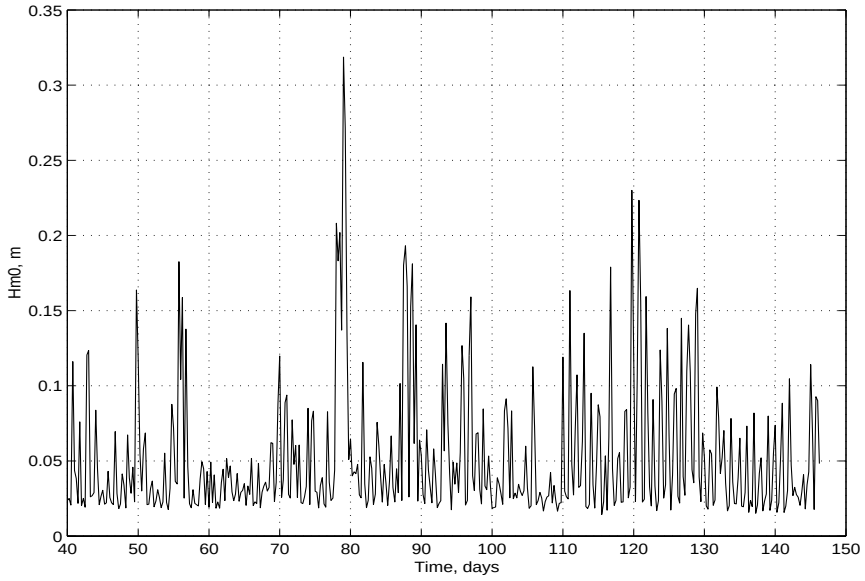

Figure E8. Significant wave height based on spectral analysis

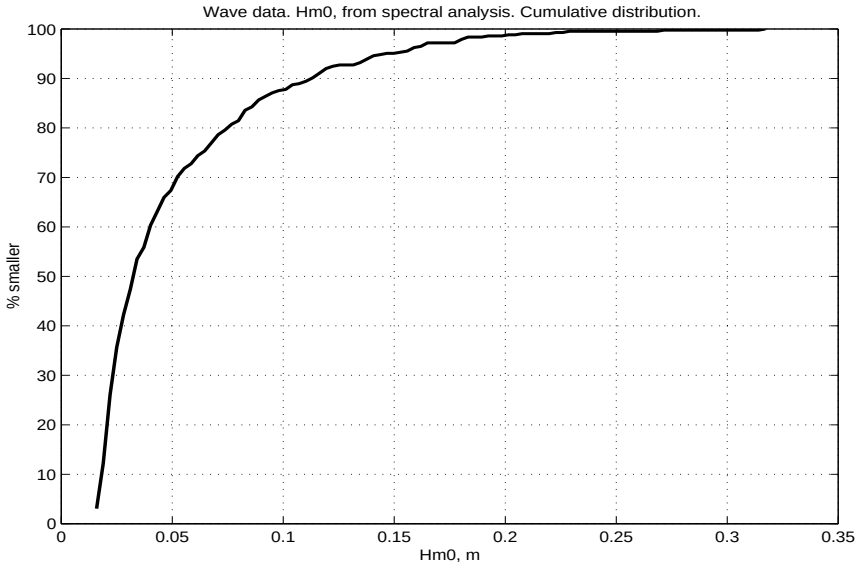

Figure E9. Cumulative distribution of the significant wave height at the mouth of the Ortega River in the St. Johns River

Table E1. Wind speed/direction distribution. Dominant speed/directions are highlighted

Wind direction, degrees	Speed, m/s 0	1	2	3	4	5	6	7	8	9	10	11	12	13	14	15	%
24	15	171	382	486	332	174	78	32	10	4	1	1	1				4.9
48	21	184	389	413	287	129	82	32	19	9	4	1	3				4.6
72	47	413	722	778	627	343	236	154	109	59	17	8	2	4			10.3
96	43	328	579	575	402	211	135	96	53	24	5	5	5	1	1		7.2
120	25	164	310	362	288	137	122	49	22	3	4						4.3
144	23	213	419	461	373	213	146	111	31	7	3	4					5.8
168	23	148	298	377	321	181	145	97	27	10	4	1	1				4.8
192	1368	916	836	766	542	318	300	112	40	15	14	2	2				15.2
216	30	178	458	453	380	243	145	89	31	13	13	10	1	5			6.0
240	24	162	371	414	412	273	193	109	55	16	8	2	1				5.9
264	29	272	527	513	519	283	183	55	9								6.7
288	24	195	380	354	308	150	104	20	8	3	8	3	1				4.5
312	33	257	576	617	463	252	186	51	16	12	8	3	2				7.2
336	11	139	330	403	308	129	69	25	7	2	5	2					4.2
360	27	214	548	814	687	274	142	50	15	5	4	1	1				8.1
% occurrence	5.1	11.5	20.8	22.7	18.2	9.6	6.6	3.2	1.3	0.5	0.3	0.1	0.1	0.0	0.0		

E3.2.5 Salinity Data

Salinity data were collected at stations TG1-TG3 during October 27–November 26, 2000. Figure E10 shows the cumulative distribution of these data for each station. The water is generally brackish; at TG1 in Cedar River the salinity is low due to freshwater outflows from the river itself as well as the creeks that flow into it.

E3.3 Discharge Data

Discharge measurements were obtained using an ADCP (Acoustic Doppler Current Profiler) Workhorse 1200 kHz (RD Instruments Inc.), on May 17, 2001. Four cross-sections of the Cedar/Ortega River confluence area were selected for data collection for almost a full semi-diurnal tidal cycle. In addition to the flow data, water samples were collected for determination of sediment concentration.

Due to the shallow nature of the estuary and poor performance of ADCP in shallow waters, the data were found to have a somewhat qualitative significance. A large fraction of the total discharge had to be estimated, Thesis Appendix EA describes the estimation algorithm, which closely follows the estimation implemented in WinRiver (RD Instruments software for ADCP systems). Table E2 presents the analyzed data for the Cedar River cross-section (all transects were made at the cross-section of the Cedar River near the confluence; see Figure E4). Positive discharge is directed west, and negative is directed east.

The mean depth at the cross-section was 1.0 m and maximum depth 1.4 m. Figure E11 shows discharge plotted on the same scale as tide data at TG2. It can be seen from the figure that as expected, the discharge curve precedes the water elevation curve.

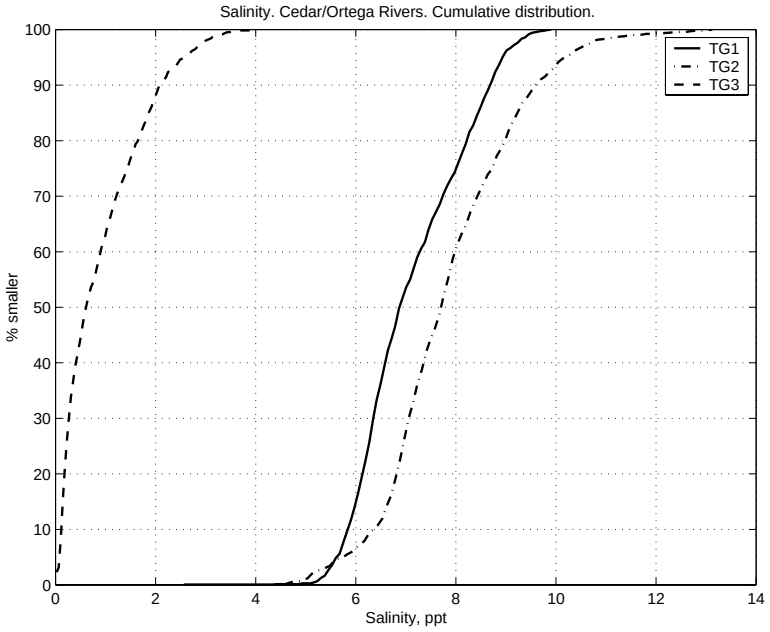

Figure E10. Cumulative distribution of salinity at stations TG1-TG3; 10/27/00-11/26/00

Table E2. Cedar River cross-section discharges, May 17, 2001

ADCP transect #	Time	Discharge, m^3/s
6	12:18	+90
14	13:25	-23
24	15:46	-69
32	17:13	-14
40	19:31	-3
50	20:29	+1

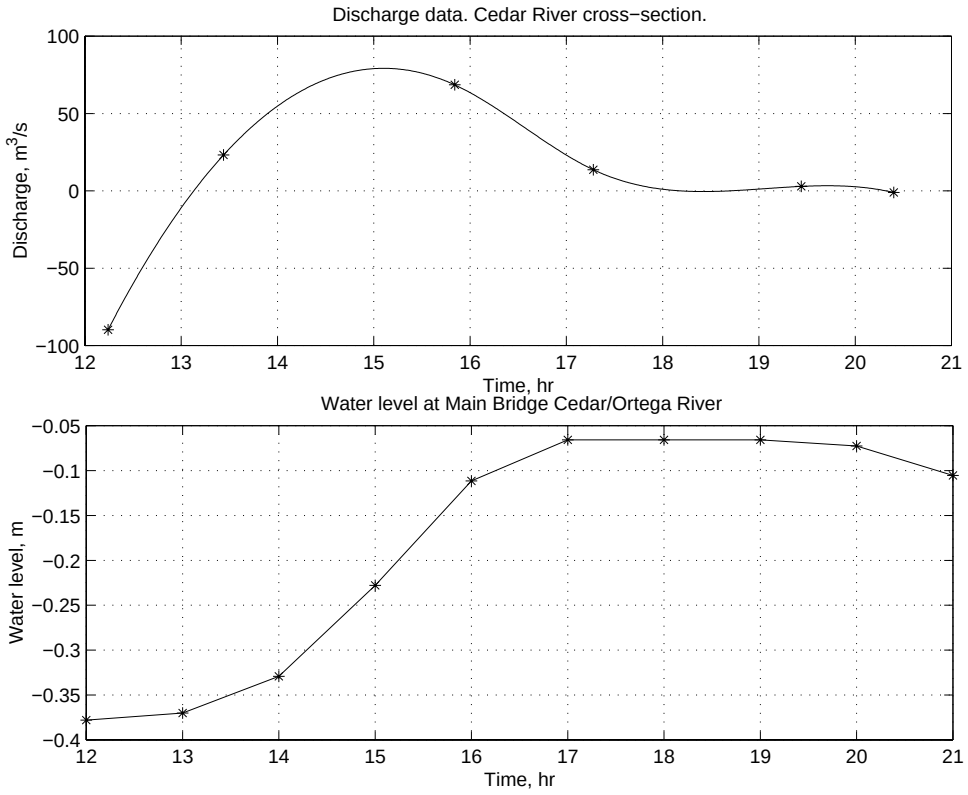

Figure E11. Cedar River cross-section discharge and Cedar/Ortega tide data, May 17, 2001

E3.4 Sediment Concentration

As noted, during the ADCP survey on May 17, 2001, a set of water samples was also collected. All samples were filtered, dried and weighed to determine the sediment concentrations. Table E3 gives the data thus obtained. The concentrations are characteristically low, and range between 8 and 101 mg/l.

Table E3. Sediment concentrations from water samples, May 17, 2001

Sample #	Concentration, mg/l	Sample #	Concentration, mg/l	Sample #	Concentration, mg/l
1	14	31	14	61	16
2	17	32	14	62	15
3	16	33	13	63	16
4	17	34	17	64	20
5	8	35	18	65	15
6	22	36	17	66	15
7	14	37	17	67	14
8	13	38	15	68	16
9	35	39	11	69	16
10	23	40	11	70	26
11	15	41	15	71	15
12	15	42	14	72	14
13	20	43	18	73	101
14	15	44	12	74	19
15	14	45	19	75	17
16	15	46	37	76	16
17	19	47	13	77	15
18	16	48	17	78	57
19	13	49	16		
20	27	50	19		
21	33	51	17		
22	17	52	21		
23	19	53	16		
24	16	54	18		
25	14	55	13		
26	16	56	13		
27	17	57	16		
28	17	58	15		
29	16	59	16		
30	13	60	16		

E3.5 Bed Sediment Distributions

In order to represent bed sediment distribution patterns, bed-sampling data supplied by the St. Johns River Water Management District were used to generate the maps showing the distribution of solids content, moisture content and organic content in the Cedar/Ortega Rivers. This set of maps, based on data obtained during March 3–October 2, 1998, were generated using approximation methods as follows.

First, maps were generated using Matlab routines for surface fitting (meshgrid, griddata). These routines generate a rectangular grid covering the data set supplied to them. Grid values are then approximated by fitting the surface to the data points and determining the values at the grid points. This approximation caused two problems:

- due to the lack of adequate spatial coverage of data, values at the river boundaries were automatically assigned zero values; and
- river boundary presence was not considered when generating the surface.

In order to avoid these problems, first the boundary points were approximated. The method used for this approximation was as follows. The distance from each data point to each boundary point was calculated (the shortest distance possible following the river). Boundary points (V_i) were then evaluated as:

$$V_i = \sum_{i=1}^{n} \varphi_i \cdot v_i \tag{E.37}$$

$$\varphi_i = \frac{e^{-\frac{r_{i,j}^2}{2\sigma^2}}}{\sum_{j=1}^{n} e^{-\frac{r_{i,j}^2}{2\sigma^2}}} \tag{E.38}$$

in which v_i = data point value, σ = standard deviation of the dataset, and $r_{i,j}$ = distance to data point i from boundary point j.

After generating the boundary points they were merged with the measured data points, and surface fitting functions were applied to the combined data. In this way contour maps were produced for moisture content (Figure E12), organic content (Figure E13), solids content (Figure E14) and thickness of the deposit (Figure E15). Measurement points are displayed as black dots and have values besides them. Also, equal-percent contours are drawn to identify the areas where the percentage of moisture/organics/solids is approximately the same.

Table E4 contains relevant statistics: minimum, maximum and the mean values of moisture content, organic content and solids content. We observe that the upstream reach of the Ortega River is characterized by the high organic content (30-35%), whereas the upstream reach of the Cedar River has a high solids percentage (25-30%). These trends reflect the more natural, vegetated surroundings of the Ortega versus more developed reaches of the Cedar. A thickness of the deposition layer is more or less constant in the Ortega/St. Johns River and is much smaller in the Cedar River.

Table E4. Statistical values associated with bed sediment distribution

Statistic	Moisture content (%)	Organic content (%)	Solids content (%)
Minimum	54	6	16
Maximum	84	51	46
Mean	76	21	24

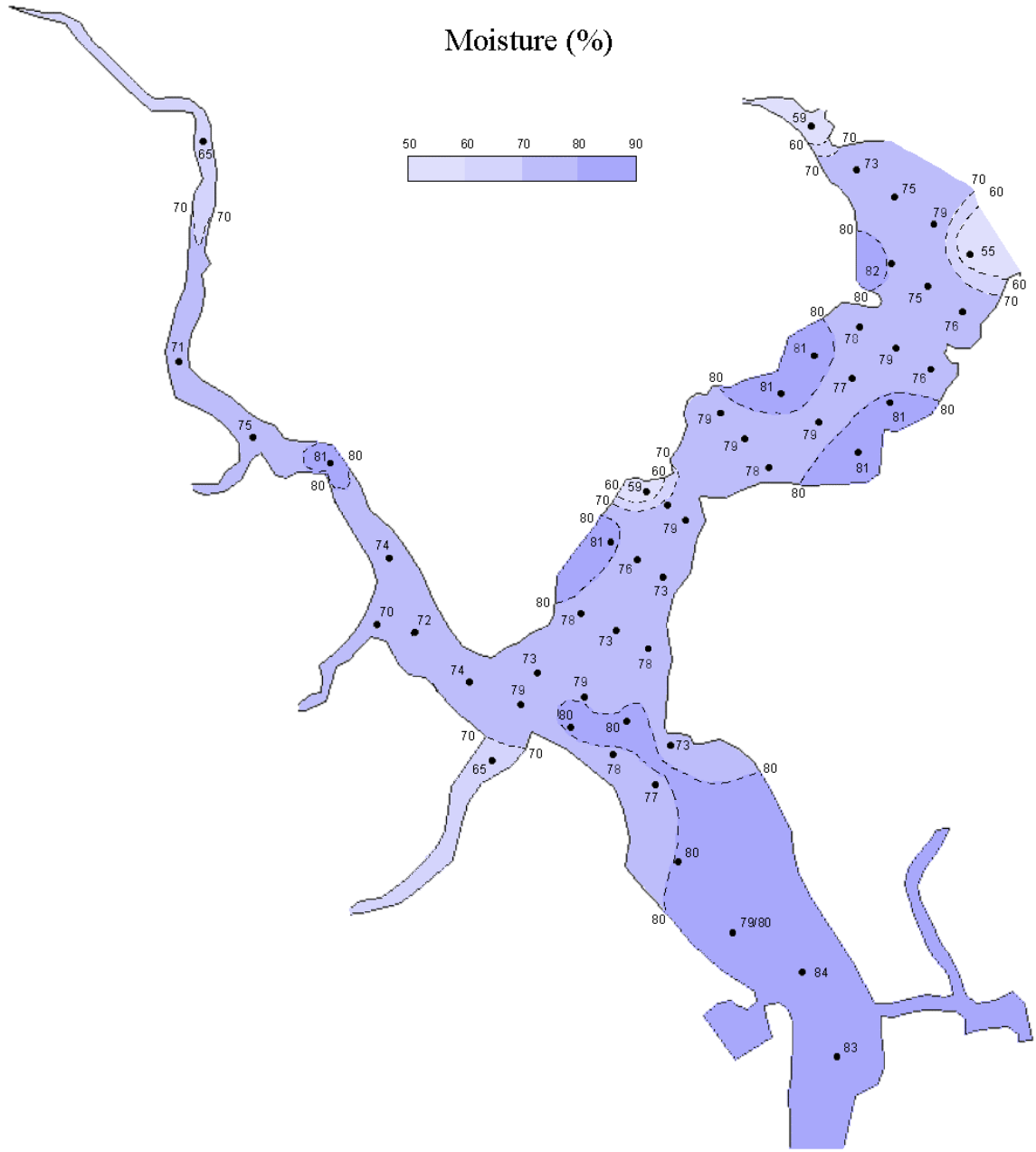

Figure E12. Moisture content distribution (%) based on 1998 sampling

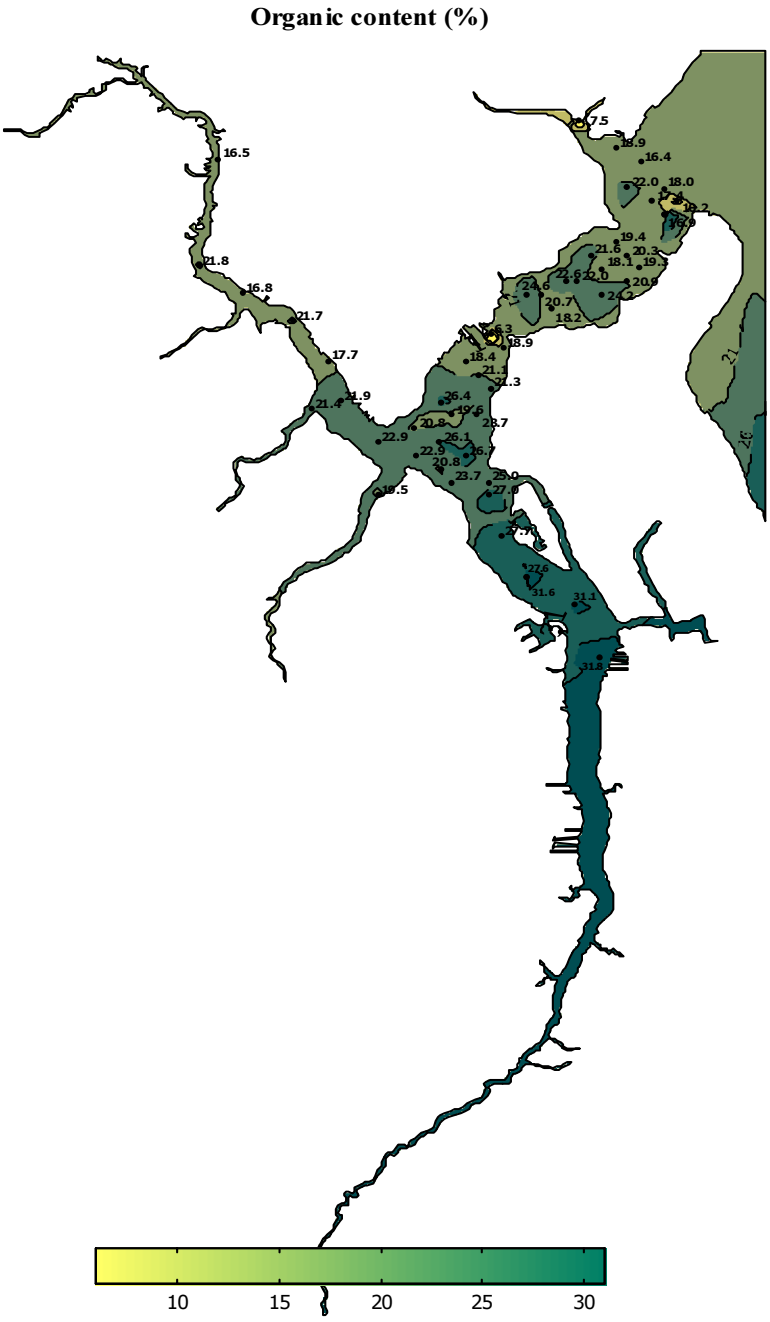

Figure E13. Organic content distribution (%) based on 1998 sampling

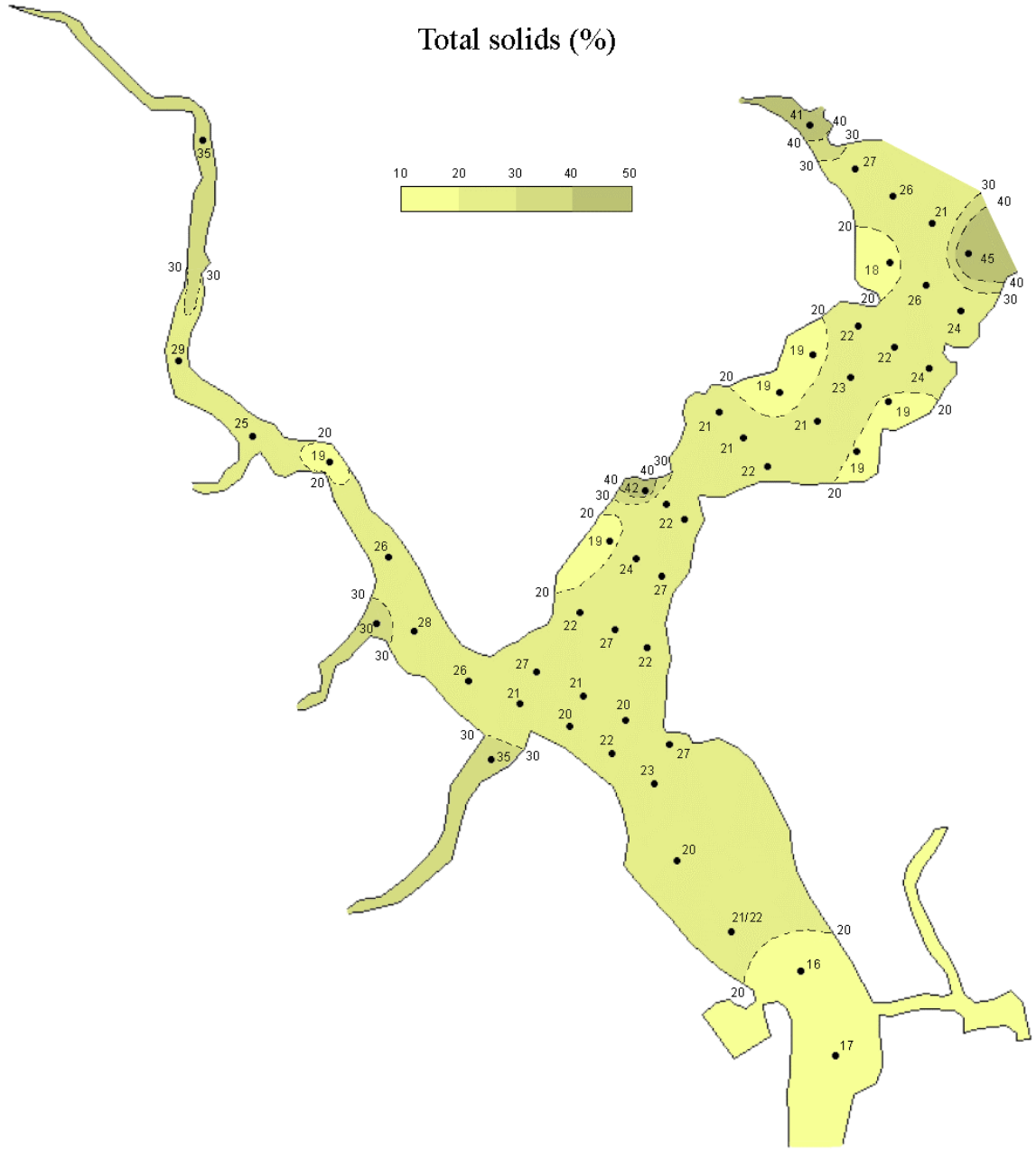

Figure E14. Solids content distribution (%) based on 1998 sampling

Figure E15. Thickness of soft deposit in the study area based on core thicknesses in 1998 sampling

E4. Assessment of Sediment Trapping Efficiency

E4.1 Flow Model Setup, Calibration and Validation

Model setup was carried out in two steps. The area of interest lies within the Cedar River, while some of the data for calibration were available for various sites within the much larger Cedar/Ortega/St. Johns River estuary. It was therefore decided to calibrate and run the model with a coarse grid covering the Cedar/Ortega/St. Johns River estuary. Running the model in this way generated the downstream boundary conditions for the Cedar River model, which was then run for sediment trapping efficiency assessment. This procedure allowed for the use of a finer grid in the Cedar River, without significantly increasing the simulation time.

Figure E16 shows the areas covered by the two model setups. Both, the coarse and fine grids are Cartesian because, as noted, the sediment transport model was found not conserve mass when run with a curvilinear grid.

E4.1.1 Cedar/Ortega/St. Johns Rivers Model Setup

The Cedar/Ortega/St. Johns River (Cartesian) grid and has dimensions of 160 by 300 cells, with a cell size of 50 by 50 m (Figure E17). The boundary conditions are labeled BC1-BC7. The grid was σ-stretched in the vertical direction with six horizontal layers.

Figure E18 shows the bathymetry of the modeled domain. The Cedar/Ortega River portion of the domain is typically shallow with 1.5–2 m depth in the channel thalweg, and an average depth of ~1 m.

Hourly water level and salinity data from the St. Johns River (supplied by the St. Johns River Water Management District) were used to define the boundary conditions at the north and south open boundaries of the St. Johns River (BC7, BC8). As an example, Figure E19 shows the time-series and the cumulative distribution of the measured water surface elevation data. The mean tide range is approximately 0.4 m.

Small creeks (Williamson Creek, Butcher Pen Creek, Big Fishweir Creek and Fishing Creek denoted on Figure E17 as BC6, BC5, BC3 and BC4, respectively) minimally affect the flow in the larger estuary. Hence, instead of using "open" boundary conditions there, they were defined in terms of sink/source cells for specifying the flow and sediment flux conditions at the heads of these creeks. The relevant boundaries BC2-BC6 are shown in Figure E20. The boundary condition time-series were supplied by the St. Johns River Water Management District.

Measured salinity time-series at open boundaries BC7 and BC8 were used. The model was run for a thee-week period to establish the salinity field (model "spin-up"), defined by these time-series. The bottom roughness z_0 was chosen as 0.04 m throughout.

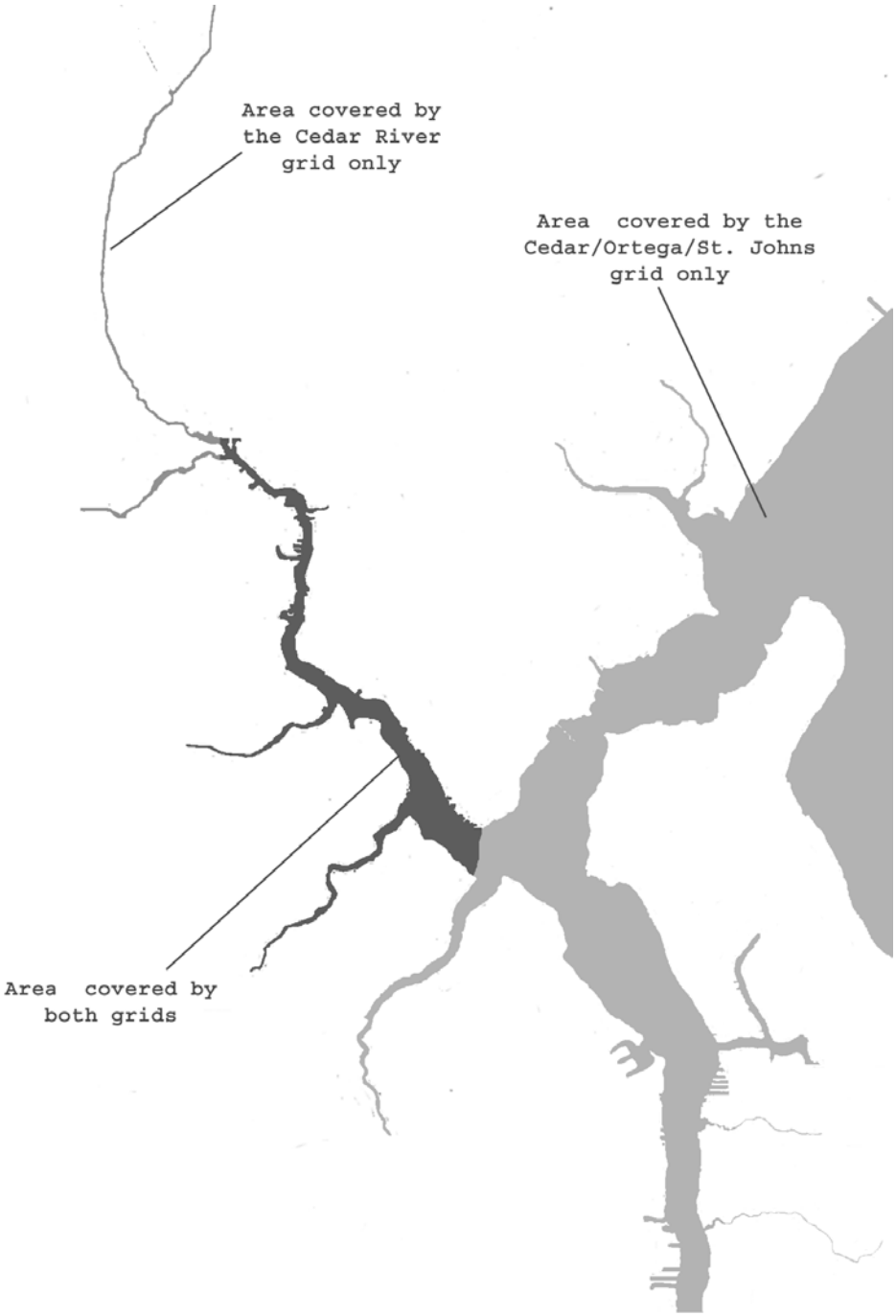

Figure E16. Areas covered by the two (coarse grid and fine grid) models

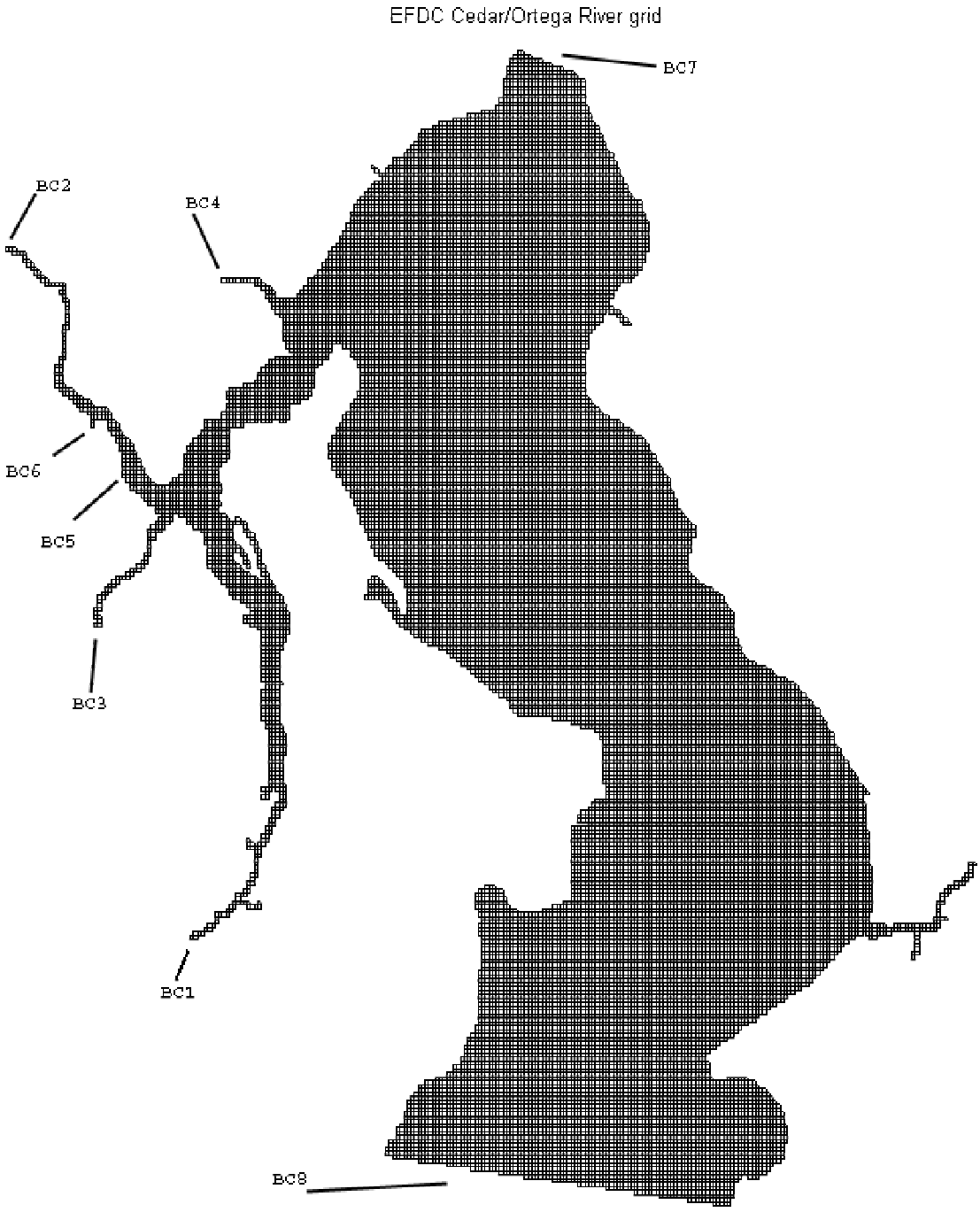

Figure E17. Cedar/Ortega/St. Johns River grid with open boundary locations

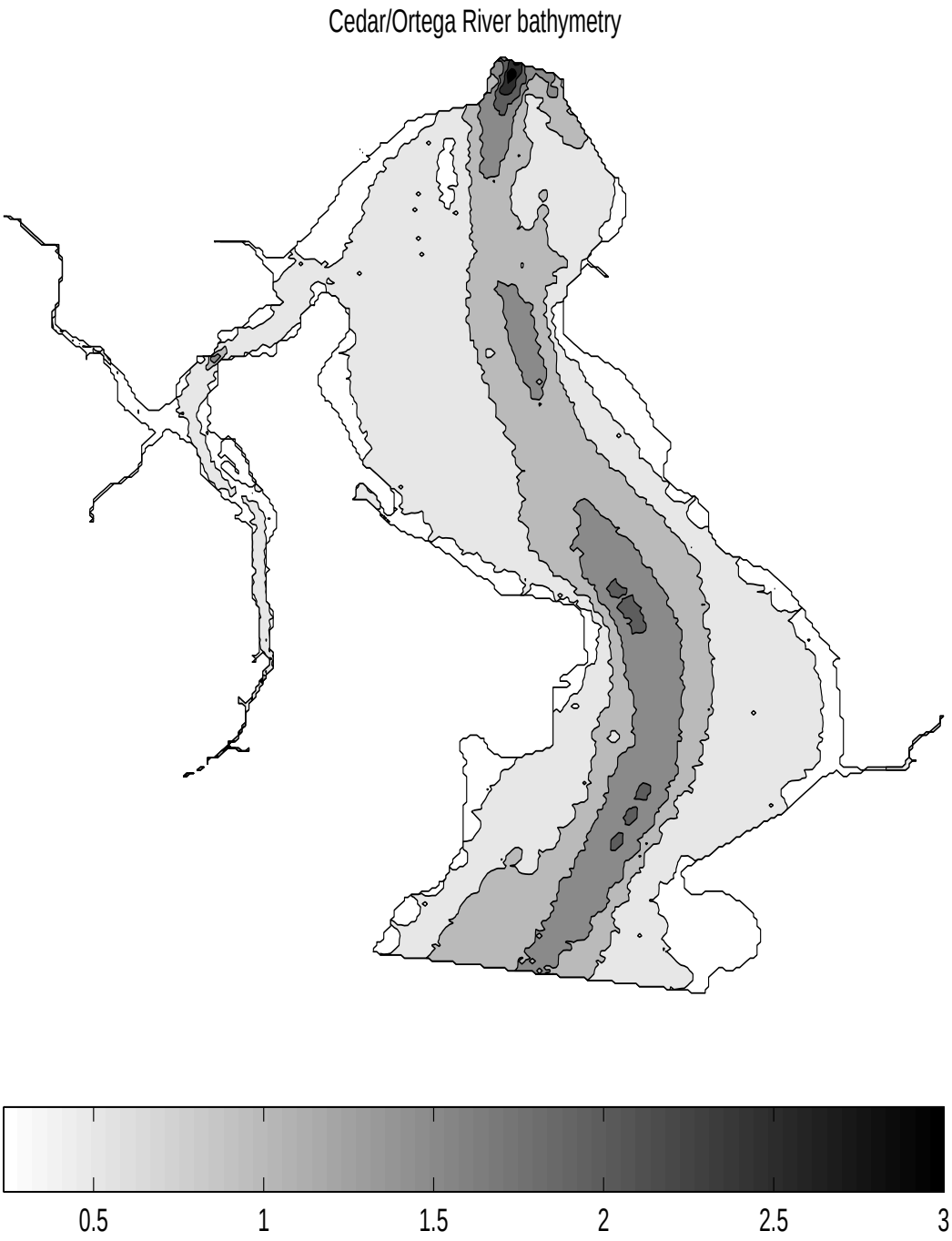

Figure E18. Cedar/Ortega/St. Johns River bathymetry (depths are in meters)

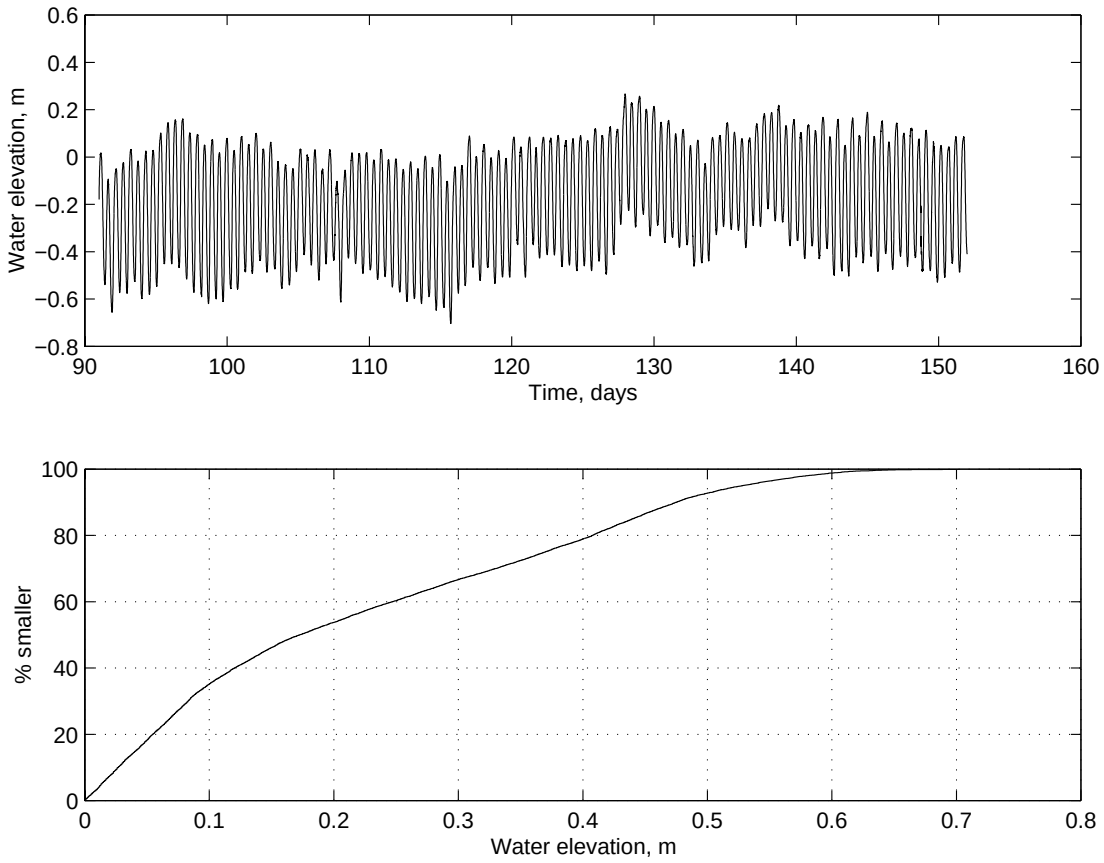

Figure E19. Cedar/Ortega/St. Johns River open boundary condition (BC7) during 2001 showing water surface elevation time-series and cumulative distribution

The kinematic viscosity and molecular diffusivity were set to 10^{-6} and 10^{-8} m^2/s, respectively [Equations E.1–E.4, Section E2.2]. The period of simulation corresponded to April 25, 2001 through May 30, 2001. A time-step of 3 s was used.

The purpose of the simulation run was to generate the flow, salinity and suspended sediment time series at the downstream boundary of the Cedar River model (near the Cedar/Ortega confluence), and also to establish a (conservative) salinity field over the estuary. These outputs were then used to generate the initial and boundary conditions for the Cedar River model.

E4.1.2 Cedar River Model Setup

The Cedar River grid was also horizontally Cartesian and vertically σ-stretched. Its horizontal dimensions were 160 by 450 cells, each cell representing an area of 15 m by 15 m, and also used six horizontal layers. The grid and bathymetry are shown in Figure E21 and Figure E22, respectively.

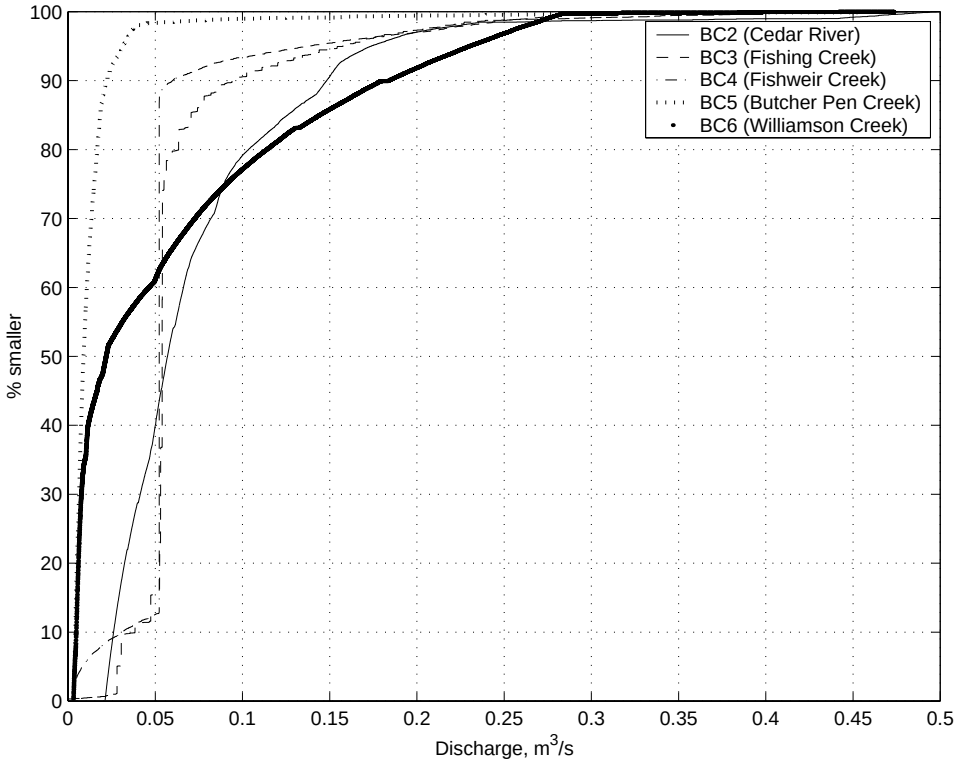

Figure E20. Cedar/Ortega/St. Johns River tributaries discharge, cumulative distribution

The boundary conditions at the upstream ends of the Butcher Pen Creek, Fishing Creek, Williamson Creek and the Cedar River were forced by establishing sink/source cells with the given discharge time-series (Figure E20). The downstream open boundary was represented by the water surface elevation forcing time series (Figure E23) generated by the Cedar/Ortega/St. Johns River model. The same physical boundary also served as a boundary condition for sediment concentration, which was defined based on the water sample data (May 17, 2001). The initial salinity field was generated by approximating the salinity field from the Cedar/Ortega/St. Johns model, which helped in decreasing the time needed for model "spin-up" required to establish a conservative salinity field. The bottom roughness coefficient, viscosity and diffusivity were unchanged from the values used in the Cedar/Ortega/St. Johns River model.

Figure E23 shows a reasonable agreement between the measurement and simulation of tide. Note that the "measured" time-series was derived by averaging the tides at stations TG2 and TG3 by taking the time lags into consideration, in order to represent tide at the open boundary, which occurred in-between the two tide stations. The mean range was 0.52 m for the measured tide and 0.50 m for the calculated one Figure E24 shows the predicted water surface elevation plotted over a short period of time at three control stations (cells): 1) at the confluence of Butcher Pen Creek and the Cedar River), 2) at the upstream-most cell of the Cedar River grid, and 3) at the cross-section in Cedar River at its confluence with the Ortega. The time lag between the upstream control station and the confluence station is equal to approximately 7.5 min, which is consistent with the registered time lag in the measured water level data, considering the distance (5.4 km) between the stations.

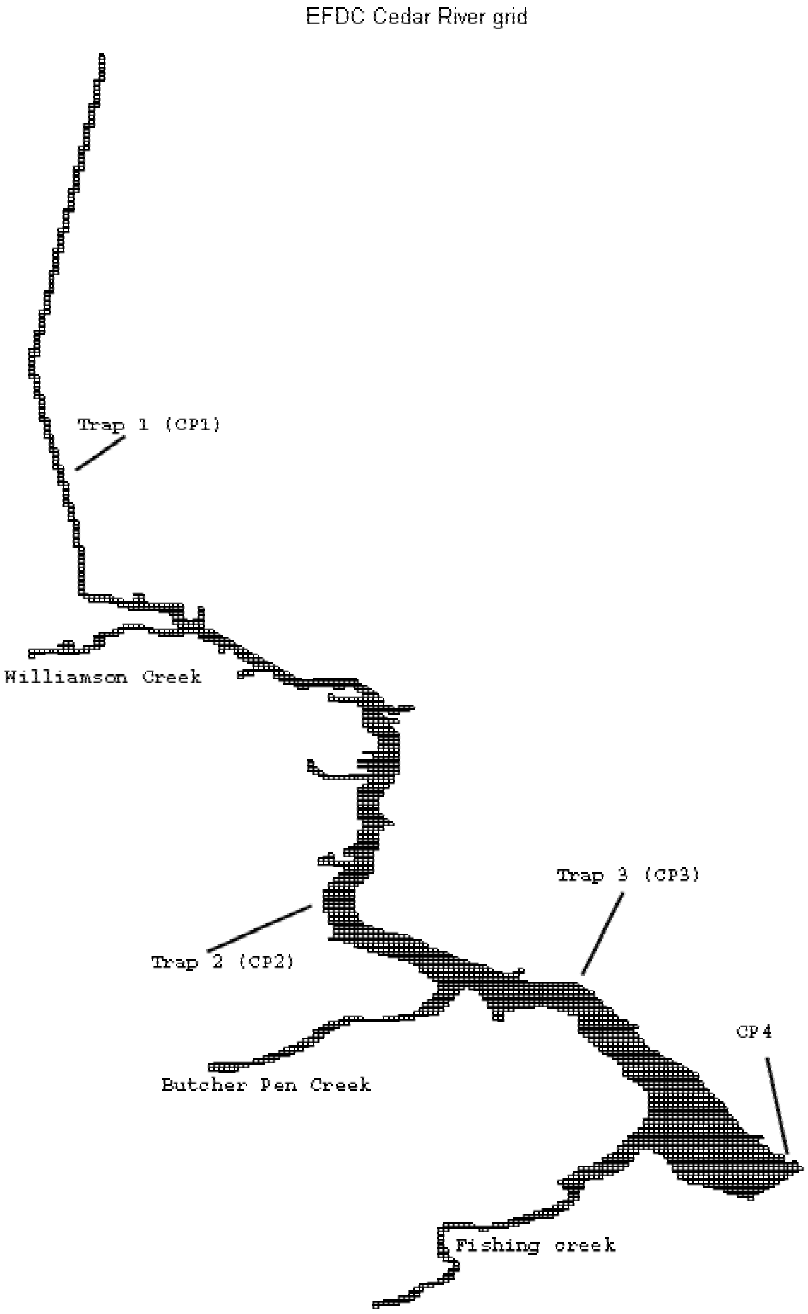

Figure E21. Cedar River model grid

Figure E22. Cedar River bathymetry (depths are in meters)

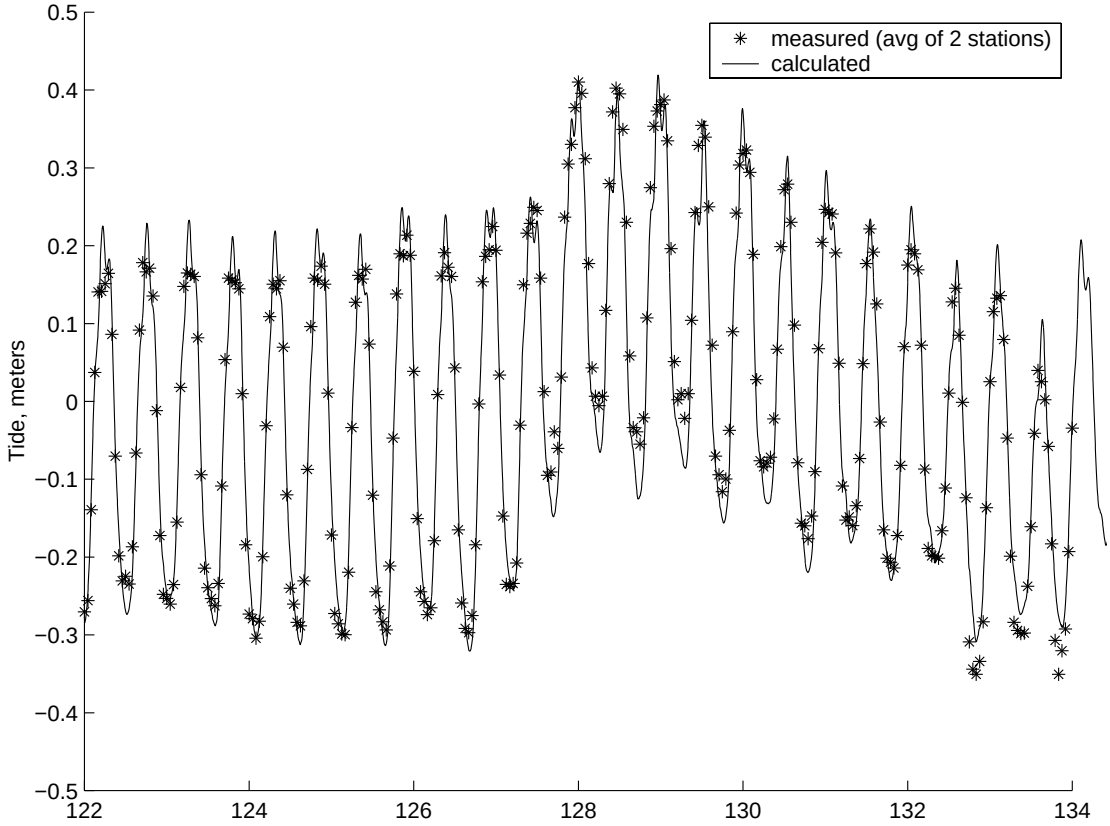

Figure E23. Measured and simulated water level variations at the downstream boundary of the Cedar River

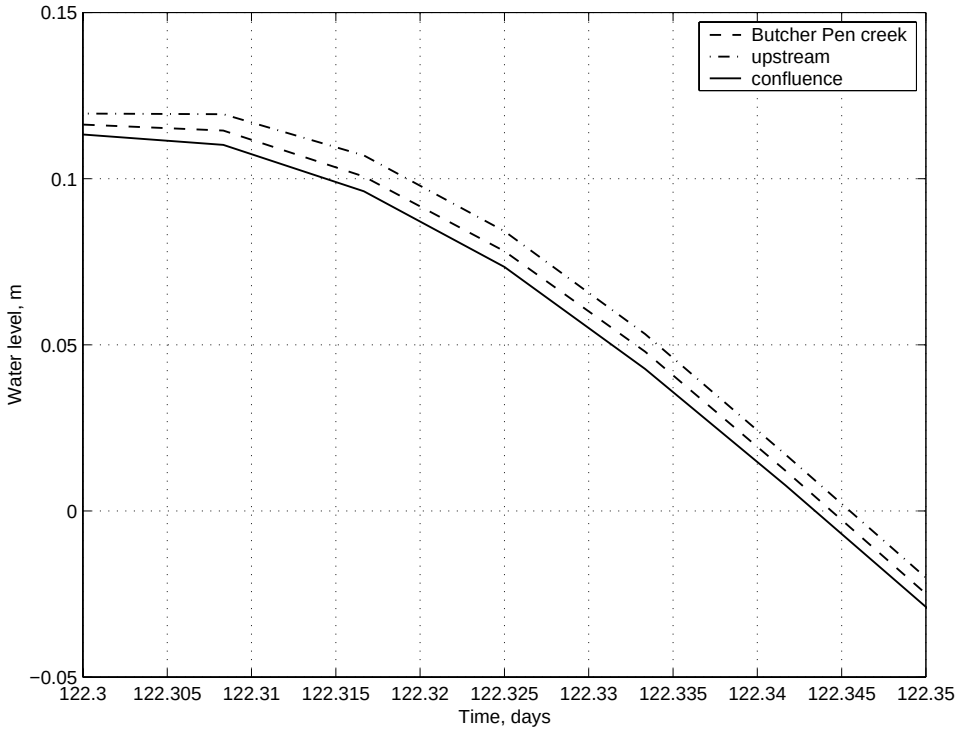

Figure E24. Water surface elevation at three control points in Cedar River

The simulated discharge data were compared to discharge obtained by the ADCP. The measured and simulated discharges in the Cedar River at the confluence are plotted on Figure E25. Figures E26 and E27 show similar results for the north and south cross-sections of the Ortega River, respectively. The latter two simulations were derived from the Cedar/Ortega/St. Johns River model. In general, the simulated discharge appears to be in a reasonable agreement with measurement, especially considering measurement errors (see Thesis Appendix EA).

E4.2 Sediment Transport Model Setup and Calibration

E4.2.1 Sediment Transport Model Setup

For running the sediment transport model the initial suspension concentration was set to 5 mg/l, the average value for the sediment concentration in the Cedar/Ortega/St. Johns River estuary. For the upstream boundary conditions in Cedar River, Williamson Creek and Butcher Pen Creek supplied by the St. Johns River Water Management District were used. It should be pointed out that at the downstream boundary of the Cedar River, the outputted values from the Cedar/Ortega/St. Johns River were significantly lower (~5-12 g/l), than the values, ranging between 8 and 57 mg/l (with an additional, exceptional value of 101 mg/l in one case), obtained from water sampling on May 17, 2001. Depth-averaged TSS concentration series simulated by the coarse grid model at the Cedar River cross-section near the confluence is shown in Figure E28 and commensurate collected samples at the same location are shown in Figure E29.

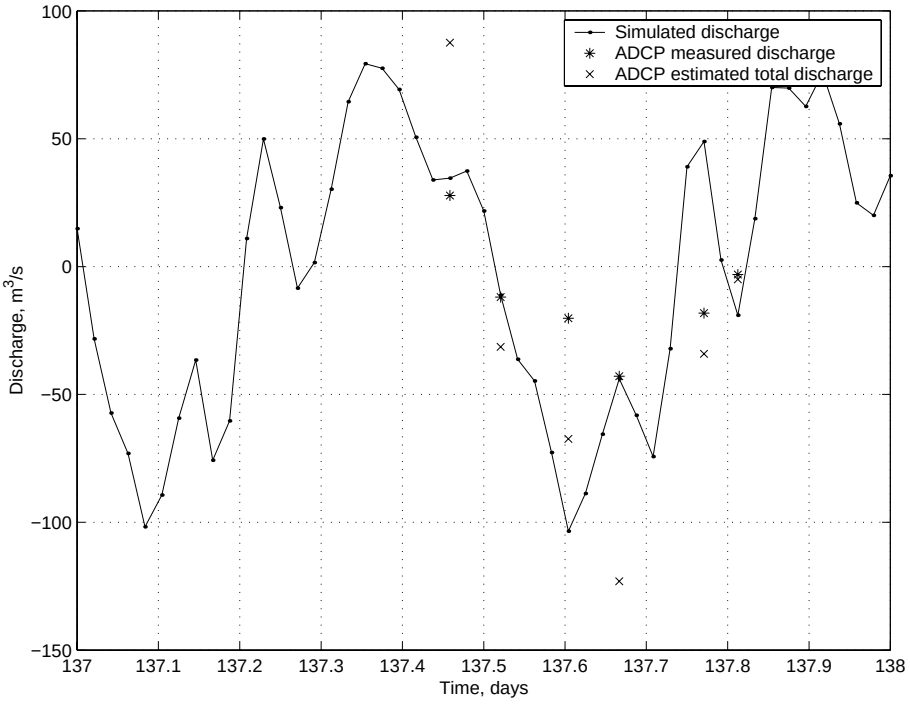

Figure E25. Measured and simulated discharges through the Cedar River cross-section

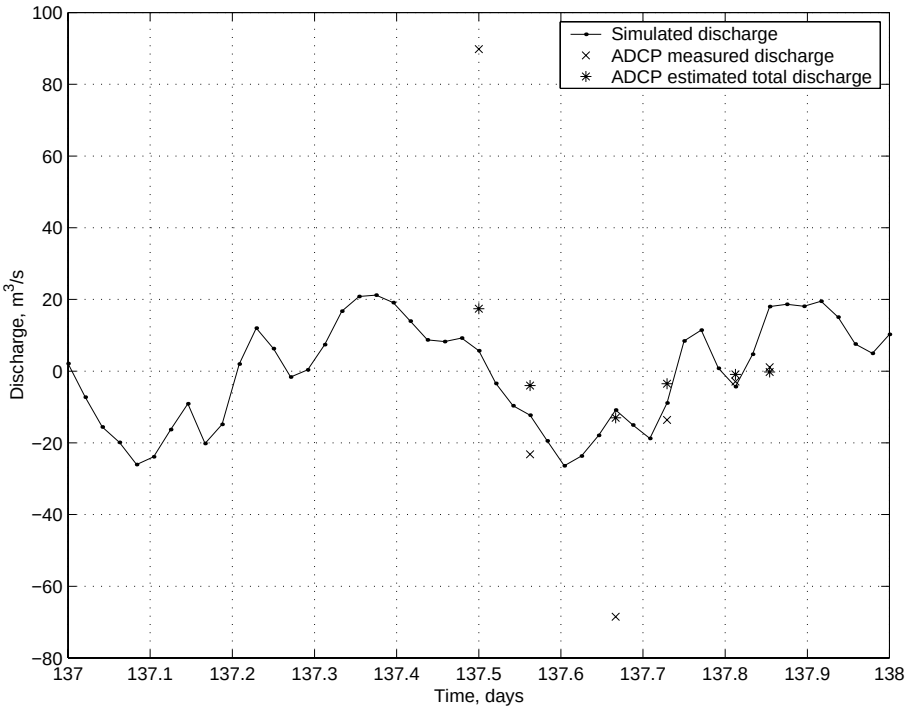

Figure E26. Measured and simulated discharges through the Ortega River cross-section (north cross-section of the confluence)

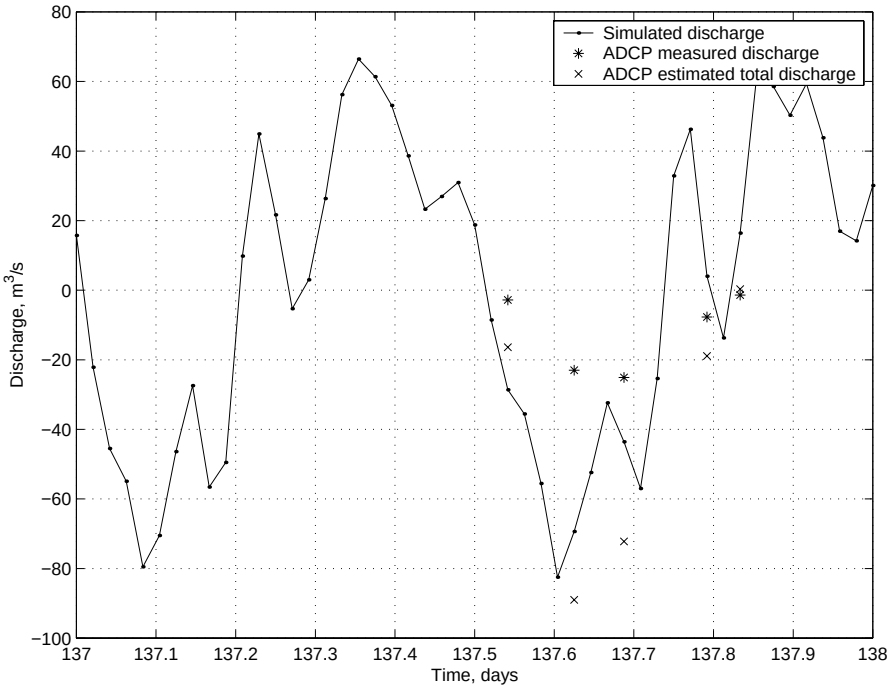

Figure E27. Measured and simulated discharges through the Ortega River cross-section (south cross-section of the confluence).

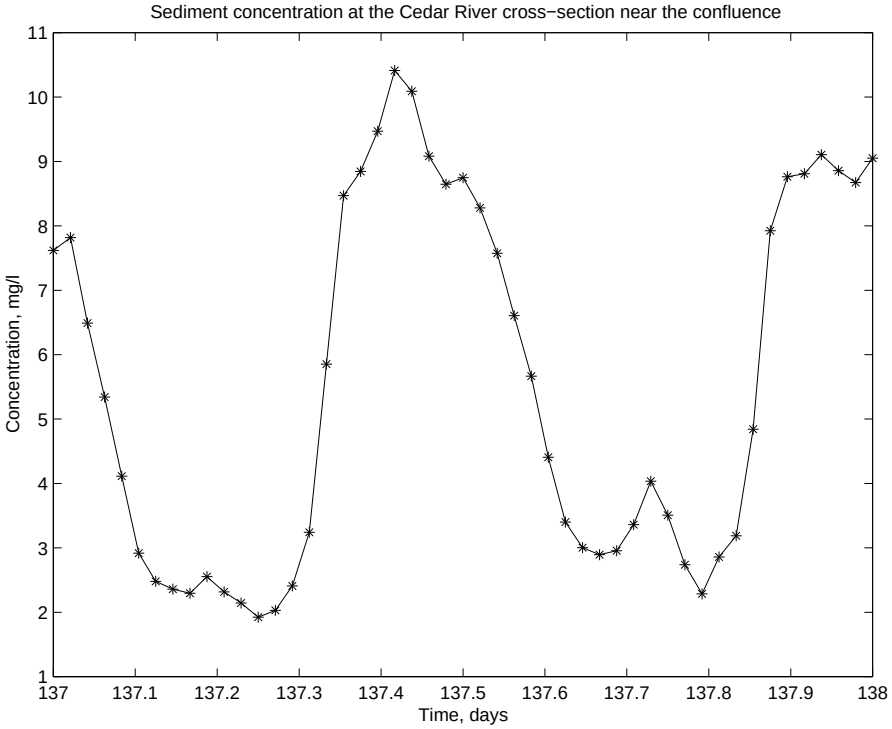

Figure E28. Depth averaged TSS concentrations at the Cedar River cross-section near the Cedar/Ortega confluence simulated by the coarse grid model (May 17, 2001)

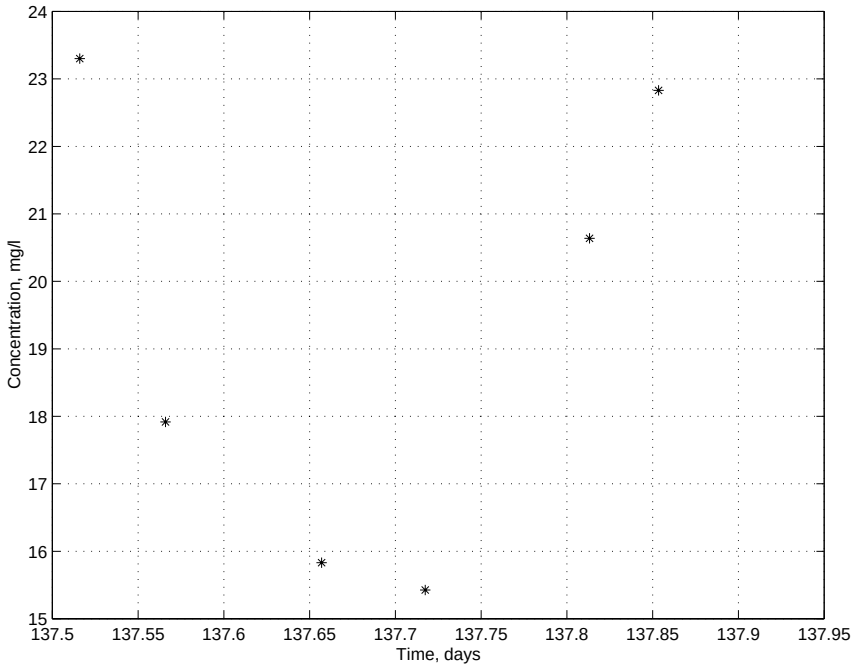

Figure 29. Depth averaged TSS concentrations from the water sample data, collected at the Cedar River cross-section near the Cedar/Ortega confluence (May 17, 2001)

The above discrepancy between the simulated and measured concentrations was found to be due to the low concentrations predicted at the head boundaries of the Cedar River and the creeks. These boundary conditions, supplied by the St. Johns River Water Management District, were not verified. The problem was unfortunately realized towards the end of the present study. It was however felt that rerunning the sediment transport calculations for the Cedar River was not necessary, because the trapping efficiency results, described later, rely on relative rather than absolute values of the sediment flux. Thus the conclusions of the study were not affected.

Since variation in the sediment concentration with time was small (8-9 mg/l), compared to the increase in concentration with depth (as found from the water sampling analysis), the sampled data were averaged, and a representative vertical profile of concentration with linearly distributed values from 14 g/l in the top layer to 27 g/l in the bottom layer, was used to set the open boundary condition at the in the Cedar River.

E4.2.2 Bed Erosion

The bed erosion function (lines representing erosion rate as a function of the bed shear stress) required for sediment model code is shown in Figure E30. It was based on laboratory experiments by Gowland (2002) using mud samples collected from the Cedar and the Ortega Rivers. This function was used for both models, i.e., coarse and fine grid.

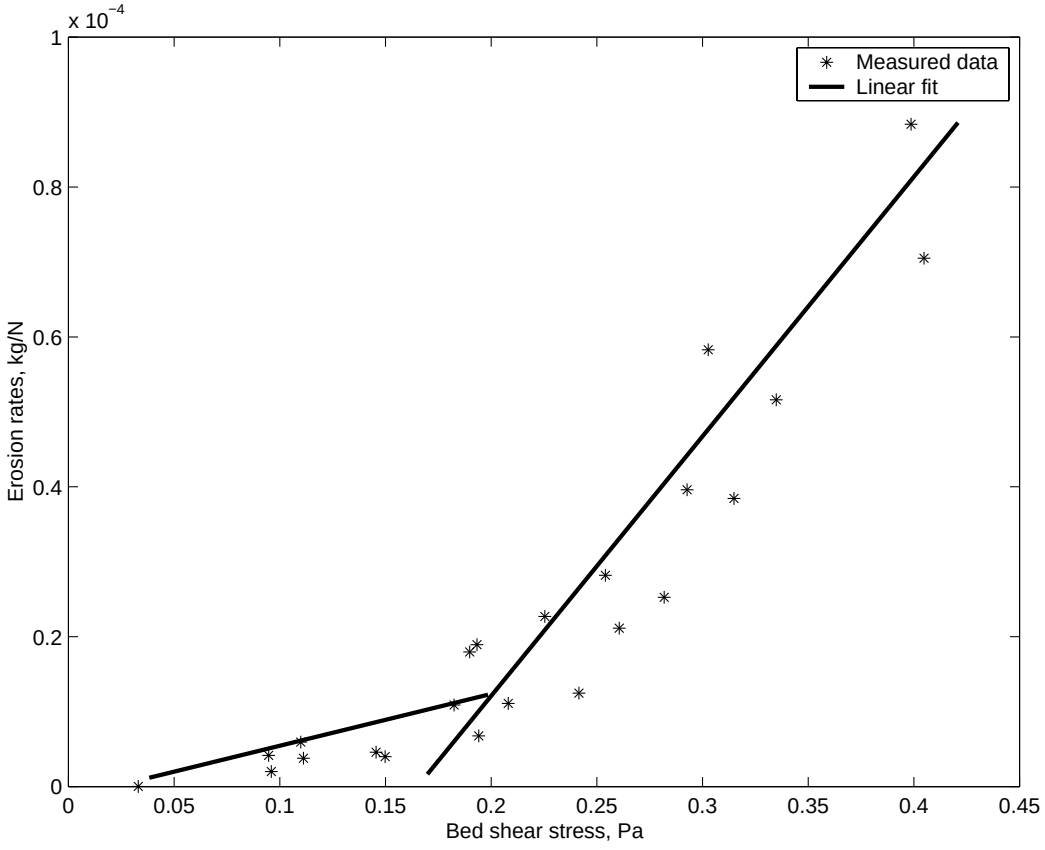

Figure E30. Bed erosion rate function obtained from laboratory experiments on mud from the Cedar/Ortega Rivers (after Gowland, 2002)

E4.2.3 Settling Velocity and Deposition

The settling velocity model (Section E2.4) was calibrated using the data obtained from laboratory settling column tests using sediment from the site (Gowland 2002). Some model tests were also carried out it against data available in the literature, the results of which are given in Thesis Appendix EB.

The model did not function for the values of the dissipation parameter G on the order of magnitude of 10^{-3} Hz and less, because very low turbulence levels caused the particle to grow infinitely large. This was due to the model formulation, in which particle size is dependent on a level of turbulence. It should be noted that in reality the volumetric concentration $\phi \propto \frac{c}{\rho_s}\frac{D}{D_p}$ cannot exceed unity, by definition, hence the constraint $D \le \frac{\rho_s}{c} D_p$ is imposed on the calculation of the diameter.

To calibrate the model against the laboratory data (Gowland 2002) the value of $G \approx 10^{-2}$ Hz was used, in order to satisfy the above constraint and, at the same time, to simulate a near-quiescent situation (the settling column being a quiescent environment). The estimated range of G for Cedar River estuary was found to be within 0.5 to 10 Hz [based on Equation E.30), which gives a relation between the flow velocity, shear stress and dissipation parameter]. The concentration in the Cedar River (from the water samples, collected in May 17, 2001) was found to be within 8 to 57 mg/l; however for the modeling purposes the range of concentrations from 0.1 to 100 was selected for convenience. Figure E31 thus obtained qualitatively resembles the Dyer diagram (Figure E31). The dissipation parameter was related to the shear stress using Equation E.30 considering the mean flow of 10 cm/s.

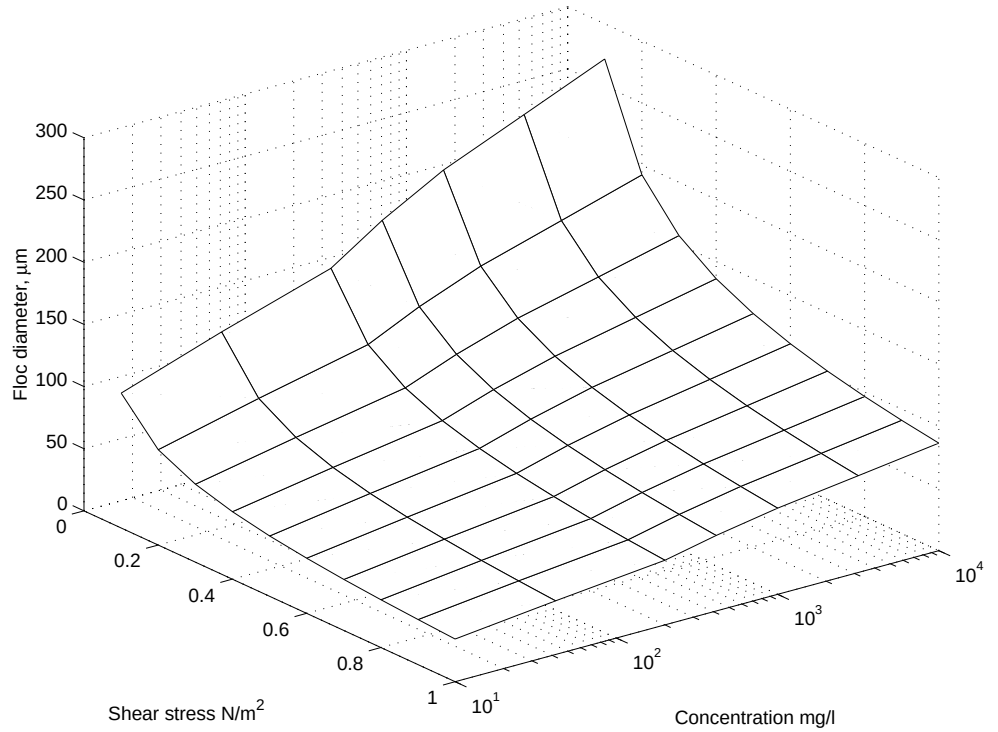

Figure E31. Calculated floc size as a function of shear stress and concentration

Figure E32 shows settling velocity as a function of concentration, based on the laboratory settling column data using sediment from the site (Gowland 2002). The curve is described by the equation

$$W_s = \frac{aC^n}{\left(b^2 + C^2\right)^m} \tag{E.39}$$

with the parameters a, b, n and m set to 0.035, 2.0, 3.5 and 2.75, respectively.

For calculation purposes, the value of the fractal diameter, nf [Equation E.26], was taken as 2.3. By fitting the settling velocity predicted by the model to the curve given by Figure E32, the parameters (k_a, k_b, p and q) for the settling calculation velocity were found. The exponents p and q were found to be 0.7 and 0.5, respectively, and the growth/breakup efficiency coefficients $k_a = 10.3$ and $k_b = 16.8 \cdot 10^3$. The values of these coefficients are of the same order of magnitude as those of Winterwerp (1998) ($k_a = 14.7$ and $k_b = 14.0 \cdot 10^3$). Fluid properties were selected as ρ_w = 1,020 kg/m^3 and $\nu = 10^{-6}$ m^2/s.

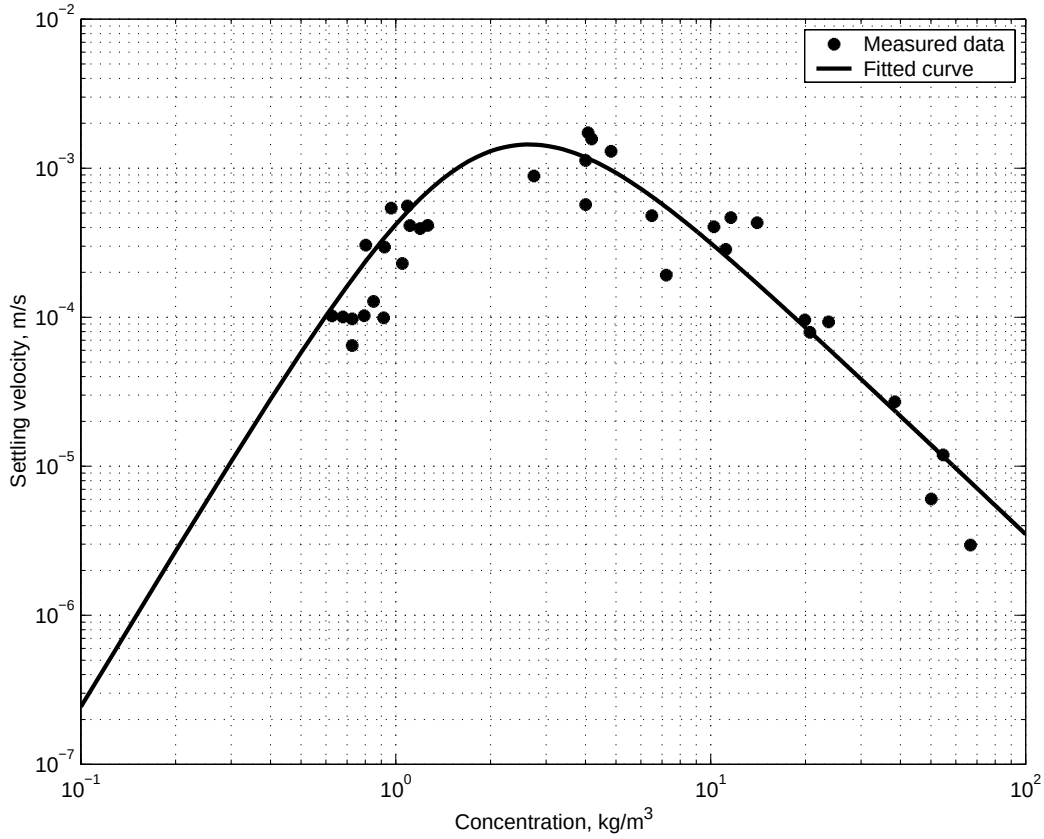

Figure E32. Settling velocity curve based on laboratory tests in a settling column using sediment from the Cedar River and vicinity (after Gowland 2002)

E4.3 Trapping Efficiency Analysis

E4.3.1 Treatment Plan

As described in Section E1.2, the effects of two sediment treatment sites were to be tested. For the present purpose the locations of the sites (1 and 2) were changed (Figure E21). Each site was tested with four assumed trapping efficiencies: 0% (no trapping), 30%, 60% and 90%. The maximum efficiency (90%) is in part based on the estimated 85% for TSS removal by Wet Detention Systems (WDS) in Florida (see Table E5).

Table E5. TSS removal efficiencies of treatment systems in Florida (after Harper 1997)

Treatment system	Estimated TSS removal efficiency (%)
Dry Retention	60-98
Off-Line Retention/Detention	90
Wet Retention	85
Wet Detention	85
Wet Detention with Filtration	98
Dry Detention	70
Dry Detention with Filtration	60-70
Alum Treatment	90

For that purpose, the resulting (calculated) settling flux (total mass of sediment passing the cross-section of the estuary in a unit of time) values at the Cedar River open boundary were compared to determine the potential effect of trapping sediment near the upstream end of the Cedar River (Site 3) on deposition downstream, where contaminated sediments derived from upstream Cedar River tend to deposit. It should be noted that in the Cedar River the direction of the water flow changes with flood and ebb tides; hence the ebb tide is the only time when there is a sediment flux out of the river.

E4.3.2 Sediment Trap Setup

The sediment trap at the treatment site typically is a water detention (i.e., temporary retention) pond. By diverting river flow into the pond where flow velocities are small, a major portion of suspended sediments will typically deposit. Such systems can also be effective for storm water treatment when the bulk of the solids is carried with the first flush, as they can be intercepted and given a sufficient residence time to allow them to deposit. While some treatment facilities may require drainage pumps, others are strictly gravity flow systems. If the water is high in nutrients, the facility may include a vegetated wetland area that will absorb the nutrients in the water before it is discharged into the receiving waters. The concern for the Cedar River treatment system was to provide as much treatment as possible; hence the effectiveness of the facility was defined by the area available for it. Due to modeling limitations and related complications in representing the site as a water body with channelized flow diverted into it, site representation in the model was simplified. Accordingly, a function was implemented that decreased the sediment flux bypassing the grid cell by a pre-defined percentage. The channel cross-section, where the treatment site would be located, was represented by cells having such a sediment removal function (in

terms of the percentage by which the effluent sediment load, leaving the site, is reduced with respect to influent load entering the site).

E4.3.3 Effect of Trap Efficiency on Settling Flux Downstream

Cedar River model runs were run without and with the sites in place (Figure E21), each for the selected four removal ratios (0%, 30%, 60%, and 90%). The model was run for three days, during May 16-18, 2001. Four output control points (CP1-CP4) were selected (Figure E21). CP1-CP3 corresponded to the sites and were placed just upstream of a site to measure sediment flux into the site, and CP4 was the control point just upstream of the open boundary, for monitoring trapping influence at the downstream end.

Net sediment fluxes at the control points averaged over three semi-diurnal tidal cycles (the second cycle on May 17 and two cycles on May 18, 2001) are presented in Table E6. As seen in this table, it can be inferred that Sites 1 and 2 in the upstream portion of the Cedar River would have a small effect on sediment transport at the lower end of the Cedar River. In contrast, Site 3 can be considerably more effective. The reason for these differences appears to be that the majority of sediment load is derived from Williamson and Butcher Pen Creeks, rather than the Cedar River.

Table E6. Comparison of sites with different removal efficiencies with a no-trapping scenario

Trap efficiencies (%)			Net sediment flux g/s				Resulting efficiency at the confluence (%)
Trap 1	Trap 2	Trap 3	CP1	CP2	CP3	CP4	
0	0	0	6.7	8.9	11.4	14.1	0.0
30	0	0	6.7	7.9	11.0	13.8	2.1
60	0	0	6.7	7.7	9.9	13.6	3.5
90	0	0	6.7	7.0	9.6	13.1	7.1
0	30	0	6.7	8.9	10.1	12.3	12.8
0	60	0	6.7	8.8	8.2	10.9	22.7
0	90	0	6.7	8.7	7.6	9.2	34.7
0	0	30	6.7	8.9	11.4	10.6	24.8
0	0	60	6.7	8.8	11.4	7.9	44.0
0	0	90	6.7	8.8	11.2	5.8	58.9
30	30	30	6.7	7.8	7.2	6.9	51.1
60	60	60	6.7	6.0	4.1	2.9	79.4
90	90	90	6.7	2.8	1.1	0.3	97.8

The above observations are further highlighted in Table E7, by taking the cases of no entrapment and 30% entrapment (which may closer to a realizable efficiency), and seeing the effect in the confluence area. From the table it appears that: 1) Any treatment facility upstream of Williamson and Butcher Pen Creeks, as presently envisaged, will not be effective in reducing sediment loading in the confluence area, 2) treatment downstream of Butcher Pen will have measurable, but possibly not significant effect, and 3) more than one treatment site may have to be developed. In the event that a downstream treatment site cannot be constructed, dredging a trap in the riverbed at that site should be considered. Such an action should preferably be coupled with a one-time dredging of the confluence area to remove soft sediment deposit there.

Table E7. Summary of the effect of treatment on sediment load in the confluence area

Upstream Cedar	Mid-stream Cedar	Downstream Cedar	Load reduction at the confluence (%)
Treatment	–	–	-2
–	Treatment	–	-13
–	–	Treatment	-25
Treatment	Treatment	Treatment	-51

E5. Conclusions

E5.1 Summary

A study of the effectiveness of fine sediment trapping in the Cedar River estuary in north Florida was carried out. A combined three-dimensional hydrodynamic and sediment model was set up and calibrated for this estuary. The original model (EFDC) was improved for fine sediment settling velocity calculations, by accounting for floc growth and breakup processes due to turbulence. The effect of selected sediment treatment sites or traps with different efficiencies (and placed in different locations upstream) on sediment transport downstream was examined.

E5.2 Conclusions

The following are the main conclusions of this study:

1. Simulated discharge and tidal variations in the Cedar River were found to agree reasonably well with measurements.

2. The settling velocity calculation routine was found to be applicable to conditions when the flow is turbulent, but not in near-quiescent waters, i.e., when the energy dissipation parameter has low values.

3. It appears that fine sediment trapping in the upstream reach of the Cedar River would have only a minor effect on sediment transport downstream near the confluence of the Cedar and Ortega Rivers. This is so because a major part of suspended sediment flux downstream appears to arrive there from creeks (especially Butcher Pen and Williamson) that flow into the middle reach of Cedar River.

4. Sediment entrapment closer to the confluence of the Cedar and Ortega rivers appears to be able to measurably reduce sediment transport to the confluence and, therefore, can be expected to lower the flux of contaminants out of Cedar River.

E5.3 Recommendations for Further Work

Further development of the settling velocity model is required, in order to extend the calculation to settling in near-quiescent water. Traps simulation should be made more realistic by incorporating the mechanics of an actual retention/detention pond in the model.

References

Dyer, K. R. 1989. Sediment processes in estuaries: Future research requirement. *Journal of Geophysical Research* 94(C10): 9489-9498.

Ganju, N. K. 2001. Trapping organic-rich sediment in an estuary. Unpublished master's thesis, University of Florida, Gainesville.

Gowland, J. E. 2002. Laboratory experiments on the erosional and settling properties of sediment from the Cedar/Ortega River system. *Report UFL/COEL-CR/2002/00*1. Coastal and Oceanographic Engineering Program, Department of Civil and Coastal Engineering, University of Florida, Gainesville.

Hamrick, J. M. 1992. A three dimensional environmental fluid dynamics computer code: Theoretical and computational aspects. *Special Report No 317*. Applied Marine Science and Ocean Engineering, Virginia Institute of Marine Science, Gloucester Point.

———. 1996. User's manual for environmental fluid dynamics computer code. *Special Report No 331*. Applied Marine Science and Ocean Engineering, Virginia Institute of Marine Science, Gloucester Point.

Harper, H. H. 1997. Pollutant removal efficiencies for typical stormwater management systems in Florida. *Proceedings.* The Biennial Stormwater Research Conference, Southwest Florida Water Management District, Tampa, Florida, 6-19.

Huang, H. 1994. Fractal properties of flocs formed by fluid shear and differential settling. *Physics of Fluids* 6(10):3229-3234.

Levich, V. G. 1962. *Physicochemical hydrodynamics*. Prentice Hall, Inc.

McAnally, W. H., and A. J. Mehta. 2000. Aggregation rate of fine sediment. *Journal of Hydraulic Engineering* 126(12): 883-892.

———. 2001. Collisional aggregation of fine estuarine sediment. In *Coastal and Estuarine Fine Sediment Processes*, W. H. McAnally and A. J. Mehta, eds., Elsevier, Amsterdam, 19-40.

Mellor, G. L., and T. Yamada. 1982. Development of a turbulence closure model for geophysical fluid problems. Reviews in *Geophysics and Space Physics* 20: 851-875.

National Research Council. 2001. A risk-management strategy for PCB-contaminated sediments. National Academy Press, Washington, DC.

Parshukov, L. N. 2001. Effect of turbulence on the deposition of cohesive flocs. Unpublished master's thesis, University of Florida, Gainesville.

RD Instruments. 1994. *Transect: User's Manual for Broadband Acoustic Doppler Current Profilers*. San Diego, California.

Smolarkiewicz, P. K. 1983. A simple positive definite advection scheme with small implicit diffusion. *Monthly Weather Review* 111: 479-486.

Stoddard, D. M. 2001. Evaluation of trap efficiency in an estuarine environment. *Report MRP-2001/003*. Department of Civil and Coastal Engineering, University of Florida, Gainesville.

Stolzenbach, K. D., and M. Elimelich. 1994. The effect of density on collisions between sinking particles: implications for particle aggregation in the ocean. *Journal of Deep Sea Research* 41(3): 469-483.

Teeter, A. M. 2001. Clay-silt sediment modeling using multiple grain classes: Part I: Settling and deposition. In *Coastal and Estuarine Fine Sediment Processes*, W. H. McAnally and A. J. Mehta, eds., Elsevier, Amsterdam, 157-170.

Van Leussen, W. 1994. Estuarine macroflocs and their role in fine-grained sediment transport. Unpublished Ph.D. dissertation, University of Utrecht, The Netherlands.

Winterwerp, J. C. 1998. A simple model for turbulence induced flocculation of cohesive sediment. *Journal of Hydraulic Research* 36(3): 309-326.

Wolanski, E., R. Gibbs, P. Ridd, A. Mehta. 1992. Settling of ocean-dumped dredged material, Townsville, Australia. *Estuarine, Coastal and Shelf Science* 35: 473-489.

Thesis Appendix EA
Water Discharge Estimation Based on ADCP

Water discharge must be calculated for each ADCP transect. Due to the inability of the ADCP used to record measurements close to the water surface and the bottom, as well as in the shallow near-bank areas, a method must be used to account for the loss of coherent signals for these blank zones in an approximate way. The following uses the method suggested and used in RD Instruments, WinRiver (software designed by RD Instruments for analysis and visualization of the ADCP data) and is described in a help system provided with the software.

The required total discharge (Q_{total}) from the instrument consists of measured ($Q_{measured}$) and estimated (Q_{est}) values:

$$Q_{total} = Q_{est} + Q_{measured} \tag{E.37}$$

The estimated discharge, which must be added to the measured value, consists of four components: top (layer close to the surface), bottom (layer close to the bottom), right and left (discharge in the zones close to the bank, where ADCP data are usually not taken because of shallow water). The "estimated" discharge is then calculated as:

$$Q_{est} = Q_{top} + Q_{bottom} + Q_{right} + Q_{left} \tag{E.38}$$

For calculating the top and bottom discharges two (user-definable) methods can be used: Constant and Power. The Constant Method assumes that the velocity is constant in the top/bottom layer and is equal to topmost/bottommost successfully measured acoustic bin. The Power Method assumes a power-law velocity (u) profile in the vertical (z) direction:

$$u = r \cdot z^{p} \tag{E.39}$$

in which the exponent p is user-defined with a default value of 1/6, and the proportionality constant r is found by fitting the power-law profile to the measured points.

For calculating the right/left discharge the following formula is used:

$$Q = c \cdot D \cdot H \cdot u_{avg} \tag{E.40}$$

where c is a user-defined coefficient equal to0.35 for a triangular near bank bottom shape (default) and 0.91 for a rectangular near bank bottom shape; D is a distance to bank (defined in a data collection process and obtained from the ADCP data files); H is a water depth of the leftmost/rightmost measured ensemble; and u_{avg} is velocity averaged over the user-defined number of leftmost/rightmost ensembles.

Thesis Appendix EB
Settling Velocity and Floc Size Calculations

EB.1 Introduction

In order to demonstrate the application of the settling velocity model described in Section E2.4 of this thesis and to test the model against the data available in the literature, the following calculation tests were performed.

EB.2 Settling Velocity Calculations

Wolanski et al. (1992) presented data on the settling of sediment from Townsville Harbor, Australia. A Plexiglas cylinder of 10 cm internal diameter and 140 cm height was used as a settling column. Turbulence could be generated in this column by oscillating 1-cm wide rings along the walls, spaced 2 cm apart. Two sets of data were obtained: in quiescent water, and with rings oscillating. Quiescent water can be characterized by very low values of dissipation parameter G.

First, model predicted settling velocity was fitted to the data in oscillating flow based on Equations E.29 and E.36, and floc aggregation coefficient in a form similar to Equation E.39, i.e., $k_a = k'_\alpha \dfrac{C^n}{\left(b + C^2\right)}$. The parameters k_a, k_b, p and q were determined in this way; p and q were found to be 0.6 and 0.45, respectively, and. $k_a = 8.7$ and $k_b = 19.1 \cdot 10^3$ for $n = 0.87$ and $b = 1.96$. A representative value of the dissipation parameter was found to be $G \approx 1.3$ Hz. Then $G \approx 10^{-2}$ Hz was used to represent quiescent water and the corresponding velocity curve was plotted (Figure E33).

In Figure E33, the simulated curve based on measurement in oscillating water indicates a reasonably good match with data points. However, measurements in quiescent water are not predicted as well. This is believed to be due to the fact that, as noted in Section E4.2.2 of this thesis, the model does not perform well for low values of dissipation parameter G (i.e., in the absence of turbulence).

EB.3 Particle Size Calculations

In steady flows and with given sediment properties, flocs tend to have a narrow size distribution and may be assumed to have an equilibrium size defined in terms of, for example, the median diameter. The equilibrium size condition implies that the growth and breakup processes balance each other. Thus, flocs that are smaller than the equilibrium size would have growth dominating over breakup, and for larger flocs the breakup process would be dominant. As a result the floc size tends to fluctuate around its equilibrium value.

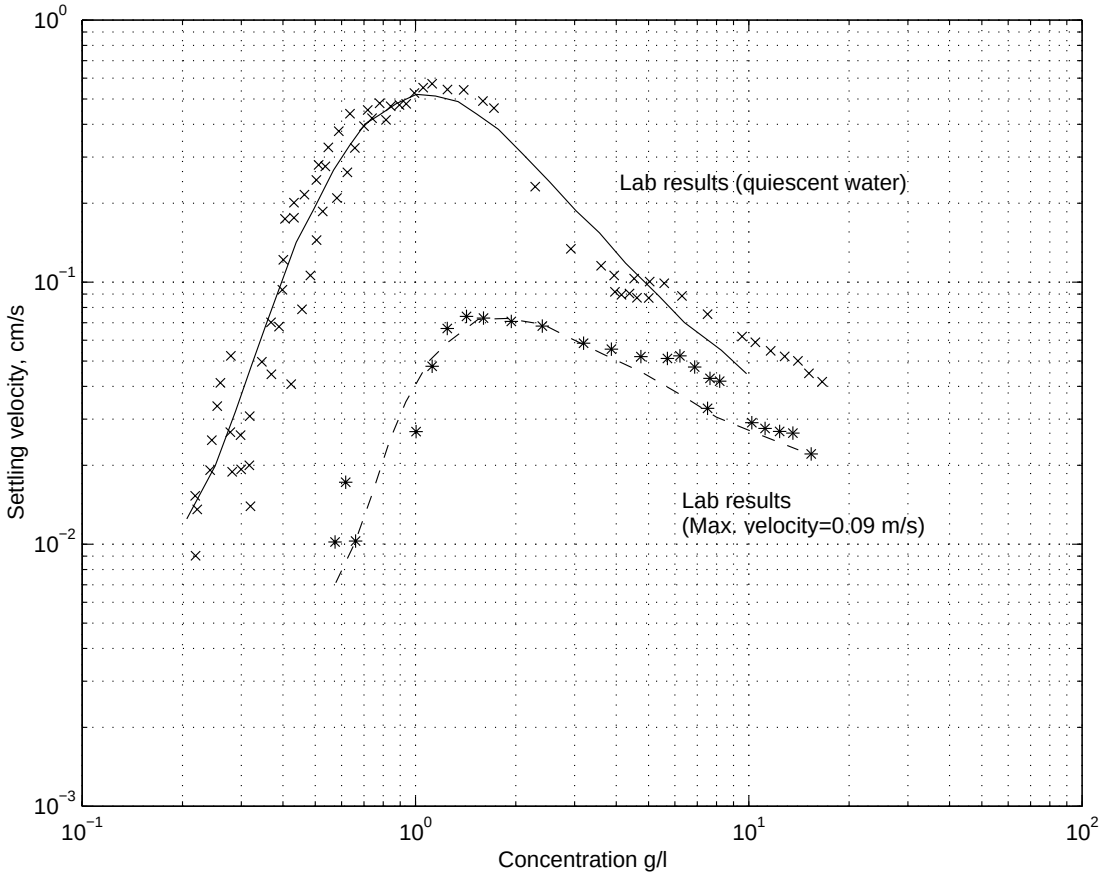

Figure E33. Settling velocity calculation test results, and comparison with data of Wolanski et al. (1992) using sediment from Townsville Harbor, Australia

The model was tested against the floc size data published by Winterwerp (1998) from two settling column tests using sediment from the Ems-Dollard River area in The Netherlands. Particle sizes were measured using a Malvern particle sizer. For simulation purposes the parameter values in Table E8, plus those provided by Winterwerp, were used. The initial particle size was taken as 4 μm, as measured by Winterwerp. Coefficients $k_a = 14.7$ and $k_b = 14.0 \cdot 10^3$ were selected.

Table E8. Data from settling column tests with Ems-Dollard mud

Test No	c (kg/m^3)	G (Hz)
T-73	1.21	81.7
T-69	1.17	28.9

Comparisons between simulations and data are shown on Figure E34. The values of concentration and dissipation parameter used are given in Table E8. The resulting curves, which lead to equilibrium sizes, appear to be the same as those of Winterwerp (1998). Floc

size is seen to grow with time until it reaches an equilibrium value (there is an equilibrium particle size for given concentration and dissipation parameter) and remains the same beyond that point.

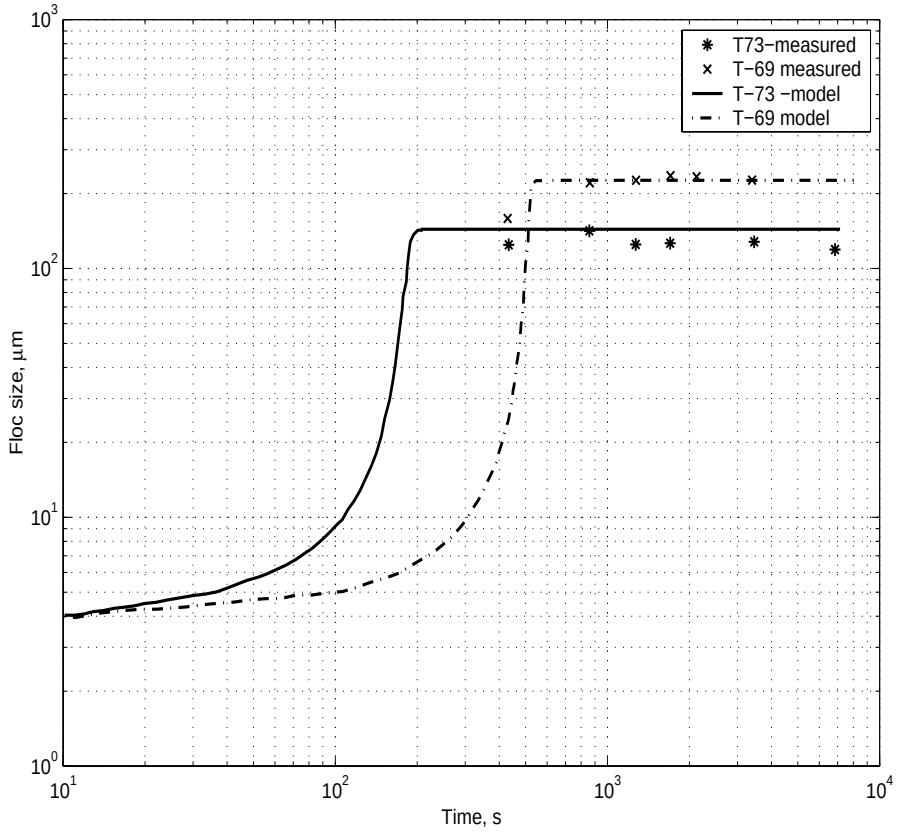

Figure E34. Floc growth with time measured and predicted for River Ems-Dollard mud (Winterwerp, 1998)

(Page intentionally blank)

Appendix F

Evaluation of Sediment Trap Efficiency in an Estuarine Environment

Daniel M. Stoddard
Department of Civil and Coastal Engineering
University of Florida

for

St. Johns River Water Management District
Palatka, Florida

May 2002

Executive Summary

Trench-traps are utilized where sediment containment is a concern. In this study, trapping efficiency is key concern. A 60 m(L) × 300 m(W) × 2 m(D) trap was incorporated into the Cedar River, near the confluence with the Ortega River. A second trap of same dimensions was also incorporated 420 m upstream.

Trap efficiency was calculated as a sediment removal ratio, or the percentage by which influent sediment load to the trap is reduced in the effluent load from the trap. Trap efficiency was carried out for varying Cedar River discharges. A specific discharge (16.4 m^3/s) was found to yield the maximum removal. At discharges above and below this discharge, the removal ratio decreases. This is attributed to the increase in tidal influence at lower discharges and velocities too large to allow settling at higher discharges.

Future work includes developing a monitoring scheme to determine actual sedimentation rates in a test trap at the chosen location.

Contents

List of Figures

List of Tables

List of Symbols

A	=	area
C	=	sediment concentration (kg/m^3)
C_1	=	sediment concentration (kg/m^3) related to Equation F.13
C_z	=	Chézy discharge coefficient
$D_x, D_{xx}, D_{xy}, D_{yx}, D_{yy}$	=	horizontal dispersion coefficients
H	=	depth (m)
H_e	=	equilibrium bed elevation related to Equation F.33
H_0	=	datum bed elevation related to Equation F.33
K	=	sedimentation coefficient related to Equation F.33
K_L, K_T	=	longitudinal and transverse dispersion constants, respectively
L	=	channel length
L_o	=	original trap length related to Equation F.31
M	=	number of time steps in one ebb tidal period
Oc	=	organic content (%)
P	=	tidal prism (m^3)
Pe	=	Peclet number
Q	=	discharge (m^3/s)
Q_d	=	depositional flux (kg/m^2-s)
Q_e	=	erosional flux (kg/m^2-s)
Q_f	=	freshwater discharge (m^3/s)
R	=	sediment removal ratio
R^2	=	correlation coefficient
R_{ave}	=	ebb-tide averaged removal ratio
S	=	sediment source/sink term
Sa	=	salinity (ppt)
S_R	=	sedimentation rate (m/d)
T	=	tidal period (s)
U	=	depth-averaged, x-direction velocity (m/s)
V	=	depth-averaged, y-direction velocity (m/s)
W_s	=	settling velocity (m/s)
W_{sf}	=	free settling velocity (m/s)
a	=	empirical coefficient related to Equation F.13
b	=	empirical coefficient related to Equation F.13
g	=	acceleration due to gravity (m/s^2)
h	=	water depth
Δh	=	deposit thickness
k	=	damped wave number
k_0	=	frictionless wave number
m	=	empirical coefficient related to Equation F.13 and F.31
n	=	Manning's flow resistance coefficient related to Equation F.13
n_s	=	sediment bed porosity
n_w	=	empirical coefficient related to Equation F.13
p	=	probability of deposition

q = sediment load (kg/s)
q_e = influent sediment load (kg/s)
q_i = effluent sediment load (kg/s)
t = time
Δt = time step
u_b = bottom, x-direction velocity
v_b = bottom, y-direction velocity
w_c = sediment water content
x = horizontal coordinate
y = horizontal coordinate
z = vertical coordinate
α_s = empirical coefficient related to Equation F.16
β_s = empirical coefficient related to Equation F.16
γ = bottom friction-dependent coefficient
ε_N = erosion rate constant (kg/m^2-s)
ε_{NO} = limiting erosion rate constant (kg-N/s)
η = water surface elevation
λ = tidal influencing factor related to Equation F.12
ν = eddy viscosity
ρ_b = sediment bulk density (kg/m^3)
ρ_d = bottom sediment dry density (kg/m^3)
ρ_s = sediment granular density (kg/m^3)
ρ_w = water density (kg/m^3)
τ_b = bed shear stress (Pa)
τ_d = critical shear stress for deposition (Pa)
τ_s = bed shear strength (Pa)
Φ = solids volume fraction
Φ_e = limiting solids volume fraction

F1. Introduction

F1.1 Problem Statement

Sediment shoaling in estuarine environments can create significant problems such as decreased discharges, degradation of water quality, and concentration of contaminants and organic compounds. One commonly employed solution to reduce sedimentation is the implementation of a trap scheme by creating a trench along the submerged bottom. To create a trench-trap, the depth at the chosen location is increased by dredging. In this study, a sediment trap is defined as an area of the submerged bottom deepened to a depth greater than the surrounding bottom, in order to reduce flow velocity. The lower velocity should allow sediment to deposit in the trap rather than move past and deposit elsewhere. This in turn allows for maintenance dredging to be performed at a specific location (the trap) rather than over a broad submerged area. The increased depth results in a decreased flow velocity, thereby allowing incoming sediment to settle in the trap itself, instead of being carried further downstream. The sediment can then be removed from the trap, rather than dredging the otherwise distributed deposit from a broader area. By holding the trap depth and location constant and varying the discharge of the river system, the efficiency of a trap can be assessed for different flow discharges. For present purposes, efficiency will be determined by the sediment removal ratio, which is the percentage by which the effluent sediment load (leaving the trap) is reduced with respect to influent load entering the trap (Ganju 2001). By creating efficient traps much of the detrimental effects of excess sediment and unwanted pollutants entering the system can be curtailed.

F1.2 Role of Florida Sediment

In Florida's biologically highly active estuarine and lacustrine environments, the fraction of fine-grained sediment that is organic is often on the order of 20-60% by weight and sometimes as high as 90-95%. There are three main sources of this organic matter. Terrestrial systems tend to be abundant in carbon (C), and the biomass produced by woodland and grassland is on the order of 50g C/m^2 (Mehta et al. 1997). Much of this material is degraded by the soil but some of it is washed away and introduced into fresh water and marine environments. The composition of this material is mainly cellulose which is non-degradable by water itself and the existing soil is less efficient in degrading the organic material making its breakdown very slow. Although aquatic plants breakdown more easily, they also contribute to the input of organic matter. The third source of organic matter is provided by phytoplankton, which usually has a biomass of 1.5C/m^2 with 5-6 crops/year for the Florida region. Trefry et al. (1992) state that the coastal waterways in Florida are stressed by inputs of fine-grained organic-rich sediments from riverine systems. Besides the alterations of the benthic community that this input causes, there are indirect problems associated with organic sediment such as sorption of contaminants like Cd, Cu, Hg, Pb, Zn and PCB's. In the Cedar River, PCB's in sediment have been documented to be up to 0.023 ppm (Campbell et al. 1993) and detectable amounts (up to 0.055 ppm) are also found in every species of fish collected from the area**.**

Most of Florida estuaries are microtidal, hence another important feature of the region is the occurrence of episodic events such as heavy rainfall and storms which act as natural dredging mechanisms due to the strong currents generated (Marván et al. 2001).

The area of study is the Cedar River system located in Northeast Florida. Trapping contaminants in the Cedar River system is important due to the elevated concentration of PCB (polychlorinated biphenyl) contaminants in the water system due to leeching of sediments and runoff from a fire at a chemical company in January 1984. The site was located approximately 0.35 miles east of the Cedar River near the headwaters north of Interstate I-10 and also adjacent to municipal storm drains and drainage ditches. The fire destroyed several tanks storing high concentrations (4,425 ppm) of PCB laden oils and other materials. It is believed that a combination of the damage to the storage tanks and the fire fighting effort created a vehicle for the PCB contaminant to enter the Cedar River basin. The surrounding groundwater and soil was sampled extensively in 1989 and the concentrations were still significantly above the regulated amount of 50 ppm.

The filtering role of estuaries makes them crucial transitional areas trapping significant quantities of particulate and dissolved matter through a wide variety of physical and biogeochemical processes. Cohesive sediments play an important role in these processes. Unlike sand, well characterized by its grain size distribution, cohesive sediments are complex mixtures of different clay minerals, mainly organic matter, and a small percentage of sand and silt. Hydrodynamic action is the most important mechanism involved in sediment transport. It advects the suspended sediments, provides the force needed to erode the bed and, through turbulence, plays a major role in the flocculation of cohesive sediments. Relatively large velocities generally occur in tidal estuaries. Because the hydrodynamic processes involved in sediment transport are mainly non-linear, the sediments are very mobile in these estuaries. They are eroded and transported upwards during flood, deposited during slack water, eroded again and transported downwards during ebb and redeposited during next slack water, to restart their movement in the forthcoming tidal cycle. Cohesive and non-cohesive sediments are different from each other in two major aspects: flocculation and consolidation of deposited material with compaction of the sediments. Flocs are formed by joining individual particles and can strongly modify the settling velocity of particulate matter. After bottom deposition, the water content is still a significant part of the bed material. The expulsion of this water is part of the sediment consolidation process. The small pore dimensions imply long times for sediment deposition, which creates conditions for fluid-mud formation in environments with very high availability of sediments (Cancino and Neves 1999).

Fine-grained cohesive sediments are important in two types of engineering problems. The first relates to the sedimentation of harbors and channels and to dredging and navigation, and the second to the mixing and dispersion of contaminants. The properties of muddy sediments are significantly affected by chemical and biological factors. As a result of their cohesive nature, mud particles absorb pollutants, especially heavy metals and pesticides. As a result, understanding pollutant dispersion depends on an understanding of particle transport. The ubiquitous bacteria and other organisms secrete films that act as a very effective glue in enhancing the resistance of the bed to erosion. However, it is noteworthy

that, in general, bioturbation acts both to increase cohesiveness and also to loosen beds and resuspend sediment (Mehta and Dyer 1990).

F1.3 Objective and Tasks

The main objective is to determine how sediment traps respond to variable discharges (concentration and velocity) in the Cedar River estuarine system by analyzing the trapping efficiency.

Several tasks must be undertaken to determine the efficiency of this selected trapping scheme. These include:

1. With the exception of two samples (O-02 and O-11), which mainly consisted of sand, the remaining 18 samples had organic content ranging from 16 to 74%.

2. Analysis of the data collected to characterize the nature of the sediment to determine the historical suspended sediment concentration data.

3. Modeling the flow field via a hydrodynamic model, in order to determine the velocities as well as the water surface elevations.

4. Reevaluation and recalculation of rating curve results from previous analysis. This new curve will be used to calculate concentrations associated with the varying discharges.

5. Utilization of a sediment transport model to determine suspended sediment concentrations. This model will incorporate the sediment characteristics determined from the sediment analysis.

6. Two trap locations will be evaluated in the calibrated flow model, and the output from that model will be applied to the calibrated sediment transport model. The influent and effluent sediment loads through the trap will be recorded in order to quantify trap efficiency of each trap.

F1.4 Report Outline

The following sections of the report will describe how the trap efficiency will be evaluated and the modeling efforts required. Next, a basic description of the Cedar and Ortega River system will be provided. The report will continue with development of the sediment rating curves, the trap design selection and the efficiency analysis of the selected trap. The summary, conclusions and recommendations will complete the report followed by a bibliography.

F2. Method of Analysis

F2.1 Trap Efficiency

The modeling of trap efficiency requires the use of a flow and sediment transport model. A flow model will provide water velocities and surface elevations, and these solutions will be applied to a sediment transport model. The sediment transport model will predict erosion, deposition, and suspended sediment concentrations in the presence of the trap.

F2.2 Flow Modeling

F2.2.1 Governing Equations

The Navier-Stokes equations govern the free surface flows of constant density and incompressible fluids (Pnueli and Gutfinger 1992). Applying the hydrostatic pressure distribution assumption yields three-dimensional model equations, and these can be vertically integrated to produce the following two-dimensional shallow water equations (Casulli 1990):

x-momentum:

$$\frac{\partial(HU)}{\partial t}+\frac{\partial(HUU)}{\partial x}+\frac{\partial(HUV)}{\partial y}=-gH\frac{\partial \eta}{\partial x}+\frac{\partial}{\partial x}\left(\nu H\frac{\partial U}{\partial x}\right)+\frac{\partial}{\partial y}\left(\nu H\frac{\partial U}{\partial y}\right)-\gamma U \tag{F.1}$$

y-momentum:

$$\frac{\partial(HV)}{\partial t}+\frac{\partial(HUV)}{\partial x}+\frac{\partial(HVV)}{\partial y}=-gH\frac{\partial \eta}{\partial y}+\frac{\partial}{\partial x}\left(\nu H\frac{\partial V}{\partial x}\right)+\frac{\partial}{\partial y}\left(\nu H\frac{\partial V}{\partial y}\right)-\gamma V \tag{F.2}$$

continuity:

$$\frac{\partial \eta}{\partial t}+\frac{\partial(HU)}{\partial x}+\frac{\partial(HV)}{\partial y}=0 \tag{F.3}$$

where H is the water depth, U is the vertically-averaged horizontal x-direction velocity, V is the vertically-averaged horizontal y-direction velocity, t is time, g is the acceleration due to gravity, η is the water surface elevation measured from the undisturbed water surface, ν is the eddy viscosity, and γ is the bottom friction dependent coefficient defined as

$$\gamma=\frac{g\sqrt{u_b^2+v_b^2}}{C_z^2} \tag{F.4}$$

where u_b and v_b are the horizontal x and y bottom velocity components respectively, and C_z is the Chézy discharge coefficient, which is related to Manning's n by

$$C_z = \frac{(H+\eta)^{1/3}}{n} \tag{F.5}$$

Solving this system of three partial differential equations (Equations F.1, F.2, and F.3) for the three unknowns (U, V,η) can be accomplished via a numerical method. The numerical algorithm used is based on the method developed by Casulli (1990). First, a characteristic analysis is performed on Equations F.1–F.3, in order to determine which terms must be discretized implicitly, such as the water surface elevation (Equations F.1, F.2), and the velocity divergence (Equation F.3). The advective terms are discretized explicitly using an upwind scheme, which is unconditionally stable when a Eulerian-Lagrangian method is used to discretize the terms. This method requires the solution of a 5-diagonal matrix at every time step. It is used in conjunction with an alternating-direction implicit (ADI) routine, which results in two simpler, linear tri-diagonal matrices (Casulli 1990).

F2.2.2 Model Operation

The 2-D vertically averaged hydrodynamic model reported by Marván (2001) which was developed by Casulli (1990) used in this study is operated using the MATLAB computational computer application. The use of MATLAB allows for the generation of the necessary graphics and data output in a simple fashion, though the computational effort is intensive, due to the necessity of large matrices. Rectangular grids with square elements are used, with numeric "ones" indicating the body of water, and "zeros" representing land boundaries developed for input into the computer model. A similar grid is required for the input bathymetry, with the depth at mean high water entered into each element.

F2.2.3 Flow Boundary Conditions

Flow boundaries are indicated by extending water cells to the grid edge. If freshwater inflow is desired, a permanent velocity can be imposed at the edge, corresponding to the desired flow condition. If a non-steady state inflow is desired, velocity as a function of time can be implemented. For a tidal flow boundary, a function specifying the water surface elevation at the boundary can be applied. If no velocity or elevation is specified at cells, which terminate at the grid edge, they become no-flow boundaries in the algorithm.

F2.2.4 Flow Model Input/Output Parameters

The area and bathymetry grids described in Section F2.2.2 are required to specify the domain to be modeled. Other required inputs are the tidal forcing function at the seaward boundary, the calculation time step, the total simulation time, a file containing Manning's n coefficient values for each cell, and velocities at the tributary flow boundaries. The output is three matrices consisting of the water surface elevations, x-direction velocities, and y-direction velocities, for every time step in the simulation.

F2.3 Modeling Sediment Removal

F2.3.1 Flow Model Input/Output Parameters

The accurate prediction of suspended sediment transport in estuaries is important for activities such as dredging, the accurate mapping of navigation channels and improved understanding of pollutant transport. The difficulty in formulating accurate suspended sediment transport formulas suitable for a range of input conditions arises because the sediment transport forms a complex feedback system with the near-bed hydrodynamics and the bed topography. One important area of research related to the accurate prediction of suspended sediment transport is the formulation of the magnitude and shape of the temporally averaged suspended sediment concentration profile in a tidal channel. This subject is of practical importance, as the product of the temporally averaged suspended sediment concentration and horizontal velocity profiles form the dominant component of the horizontal suspended sediment flux in tidal and steady flow conditions (Rose and Thorne 2001).

The sediment removal will use a 2D MATLAB based horizontal depth-averaged fine sediment transport model with the capability to manipulate erosion and deposition functions based on organic content. Initially the model hydrodynamics are determined by a finite difference semi-implicit algorithm developed by Casulli (1990). In this, the water surface elevation is obtained implicitly and the velocity is determined in an explicit fashion.

F2.3.2 Governing Advection-Diffusion Equation

Advection-diffusion is calculated with Equation F.6 using a finite-volume explicit method based on the quadratic upstream (QUICKEST) method of Leonard (1977) (Marvan et al. 2001):

$$\frac{\partial hC}{\partial t}+\frac{\partial (huC)}{\partial x}+\frac{\partial (hvC)}{\partial y}-\frac{\partial}{\partial x}\left(D_{xx}\frac{\partial hC}{\partial x}+D_{xy}\frac{\partial hC}{\partial y}\right)+\frac{\partial}{\partial x}\left(D_{yx}\frac{\partial hC}{\partial x}+D_{yy}\frac{\partial hC}{\partial y}\right)=S \qquad \text{(F.6)}$$

where t is time, C is the depth-averaged suspended sediment concentration, u and v are the longitudinal and transversal depth averaged velocities, h is the water depth and S is a source-sink term. The dispersion coefficients D_{xx}, D_{xy}, and D_{yy} are treated as follows (Preston 1985):

$$D_{xx}=\frac{K_l u^2+K_t v^2}{C_z\sqrt{u^2+v^2}}h\sqrt{g} \qquad \text{(F.7)}$$

$$D_{yy}=\frac{K_l v^2+K_t u^2}{C_z\sqrt{u^2+v^2}}h\sqrt{g} \qquad \text{(F.8)}$$

$$D_{xy} = D_{xy} = \frac{(K_l - K_t)uv}{C_z\sqrt{u^2 + v^2}} h\sqrt{g} \tag{F.9}$$

where K_l and K_t are the dispersion coefficients in the longitudinal and transversal directions taken to be 13 and 1.2, respectively, C_z is the Che|y coefficient and g is the acceleration due to gravity. The source-sink term in Equation F.6 accounts for the erosion and deposition in the following way:

$$S = Q_e + Q_d \tag{F.10}$$

where Q_e is the erosion flux at every time step and Q_d is the corresponding deposition flux.

F2.3.3 Deposition Flux

The deposition flux is expressed according to Krone (1962) as:

$$Q_d = -pW_sC \tag{F.11}$$

where W_s is the sediment settling velocity and p is the probability for deposition defined as:

$$p = \left(1 - \frac{\tau_b}{\tau_d}\right) \tag{F.12}$$

where τ_b the bed shear stress and τ_d a critical shear stress for deposition. In this analysis, the parameter τ_d is set to a value above the highest shear stress found in the modeled domain, thus allowing deposition to occur at all times as long as suspended sediment is present.

Generally, the settling velocity of fine sediment is dependent on concentration. As a result, the settling velocity differs depending on three identifiable regimes: free settling, flocculation settling, and hindered settling. In the free settling range, relatively low concentrations permit the individual flocs to settle without interference from other flocs. The settling velocity in this range is a function of the drag coefficient and the submerged weight of the floc. As concentration increases, the collision frequency of flocs increases, resulting in the formation of larger flocs. These flocs are able to settle quicker due to their increased mass, and characterize the flocculation settling range. Eventually, the concentration in the water column reaches a point where a floc is unable to settle quickly due to significant interference from other flocs, and the limited pore space for the fluid. This interference reaches a maximum when the water column resembles a bed of mud with negligible settling (Mehta 1994). Hwang (1989) formulated a fit of the flocculation and hindered settling ranges, relating settling velocity to concentration as follows:

$$W_s = \frac{aC^{n_w}}{\left(C^2 + b^2\right)^m} \tag{F.13}$$

where a, b, m, and n_W are empirical constants. For the free settling range, at concentrations ($C \leq 0.25$ kg/m^3) a constant settling velocity (W_{sf}) is provided. Laboratory tests performed in a settling column are required to determine the site-specific constants. The settling velocity of the aggregates is a function of concentration and of shear stress, because the aggregation of particles depends on the number concentration of particles in the flow, but their ultimate size is limited by turbulent shearing (Mehta and Dyer 1990).

F2.3.4 Suspended Sediment Boundary Conditions

The boundary conditions at the tributary connections can be expressed as steady-state concentrations, or sediment rating functions can be applied if unsteady tributary flows are desired. This also holds true at the tidal entrance, where incoming concentrations can be specified, varying with tidal stage and/or current velocity.

F2.3.5 Erosion Flux

In contrast to τ_d, Q_e cannot be treated in this way because erosion depends on the shear strength of the soil and is therefore considered in the following form:

$$Q_e = \varepsilon_N \left(\tau_b - \tau_s\right) \tag{F.14}$$

where ε_N is the erosion rate constant and τ_s is the bed shear strength. The bed shear stress is computed as

$$\tau_b = \frac{\rho_w g n^2 U^2}{\left(H + \eta\right)^{1/3}} \tag{F.15}$$

where ρ_w is the density of water. The shear strength of the bed is calculated via Mehta and Parchure (2001):

$$\tau_s = \alpha_s \left(\phi - \phi_s\right)^{\beta_s} \tag{F.16}$$

where ϕ is the solids volume fraction (ρ_D/ρ_s), ρ_D is the dry density, ρ_s is the grain density, ϕ_s is the limiting solids volume fraction value of ϕ at which $\tau_s = 0$ and α and β_s are sediment-specific empirical coefficients.

F2.4 Sedimentation, Sediment Trap, and Trap Efficiency

F2.4.1 Sedimentation

Sedimentation at any point in the estuary can be calculated from the deposit thickness Δh given by

$$\Delta h = \sum_{i=1}^{\frac{t_S}{\Delta t}} \frac{Q_{d_i} \Delta t}{\rho_d} \tag{F.17}$$

where t_s is the total simulation time, Δt is the time step, i is the time step index, Q_{di} is the deposition flux, and ρ_d is the deposit dry density. The sedimentation rate is then calculated by

$$S_R = \frac{\Delta h}{t_s} \tag{F.18}$$

where S_R is the sedimentation rate.

It is well known that in rapidly moving waters, fine particles are not deposited. Consequently, consideration must be made that sedimentation increases as flow velocity decreases. Since there is a close relationship between flow velocity and bottom shear, the following hypothesis has been proposed: shear stress in moving waters is an important controlling (reducing) factor on sedimentation. In aquatic systems, there are cohesive and noncohesive particles. The theoretical basis of cohesive material sedimentation in moving waters was derived from the fundamental flume experiments of Partheniades (1965; 1972). These experiments showed that sedimentation, as well as resuspension, depend on bottom shear stress. There are threshold values, one for sedimentation and a much higher value for resuspension. It was found that the degree of deposition (the proportion of the initially resuspended material, which settles) as well as the rate of deposition is controlled by the bottom shear. Partheniades (1972) wrote: "We may distinguish two groups of flocs: those with sufficient high strength to resist the flow induced disruptive shear stresses, which are highest near the bed, and those with insufficient strength. The first will be able to reach the bed, will develop several bonds with it and will become a part of it; the remaining flocs will be disrupted and reentrained" (Kozerski and Leuschner 1999).

F2.4.2 Definition of Trap

In this study, a sediment trap is defined as an area of the submerged bottom deepened to a depth greater than the surrounding bottom, in order to reduce flow velocity. The lower velocity should allow sediment to deposit in the trap rather than move past and deposit elsewhere. This in turn allows for maintenance dredging to be performed at a specific location (the trap) rather than over a broad submerged area.

F2.4.3 Definition of Trap Efficiency

Trap efficiency is defined as the percent by which effluent suspended sediment load is reduced with respect to the influent suspended sediment load (removal ratio). In a tidal situation, the seaward edge of the trap will be the influent side during flood tide, and the effluent side during ebb tide, and vice versa for the landward edge.

F2.4.4 Calculation of Trap Efficiency

At each time-step in the sediment transport simulation the concentration, the velocity, and the water surface elevation will be calculated in each cell. The cells that border the trap and are flow-normal are also of interest. Sediment loads can be calculated for these border cells as follows:

$$q = UCH\Delta x \tag{F.19}$$

where q is the sediment load, U is the flow velocity, and Δx is the cell width. The sediment load on each side of the trap will be used to compute the sediment removal ratio as follows:

$$R = \frac{q_i - q_e}{q_i} \tag{F.20}$$

where R is the removal ratio, q_i is the influent sediment load, and q_e is the effluent sediment load. The removal ratio will be averaged over a tidal cycle, using the removal ratio values from each time-step.

F2.4.5 Calculation of Trap Efficiency as a Function of Discharge

Simulations will be run for different discharges of the Cedar River. The average removal ratio for each trap will be compared for a given flow discharge. The normal flow will be used as the benchmark by which the efficiency of the trap will be assessed under the other discharge cases. The removal ratio as a function of discharge will be plotted to determine what effect discharge has on trap efficiency.

F3. Cedar, Ortega, and St. Johns River System

F3.1 History and Description of the System

Before European involvement in North America, the Timucuan Indians called the St. Johns River Welaka, or river of lakes. In the early 1500s, Spanish seamen called the river Rio de Corrientes or River of Currents. In 1562, almost 50 years before the settlement in Jamestown, the French established Fort Caroline on a high bluff overlooking a river they called Riviere de Mai (River of May) because they arrived there on May 1. In 1565, Spanish soldiers marched north from St. Augustine, captured Fort Caroline and slaughtered the

French. The Spanish renamed the river San Mateo to honor the saint whose feast followed the day they captured the river. Later, the river was renamed Rio de San Juan after a mission near its mouth named San Juan del Puerto. The English translation of the name Rio de San Juan, St. Johns River, lasted through English, Confederate and American possession of the river and remains today. Soon after England acquired Florida in 1763, King George III sent botanist John Bartram to explore Florida. His son, William Bartram, stayed in Florida and published his book Travels in 1791. It describes his exploration of the river as far south as Lake Harney. In the 1800s, steamboats made the St. Johns River a popular winter destination for northerners. By the 1860s, several steamers were making weekly round trips from Charleston and Savannah to Jacksonville and Palatka, and other settlements. In the 1900s, miles of floodplain were drained to make room for indigo, sugar cane, citrus and other profitable crops. Encroachment through draining of the headwater marshes at the river's southern end was neither planned nor controlled. More than 70 percent of the marsh was claimed for agricultural and urban uses. In 1954, Congress authorized flood-control works in the southern part of the St. Johns River. To store water and to move floodwaters, large reservoirs and canals were designed by the U.S. Army Corps of Engineers. The Corps' project was halted in the 1970s. In 1974, the project was deemed unacceptable for environmental reasons. In 1980, a redesigned project by the St. Johns River Water Management District favored restoring wetlands to hold and release floodwaters and managing water levels to simulate natural marsh conditions. Since the project began, the District has restored more than 610 km^2 of original marsh, an area about the size of Delaware.

The St. Johns River is an ancient intracoastal lagoon system. As sea levels dropped, barrier islands became an obstacle that prevented water from flowing east to the ocean. The water collected in the flat valley and slowly meandered northward, forming the St. Johns River. The St. Johns River is the longest river in Florida at 500 km in length. The width of the river varies between a flat marsh at its headwaters and averages about two miles in width between Palatka and Jacksonville. In central Florida, the St. Johns River widens to form large lakes. Additionally, it is one of the few rivers in the United States that flows north. The total drop of the river from its source in marshes south of Melbourne to its mouth in the Atlantic Ocean near Jacksonville is less than 9 m, or about 1.6 cm per kilometer, making it one of the "laziest" rivers in the world. Because the river flows slowly, it is difficult for the river current to flush pollutants. Major pollution sources include discharges from wastewater treatment plants and stormwater runoff from urban and agricultural areas. This runoff carries pesticides, fertilizers and other pollutants into canals, ditches and streams that lead to the river with much of the river pollution is concentrated around urban areas. Salt water enters the river at its mouth in Jacksonville. In periods of low fresh water flow, tides may cause a reverse flow as far south as Lake Monroe, 260 km upstream from the river's mouth. The Ortega River basin is located west of the St. John's River in south-central Duval County in northern Florida and is an important tributary of the St. Johns River (see Figure F1). The Ortega River is the main tributary of the system, discharging approximately half of the total system's volume to the St. Johns River. The Cedar River is the second most important tributary and there are three other secondary tributaries of the system (Fishing Creek, Butcher Pen Creek and Williamson Creek). The upstream portion of the Ortega River is known as McGirt's Creek. The creek lies within the Duval uplands physiographic province and flows

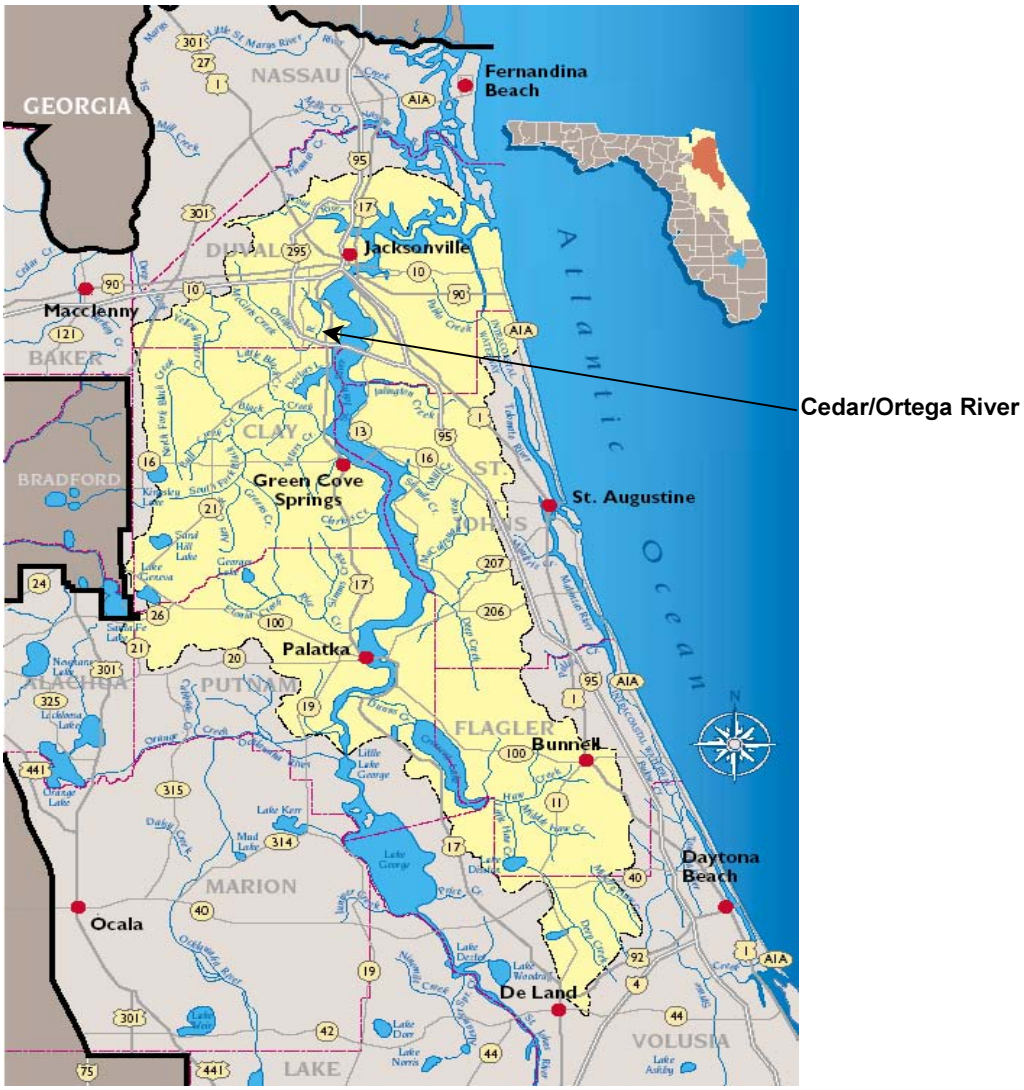

Figure F1. Regional map of Lower St. Johns River basin

generally north to south. The Ortega River continues this course until it reaches the Eastern Valley physiographic province, where the river gradually turns 180 degrees to a north-northeasterly course before reaching the St. John's River north of the Jacksonville Naval Air Station.

The Cedar River, the largest tributary of the Ortega River (Figure F.2), is actually a major system itself. From its headwaters north of Interstate 10 and west if Interstate 295, this river flows southeast to its confluence with the Ortega River. Major tributaries to the Cedar River are Willis Branch, Williamson Creek, Butcher Pen Creek, and Fishing Creek. The tidal interface for the Ortega River is at Collins Rd., while the tidal interface for the Cedar River is near Lane Ave. (These two and other road locations are not highlighted in any drawings herein; they are found in road maps of the Jacksonville area.)

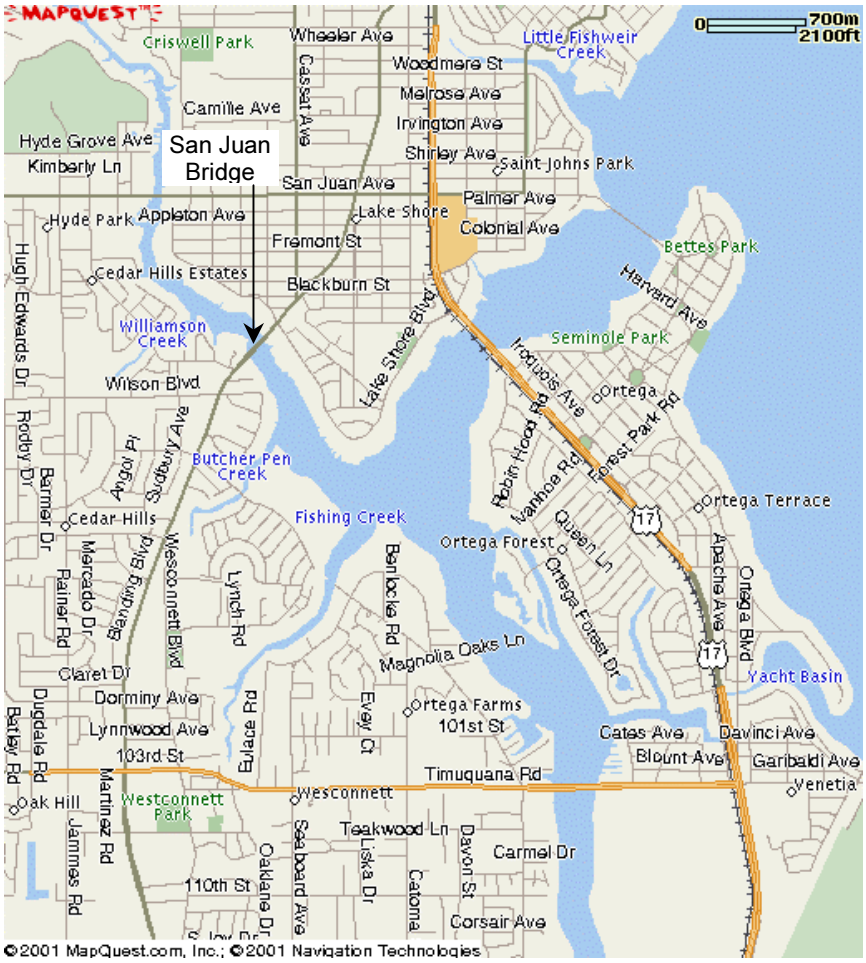

Figure F2. Cedar/Ortega River system and tributaries (from Mapquest.com)

In the early 1990's, approximately one-third of the Ortega/Cedar River basin was residential, with commercial/industrial and vacant land comprising the other major land uses. Since then, vacant land has decreased significantly (Mehta et al. 2000). The average annual rainfall in the Ortega/Cedar basin is approximately 132 cm and the major portion of it falls between June and September (Campbell et al. 1993). Water depths in the Ortega/Cedar basin study area range between 1 and 7 m, with the range in the Cedar River between 0.65 m and 4.3 m. At the mouth of the Ortega River with St. Johns River, the semidiurnal tide ranges from 0.14 m (neap tide) to 0.28 m (spring tide) having a mean of 0.19 m (this was the value used in the hydrodynamic model). The bottom and suspended sediment is mostly a mixture of clay, silt and organic matter. Typical suspended sediment concentration is approximately 15 mg/l; however, during storm runoff events it rises to as much as 105 mg/l**.** The mean organic content was found to be 28%. Previous samples from Mehta et al. (2000) show similar results for the sampled area having values between 22 and 36%. Measurements were also obtained from the St. Johns River Water Management District (SJRWMD), which showed less organic content ranging from 8–22% within the study area (Marván et al. 2000). For this analysis the mean organic content value will be used for calculation purposes.

F4. Assessment of Trap Efficiency

F4.1 Sediment Rating Relations

F4.1.1 Sediment Rating Curve Definition

In many lowland rivers a major part of the sediment is transported in suspension. As the finest fraction of the suspended sediment load often is a non-capacity load it cannot be predicted using stream power related sediment transport models. Instead, empirical relations such as sediment rating curves often are applied. A sediment rating curve describes the average relation between discharge and suspended sediment concentration for a certain location. The most commonly used sediment rating curve is a power function (e.g., Walling 1974; 1978):

$$C = aQ^b \tag{F.21}$$

where C is suspended sediment concentration (kg/m^3), Q is water discharge (m^3/s), and a and b are regression coefficients. Equation F.21 covers both the effect of increased stream power at higher discharge and the extent to which new sources of sediment become available in weather conditions that cause high concentrations are related to the statistical method used to fit the sediment-rating curve and to the scatter about the discharge. Despite its general use several problems are recognized that regard the accuracy of the fitted curve as well as the physical meaning of its regression coefficients. Statistical inaccuracies related to the fitting procedure are discussed by Ferguson (1986; 1987), Jansson (1985), Singh and Durgunoglu (1989), and Cohn et al. (1992). They concluded that the sediment load of a river is likely to be underestimated when concentrations are estimated from water discharge using least squares regression of log-transformed variables. Scatter, among other things, caused by variations in sediment supply due to, for instance, seasonal effects, antecedent conditions in the river basin, and differences in sediment availability at the beginning or the ending of a flood. This is not accounted for by the rating curve. As a sediment rating curve can be considered a 'black box' type of model, the coefficients a and b in Equation F.21 have no definite physical meaning. Nevertheless, some physical interpretation is often ascribed to them. Peters-Kümmerly (1973) and Morgan (1995) state that the a-coefficient represents an index of soil erosion severity. High a-values indicate intensively weathered materials, which can easily be eroded and transported. According to Peters-Kümmerly (1973), the b-coefficient represents the erosive power of the river, with large values being indicative for rivers where a small increase in discharge results in a strong increase in erosive power and sediment transport capacity of the river. Others state that the b-coefficient indicates the extent to which new sediment sources become available when discharge increases. Several authors compare the values of the b-coefficient obtained for different rivers to discuss differences in sediment transport characteristics in the different basins (Peters-Kümmerly 1973; Walling 1974; Sarma 1986; Morgan 1995; Kern 1997).

As discussed previously, the values of the regression coefficients of sediment rating curves are assumed to depend on the severity of erosion, or the availability of sediment in a certain area, the power of the river to erode and transport the available material, and on the

extent to which new sediment sources become available in weather conditions that cause high discharge. According to Walling (1974) *b*-values are also affected by the grain size distribution of the material available for transport, i.e., in streams characterized by sand sized sediments the power of the stream to transport sediment will be more important than in streams that mainly transport silt and clay. This will result in high *b*-values. However, as the *a*- and *b*-coefficients of sediment rating curves are inversely correlated (Rannie 1978; Thomas 1988) it seems more appropriate to use the steepness of the rating curve, which is a combination of the *a*- and *b*-values, as a measure of soil erodibility and erosivity of the river. Steep rating curves, i.e. low *a*- and high *b*-values, should thus be characteristic for river sections with little sediment transport taking place at low discharge. An increase in discharge results in a large increment of suspended sediment concentrations, indicating that either the power of the river to erode material during high discharge periods is high, or that important sediment sources become available when the water level rises.

Flat rating curves should be characteristic for river sections with intensively weathered materials or loose sedimentary deposits, which can be transported at almost all discharges. When this line of reasoning is accepted for the Cedar River, the following interpretation can be assigned to the rating curves shown in Figure F3. This suggests a limited amount of fine sediment, which can be picked up from the bed at low discharge. Once a certain discharge threshold is exceeded, sediment supply to the river increases, and sediment can be picked up from the riverbed, resulting in a rapid increase in suspended sediment concentrations. This argument leads to the hypothesis that steeper rating curves are indicative of rivers, or river sections, where most of the sediment transport takes place at high discharge. Sediment transport rates estimated using a sediment-rating curve always differ somewhat from measured sediment loads. Hence, the sediment-rating curve produces only reasonable estimates of long-term total sediment loads (Asselman 2000).

F4.2 Determination of Rating Curve

In the original analysis performed by Marván (2001), the number of suspended sediment measurements were limited, hence, in order to set the boundary conditions for the tributaries a rating curve was developed by relating the peak and mean values of concentration C to the corresponding peak and mean river discharge Q in the Ortega and Cedar Rivers, obtaining the following relations (Figure F4).

$$C = 2 \times 10^{-5} Q^{2.23} \tag{F.22}$$

At the mouth of the Ortega River, this boundary condition was only applied when the flow was entering the system from St. Johns River. Since no concentration data were available from this site, by using the sediment characteristics and a zero-dimensional resuspension model (Mehta and Li 1999) the following rating curve was developed for the Cedar River:

$$C = 1.65 \times 10^{-2} Q^{0.52} \tag{F.23}$$

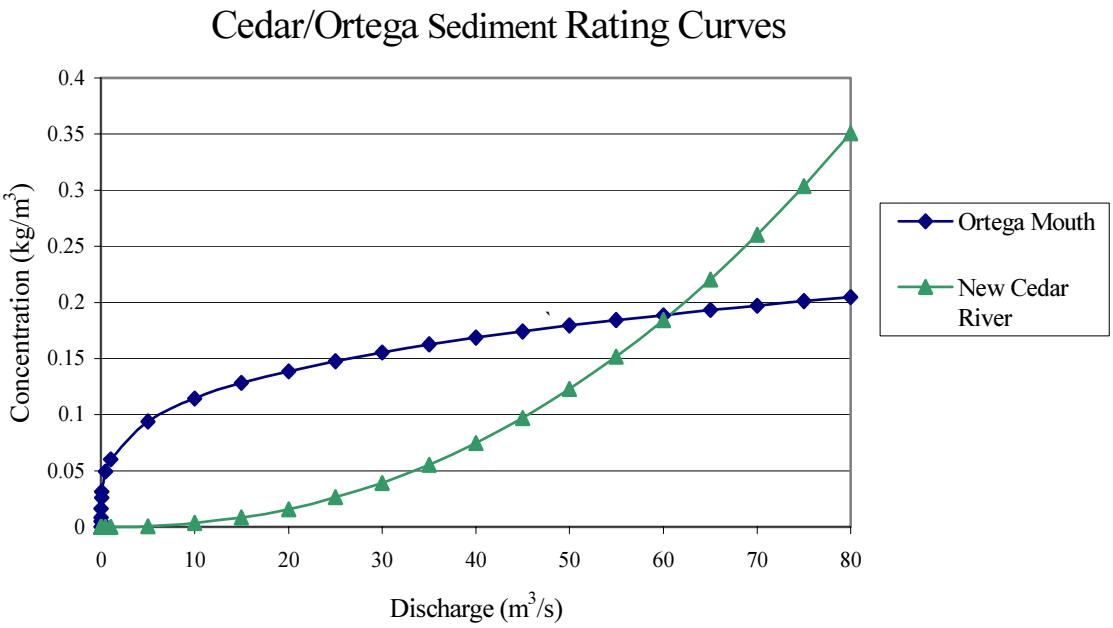

Figure F3. Cedar/Ortega River sediment rating curves

At the time of Marván's analysis, only limited data were available. Further analysis was performed to validate the Cedar River rating curve utilizing additional data from the SJRWMD. The additional discharge data were included with original data and averaged by month and plotted against the concentration, the resulting data were band averaged to reduce scatter. A new rating curve was fit to the band averaged data as shown in Figure F4. Following is the recalculated rating curve for the Cedar River:

$$C = 6 \times 10^{-2} Q^{0.28} \tag{F.24}$$

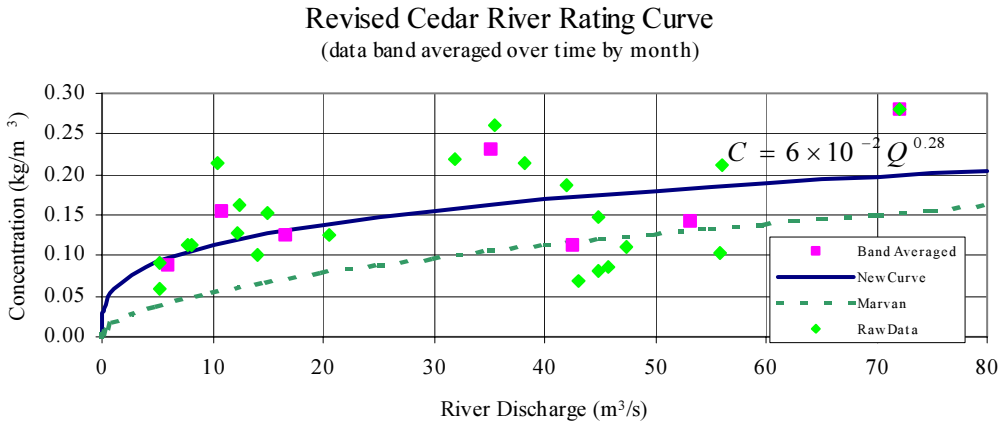

Figure F4. Revised Cedar River sediment rating curve

Figure F5 shows a comparison between the original Cedar River rating curve and the revised curve. The new curve values were incorporated into the sediment model. Figure F3 shows the sediment rating curves for the Cedar/Ortega system that serve as sediment concentration boundary conditions for the sediment transport model.

F4.3 Trap Design Selection

F4.3.1 Factors and Considerations

Some basic design factors were considered in sizing and locating the traps. The following are some basic factors as Parchure et al. (2000) indicates to consider when designing a sediment trap:

1. Locate the trap at a place of maximum sediment transport.

2. It should have navigational access for a dredge to get in and get out without difficulty.

3. The depth and size of the trap should permit safe operation of a dredge.

4. The storage volume of the trap should permit adequate temporary storage of the sediment.

5. Preferably, the trap should catch both fine and coarse sediment.

6. The prevailing flow pattern should be approximately normal to the longer side of the trap.

These factors were evaluated and applied in varying degrees when selecting the size and location of the test traps.

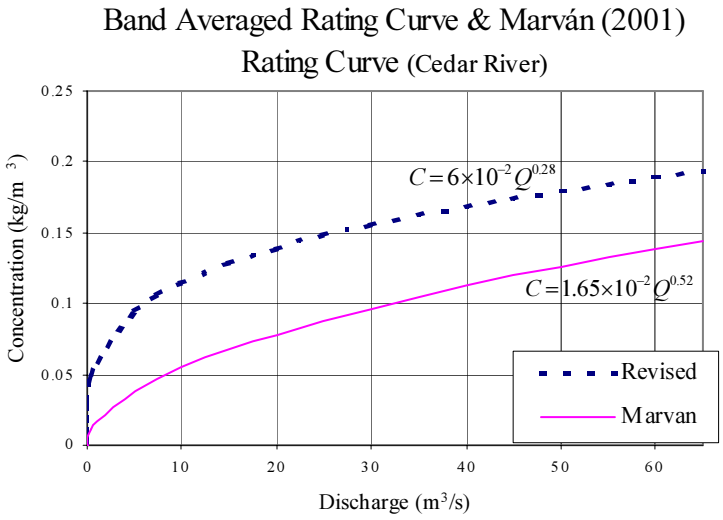

Figure F5. Comparison between Marván (2001) and new Cedar River sediment rating curves

F4.3.2 Evaluation

Based on flow data and previous hydrodymanic and sediment transport analyses of the Cedar River system by Marván et al. (2000) and Mehta et al. (2000), Trap 1 is placed near the confluence of the Cedar and Ortega Rivers (Figure F6). Trap 2, conversely is located approximately 420 m upstream. Both traps were selected 60m (1 cell) wide by 300m (5 cells) long with a surface area of 18,000 m^2 and a volume of 36,000 m^3. The traps are to have an initial dredged depth of 2 meters (from original bed depth) of the river cross-section, which for Trap 1 the dredging depth is 3.8 m and the dredging depth for trap 2 is 3.2 m. These were considered sufficient to reduce the velocity in the canal to allow measurable sediment to settle. For example, with a flow of 3 m^3/s and regular tidal forcing in the Cedar River, the average velocity over trap 1 was found to be 0.13 m/s. Over the same location with no trap in place, the average velocity was 0.24 m/s, which results in a 49% reduction in velocity over the trap. The range of velocity reduction for trap 1 and trap 2 were from 44% to 51% and 43% to 53%, respectively, with an overall average velocity reduction of 48%.

In order to correctly incorporate the trap into the computer model, the existing bathymetry file (Figures F7 and F8) was updated with the location and depths of the traps at the selected cells. The output from the flow model was then input into the sediment transport model. Sediment removal ratio, as defined by Equation F.20, was calculated from the influent and effluent sediment loads in units of kg/s (Equation F.19) at the cells adjacent to the trap on the upstream and downstream edges of the trap. The input densities (dry, bulk, granular) required for the trap were determined from Figure F9, and the values are 157 kg/m^3, 1099 kg/m^3, 2188 kg/m^3, respectively. The settling velocity function used for removal ratio calculations is shown in Figure F10.

Influent and effluent sediment loads were calculated for each time step, and then the removal ratio averaged over one ebb tidal cycle as follows:

$$R_{ave} = \frac{\sum_{i-1}^{M} R_i}{M} \tag{F.25}$$

where R_{ave} is the ebb tide averaged removal ratio, i is the index for each time step Δt, R_i is the removal ratio from a single time step, and M is the total number of time steps over a complete tidal period, as follows:

$$M = \frac{T}{2\Delta t} \tag{F.26}$$

where T is the tidal period (12.42 h). Flood tidal data were not used to calculate the removal ratio because the effluent load (downstream edge) contained only the sediment which escaped the trap on the previous ebb tide. It was observed that for 63% flow (35.4 m^3/s) was the only discharge that produced a constant flow toward the St. Johns River even while the

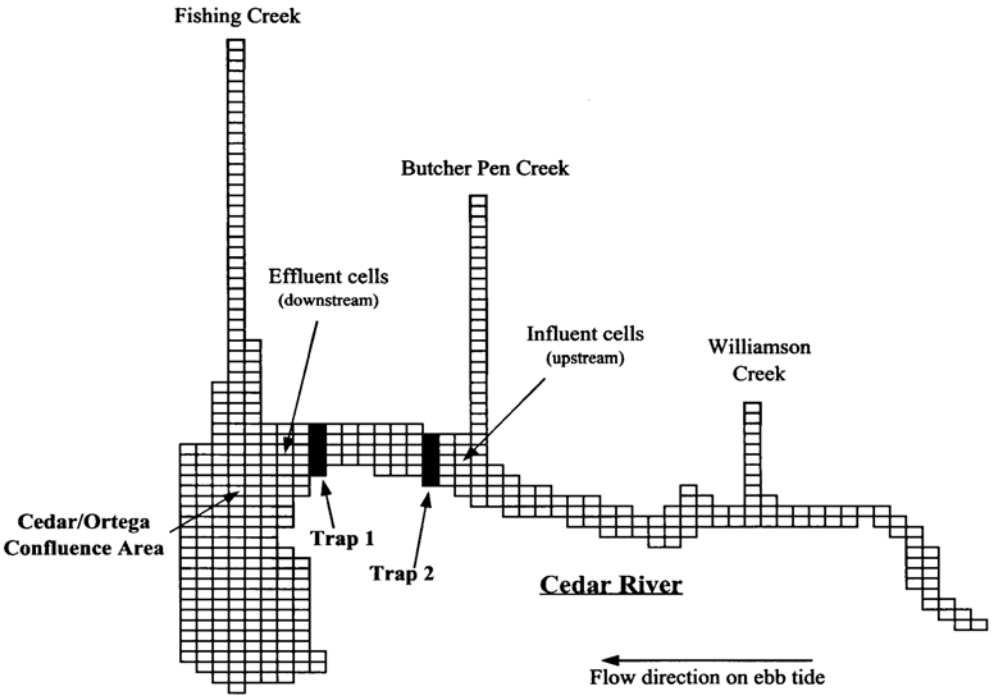

Figure F6. Cedar River section of the computational grid (trap cells are shown in black)

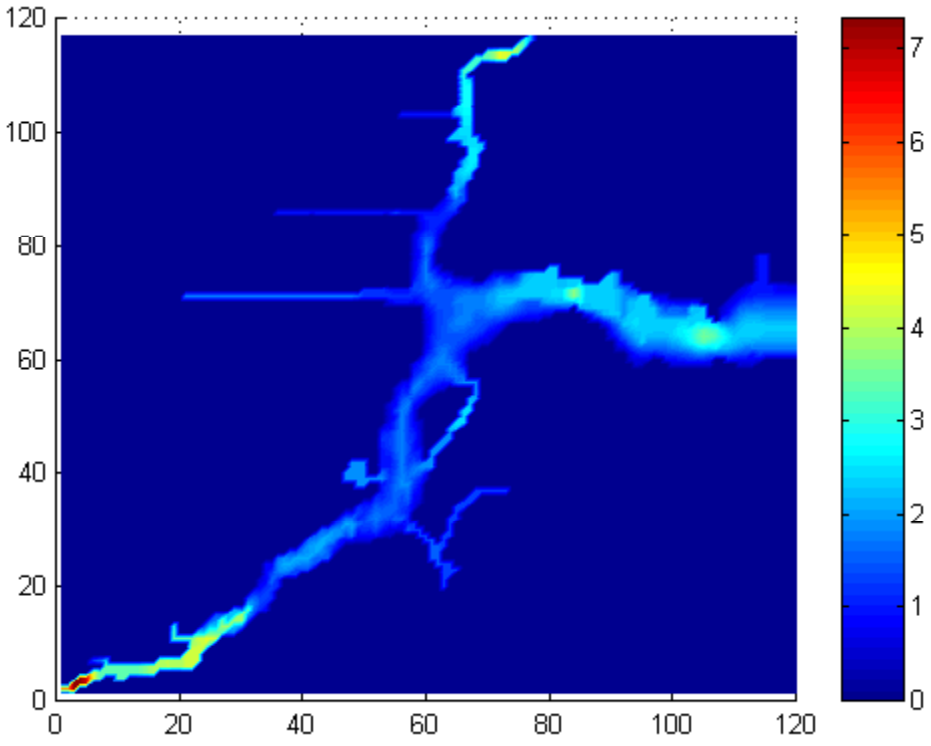

Figure F7. Bathymetry of Cedar/Ortega River as used in hydrodynamic/sediment transport models

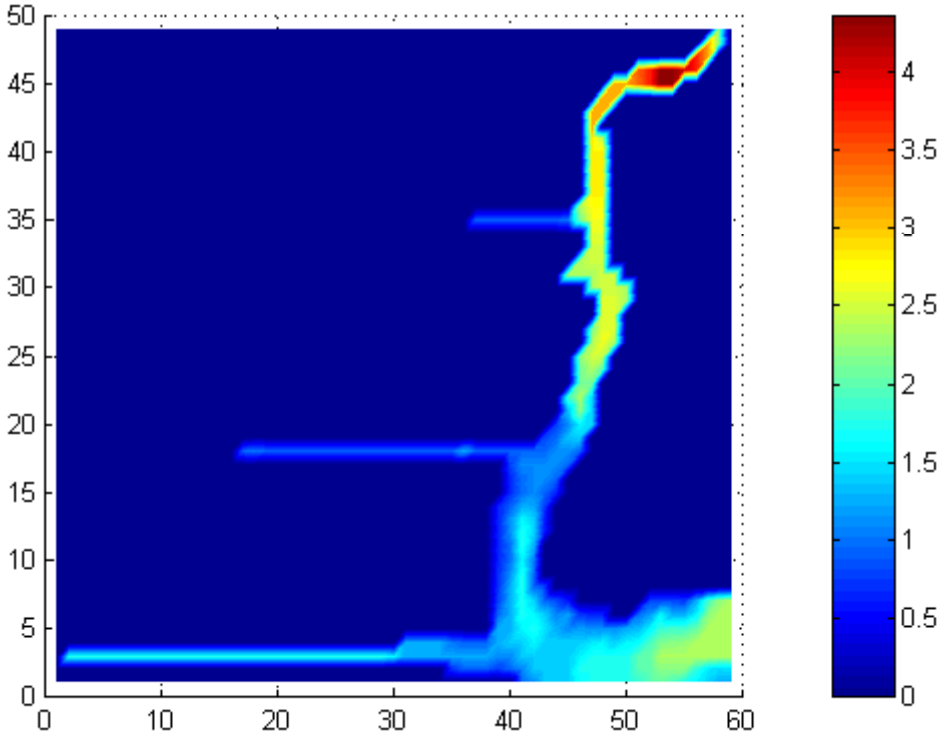

Figure F8. Bathymetry of Cedar River as used in hydrodynamic/sediment transport models

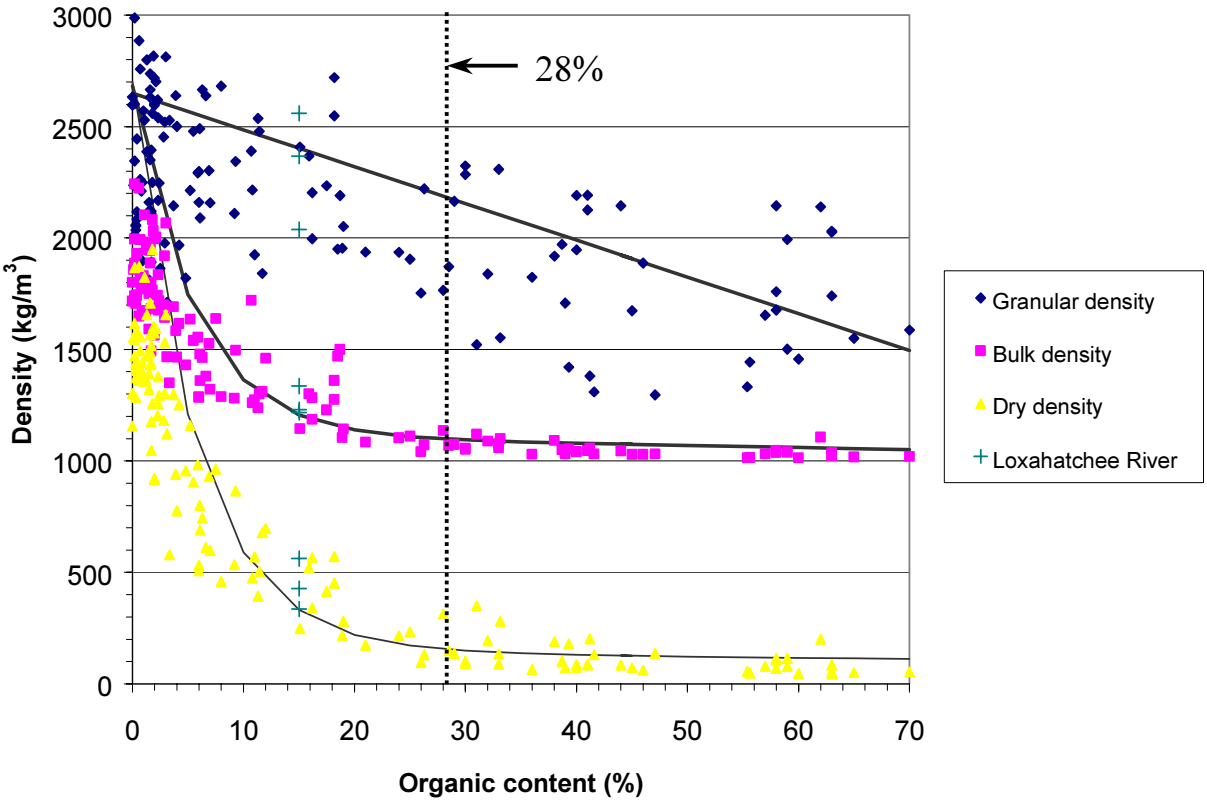

Figure F9. Variation of granular, bulk, and dry densities with organic content using data from three Florida locations and the Loxahatchee River (from Ganju 2001)

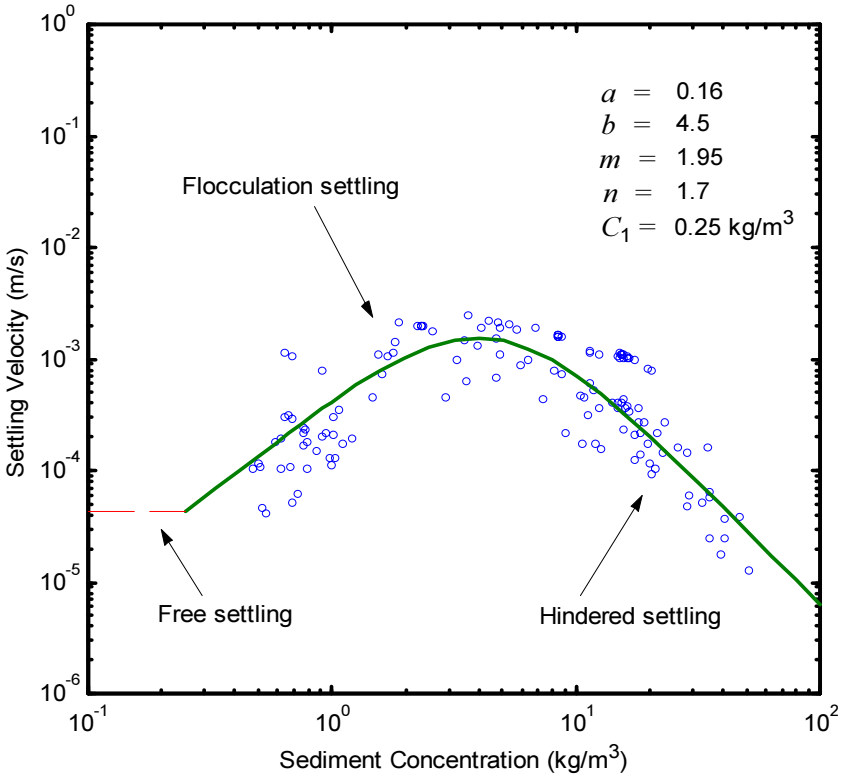

Figure F10. Settling velocity vs. sediment concentration

tide was flooding although small flood values appeared at a discharge of 16.4 m^3/s. For the 35.4 m^3/s flow, the removal ratio was calculated for the entire tidal period.

F4.4 Trap Efficiency as a Function of Discharge

F4.4.1 Trap Performance

Harmonic analysis was carried out by Marván (2001) for tide at the Ortega River mouth at the St. Johns River in order to generate a one-year water level record. Water surface elevation and velocity data from San Juan Bridge (Figure F2) provided by SJRWMD was used for calibration of the hydrodynamic model. River discharge was also available in Ortega River having a mean discharge of 1.4 m^3/s and a maximum of 112 m^3/s. By measuring the watersheds of the other main tributaries (Fishing Creek, Butcher Pen Creek, Williamson Creek and Cedar River), an estimate of the river discharge was made, yielding the rates given in Table F1.

The hydrodynamic and sediment transport models used were previously calibrated as discussed in Marván et al. (2000) and utilized for the trap analysis. Using the calibrated model, several discharges were used for evaluation. Table F2 provides the evaluation discharges and associated concentrations using the recalculated Cedar River rating curve.

Table F1. Cedar/Ortega and tributary discharges in m^3/s

Tributary	Normal conditions	Storm runoff event
Ortega River	8.50×10^{-1}	7.80×10^{1}
Fishing Creek	1.60×10^{-1}	1.46×10^{1}
Butcher Pen Creek	4.00×10^{-2}	3.75×10^{0}
Williamson Creek	3.90×10^{-2}	3.64×10^{0}
Cedar River	6.50×10^{-1}	5.52×10^{1}

Source: Marván et al. 2001.

Due to model limitations at the time of evaluation, the 100% discharge of 55 m^3/s was not evaluated. The organic content included in the model was 28%, which is the mean organic content of the Cedar River sediment. Removal ratios were calculated only during periods of ebb tide flow through the trap (Section F4.3), and plotted against Cedar River discharge (Figure F11) and velocity (Figure F12). These simulations show that the removal ratio is maximum at a discharge of approximately 16.4 m^3/s. At higher discharges the removal declines meaning that the velocity is too large to allow particles to settle in the trap and are subsequently transported past the trap. Conversely, at significantly lower discharges the same particles settle before arriving at the trap.

To provide a performance comparison, the trap was moved 420 m upstream from its previous location. The dredge depth and surface area of the trap remained the same at 18,000 m^2. The original bathymetric grid was adjusted to reflect the new depth. The removal ratio for Trap 2 was calculated for the same discharges. Table F2 compares the removal ratios for the discharges at each trap location. Trap 2 performed 28 % better at the peak removal ratio flow rate (16.4 m^3/s) and by an overall average of 56% over Trap 1. This reduced performance by Trap 1 can be partly attributed to the increased tidal action near the confluence of the Cedar and Ortega Rivers where Trap 1 is located. Trap 2 performed more

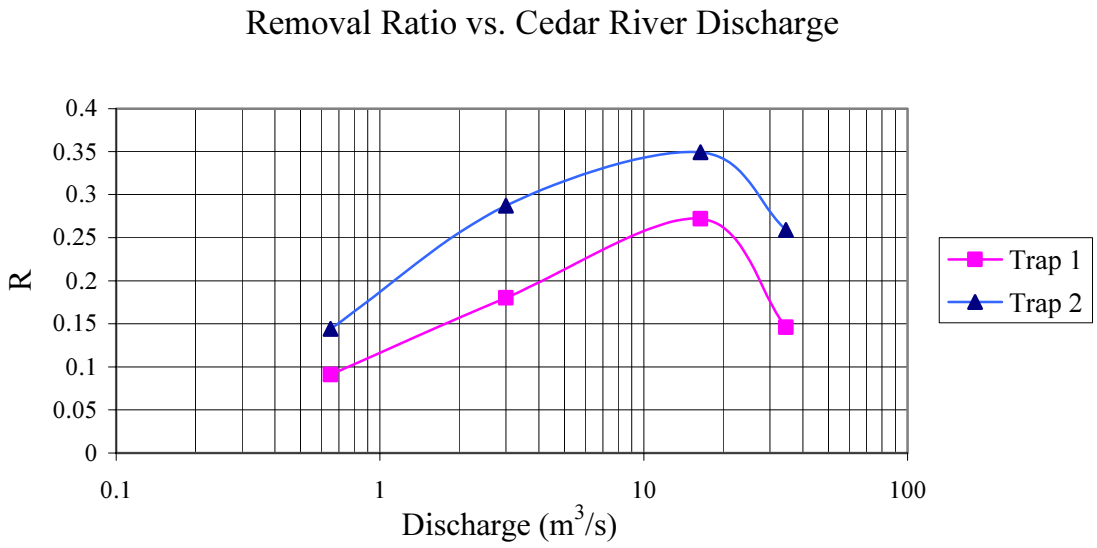

Figure F11. Removal ratio of trap 1 and 2 as a function of Cedar River discharge

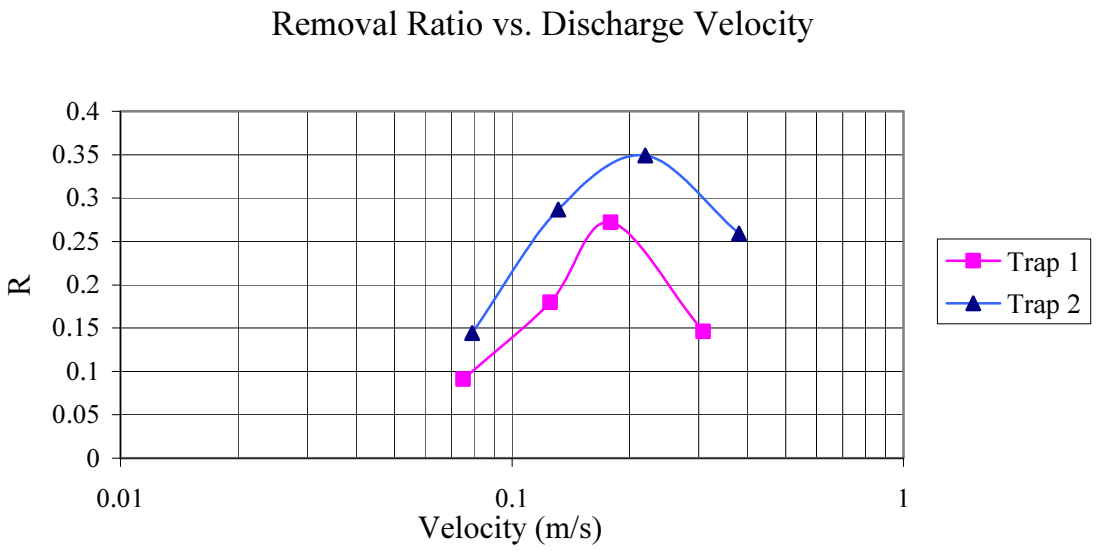

Figure F12. Removal ratio of trap 1 and 2 as a function of Cedar River velocity

Table F2. Removal ratio as a function of Cedar River discharge for Trap 1 and Trap 2

Cedar River Discharge (m^3/s)	Trap 1 Removal Ratio	Trap Removal Ratio
0.65	.09	.14
3.0	.18	.29
16.4	.27	.35
34.5	.15	.26

effectively due to more consistent flow direction and velocity since the location is well within the Cedar River. Trap 1, being closer to the Ortega River confluence area experienced more “mixing”, reducing trapping efficiency.

To provide a performance comparison, the trap was moved 420 m upstream from its previous location. The dredge depth and surface area of the trap remained the same at 18,000 m^2. The original bathymetric grid was adjusted to reflect the new depth. The removal ratio for Trap 2 was calculated for the same discharges. Table F2 compares the removal ratios for the discharges at each trap location. Trap 2 performed 28 % better at the peak removal ratio flow rate (16.4 m^3/s) and by an overall average of 56% over Trap 1. This reduced performance by Trap 1 can be partly attributed to the increased tidal action near the confluence of the Cedar and Ortega Rivers where Trap 1 is located. Trap 2 performed more effectively due to more consistent flow direction and velocity since the location is well within the Cedar River. Trap 1, being closer to the Ortega River confluence area experienced more “mixing”, reducing trapping efficiency.

F4.4.2 Tidal Influence on Performance

Similar to the results in Ganju (2000), the removal ratios for both traps increase until a critical discharge is reached and then decrease. For this system, each trap, the "break-even" discharge was 16.4 m^3/s. Considering the graphical removal ratio solution from Mehta (1984) for a basin with two entrances, the Cedar River trapping schemes results in the relationship

$$R \propto \frac{1}{U} \tag{F.27}$$

with settling velocity, trap length constant, the removal ratio is proportional to the discharge velocity. As verification, recalling the depositional flux is:

$$Q_d = W_s CL \tag{F.28}$$

and the total sediment flux entering the trap is

$$Qi = CUh \tag{F.29}$$

and taking the removal ratio as

$$R = \frac{q_i - q_e}{q_i} = \frac{Q_d}{Q_i} = \frac{W_s L}{Uh} \tag{F.30}$$

it can be shown to be proportional to U^{-1} since W_s, L, and h are essentially constant. Conceptually, as the velocity decreases, the removal ratio should increase. This theory is supported by Baker et al. (1988), but for both of these situations, the velocity was unidirectional. Baker et al. showed that for a sediment trap in a unidirectional flow the removal ratio increased as the velocity approached zero. For the chosen trap locations, as the discharge velocities decrease, tidal influences increase. Starting with the highest discharge (unidirectional flow) and working toward the minimum discharge (bi-directional flow), the removal ratio increases until a maximum value is reached for each trap. Traps 1 and 2 had maximum removal ratios of 0.27 and 0.35, respectively. Continuing to reduce the discharge from the peak removal ratio at 16.4 m^3/s, the tidal influences begin to appear changing the flow from unidirectional to bi-directional. As the discharge approaches zero the tidal forcing effect increases and becomes maximum, which keeps the sediment in the vicinity of the trap in a semi-resonant pattern for a longer period of time before being pushed through the system as in the unidirectional or runoff induced flow case.

Based on the results and observations thus far, it is believed that tidal influence is a contributing factor in removal ratio calculation and should be evaluated. In a unidirectional flow, the sediment is more likely to settle because external disturbances are reduced versus the directional velocity changes that take place in a bi-directional flow situation. By changing direction, some of the previously deposited sediment may become resuspended if consolidation has not occurred. If the discharge is minimal and tidal forcing is near maximum, the consolidation would be small and resuspension more likely. With this in

mind, the removal ratio would decrease. Of course, actual sediment characteristics that would have to be evaluated for each system depends significantly on settling velocity. In this analysis, the settling velocity is free settling and constant because the concentrations are small. Each estuarine system would have to be evaluated to determine the discharge value where tidal influence begins to impact removal ratio. A general relationship can be developed for both tidal and non-tidal influenced removal ratio portions.

As tidal influence increases, the equivalent trap length theoretically increases due to the resonance in the system. This tidal equivalent trap length (L) can be illustrated by using the following expression:

$$\frac{L}{L_O} = k\left(\frac{U}{U_O}\right)^m, \; m > 1 \tag{F.31}$$

where L_o is the original trap length (Figure F13) and U_o is a characteristic velocity of the non-tidal portion of the removal ratio (most likely for the desired evaluation discharge). The value m is a scaling factor to account for the varying tidal influences as the discharge changes. Substituting this expression into Equation F.20 and converting the velocities into discharges, the following expression results for the tidal-influenced removal ratio:

$$R = \frac{W_s L_O B}{Q} k\left(\frac{Q}{Q_O}\right)^m = \lambda \frac{W_s L_O B}{Q}; \text{ where } \lambda = k\left(\frac{Q}{Q_O}\right)^m \tag{F.32}$$

where λ is the dimensionless tidal influence factor. Figure F14 shows the tidal/non-tidal influenced removal ratio using Equations F.20 and F.22 for k=1, m=1.5, and Q_o=5 m^3/s.

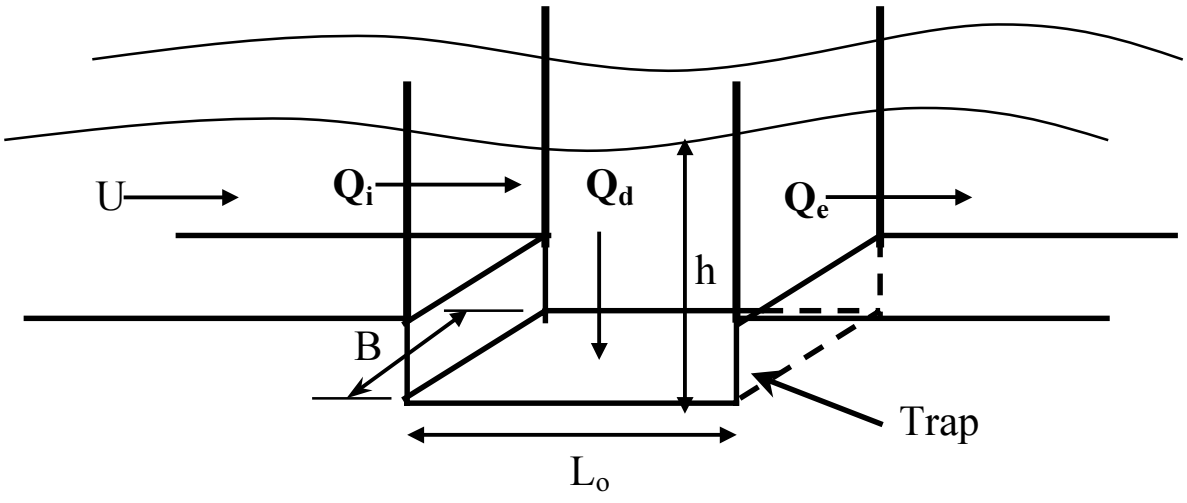

Figure F13. Single-box model for illustration of tidal/non-tidal removal ratio as a function of deposition and erosion fluxes

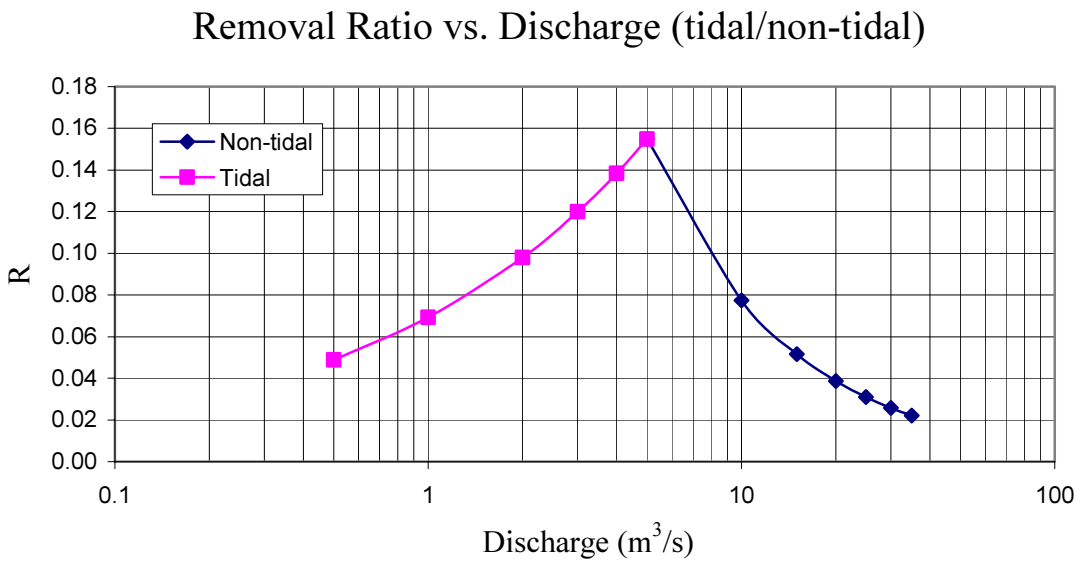

Figure F14. Tidal/non-tidal removal ratio as a function of discharge

The resulting trend from Equation F.32 is very similar to the model results verifying that a tidal influence that reduces the removal ratio is present at lower discharges. To ensure a valid and accurate application, the appropriate scaling factors (m and k) need to be adjusted for each system and trap configuration.

5. Conclusions

5.1 Summary

The objective of this study was to determine the effect of discharge on trapping efficiency for a given trap design in different locations. The Cedar River was chosen as the location of the study due to the influx of organic rich fine sediment and contaminants from upstream sources desired to be kept in the traps rather than spread through the entire biologically sensitive estuarine system. Flow (hydrodynamic) and transport models were utilized to calculate the water levels, velocities, and sediment concentrations in the Cedar/Ortega River system. The models were calibrated using data previously collected from available sources and field investigations (see Marván 2001). Tidal elevations and currents were measured, and historical tributary flow data were obtained from St. Johns River Water Management District (SJRWMD) in order to calibrate the flow model.

Utilizing the calibrated model, a sediment trap in two locations was incorporated into each of the models to determine the trapping efficiency as a function of discharge. The results of these simulations and conclusions are discussed in the following section.

5.2 Conclusions

The simulations for trap efficiency as a function of Cedar River discharge demonstrate a specific discharge (16.4 m^3/s) at which the sediment removal ratio is a maximum. Above this discharge, particles are moving fast enough to bypass the trap and below this discharge the particles deposit before arrival at the trap. A comparison trap was evaluated 420 m upstream. The trap performed 28% better while maintaining the maximum removal ratio at 16.4 m^3/s.

Comparing the trapping efficiency results against the expected relationship for removal ratio, the inconsistencies appear at lower velocities. According to the theory, as velocity decreases the trapping efficiency increases since the removal ratio is proportional to U^{-1}. This indicated another influence was present in the system reducing the efficiency at lower velocities. Also noticed as the discharge velocities decreased, the tidal influence became stronger. A relationship was developed and applied to account for the increase tidal influence at lower velocities Equation F.32.

5.3 Recommendations for Further Work

The trapping efficiency calculation would be more accurately performed with a 3-D model to more effectively account for the mud suspension in high concentrations just above the bed.

Prior to any full scale dredging, a test pit should be dredged to accurately determine sedimentation, flow velocity (to calculate discharge), pressure (to determine water elevation), and deposition thickness in the test pit in the Cedar River. A proposed trap is showed in Figure F15. The system setup would have a central data logger to record output from the

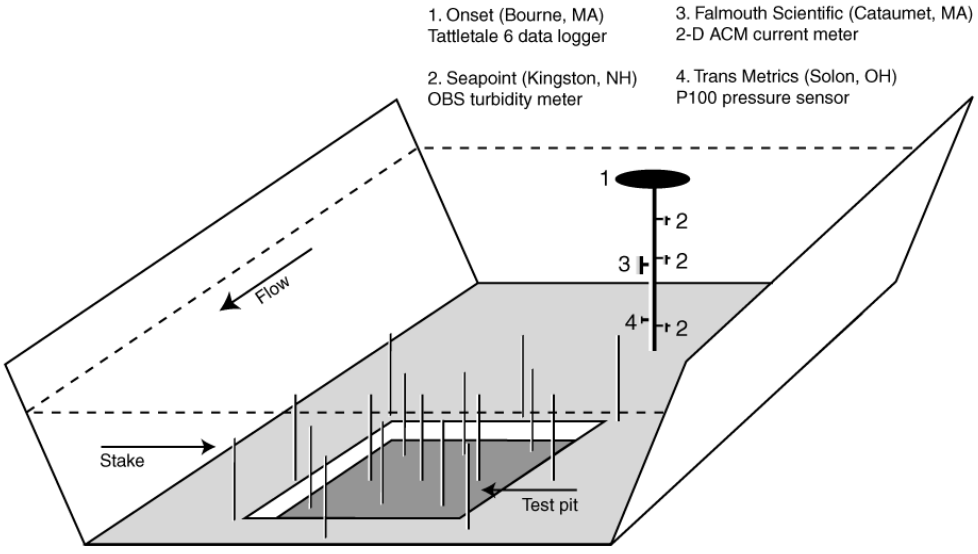

Figure F15. Possible layout of an experimental test pit from Ganju (2001)

turbidity meters, current meter, and pressure sensor. To determine the equilibrium bed elevation and the pit bed level, divers would be needed. A similar system was deployed by Harley and Dean (1982) off the coast of Colombia.

Vicente (1992) provides a method to calculate a constant sedimentation coefficient (K), which can be used to calculate bed elevation through time, as follows:

$$H(t) = H_O + \left(H_h - H_O\right)\left(1 - e^{-Kt}\right) \tag{F.33}$$

where H(t) is the bed elevation at any time, H_o is a datum elevation, and H_e is the equilibrium bed elevation (in absence of dredging). In order to determine K, test pit bottom elevations must be recorded over time, referenced to H_e. Once the time/elevation data are recorded for different areas of the pit, K is determined. One benefit of this method is that only two monitoring visits are needed to determine K. Shoaling depth through time can then be estimated for the site, with the final shoaling depth approaching the equilibrium bed elevation (Ganju 2001).

References

Asselman, N.E.M. 2000. Fitting and interpretation of sediment rating curves. *Journal of Hydrology* 234:228-248.

Baker, E.T., H.B. Milburn, and D.A. Tannant. 1999. Field Assessment of sediment trap efficiency under varying flow conditions. *Journal of Marine Research* 46:573-592.

Campbell, D., M. Bergman, R. Brody, A. Keller, P. Livingston-Way, F. Morris, and B. Watkins. 1993. *Lower St. Johns River Basin SWIM Plan*. St. Johns River Water Management District.

Cancino, L. and R. Neves. 1999. Hydrodynamic and sediment suspension modeling in estuarine systems, Part I: Description of the numerical models. *Journal of Marine Systems* 22: 105-116.

Casulli, V. 1990. Semi-implicit finite difference methods for the two-dimensional shallow water equations. *Journal of Computational Physics* 86: 56-74.

Cohn, T.A., D.L. Caulder, E.J. Gilroy, L.D. Zynjuk, and R.M. Summers. 1992. The validity of a simple statistical model for estimating fluvial constituent loads: An empirical study involving nutrient loads entering Chesapeake Bay. *Water Resources Research* 28: 2353-2363.

Ferguson, R.I. 1986. River loads underestimated by rating curves. *Water Resources Research* 22: 74-76.

———. 1987. Accuracy and precision of methods for estimating river loads. *Earth Surface Processes and Landforms* 12: 95-104.

Ganju, N.K. 2001. Trapping organic-rich fine sediment in an estuary. Master's thesis, University of Florida, Gainesville.

Ghosh, L.K., N. Prasad, V.B. Joshi, and K.K. Kunte. 2001. A study on siltation in access channel to a port. *Coastal Engineering* 43: 59-74.

Harley, R., and R.G. Dean. 1982. Channel shoaling prediction: A method and application. *Proceedings.* 18th International Conference of Coastal Engineering, American Society of Civil Engineers, 1199-1218.

Hwang, K. 1989. Erodibility of fine sediment in wave-dominated environments. Master's thesis, University of Florida, Gainesville.

Jansson, M. 1985. A comparison of detransformed logarithmic regressions and power function regressions. *Geografiska Annaler* 67A, 61-70.

Kern, U. 1997. *Transport von Schweb- und Schadstoffen in staugeregelten Fließgewässern am Beispiel des Neckars*. Mitteilungen Institut für Wasserbau, Universität Stuttgart, Stuttgart, Germany.

Kozerski, H.-P., and K. Leuschner. 1999. Plate sediment traps for slowly moving waters. *Water Resources* 33(13): 2913-2922.

Krone, R.B. 1962. Flume studies of the transport of sediment in estuarial shoaling processes. *Final Report*. Hydraulics Engineering Laboratory and Sanitary Engineering Research Laboratory, University of California, Berkeley, 118 p.

Leonard, B.P. 1977. A stable and accurate convective modeling procedure based on quadratic upstream interpolation. *Computer Methods in Applied Mechanics and Engineering* 19: 59-98.

Marván, F.G. 2001. A two-dimensional numerical transport model for organic-rich cohesive sediments in estuarine waters. Ph.D. thesis, Heriot-Watt University, Edinburgh, UK.

Marván, F.G., S.G. Wallis, and A.J. Mehta. 2001. Episodic transport of organic-rich sediments in a microtidal estuarine system. Research paper to be published in *Proceedings.* INTERCOH 2000.

Mehta, A.J., R. Ariathurai, M. Peng-Yea, and E.J. Hayter. 1984. Fine sedmentation in small harbors. *Report UFL/COEL-TR/051.* Coastal and Oceanographic Engineering Department, University of Florida, Gainesville, 113 p.

Mehta, A.J., and K.R. Dyer. 1990. Cohesive sedimant transport in estuarine and coastal waters. In: *The Sea (Vol. 9, Part B), Ocean Engineering Science*, B. Le Mehaute and D.M. Hanes, Wiley and Sons, New York.

Mehta, A.J., R. Kirby, and E.J. Hayter. 2000. Ortega/ Cedar river basin, Florida, restoration: Work plan to assess sediment-contaminant dynamics. *Report No.UFL/COEL-99/019.* Department of Civil and Coastal Engineering, University of Florida, Gainesville, 30 p.

Mehta, A.J., R. Kirby, J.D. Stuck, J. Jiang, and T.M. Parchure. 1997. Erodibility of organic rich sediments: A Florida perspective. *Report UFL/COEL-99/019.* Coastal and Oceanographic Engineering Department, University of Florida, Gainesville, 60 p.

Mehta, A.J., S.C. Lee, Y. Li, S.B. Vinzon, and M.G. Aberu. 1994. Analysis of some sedimentary properties and erodibility characteristics of bottom sediment for the Rodman Reservoir, Florida. *Report No. UFL/COEL-90/008.* Coastal and Oceanographic Engineering Department, University of Florida, Gainesville.

Mehta, A.J., and T.M. Parchure. 2001. Surface erosion of fine-grained sediment revisited. In: *Muddy Coast Dynamics and Resource Management*, B.W. Flemming, M.T. Delafontaine, and G. Liebezeit, eds., Elsevier, Oxford, UK (in press).

Morgan, R.P.C. 1995. *Soil Erosion and Conservation.* 2nd ed., Longman, London.

Parchure, T.M., B. Brown, and R.T. McAdory. 2000. Design of sediment trap at Rollover Pass, Texas. *Report No. ERDC/CHL TR-00-23.* United States Army Corps of Engineers Coastal and Hydraulics Laboratory, Vicksburg, Mississippi.

Peters-Kümmerly, B.E. 1973. Untersuchungenüber Zusammensetzung und Transport von Schwebstoffen in einigen Schweizer Flüssen. *Geographica Helvetica* 28: 137-151.

Pnueli, D., and C. Gutfinger. 1992. *Fluid Mechanics*. Cambridge University Press, New York, 473 p.

Preston, R.W. 1985. The representation of dispersion in two-dimensional shallow-water flow. *Report TPRD/L/2783/N84*. Technology Planning and Research Division, Central Electricity Research Laboratories, 13 p.

Rose, C. P., and P.D. Thorne. 2001. Measurements of suspended sediment transport parameters in a tidal estuary. *Continental Shelf Research* 21: 1551-1575.

Sarma, J.N. 1986. Sediment transport in the Burhi Dihing River, India. In: *Drainage Basin Sediment Delivery*, R.F. Hadley, ed., IAHS publication 159, 199-215.

Singh, K.P., and A. Durgunoglu. 1989. Developing accurate and reliable stream sediment yields. *Sediment and the Environment*, IAHS publication 184, Wallingford, Proceedings of the Baltimore Symposium— May 1989, 193-199.

Trefry, J.H., N.C. Chen, R.P. Trocine, and S. Metz. 1992. Impingement of organic-rich, contaminated sediments on Manatee Pocket, Florida. *Florida Scientist* 55(3): 160-171.

Vicente, C.M. 1992. Experimental dredged pit of Ka-Ho. *Proceedings.* International Conference on the Pearl River Estuary, Analysis of shoaling rate. Macao, 459-471.

Walling, D.E. 1974. Suspended sediment and solute yields from a small catchments prior to urbanization. In: *Fluvial Processes in Instrumented Watersheds*, K. J. Gregory, and D.E. Walling, eds., Institute of British Geographers Special Publication #6, 169-192.

———. 1978. Suspended sediment and solute response characteristics of the river Exe, Devon, England. In: *Research in Fluvial Systems*. R. Davidson-Arnott, and W. Nickling, eds., Geoabstracts, Norwich, 169-197.

(Page intentionally blank)

Appendix G

Hydrodynamic and Sediment Transport Modeling

Appendix G

Hydrodynamic and Sediment Transport Modeling of the Cedar/Ortega/St. Johns River System

G.1 Introduction

This report describes the application of the Environmental Fluid Dynamics Code (EFDC) numerical model (described below) to the Cedar/Ortega/St. Johns Rivers system. Figure G.1 shows a site map for the Cedar/Ortega River basin, whereas Figure G.2 shows the confluence of the Cedar and Ortega Rivers as well as the confluence of the Ortega and St. Johns Rivers. The problem being investigated by the St. Johns River Water Management District (SJRWMD) is contamination of bottom sediments in the Cedar River and Ortega/Cedar River confluence area. The principle chemicals of concern are PCBs and PAHs. The purpose of the modeling study described herein is to simulate the hydrodynamics and sediment transport in the identified area of contamination, and evaluate present and future rates of sediment deposition, erosion and transport under selected remediation scenarios provided by SJRWMD. A specific objective of the modeling study was to evaluate the impact of placing both in-channel and off-channel sediment traps at selected locations, with three different removal efficiencies (i.e., 40%, 60%, 80%) for the off-channel traps, on the net sediment flux out of the Cedar River.

The EFDC model was developed by John M. Hamrick while he was a faculty member at the Virginia Institute of Marine Science (Hamrick 1992). Dr. Hamrick now works for Tetra Tech, Inc. in Fairfax, VA. Continued development and support of EFDC has been provided by Tetra Tech, with this work mostly funded by the U.S. Environmental Protection Agency (EPA). The model has been applied to numerous rivers and estuaries in this country. It has

been used to investigate a wide range of environmental problems including: a) sediment, contaminant and pathogenic organism transport and fate from both point and nonpoint

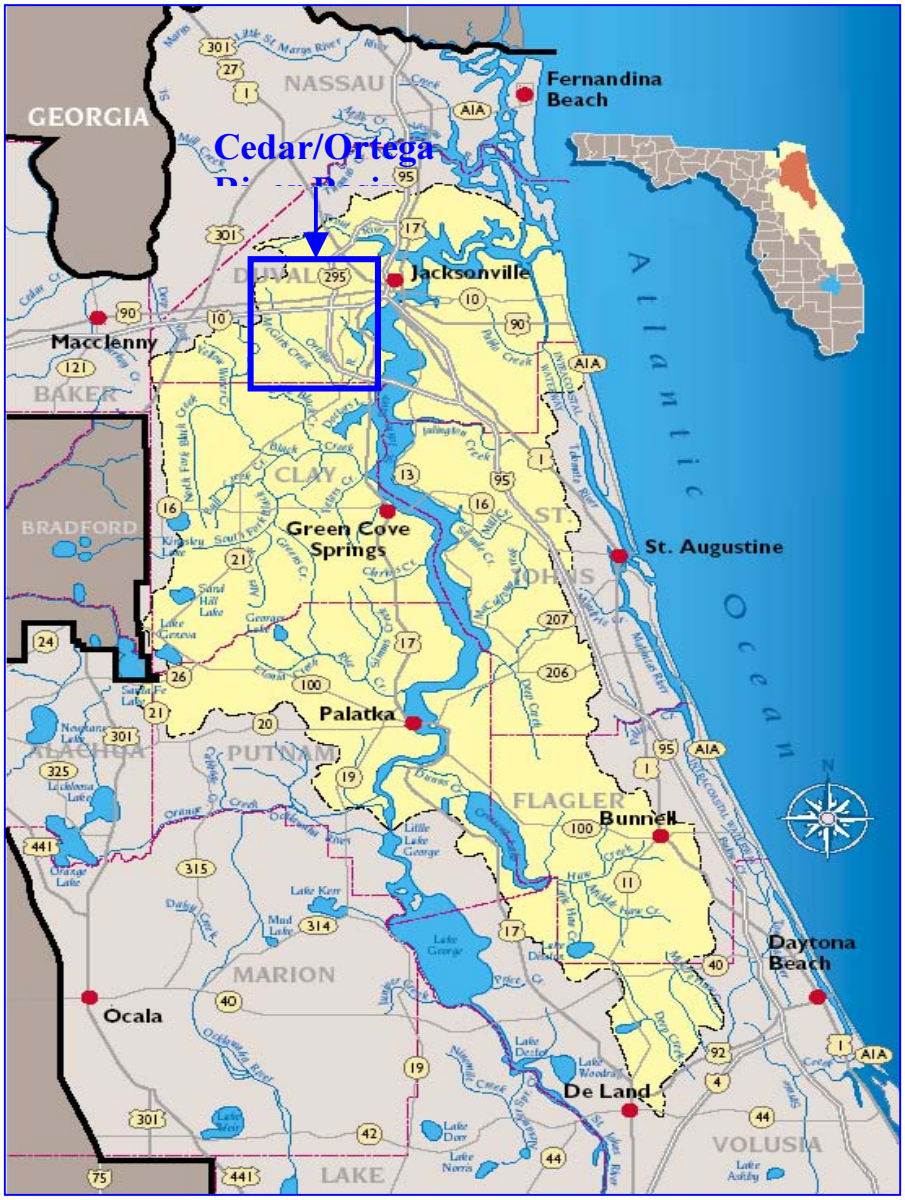

Figure G.1 Regional map of the Lower St. Johns River basin and the general area of the Ortega/Cedar River basin.

sources; b) power plant cooling water discharges; c) oyster and crab larvae transport; d) dredging and dredge spoil disposal alternatives, and e) water quality problems in estuaries. A recent evaluation of contaminated sediment transport models reported that EFDC is one of

the top-ranked public domain models for simulated the transport of sediments and contaminants in surface waters (Imhoff *et al*. 2003).

Figure G.2 Cedar/Ortega River system and St. Johns River

The theoretical and computational basis for EFDC is described in Hamrick (1992), and a user manual for EFDC is given in Hamrick (1996). The description of the sediment transport algorithms incorporated in EFDC is given by Hamrick (2000). Updated versions of these documents are currently being produced (under contract to EPA) by Tetra Tech. It is

scheduled to be delivered to EPA in April 2004. The updated manual will be delivered to the SJRWMD after being peer reviewed by EPA.

G.2 Modeling Strategy

To accomplish the task of modeling various sediment trap efficiency scenarios in the Cedar River, two curvilinear-orthogonal models were setup. The modeling domain for the coarser Cedar/Ortega/St. Johns Rivers (COSJR) model consisted of the reach of the St. Johns River between the Buckman Bridge and the Main Street Bridge, and included the Ortega River (upstream to TG3 – see Figure G.3) and a reach of the Cedar River that extended upstream of the sites of the proposed off-channel sedimentation ponds. The modeling domain for the second model was the Cedar River (CR) and extended from the confluence with the Ortega River to upstream of the proposed sedimentation ponds. The former was used to generate the downstream boundary conditions for the latter. The reasons for using this modeling strategy were the following: 1) a more detailed representation of the Cedar River than was possible with the coarser COSJR model was needed to more accurately simulate the hydrodynamics, and salinity and sediment transport in the Cedar River; and 2) the hydrodynamic and salinity boundary conditions at the downstream end of the CR modeling domain had to be predicted using a model in which that boundary (of the CR model) was located at an interior location in the COSJR model.

G.3 Model Setup

The setup of both the COSJR and CR models is described in this section.

G.3.a Cedar/Ortega/St. Johns Rivers Model

The curvilinear-orthogonal grid for the COSJR model consists of 2,856 computational cells. To simulate the partially stratified estuarine flow in the modeled reach of the St. Johns

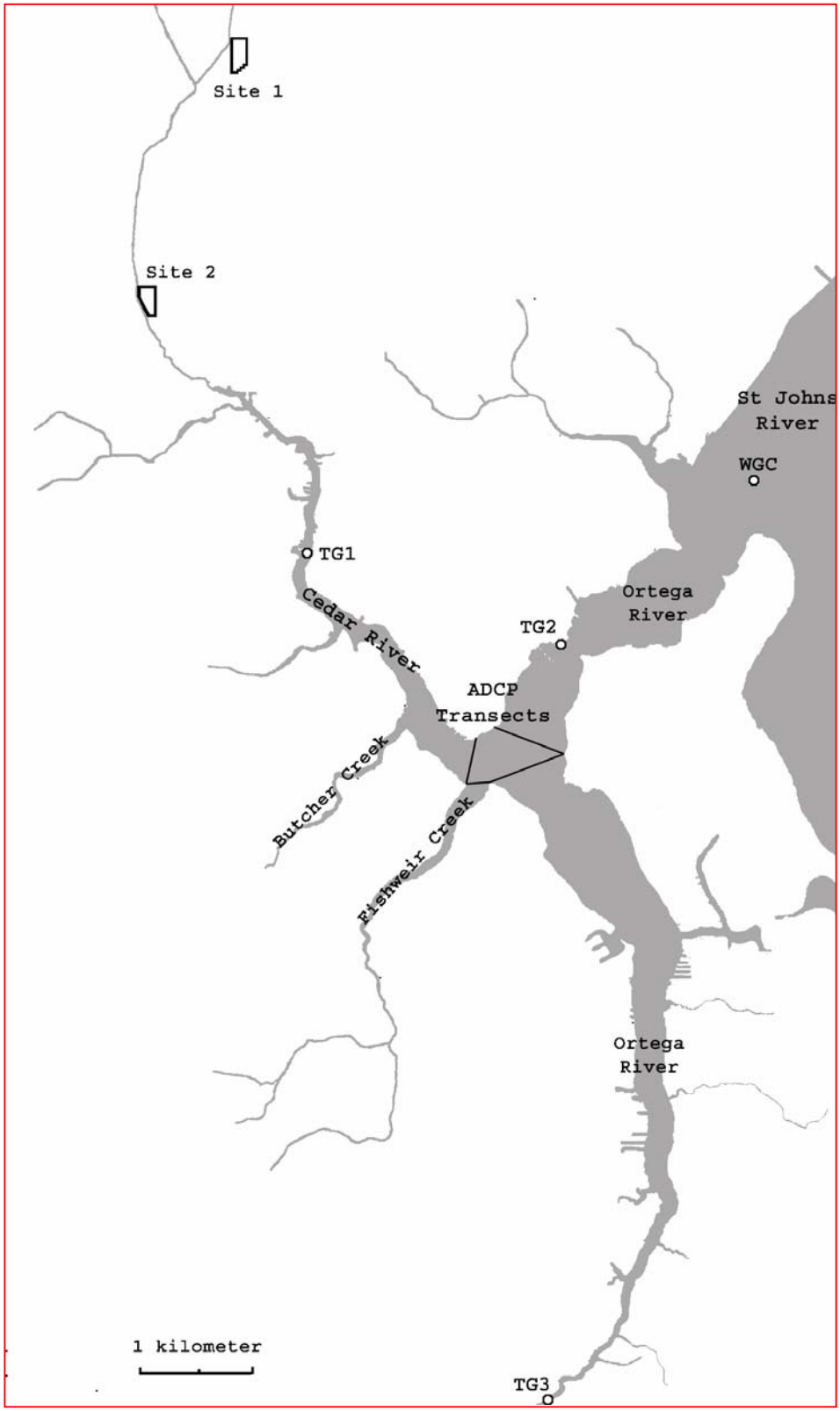

Figure G.3 Confluence of Cedar, Ortega and St. Johns Rivers (after Paramygin 2002). Fishing Creek is incorrectly labeled as Fishweir Creek, and Butcher Pen Creek is incorrectly labeled as Butcher Creek.

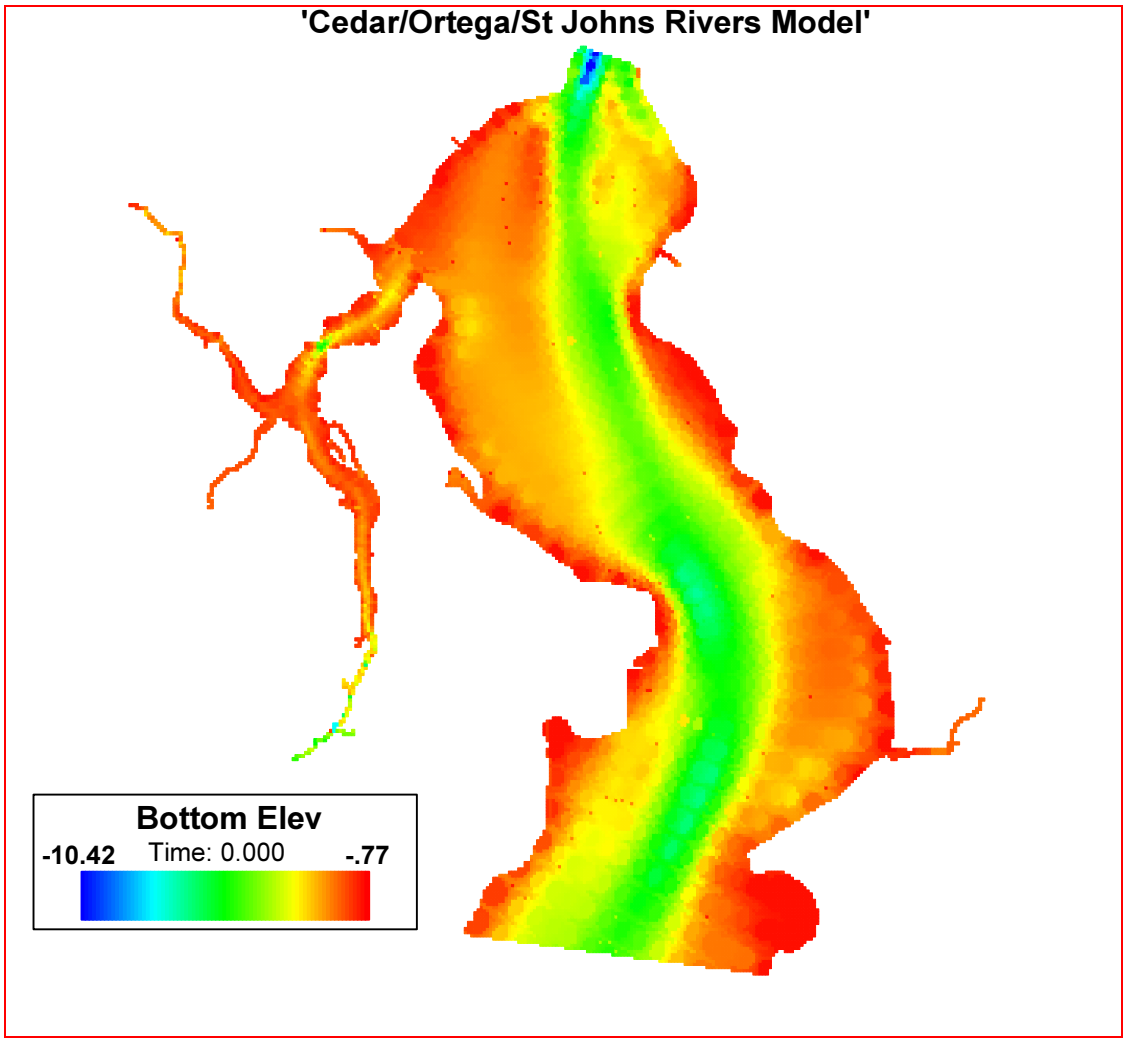

Figure G.4 Bathymetry of the COSJR modeling domain. Bottom elevations are in meters with respect to NGVD.

River, six vertical layers to represent the water column. The bathymetry of the modeling domain is shown in Figure G.4, while the grid with the locations of the open water boundaries are shown in Figure G.5. At BC8 and BC9 (see Figure G.5), measured water surface elevations and salinities at three levels over the water column were used for the boundary conditions (see Figures G.6 and G.7). In these figures, the units on the abscissa are the day numbers in 2001. The average of the three vertical salinity measurements is plotted in Figure G.7. At BC1 – BC7, the boundary values for discharge were obtained by the SJRWMD using

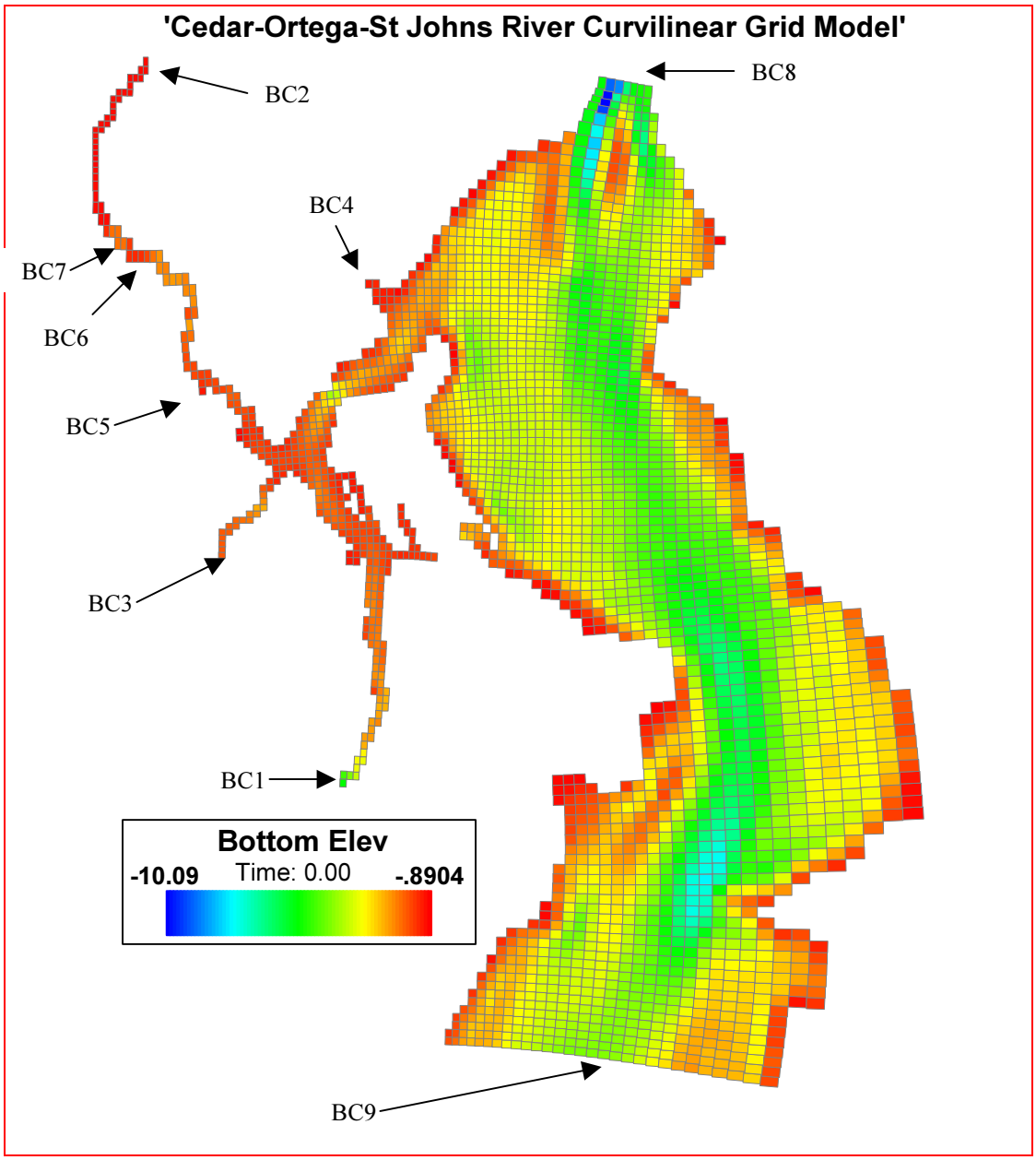

Figure G.5 COSJR model grid with locations of open water boundary conditions (BC1 – BC9)

the SWMM model (Freeman 2001). Figures G.8 and G.9 show representative time series plots of the SWMM predicted discharges and suspended sediment concentration at BC1 – BC7. In addition, the SWMM predicted time series of direct runoff and nonpoint source sediment loads from subwatersheds along the Ortega and Cedar Rivers were added to the appropriate computational cells along these rivers.

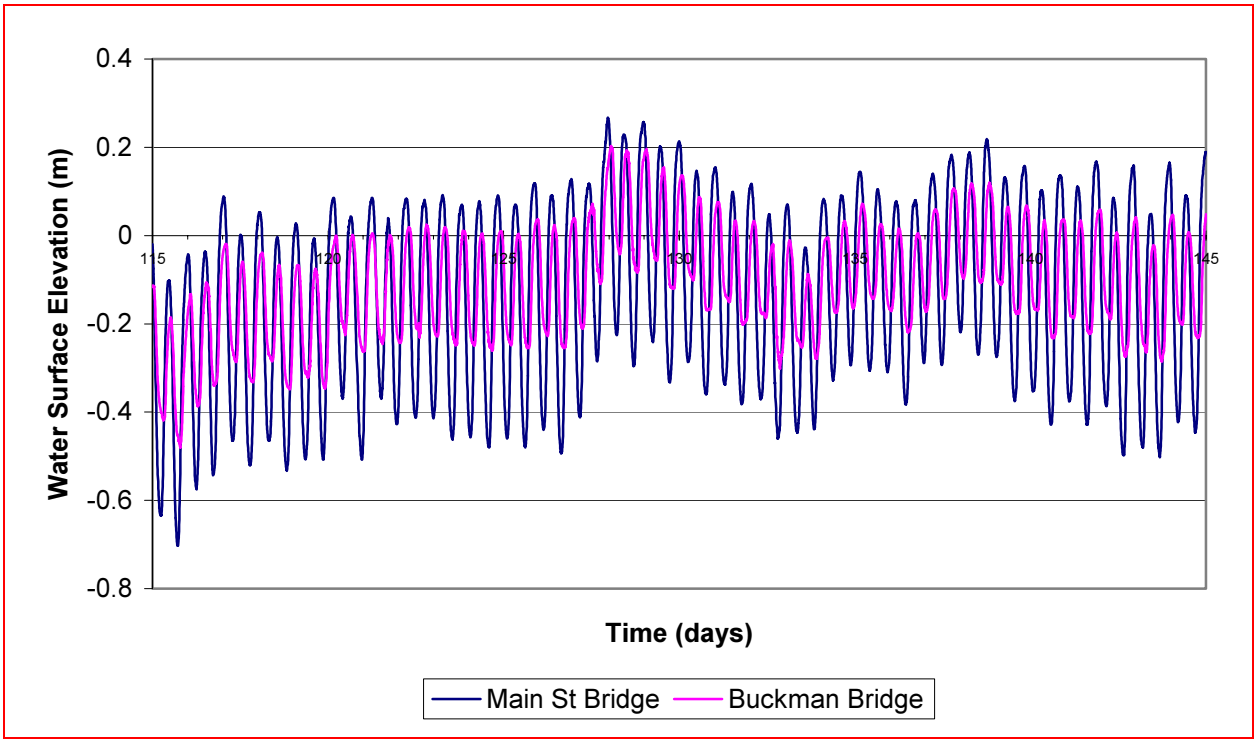

Figure G.6 Representative time series plots of water surface elevations at the upstream and downstream boundaries in the St. Johns River

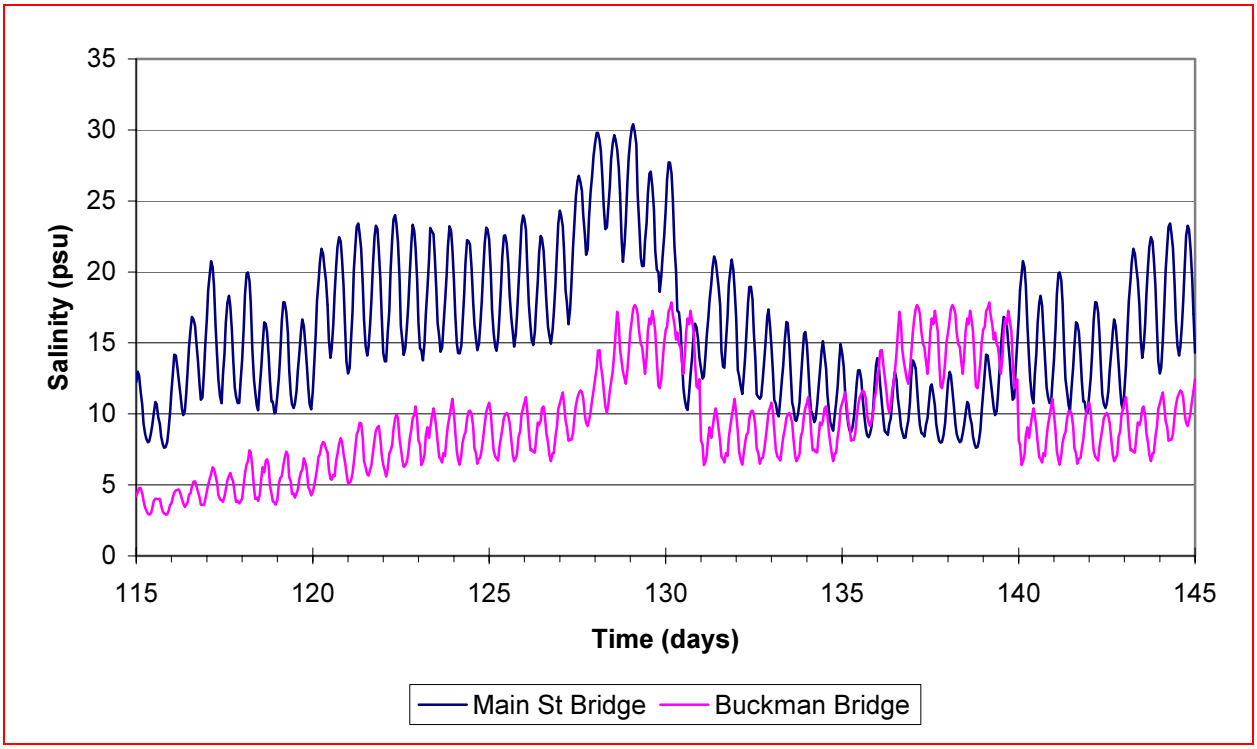

Figure G.7 Representative depth-averaged salinities at the upstream and downstream boundaries in the St. Johns River

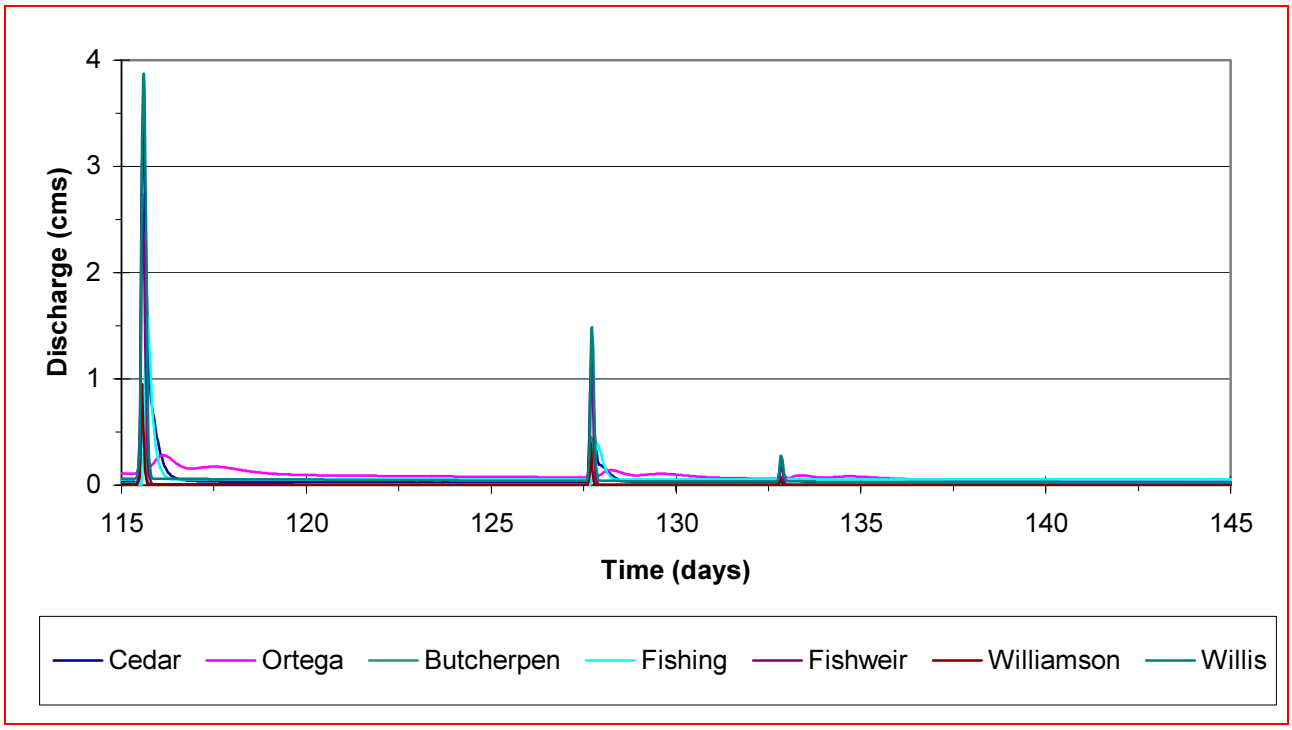

Figure G.8 Representative time series of SWMM predicted discharges at BC1 – BC7

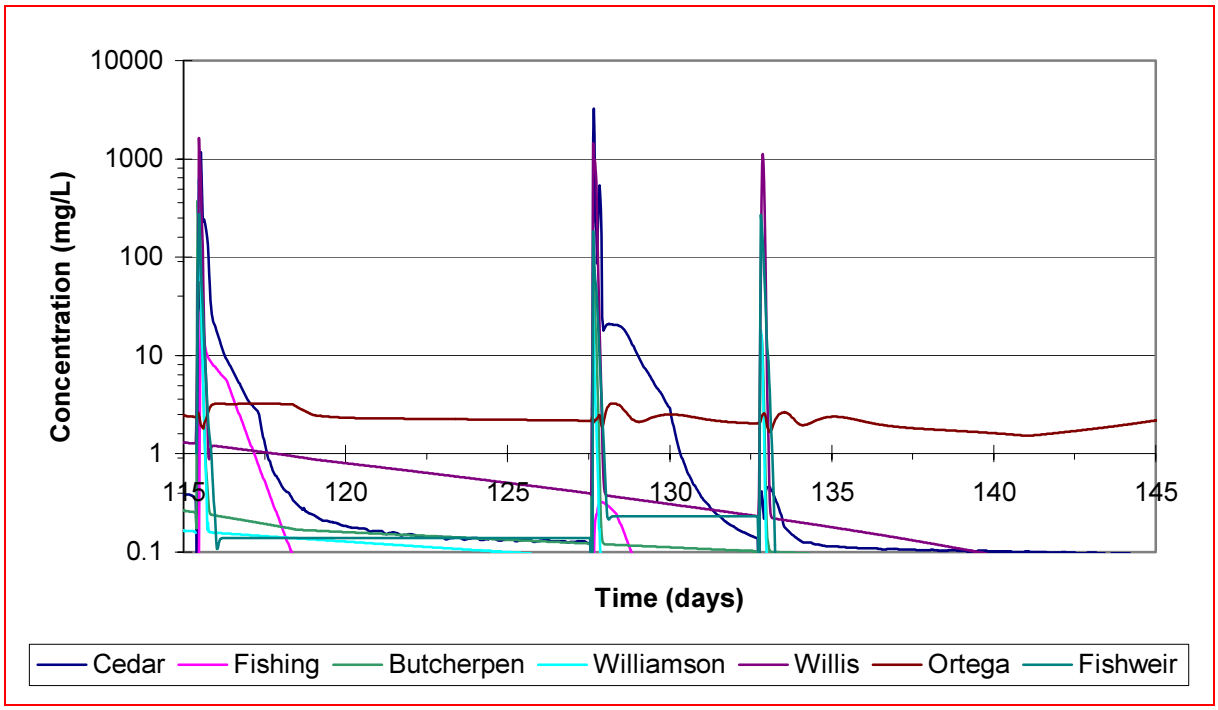

Figure G.9 Representative time series of SWMM predicted suspended sediment concentrations at BC1 – BC7

The COSJR model was initially run (cold-started) for a 60-day spin-up period (01 Jan – 01 Mar 2001). To achieve a stable solution, a constant 4-sec time-step was used in this simulation. The restart file generated by this run was used to hot-start the runs made during the 90-day calibration period (01 March – 29 May 2001), the results of which are described in the Section 4. This model runs at a speed of 100 simulated days per day on a 2.4 GHz Pentium 4 computer.

G.3.b Cedar River Model

The curvilinear-orthogonal grid for the CR model consists of 845 computational cells. As with the COSJR model, six vertical layers were used. The bathymetry of the modeling domain is shown in Figure G.10. Enlargements of the downstream and upstream ends of the CR grid are shown in Figures G.11 and G.12, respectively. As seen in these figures, five cells were used to represent the lateral variability in flow and transported constituents, i.e., dissolved salt and sediment, over the entire length of the modeling domain. To simulate the partially stratified estuarine flow in the lower reach of the Cedar River, six vertical layers were used in every computational cell. Also shown in Figure G.10 are the locations of the six open water boundaries (BC1 – BC6) where boundary conditions were applied. The same boundary conditions used for BC1 – BC5 in the COSJR model were used for the CR model. The stage, salinity and suspended sediment concentration boundary conditions at the downstream boundary (BC6) were generated by the COSJR model. The five cells at the downstream boundary match five cells are coincident with five cells in the COSJR model.

For this model application, time-variable freshwater inflows (shown in Figure G.13) and suspended cohesive sediment concentrations (shown in Figure G.14) were applied at the following locations: BC1 – Cedar River; BC2 – Williamson Creek; BC3 – Butcher Pen Creek; BC4 – Fishing Creek; BC5 – Willis Branch. These time series were generated using

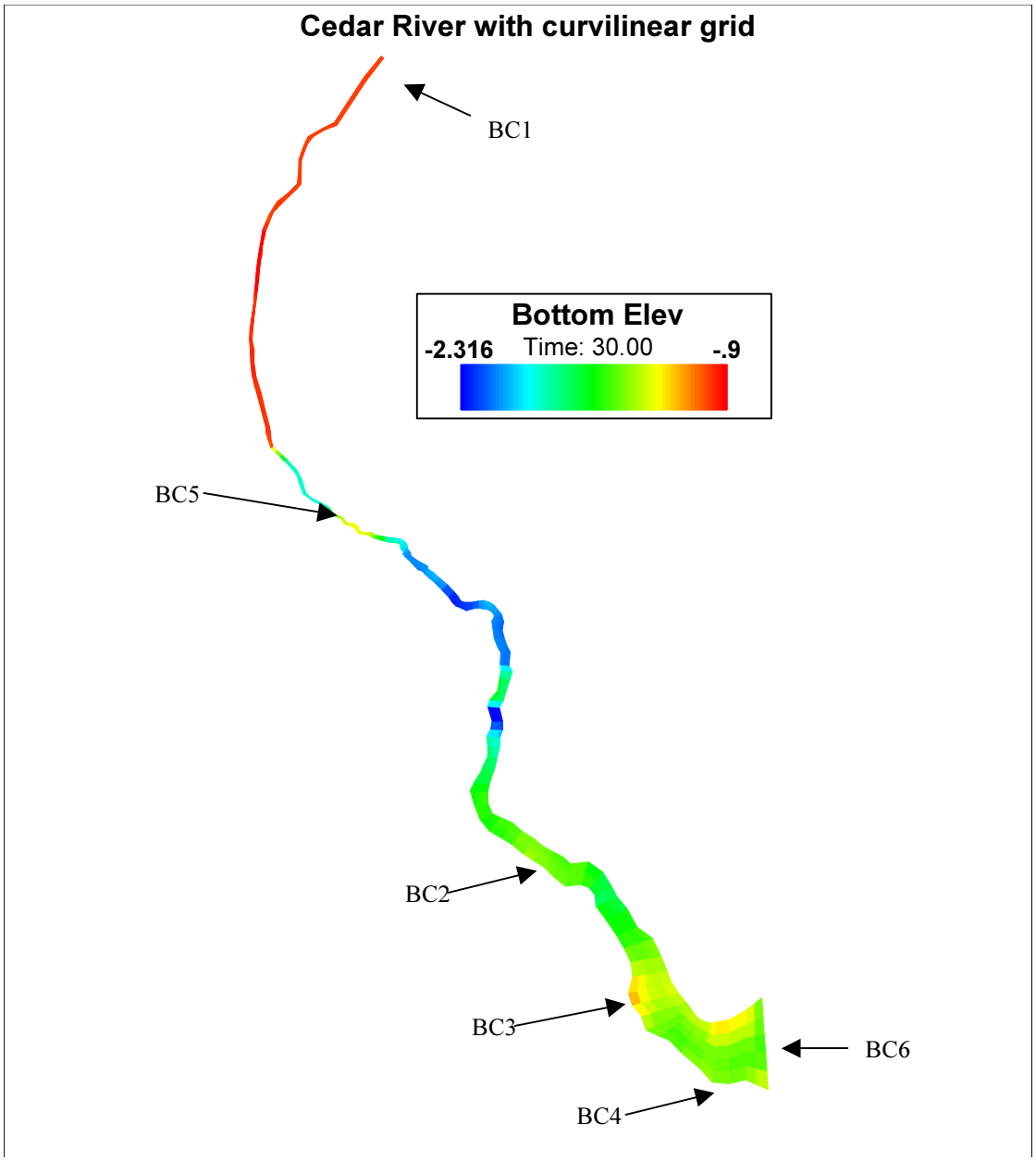

Figure G.10 Bathymetry of the Cedar River Modeling Domain. Bottom elevations are in meters with respect to NGVD.

the SWMM (Freeman 2001). The semi-diurnal tidal signal applied at the downstream boundary (BC6) is shown in Figure G.15. The vertically varying salinity time series applied at the middle cell at the downstream boundary are shown in Figure G.16. Similar time series are applied at the other four cells at BC6.

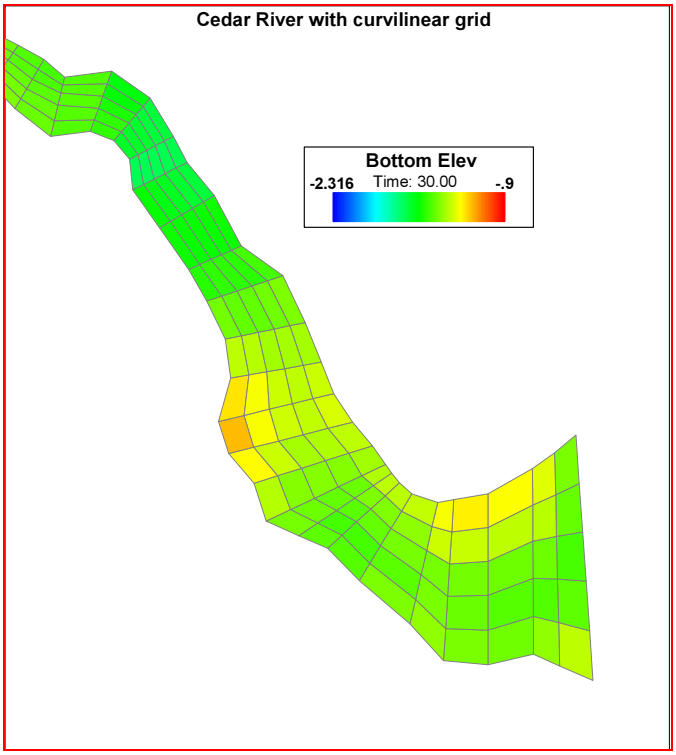

Figure G.11 Downstream End of the Cedar River grid

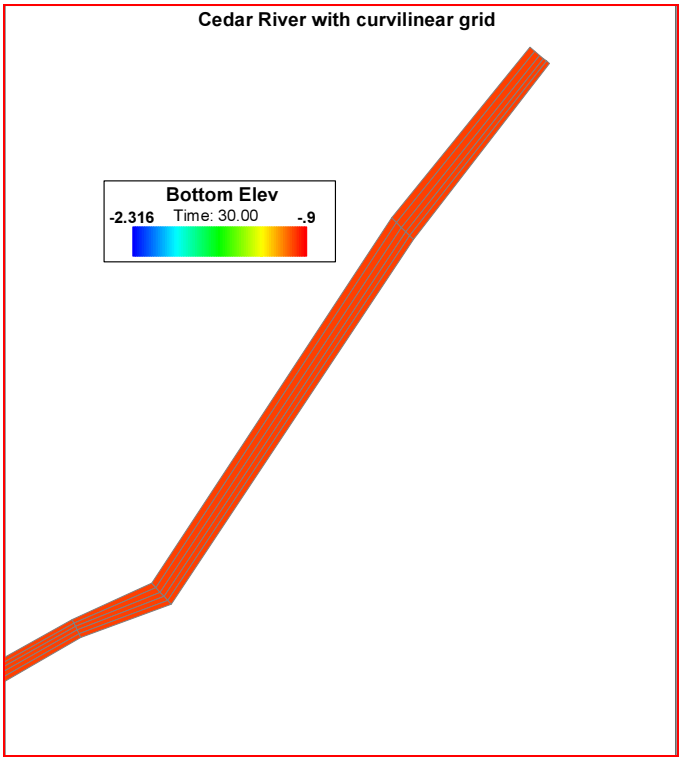

Figure G.12 Upstream end of the Cedar River grid

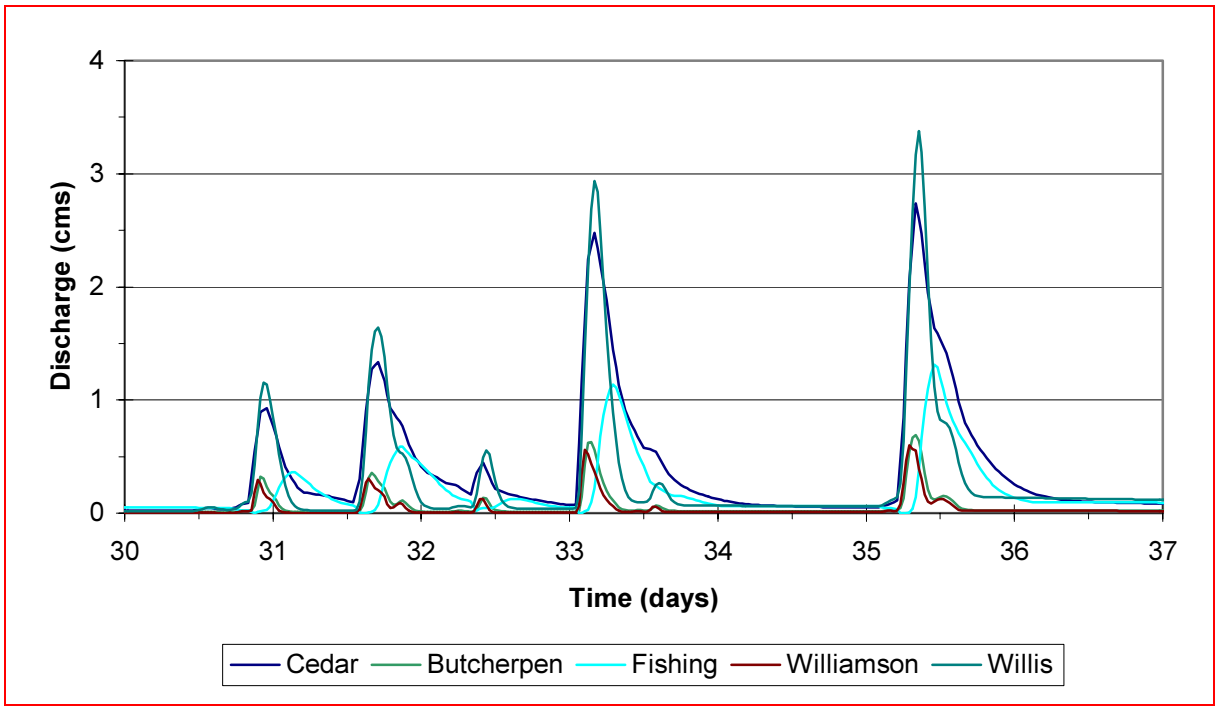

Figure G.13 Freshwater inflow time series for the Cedar River at BC1 – BC5

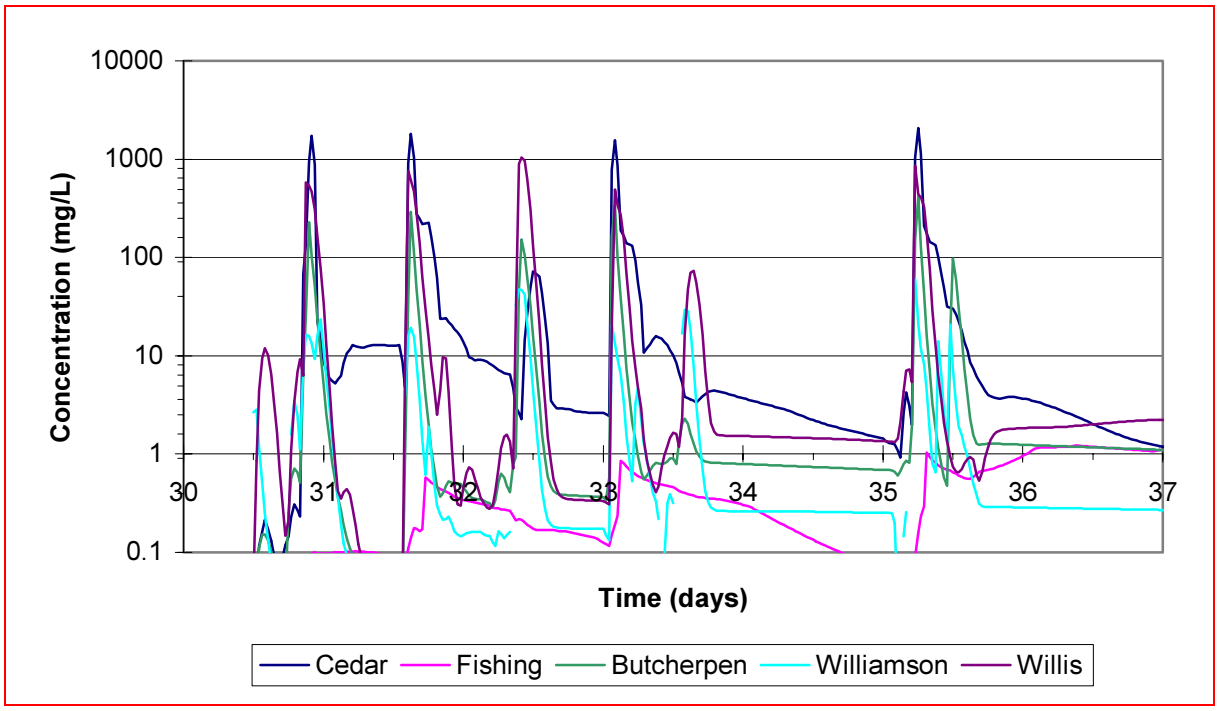

Figure G.14 Suspended cohesive sediment concentration time series for the Cedar River at BC1 – BC5

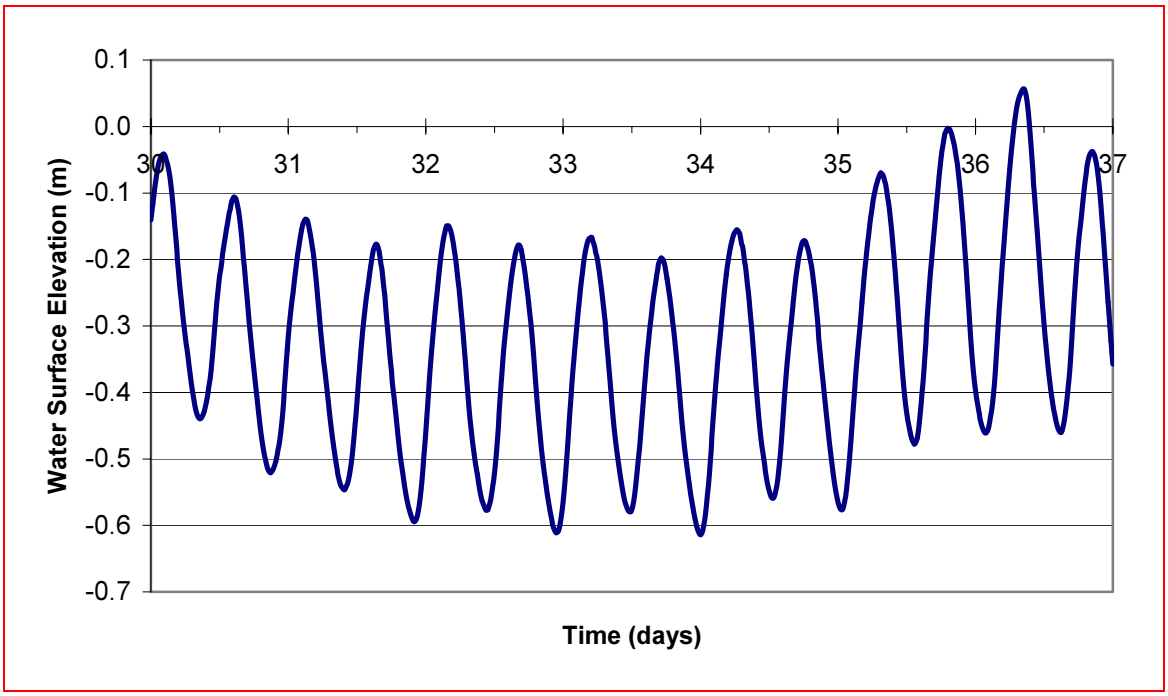

Figure G.15 Tidal signal used for the CR hydrodynamic boundary condition at BC6

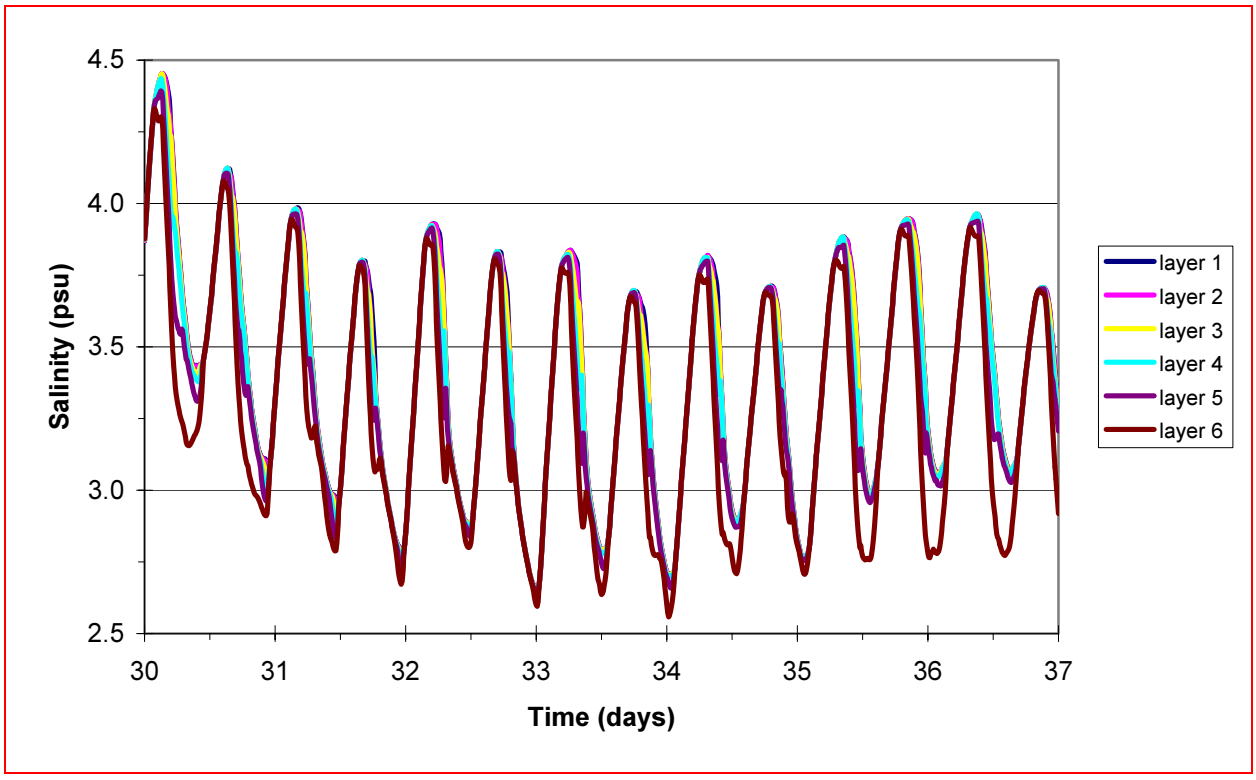

Figure G.16 Cedar River salinity time series used for the middle cell at BC6, with layer 1 being the bottom layer

Driven by the specified boundary conditions, the CR model was initially run (cold-started) for a 30-day spin-up period. A time-step of 2 seconds was used. This model runs at a speed of 148 simulated days per day on a 2.4 GHz Pentium 4 computer. The restart file generated by this run was used to hot-start the remediation scenario runs specified by the SJRWMD.

G.4 Model Calibration

A 90-day calibration period (01 March – 29 May 2001) was used for the COSJR model. Results obtained from calibration of the COSJR model are presented next. The hydrodynamic model was calibrated by adjusting the spatially uniform value of the bottom roughness height z_o until the best agreement between measured and predicted state variables was obtained. A value $z_o = 0.04$ was found to result in the optimum agreement.

Figures G.17 and G.18 show the predicted horizontal salinity distributions at two times (approximately one-half tidal cycle apart) during day 66 (Julian day 126) of the calibration run. Since no salinity measurements are available for this period, these two figures are included only for qualitative assessment of the model's ability to predict salinity distributions throughout the modeling domain.

Figure G.19 shows the comparison between predicted and measured water surface elevations at TG2 for days 107 - 137. Figure G.20 shows the same comparison for days 130 – 137, which are the last seven days of the record at TG2. The latter figure enables a more detailed comparison of differences between the predicted and measured water surface elevations and phases. As seen in these figures, the predicted and measured elevations and phases agree satisfactorily at this location. The small differences in both phase and elevations may be attributed to, among other factors, the differences between the actual local winds over

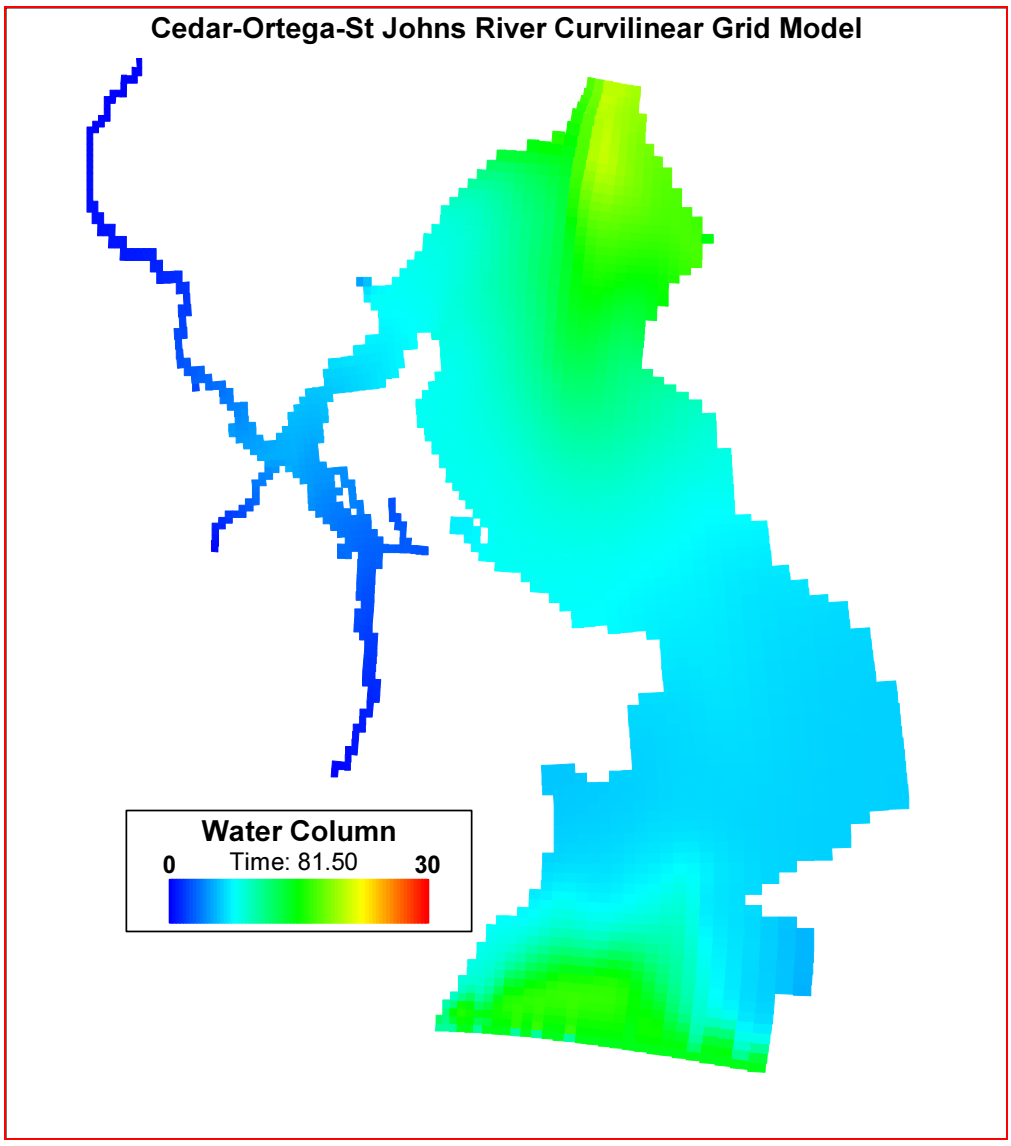

Figure G.17 Predicted salinity distribution at approximately low water

the simulated period and those measured at the recording weather station, which is located a few miles from the Cedar/Ortega/St. Johns Rivers confluences. The measured wind speeds and directions were used in this simulation.

Figure G.21 shows the comparison between predicted and measured water surface elevations at TG1 for days 60 - 90. Figure G.22 shows the same comparison for days 90 – 120. Note that the tide gage started to malfunction sometime around day 80. This is even more apparent in Figure G.22. Examination of the first 20 days in Figure G.21 shows good

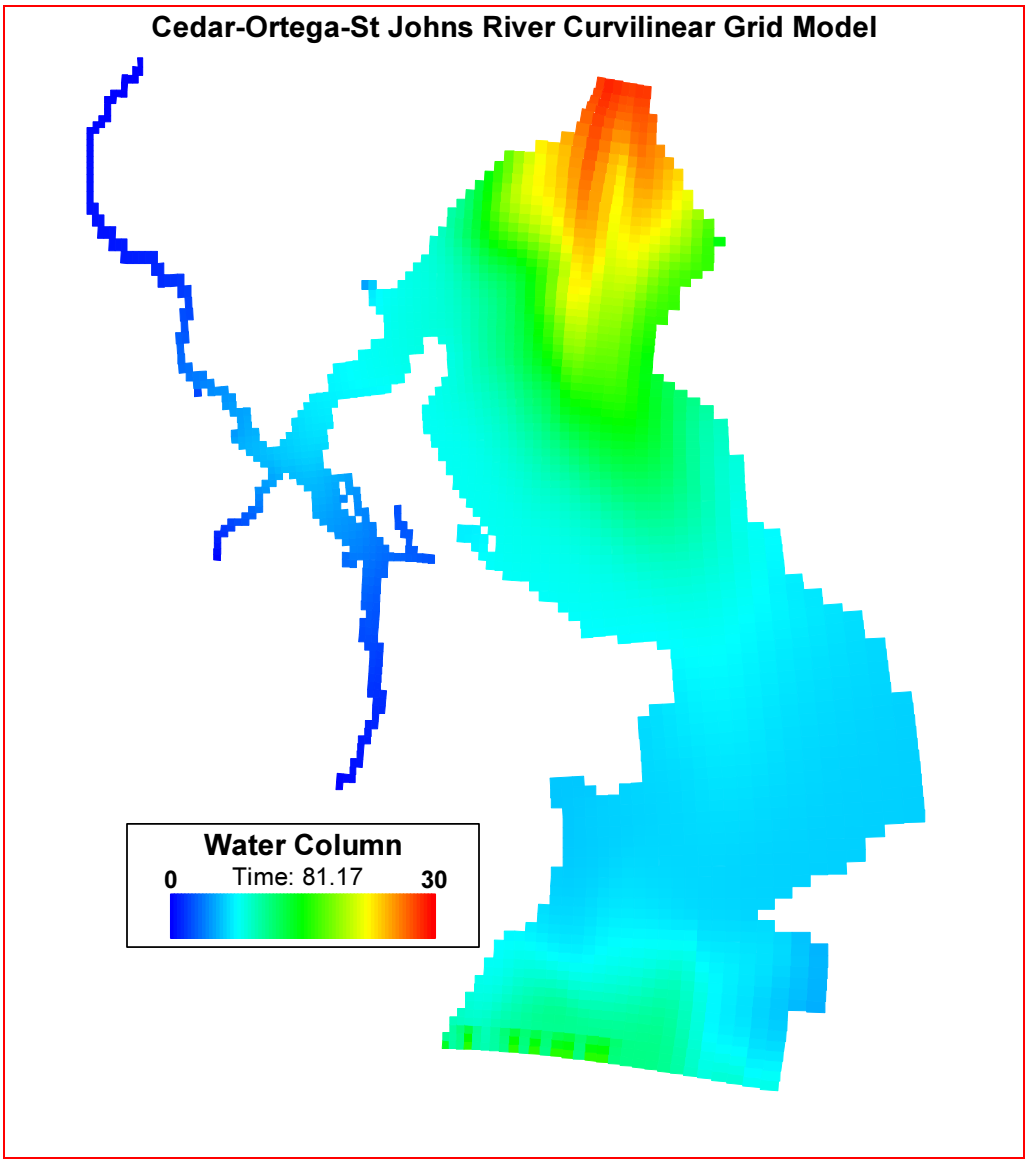

Figure G.18 Predicted salinity distribution at approximately high water

agreement between the predicted and measured phases, though the agreement with the water surface elevation was not as good as that obtained at TG2. This result is not totally surprising considering the coarseness of the grid used to represent the Cedar River in the COSJR model.

Figures G.23 – G.25 show the comparisons obtained between the predicted and ADCP-measured discharges at transects 3, 4 and 6 (see Figure 3) on day 137, which corresponds to 17 May 2001. In these figures, series 1 is the predicted discharge (data points are 30 minutes apart), series 2 is the ADCP measured discharge, and series 3 is the total

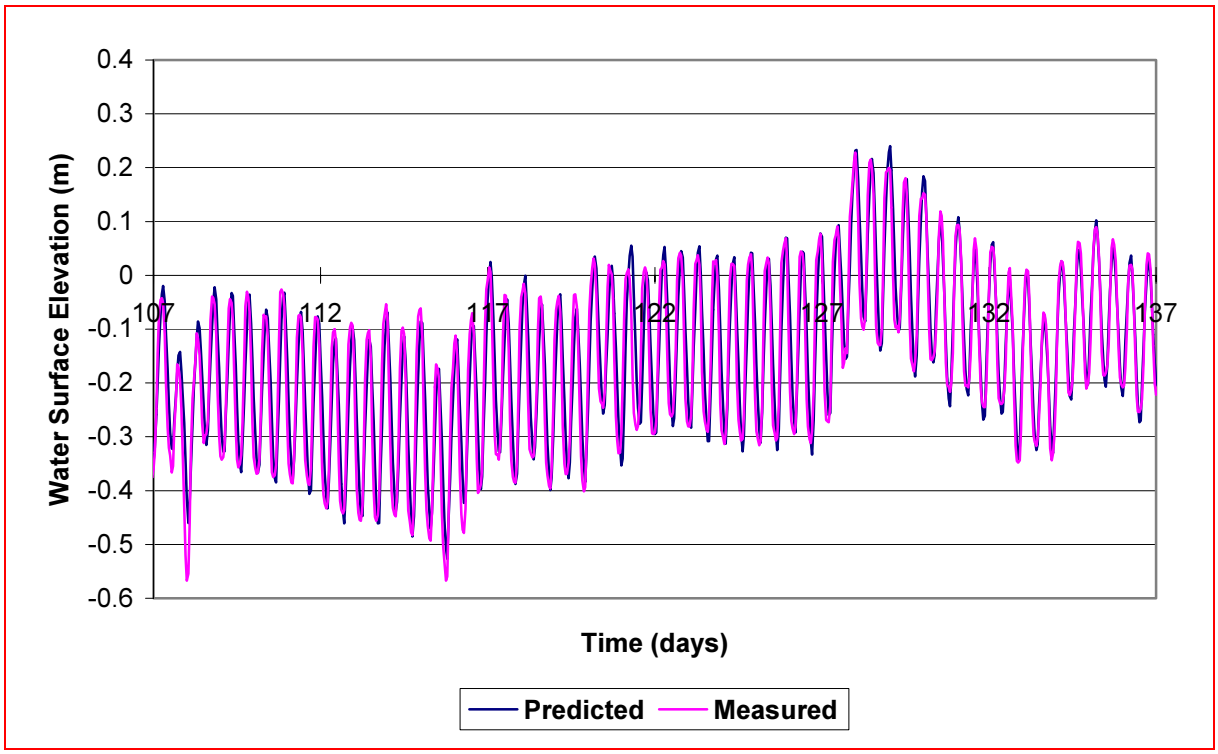

Figure G.19 Predicted versus Measured Water Surface Elevations at TG2 for days 107–137

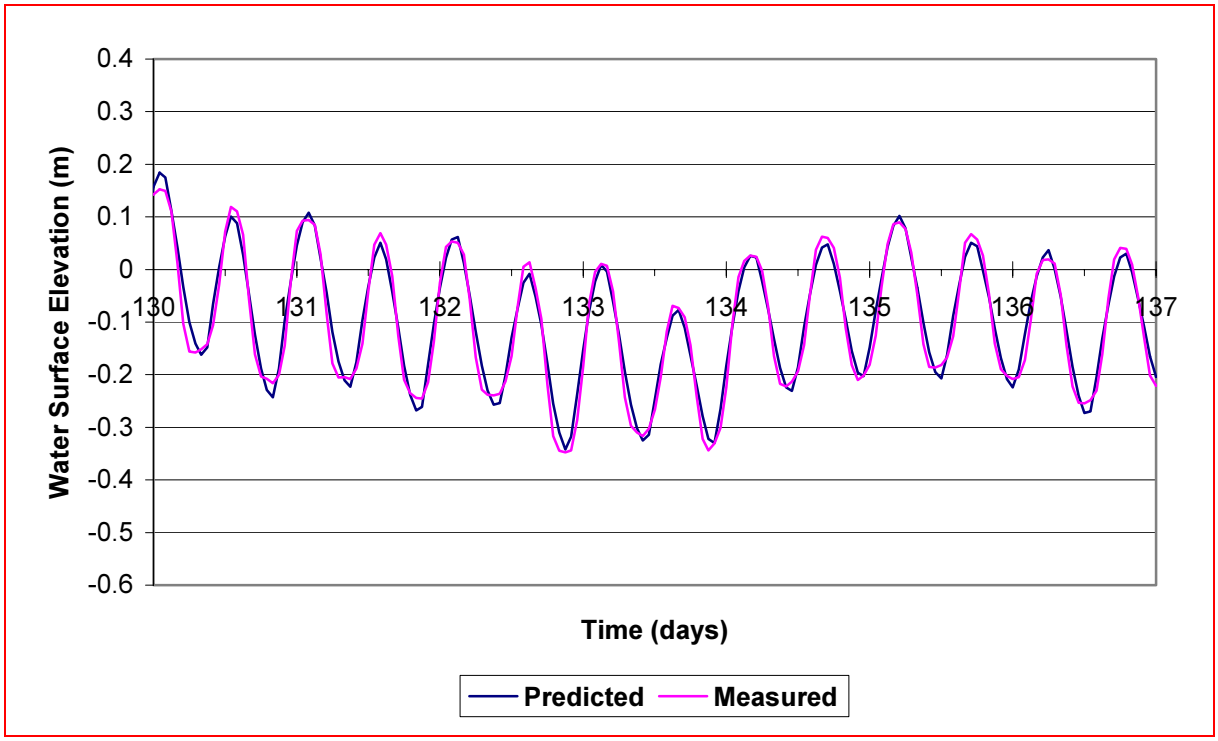

Figure G.20 Predicted versus Measured Water Surface Elevations at TG2 for days 130–137

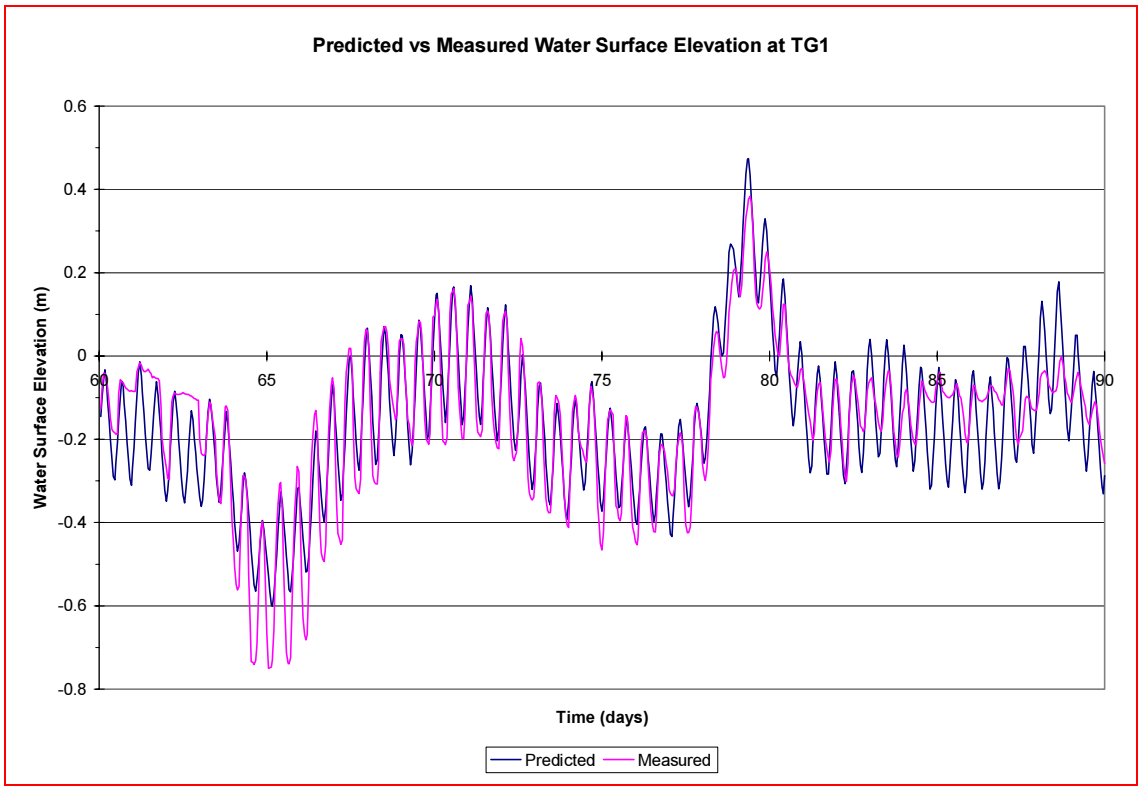

Figure G.21 Predicted versus Measured Water Surface Elevations at TG1 for days 60–90

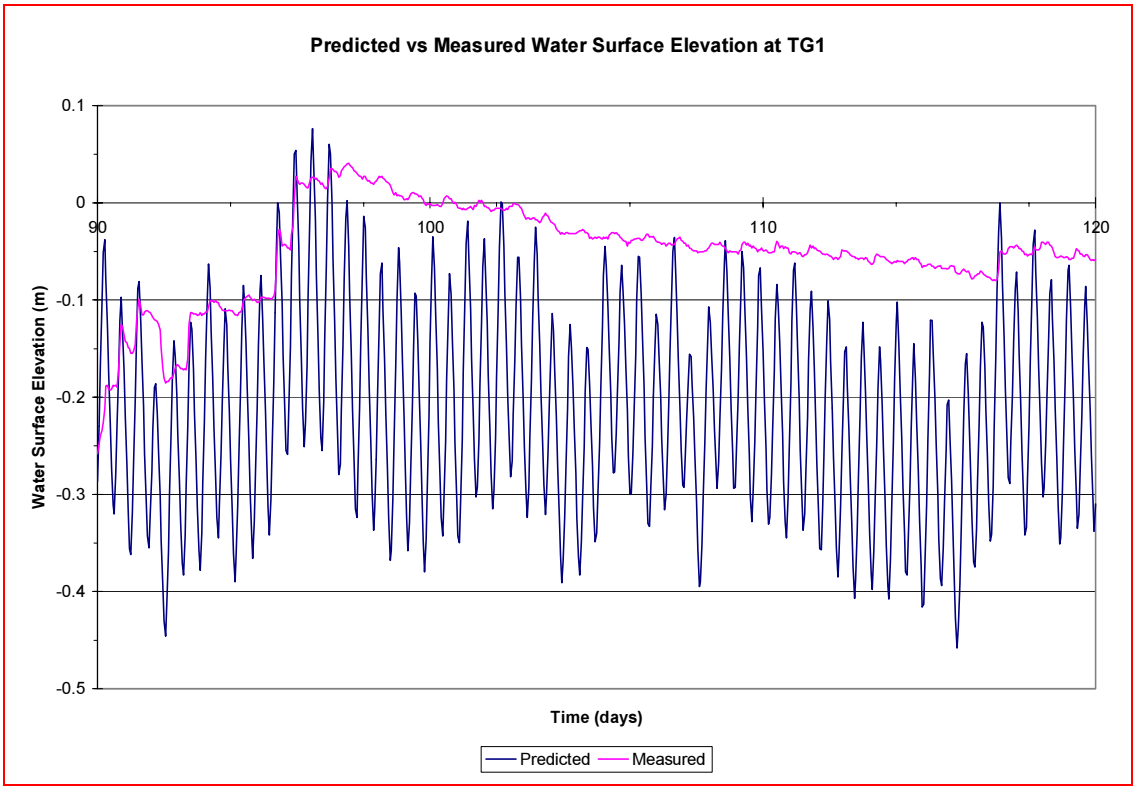

Figure G.22 Predicted versus Measured Water Surface Elevations at TG1 for days 90–120

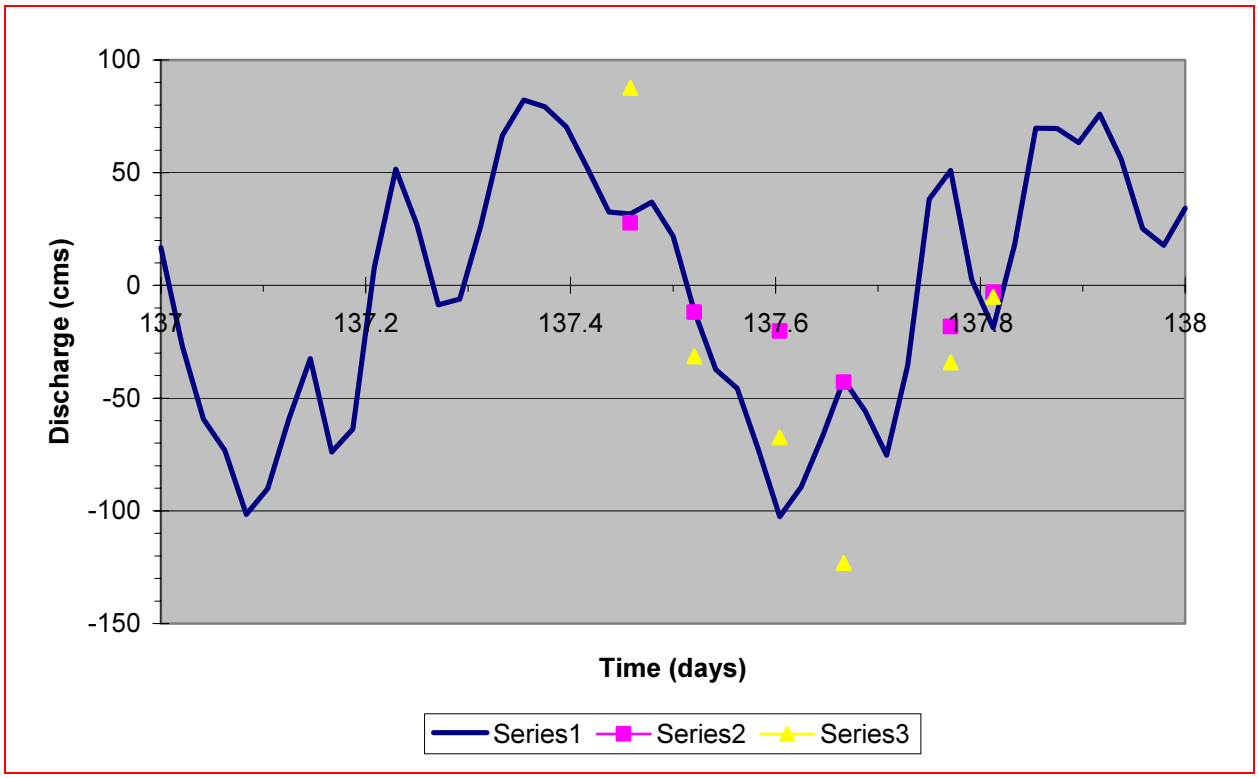

Figure G.23 Predicted vs. Measured Discharges for Day 137 at Transect 3

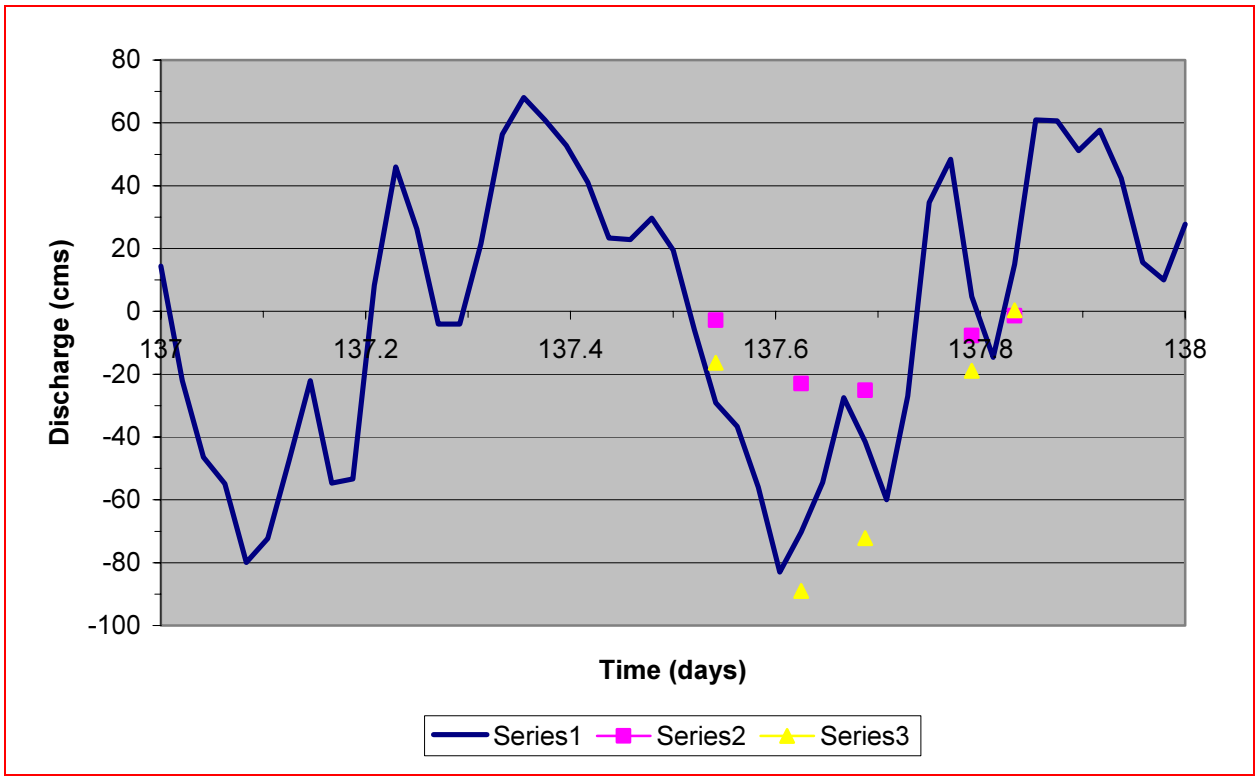

Figure G.24 Predicted vs. Measured Discharges for Day 137 at Transect 4

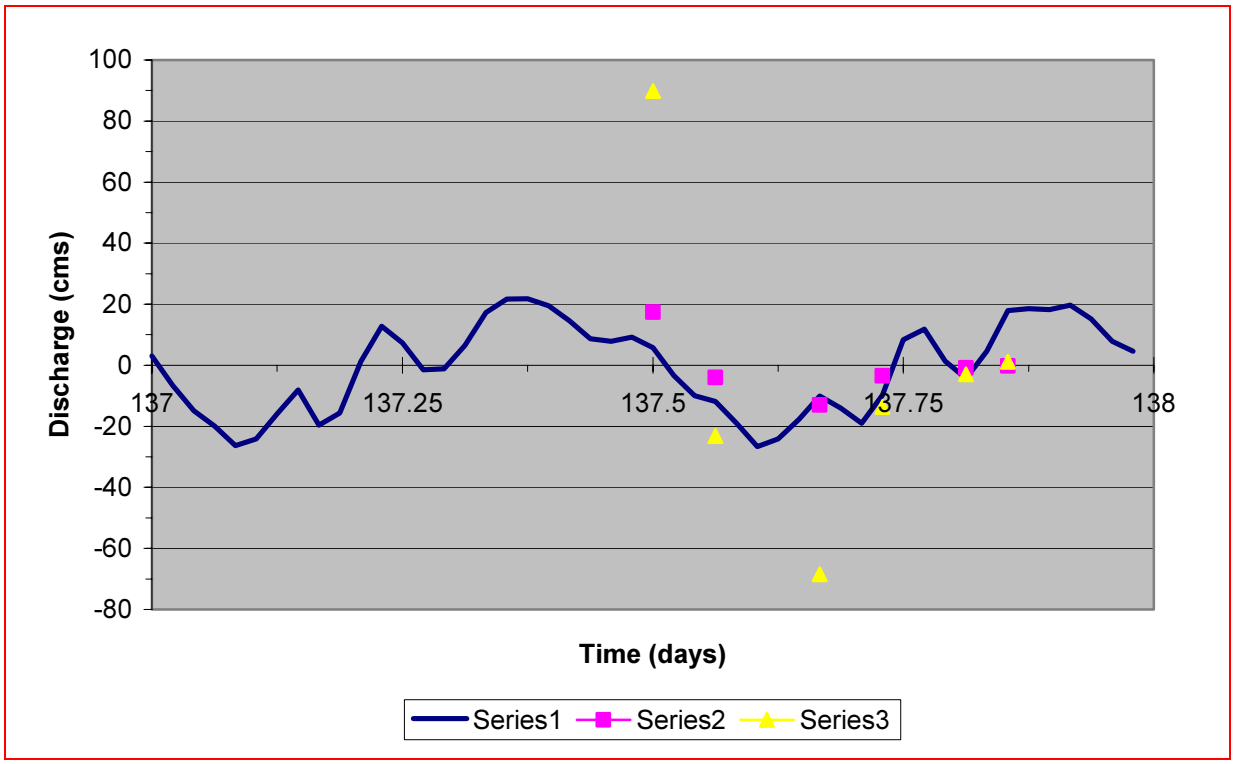

Figure G.25 Predicted vs. Measured Discharges for Day 137 at Transect 6

estimated measured discharge (see Paramygin (2002) for a discussion of the method used to obtain the total estimated measured discharge). In general, the measured discharges are reasonably close to the predicted discharges.

Figures G.26 – G.28 show the agreement obtained between the absolute value of the predicted (series 1) versus the measured (series 2) sediment fluxes. Paramygin (2002) discusses the procedure used to calculate the sediment fluxes. The absolute value of the fluxes had to be plotted due to the need to use a log scale on the ordinate. Relatively good agreement is seen in Figures G.26 and G.27 between the measured and predicted fluxes. Less than satisfactory agreement is seen in Figure G.28 for three of the six measured fluxes, though considering the errors associated with determination of the measured fluxes, the differences seen in these three figures are not unreasonable.

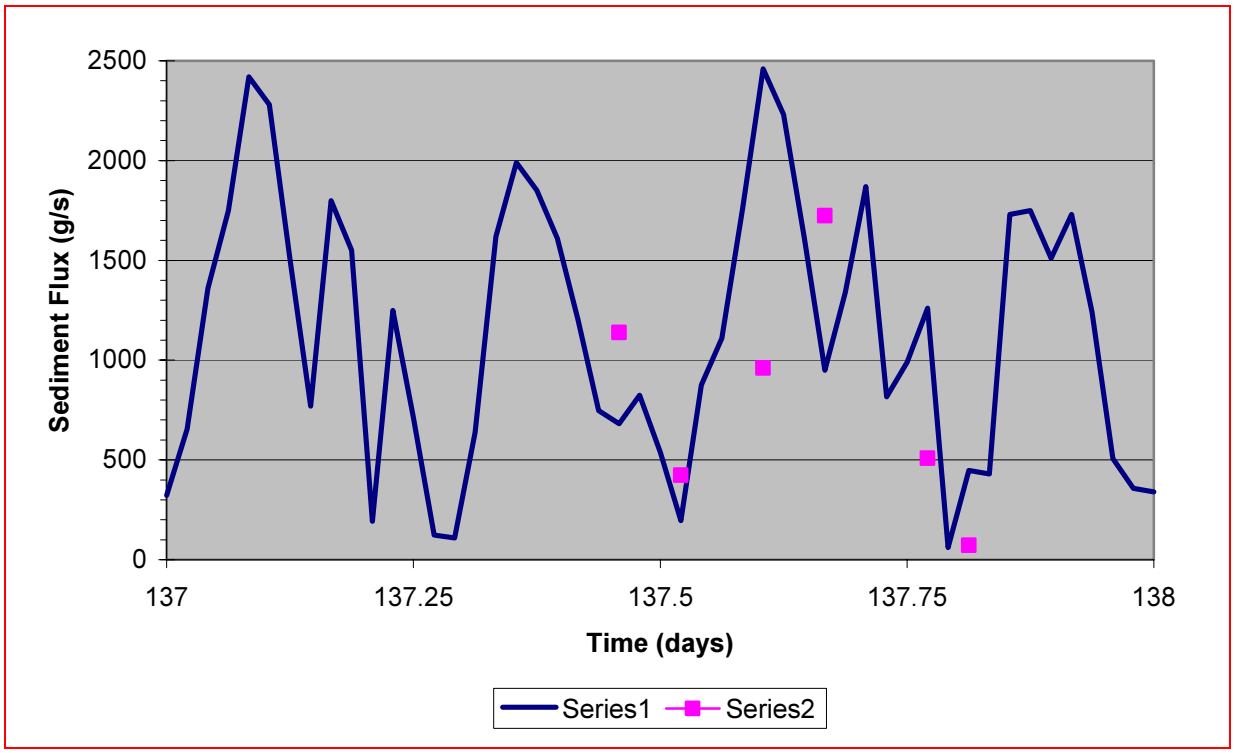

Figure G.26 Absolute Value of the Predicted vs. Measured Sediment Fluxes at Transect 3

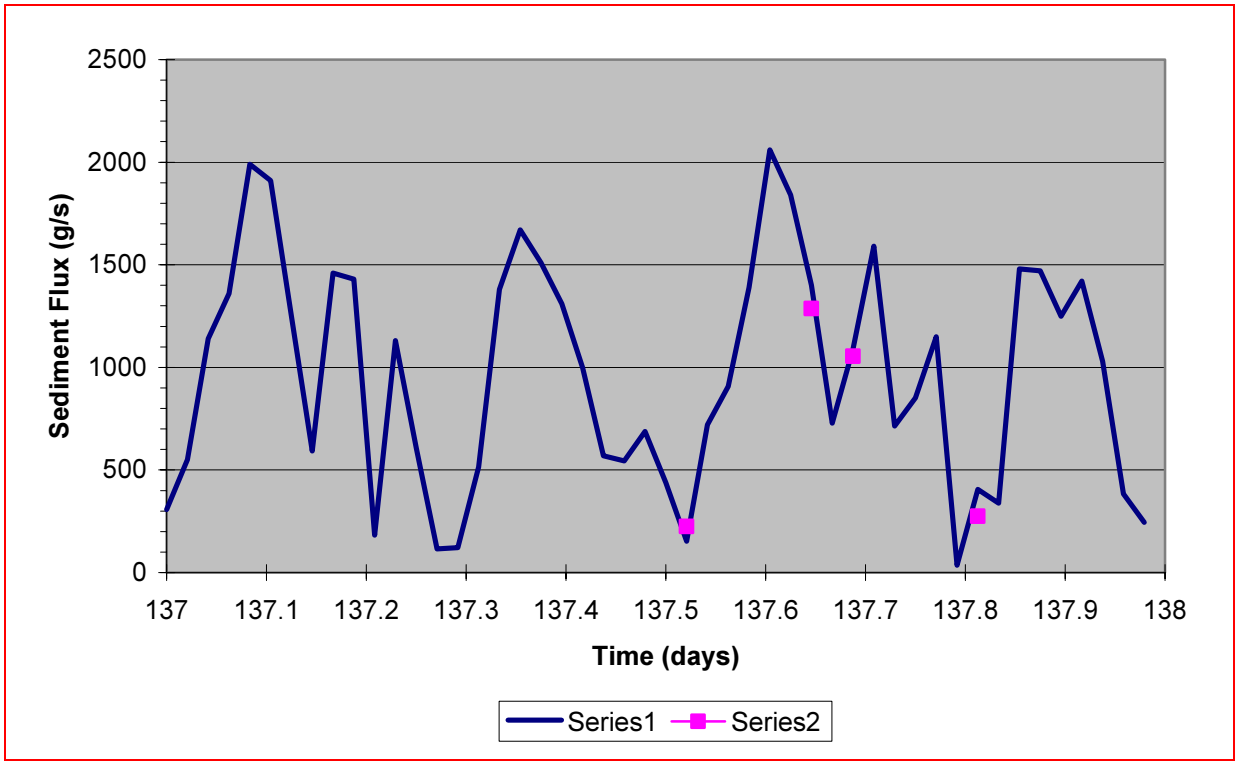

Figure G.27 Absolute Value of the Predicted vs. Measured Sediment Fluxes at Transect 4

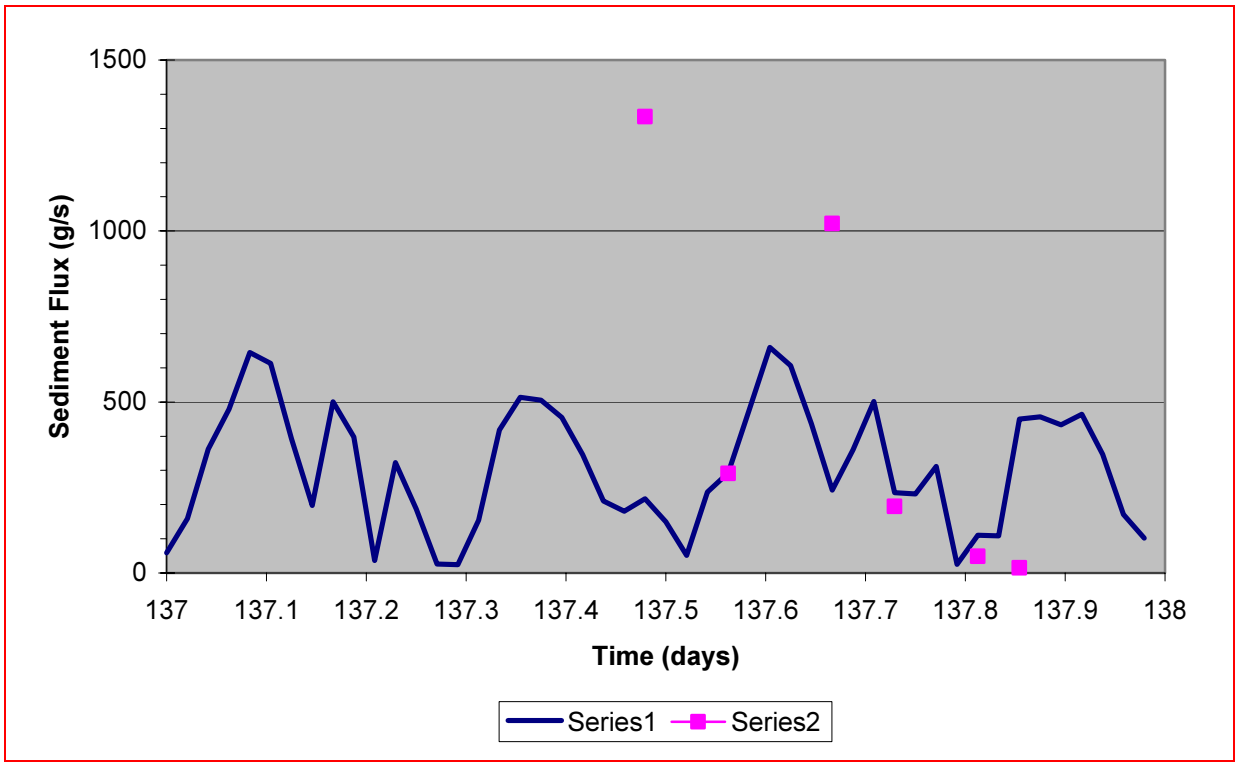

Figure G.28 Absolute Value of the Predicted vs. Measured Sediment Fluxes at Transect 6

G.5 Model Validation

A 30-day validation period (30 January – 28 February 2001) was used for the COSJR model. The COSJR model was initially run (cold-started) for a 29-day spin-up period (01 January – 29 January 2001). The restart file generated by this run was used to hot-start the runs made during the specified validation period, which corresponds to days 30 - 59, the results of which are described in this section.

Figure G.29 shows the comparison between predicted and measured water surface elevations obtained at TG1 for days 30 – 59. As seen in Figure G.21, good agreement was obtained between the predicted and measured phases, though the agreement with the water surface elevation was again (as during model calibration) not as good. As mentioned previously, some of these differences in stages may be attributable to the coarseness of the grid used to represent the Cedar River in the COSJR model, and some to problems with the

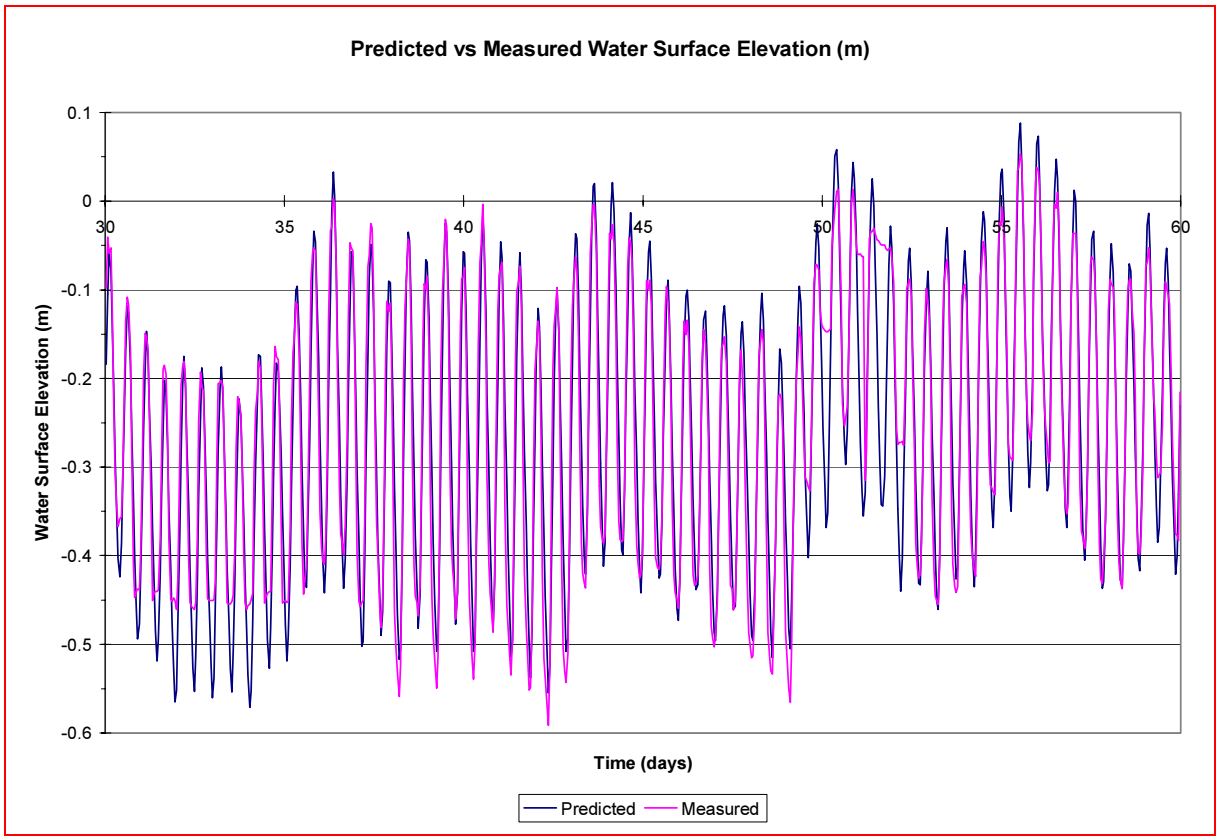

Figure G.29 Predicted versus Measured Water Surface Elevations at TG1 for Days 30-59

operation of TG1 (as can be seen around days 31 – 35, where is looks like the float in the stilling well might have bottomed out, and again around days 50 – 53). TG1 was serviced on 06 February 2001 (day 37), at which time this problem might have been corrected as it does not appear to occur again. A detailed examination of this figure shows that during some tidal cycles, the predicted tidal range is greater than the measured, and on approximately an equal number of cycles (excluding the days noted above), the reverse trend is observed. The same comparison was observed between both predicted versus measured high water elevations and low water elevations. A statistical comparison was not made between the predicted and measured water surface elevations at TG1 because of the heretofore problems noted in the operation of this gage.

Figure G.30 shows the comparison between predicted and measured water surface elevations obtained at TG2 for days 37.5 – 59. The comparison was started at day 37.5 since the measured record was not available before this date. Good agreement was again obtained between the predicted and measured phases, though as seen in this figure, the agreement between the predicted and measured water surface elevations was not as good as that obtained

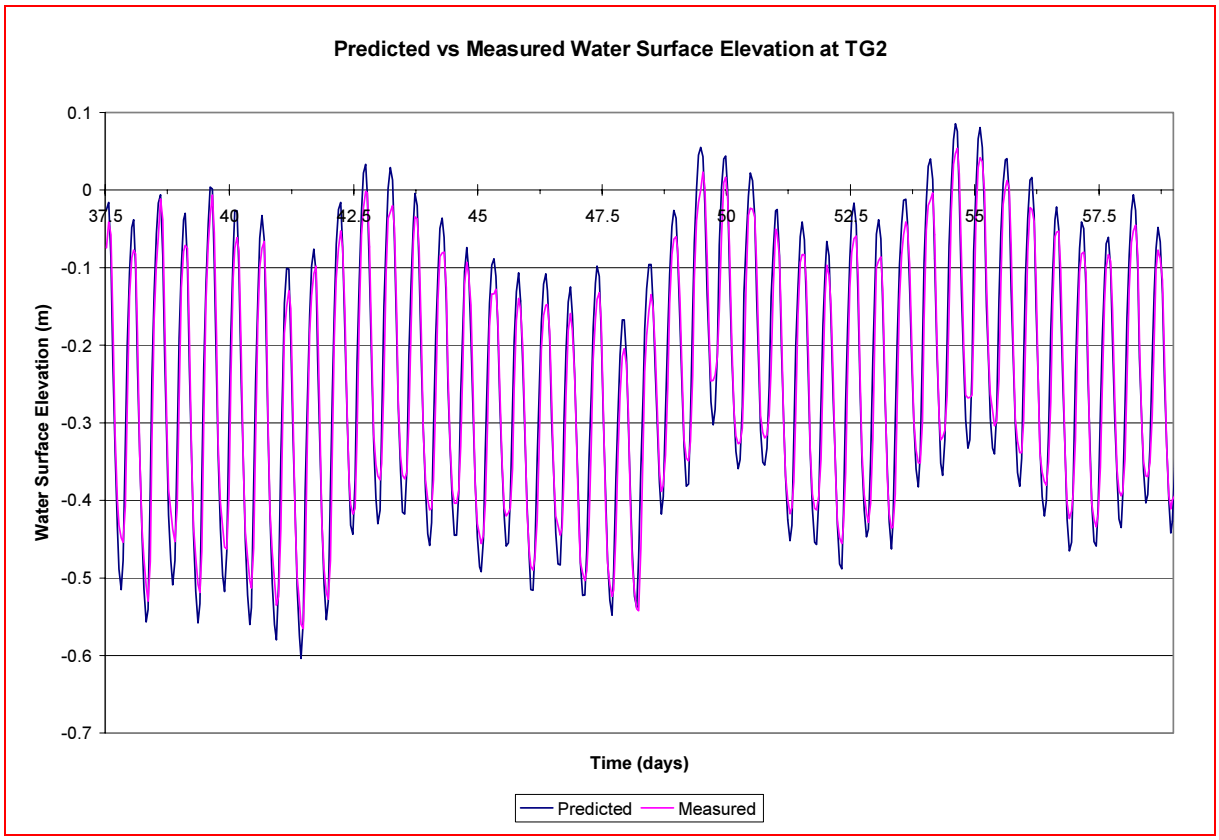

Figure G.30 Predicted versus Measured Water Surface Elevations at TG2 for Days 37.5-59

during model calibration. The average predicted tidal range during this 21.5-day period is 16% greater than the measured range. A more comprehensive model validation will be performed by comparing measurements made by the University of Florida during 2002, as reported by Patra and Mehta (2003), with model simulations once the SWMM modeling of the Ortega-Cedar drainage basins has been performed by SJRWMD.

G.6 Cedar River Sediment Trapping Modeling Results

Using the boundary conditions generated by the COSJR model, the 21 trapping scenarios defined in Tables G.1 and G.2 were run using the CR model. The purpose of running these 21 scenarios was to allow for relative comparisons of the proposed remediation measures under varying hydrodynamic and sediment loading conditions. The 18 scenarios given in Table G.1 define off-channel (i.e., sedimentation ponds) sediment traps, whereas the three scenarios given in Table G.2 define in-channel sediment traps. Each of the 21 scenarios was run for seven days (days 30 – 37 during the validation period).

G.6.a Off-Channel Sediment Traps

The locations of the three off-channel sediment traps (designated Sites OFL1 – OFL3 in Table G.1) are as follows: Sites OFL1 and OFL2 are shown in Figure G.3 (labeled Sites 1 and 2), whereas Site OFL3 is located approximately 200 m downstream of the location of TG 1 (see Figure G.3). For each scenario, the assumed sediment trapping (or removal) efficiency (0, 40, 60 or 80%) is given for each of the three proposed remediation sites. The numbers in the "CR Inflow", "CR TSS" and "Downstream tide BC" columns in Table G.1 indicate the factors the corresponding time series are multiplied by during the model run. For example, in Scenario 15, both the CR inflow time series and the CR TSS time series are multiplied by a factor of 2.5 to simulate a higher flow (and corresponding higher TSS) than that predicted by the SWMM. In Scenario 14, the downstream water surface elevation time series (predicted by the COSJR model) is multiplied by a factor of 1.5 to simulate a tide with a 50% larger tidal range.

For scenarios 1 and 2, no sediment traps were simulated. These are considered the low-flow baseline cases. As seen in Table G.1, the difference between these two scenarios is that in Scenario 1 wind was not included as a driving force, whereas in Scenario 2 the

Table G.1 Cedar River off-channel sediment trapping scenarios

Scenario No.	Off Channel Trap efficiencies (%)			Hydrodynamic/Sediment Conditions			
	OFL1	OFL2	OFL3	Wind	CR inflow	CR TSS	Downstream tide BC
1	0	0	0	none	1	1	1
2	0	0	0	measured	1	1	1
3	40	0	0	none	1	1	1
4	60	0	0	none	1	1	1
5	80	0	0	none	1	1	1
6	40	40	0	none	1	1	1
7	80	80	0	none	1	1	1
8	40	40	40	none	1	1	1
9	80	80	80	none	1	1	1
10	40	40	40	measured	1	1	1
11	40	40	ONL3	measured	1	1	1
12	40	40	40	30 mph S	1	1	1
13	40	40	40	30 mph N	1	1	1
14	40	40	40	measured	1	1	1.5
15	40	40	40	measured	2.5	2.5	1
16	40	40	40	measured	5	5	1
17	40	40	40	measured	10	10	1
18	40	40	ONL3	measured	10	10	1

Table G.2 Cedar River in-channel sediment trapping scenarios

Scenario No.	In Channel Trap			Hydrodynamic/Sediment Conditions			
	ONL3	ONL1	ONL2	Wind	CR inflow	CR TSS	Downstream tide BC
19	yes	0	0	None	1	1	1
20	yes	yes	0	None	1	1	1
21	yes	yes	yes	None	1	1	1

measured wind velocity at the NAS_Jax weather station was used to calculate the (assumed) spatially constant wind-induced surface shear stress over the modeling domain.

In Scenarios 3 – 9, the number of sediment traps and their efficiencies were systematically varied. The difference between Scenarios 8 and 10 is that wind was included as a driving force in Scenario 10, whereas it was not in Scenario 8. Due to modeling limitations and related complications in representing each of the three proposed remediation sites as a water body with channelized flow diverted into it, the representation of the off-

channel sediment traps in the model was simplified. Accordingly, a function was implemented that decreased the sediment flux bypassing the five lateral grid cells (that represented an off-channel sediment trap) by a pre-defined percentage, i.e., 40, 60 or 80%. The channel cross-sections where the three proposed treatment sites would be located were represented by designated grid cells having such a sediment removal function (in terms of the percentage by which the effluent sediment load, leaving the site, is reduced with respect to the influent load entering the site).

In Scenarios 12 – 17, in which three traps with 40% sediment trapping efficiencies were represented, one or more of the driving forces were varied. The hydrodynamic/sediment boundary conditions changed in Scenarios 14 and 15 were described above. In Scenarios 16 and 17, the CR inflow and TSS time series were multiplied by factors of 5 and 10, respectively, to represent increasing flows and sediment loads from the watershed upstream of the upstream CR boundary.

In Scenarios 11 and 18, the two upstream most off-channel traps were represented along with the upstream most in-channel trap (ONL3). The latter is located at the same location as OFL3. These two scenarios were run (with the difference between them indicated in Table G.1) to investigate the use of both off-channel and in-channel traps.

G.6.b On-line Sediment Traps

The locations of the three on-line (i.e., in-channel) sediment traps (designated Sites ONL1 – ONL3 in Table G.2) are as follows: Sites ONL1 and ONL2 are shown in Figure 4.2, whereas Site ONL3 is located at the same location as OFL3. As seen in Figure G.26, each trap was three cells wide and had an initial bottom elevation 2 m lower than that of the surrounding cells. The lengths of ONL1, ONL2 and ONL3 were 298 m, 287 m, and 319 m, respectively.

G.6.c Results from Sediment Trap Simulations

For each of the 21 scenarios, net sediment fluxes, in units of grams per second (g/s), over the seven-day simulation at five transects along the CR were computed. The results are presented in the second through the sixth columns in Tables G.3 and G.4. The five transects, identified as T1 – T5 in Tables G.3 and G.4 and showed in Figure G.27, were located as follows: T1: immediately downstream of Site 1 (see Figure G.27); T2: immediately downstream of Site 2 (see Figure G.27); T3: immediately downstream of Site 3, which is located in the middle of ONL3 (see Figures G.26 and G.27); T4: immediately downstream of ONL1 (see Figures G.26 and G.27); and T5: immediately downstream of ONL2 (see Figures G.26 and G.27). The last four columns in Tables G.3 and G.4 give the percentage decrease in the net downstream sediment flux at transects T1 – T4 relative to that for each of these transects calculated for Scenario 1 (the dashes in the first row of these last four columns indicate that the percentages were not calculated for these transects since the relative differences are meaningless for Scenario 1). The dashes in the last four columns in Table G.3 for Scenarios 15 – 18 were not calculated since the changes in the boundary conditions for these scenarios nullified comparisons in terms of the relative net sediment fluxes. The negative sediment fluxes given under T1 and T4 in Table G.4 indicate that the net flux increases at these transects relative to Scenario 1.

Percentage changes (relative to Scenario 1) in reach average bed elevation change for six reaches over the seven-day simulations are shown in Table G.5. A positive percentage in this table indicates that there was more erosion in that reach than that which occurred in Scenario 1. The first reach, designated u/s – T1, extends from the upstream (u/s) boundary to T1, reach T1 – T2 extends from T1 to T2, reach T2 – T3 extends from T2 to T3, reach T3 – T4 extends from T3 to T4, reach T4 – T5 extends from T4 to T5, and reach T5 – d/s extends

from T5 to the downstream (d/s) boundary. The actual reach average erosion (not the percentage change in reach average erosion) is given in Table G.5 for reach T4 – T5 since

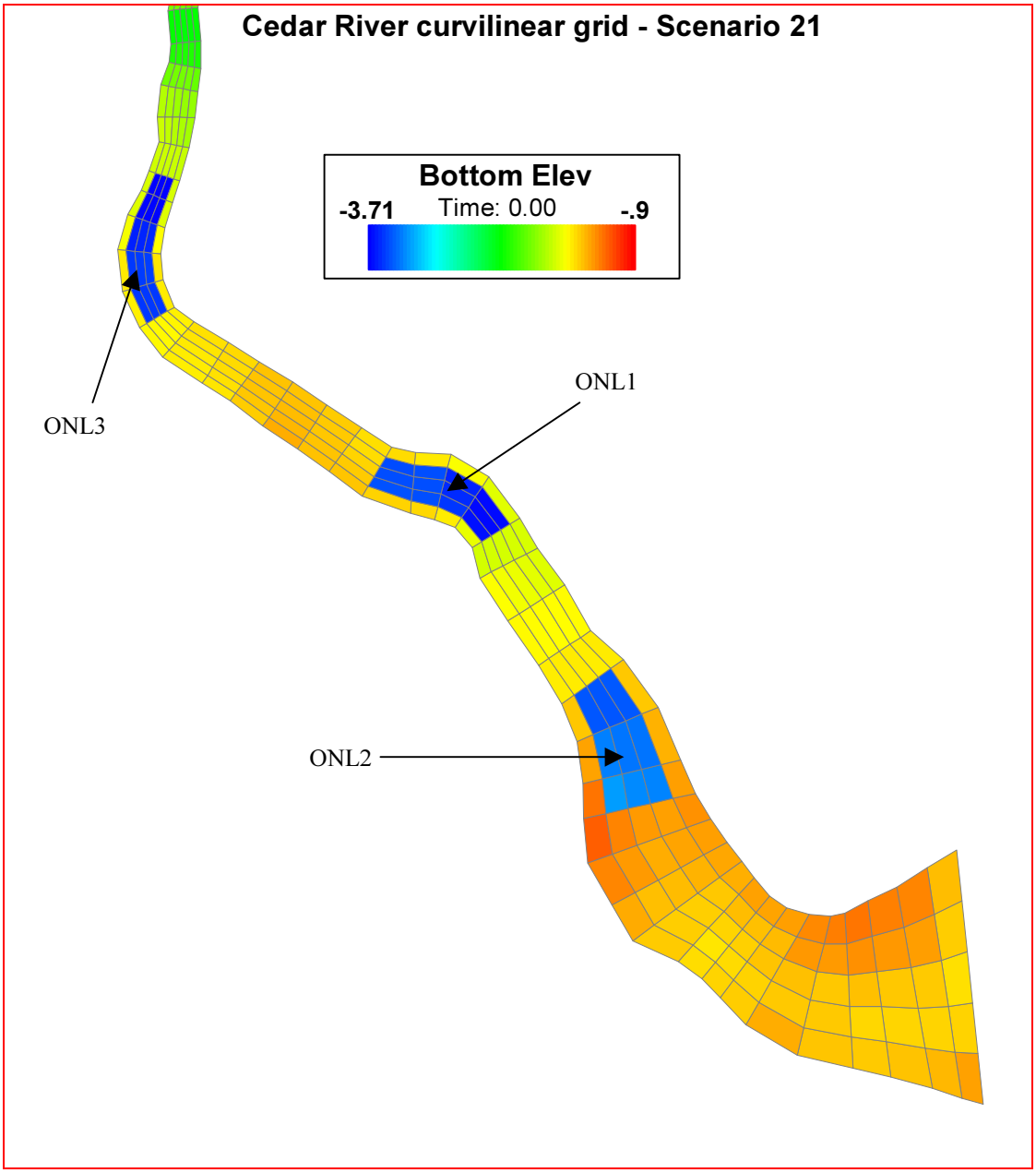

Figure G.26 Location of Three In-Channel Sediment Traps

the reach average erosion for reach T4 – T5 for Scenario 1 was zero, thus not allowing the percentage change to be calculated.

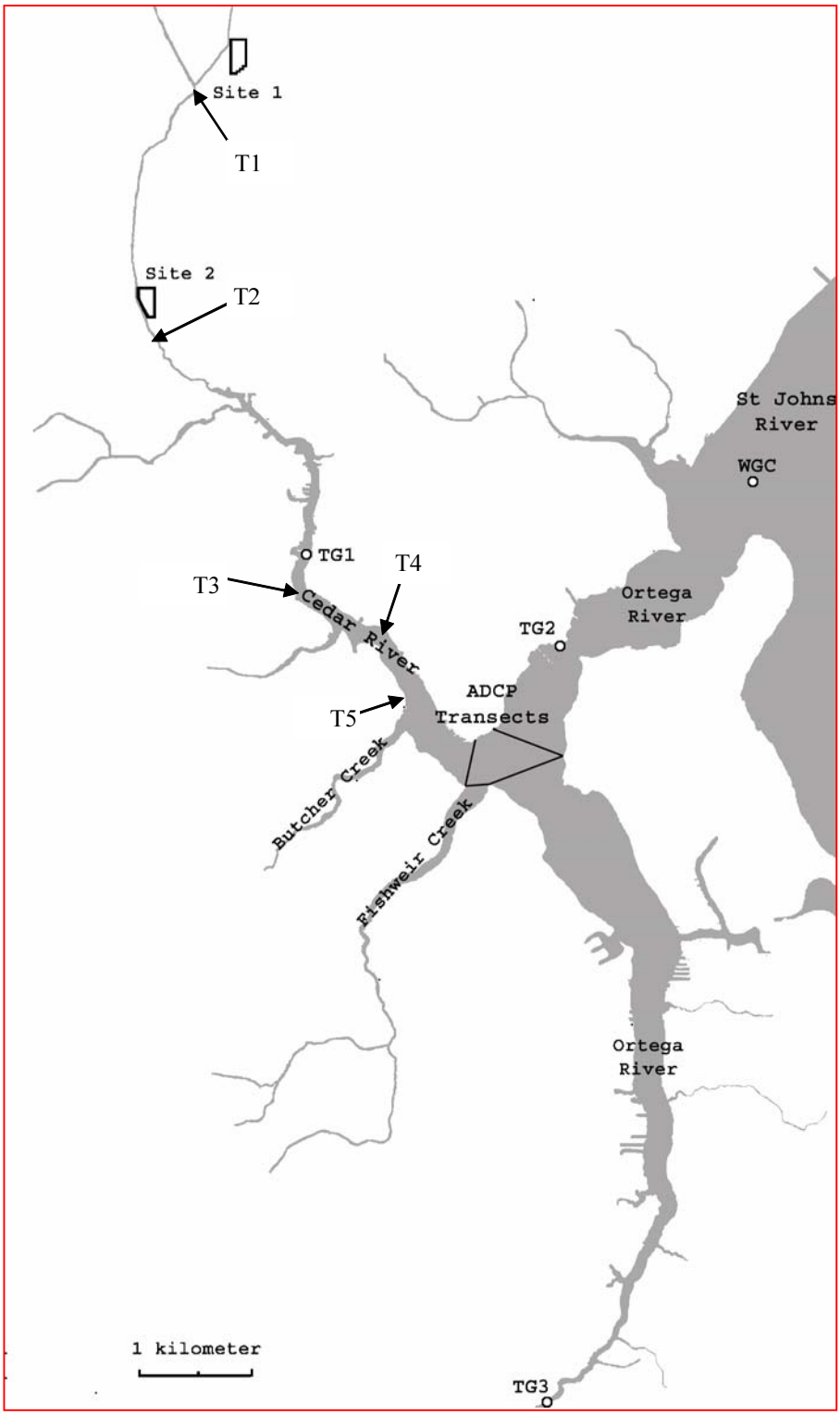

Figure G.27 Location of Transects 1 - 5

Table G.3 Results from off-channel sediment trapping scenarios

Scenario No.	Net sediment flux (g/s) at indicated transects					Decrease in net sediment flux (%)			
	T1	T2	T3	T4	T5	T1	T2	T3	T4
1	4.91	19.47	2.00	4.26	2.85	-	-	-	-
2	4.91	19.47	2.00	4.26	2.85	0	0	0	0
3	3.54	17.81	1.98	4.25	2.85	28	9	1	0.2
4	3.11	17.28	1.97	4.25	2.85	37	11	1.5	0.2
5	2.78	16.86	1.96	4.25	2.85	43	13	2	0.2
6	3.54	11.00	1.92	4.23	2.85	28	44	4	0.7
7	2.78	7.54	1.88	4.22	2.84	43	61	6	0.9
8	3.54	11.00	1.03	3.63	2.77	28	44	49	15
9	2.78	7.54	0.742	3.43	2.74	43	61	63	19
10	3.54	11.00	1.03	3.63	2.77	28	44	49	15
11	3.64	10.06	1.53	4.26	2.84	26	48	24	0.9
12	3.54	11.00	1.03	3.63	2.77	28	44	49	15
13	3.54	11.00	1.53	4.05	2.83	28	44	24	5
14	3.56	11.21	1.01	4.12	1.45	27	42	50	3
15	20.76	68.39	8.42	12.87	4.66	-	-	-	-
16	75.88	215.5	64.46	111.5	30.10	-	-	-	-
17	286.9	659.9	394.9	870.1	271.8	-	-	-	-
18	278.8	638.7	382.1	1024	327.9	-	-	-	-

Table G.4 Results from in-channel sediment trapping scenarios

Scenario No.	Net sediment flux (g/s) at indicated transects					Decrease in net sediment flux (%)			
	T1	T2	T3	T4	T5	T1	T2	T3	T4
19	5.05	18.46	1.57	4.28	2.84	-3	5	22	-0.5
20	5.04	18.54	1.59	4.02	2.95	-3	5	21	6
21	5.04	18.63	1.60	4.15	2.14	-3	4	20	3

As seen by comparing the results for Scenarios 1 and 2 in Tables G.3 – G.5, the measured wind had no impact on net sediment fluxes or reach average erosion. The impact of adding OFL1 is seen for Scenarios 3 – 5 in Table G.3. With increasing trap efficiency, the net sediment flux decreases at T1 – T3. As expected, the largest decreased occurred at T1 as this transect was located immediately downstream of OFL1. Essentially no reduction in net sediment flux occurred at T4. The results in Table G.5 for these same three scenarios show that the reach average net erosion increased with increasing trap efficiency for the three upstream-most reaches. The increase in the net erosion for these three reaches, possibly

explained by the decreasing suspended sediment concentrations (due to the increasing trap efficiencies) partially counters the decrease in the net sediment flux noted above.

Table G.5 Percentage change in reach average net erosion

Scenario Number	Change in Reach Average Net Erosion (%)					
	u/s–T1	T1–T2	T2–T3	T3–T4	T4–T5 *	T5–d/s
1	-	-	-	-	-	-
2	0	0	0	0	0	0
3	0.6	8.4	9.8	0	0	0
4	0.9	10.8	13.0	0	0	0
5	1.2	12.7	15.4	0	0	0
6	0.6	14.0	53.1	0	0	0
7	1.2	19.9	75.3	0	0	0
8	0.6	14.0	53.2	0	0	0
9	1.2	19.9	75.5	0	0	0
10	0.6	14.0	53.2	0	0	0
11	17.0	21.9	16.8	-76.6	0	21.2
12	0.6	14.0	53.2	0	0	0
13	0.6	13.9	70.3	0	0	0
14	2.2	17.7	57.2	19.6	8.77×10^{-5}	4.03×10^{5}
15	374	402	178	-1.85×10^{3}	5.79×10^{-5}	823
16	1.03×10^{3}	1.20×10^{3}	695	-2.09×10^{4}	2.16×10^{-3}	-9.52×10^{3}
17	2.41×10^{3}	2.88×10^{3}	2.07×10^{3}	-7.08×10^{4}	1.51×10^{-2}	-9.69×10^{4}
18	2.55×10^{3}	3.00×10^{3}	2.33×10^{3}	-8.52×10^{4}	1.73×10^{-2}	-1.17×10^{5}
19	16.1	6.9	-43.4	-76.6	0	21.2
20	16.1	7.6	-41.9	-29.8	0	37.4
21	15.9	8.4	-39.7	16.6	0	79.9

* the numbers in this column are the reach average bed elevation change (m)

The impact of adding OFL2 (in addition to OFL1) is seen in Table G.3 for Scenarios 6 and 7. The percentage decrease in the relative net sediment flux at T2 increases from 9% to 44% for Scenario 6 and from 13% to 61% for Scenario 7. Similar, though smaller, increases are noted at both T3 and T4 for both Scenarios. These results show that OFL2 has a larger impact on reducing the net sediment flux to the lower portion of the Cedar River than OFL1 by itself. Also note that increasing the trapping efficiencies of both OFL1 and OFL2 from 40% to 80% results in only a 17% decrease in the relative net sediment flux at T2, though the relative decrease at T3 is 50%. Also as seen in Table G.3, the net sediment flux at T4

decreases from 0.2% for Scenario 5 to 0.9% for Scenario 7. The additional increase in the reach average net erosion is noted in Table G.5 for Scenarios 6 and 7.

The impact of adding OFL3 (in addition to OFL1 and OFL2) is seen in Table G.3 for Scenarios 8 and 9. The percentage decrease in the net sediment flux at T3 increases from 4% to 49% for Scenario 8 and from 6% to 63% for Scenario 9. The percentage decrease in the net sediment flux at T4 increases from 0.7% to 15% for Scenario 8 and from 0.9% to 19% for Scenario 9. Thus, adding OFL3 has a large impact in reducing the net sediment flux at both T3 and T4. Also note that increasing the trapping efficiencies for all three off-channel traps from 40% to 80% results in a moderate 14% decrease in the net sediment flux at T3 and a minimal 4% decrease at T4. The reach average net erosion is essentially the same for Scenario 8 (in comparison to Scenario 6) and for Scenario 9 (in comparison to Scenario 7). Similar to the comparison between Scenarios 1 and 2, no change due to the measured wind is noted in Tables G.3 or G.5 between Scenarios 8 and 10.

In Scenario 11, the addition of ONL3 instead of OFL3 results in a 49% higher net sediment flux at T3 than that in Scenario 8, a 17% higher flux at T4, and a 3% higher flux at T5. The -76.6% change in net erosion given in Table G.5 for Scenario 11 at reach T3 – T4 is attributable to the deposition that occurs in ONL3. Thus, using three off-channel traps is more efficient at reducing the net sediment flux in the Cedar River than the use of two off-channel traps and one in-channel trap. Comparison of Scenarios 6 and 11 shows that the relative net sediment flux at T3 is reduced from 4% to 24% by the addition of ONL3. The difference in the net fluxes at T4 is negligible.

Next, Scenarios 12 and 13 were compared with Scenario 8. As seen in Table G.3, the results obtained for Scenario 8 (no wind) and Scenario 12 (constant 30 mph Southerly wind over the seven-day simulation) were surprisingly identical. The constant 30 mph Northerly

wind simulated in Scenario 13 resulted in a 25% less relative decrease in the net sediment flux at T3, and a 10% less relative decrease in the net sediment flux at T4. Taken together, these three scenarios show that low to moderate winds (i.e., less than that during tropical storms) have an insignificant impact on the sedimentary regime in the relatively narrow and winding Cedar River.

Scenario 14 shows the impact that a 50% higher tidal range at the downstream boundary has on the net sediment flux in the Cedar River. A smaller decrease in net sediment flux occurs at T4 in Scenario 14 (3%) than that in Scenario 8 (15%). Insignificant differences occur at the upstream transects. The biggest differences between these two scenarios are seen in Table G.5, in which the higher tidal range at the downstream boundary results in reach average net erosion for the three downstream-most reaches, i.e., reaches T3 – T4, T4 – T5, and T5 – d/s. The latter is particularly significant in reach T5 – d/s.

Scenarios 15 – 17 simulate the impact of increasing both the flow and TSS boundary conditions at the upstream boundary of the Cedar River by factors of 2.5, 5 and 10, respectively. These three scenarios are compared to Scenario 8. As seen in Table G.3, the net sediment fluxes at all five transects increase in proportion to the increase of inflow and TSS loads at the upstream boundary. Scenario 18 is identical to Scenario 17 except that an in-channel trap is used at the location of OFL3 instead of the off-channel trap. The ONL3 in-channel trap results in higher net sediment fluxes at T4 and T5 than those obtained with the OFL3 off-channel trap. This same finding was obtained by comparing Scenarios 10 and 11.

The results for Scenarios 19 – 21 seen in Table G.4 show that the only transect at which a significant reduction in the net sediment flux occurs is T3, which is located immediately downstream of ONL3. Scenarios 11 and 19 show that the reductions in the net

sediment flux at T3 is essentially the same. This indicates that OFL1 and OFL2 have minimal impact at T3.

REFERENCES

Craig, P.M. 2003. *User Manual for EFDC_Explorer: A Pre- / Post-Processor for the Environmental Fluid Dynamics Code*. Dynamic Solutions, LLC, 53 pp.

Freeman, R.J. 2001. Simulation of Total Suspended Solids Loads into the Cedar/Ortega River, Duval County, Florida Using SWMM. St. Johns River Water Management District, Palatka, Florida. *Department of Water Resources Technical Memorandum No. 46*.

Hamrick, J.M. 1992. A Three-Dimensional Environmental Fluid Dynamics Computer Code: Theoretical and Computational Aspects. The College of William and Mary, Virginia Institute of Marine Science. *Special Report 317*, 63 pp.

Hamrick, J.M. 1996. Users manual for the environmental fluid dynamic computer code. The College of William and Mary, Virginia Institute of Marine Science, *Special Report 328*, 224 pp.

Hamrick, J.M. 2000. Theoretical and Computational Aspects of Sediment Transport in the EFDC Model. *Technical Memorandum*, Tetra Tech, Inc, Fairfax, VA, 47 pp.

Hayter, E.J., V. Paramygin, and C.V. John. 2003. Three-Dimensional Modeling of Cohesive Sediment Transport in a Partially Stratified Micro-tidal Estuary to Assess Effectiveness of Sediment Traps. *7th International Conference on Nearshore and Estuarine Cohesive Sediment Transport Processes*, Virginia Institute of Marine Science.

Imhoff, J.C., A. Stoddard, and E.M. Buchak. 2003. Evaluation of Contaminated Sediment Fate and Transport Models. *Final Report*, U.S. EPA, National Exposure Research Laboratory, Athens, GA, 141 pp.

Mehta, A.J., E.J. Hayter, and R. Kirby. 2003. Ortega/Cedar River basin, Florida, restoration: An assessment of sediment trapping in the Cedar River: Phase 2 final report. *Report UFL/COEL-2002/004*, Coastal and Oceanographic Engineering Program, University of Florida, Gainesville.

Paramygin, V. 2002. Sediment trapping in a Microtidal estuarine system. *MS Thesis*, University of Florida.

Patra, R.R., and A.J. Mehta. 2003. Remediation/Restoration of Cedar/Ortega Rivers Phase 2 Amendment Part I: Data Collection. *Report UFL/COEL-2003/002*, Coastal and Oceanographic Engineering Program, University of Florida, 44 pp.

REMEDIATION/RESTORATION OF CEDAR/ORTEGA RIVERS PHASE 2 AMENDMENT: EPISODIC SEDIMENT FLUX DATA COLLECTION AND INTERPRETATION, AND EFDC MODELING IN CEDAR/ORTEGA RIVERS

1. BACKGROUND

The St. Johns River Water Management District (SJRWMD) has identified the Cedar/Ortega Rivers in North Florida, that drain into the Lower St. Johns River main-stem, to be contaminated with polychlorinated byphenyls (PCBs), polycyclic aromatic hydrocarbons (PAHs), heavy metals (e.g., mercury and cadmium), and pesticides. Cedar River flows through an industrial zone within the City of Jacksonville, and is believed to be a greater source of these contaminants than the Ortega River. A significant source of the PCBs is believed to be an industrial source in the proximity of Cedar River. The PAHs are derived from various point and non-point sources ultimately associated with petroleum hydrocarbons. Both PCBs and PAHs have high particle affinity, and their rates of biogeochemical degradation are low. Heavy metals also show a similar affinity. These contaminants are transferred to fish and shellfish at levels that may pose a threat to these organisms.

2. SCOPE AND TASKS

The Civil and Coastal Engineering Department of the University of Florida (UF) has completed the Phase 2 study - “Assessment of fine sediment deposition, erosion and transport rates and evaluation of dredge scenarios for the Cedar/Ortega Rivers”.

This amendment will continue the above data collection effort to address the issue of episodic exchange of suspended sediment across the mouth of Ortega River

in order to quantify the rate of exchange of sediment between Cedar/Ortega Rivers and Lower St. Johns River, a critical, presently unknown factor related to the sediment remediation plan for Cedar/Ortega Rivers. Previous work on this project has demonstrated that, depending on the Cedar/Ortega River runoff conditions and wave action in the St. Johns River, a large amount of sediment is transported from the Cedar/Ortega Rivers into the St. Johns River, or from the St. Johns into the Cedar/Ortega. It is now proposed to verify this prediction, since it is evident that any strategy for sediment containment within the Cedar/Ortega Rivers must account for the influx of sediment from the St. Johns. Sediment flux relationships developed in this study can be later applied to exchange processes in other main stem/tributary interfaces within the Lower St. Johns River watershed.

2.2 Tasks

All measurements required are listed below. Items 1, 2, 3 and 4 below shall be conducted for deployments over 4 months that are expected to cover several storm episodes. In each case the measure of storm will be an increase in the suspended sediment concentration, minimally doubling, over the ambient (non-storm) levels. This rise can come about due to the following forcing functions, either individually or in combinations: 1) river runoff, 2) wind waves and 3) wind-induced storm surge. Stations locations are presented in Figure 2. An important component of data analysis will be to identify the relative roles of the three forcing functions on suspended sediment concentration.

1. Water levels at sites TGCTD 1 and TGCTD 2.

2. Salinity measurements using CTD sensors at TGCTD 1 and TGCTD 2.

3. Wave data at site WGOBS.

4. Point-current velocity using a Marsch-McBirney meter at WGOBS.

5. Suspended solids concentration using OBS sensors at 4 elevations in the water column at WGOBS. Bottle sampling of suspended solids over a spring tidal cycle (14-days) for OBS calibration.

6. Current profiling at transect shown in Figure 2 using an ADCP for one spring tidal cycle.

3. DATA COLLECTION, PROCESSING, INTERPRETATION AND MODEL SIMULATIONS

3.1 Data Collection and Processing

Data collection will be of two types - long term and short term. Water levels, salinity, single-point current velocity, waves and suspended solids concentration, all to be collected over a 4 month period (January-April, 2002). Data from all relevant sensors will be recorded and stored *in situ*. Short term measurements include ADCP transects and suspended solids collection in bottles for calibration. The ADCP will be vessel-mounted with data-acquisition system on board. The bottled suspended solids will be analyzed gravimetrically at UF.

Data processing will be carried out to yield the following:

1. Suspended solids characterization, i.e., grain sizes, erosion/deposition of various size classes.

2. Time series of wind, water levels, salinity, point-current speed and direction, wave height and suspended solids concentration.

3. Three-dimensional images of velocity profiles at the ADCP transect, corresponding time series of discharge over a spring tide cycle.

3.2 Calculation of Sediment Fluxes and Interpretation

Given the above raw data, the following calculations and interpretations will be made:

1. Estimation of the time series of suspended sediment flux across the mouth of the Ortega including sediment characterization.

2. Water surface slope in the mouth area and its correlation with discharge and salinity gradient.

3. Correlation of the suspended sediment flux direction and magnitude with runoff discharge, wave action and storm surge, for each major sediment size and type.

4. Calculation of the suspended sediment size, type and load and its correlation with sediment deposition patterns in the mouth area developed by UF as part of the ongoing Phase 2 investigation.

5. Interpretation of the results from item 4 above with reference to strategies for containment of contaminated sediment in the Cedar/Ortega Rivers.

3.3 3D Sediment model calibration and delivery of calibrated model

The following tasks shall be completed with the EFDC sediment model:

1. Modification of the EFDC model grid if and as required.

2. Under the ongoing component of the Phase 2 study, the hydrodynamic algorithm has been calibrated using data being collected. Further calibration/validation of the hydrodynamic model with additional water level, salinity, wave and current velocity data, and the sediment transport algorithm using newly acquired data on suspended solids concentration and associated sediment characteristics during storm periods.

Various sediment model simulations to evaluate sediment exchanges during extreme storm events including the 1997-98 El Nino event.

4. DELIVERABLES FROM UNIVERSITY OF FLORIDA

1. Both plots and digital copies of all water levels, salinity, point-current speed and direction, wave height, sediment types, and suspended solids concentration including site names/coordinates, dates and times of measurements, and transducer types.

2. Three-dimensional images of velocity profiles along the ADCP transect, and corresponding time series of discharge over one spring tidal cycle.

3. Electronic copy of model source code and executables, model input and boundary condition files, and simulation results.

4. Quarterly progress reports. The progress reports will briefly describe the progress made during the reporting period, the overall status of the project; problems encountered during the reporting period and anticipated for next quarter, suggested remedial action.

5. Final report. The final report shall provide, but is not limited to, executive summary, introduction, literature review, description of the data collection and analysis, model calibration and simulation results, discussions, conclusions and recommendations.

5. SCHEDULE

The total project time frame for this amendment to Phase 2 will be 14 months.

Tasks	**Start Date**	**End Date**
Field deployment and data retrieval	January 1, 2002	May 31, 2002
Data analysis and interpretation	February 1, 2002	August 15, 2002
Model calibration and simulations of scenarios	February 1, 2002	September 30, 2002
Draft Final Report and oral presentation	October 1, 2002	November 30, 2002
Review of Final Report by the District	December 1, 2002	January 15, 2003
Revised Final Report	January 16, 2003	February 28, 2003

6. BUDGET

6.1 Cost of Study

Total budget for this Phase 2 extension project "Episodic sediment flux data collection and interpretation, and EFDC model calibration in Cedar/Ortega Rivers" is $45,000.

6.2 Invoicing

On a quarterly basis, as percentage of total work completed.

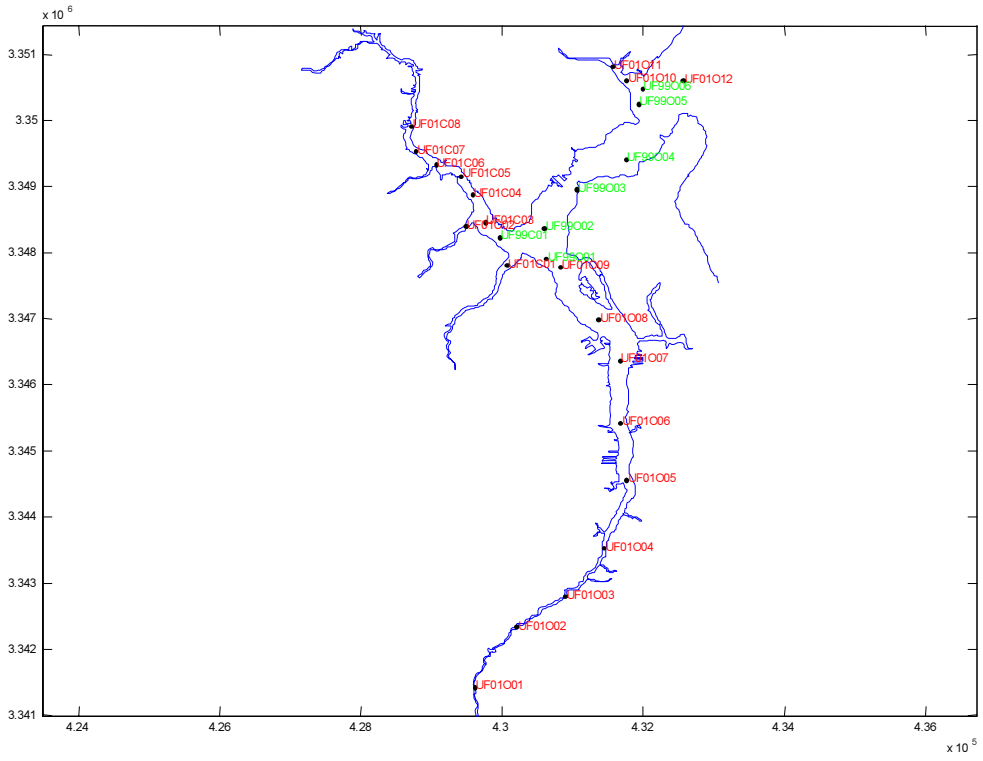

Figure 2 The Cedar/Ortega River basin in north Florida.

Figure 2 Ortega River mouth at the St. Johns River and instrument deployment. Legend: TGCTD 1 and TGCTD 2 = Locations of water level and CTD gages; WGOBS = Location of the wave gage point-current meter and OBS sensors; ADCP = ADCP transect.

1. INTRODUCTION

This progress report provides selective data blocks on tides, currents, waves and TSS concentrations from blocks collected between April 4 2002 through February 28 2003 at the mouth of the Ortega River. The two setups – Tower and Bridge – are shown in Fig. 1. These sites had the following coordinates:

- Tower 30^0 17.050’ 81^0 41.994’
- Bridge 30^0 16.483’ 81^0 43.070’

From the Bridge setup tide and wave data are reported, and from the Tower setup tide, currents and TSS concentrations.

2. TIDE

Tide data from the Bridge and the Tower are shown in Figs. 2 and 3. Note that the following vertical level corrections are required (relative to NAVD88):

- Bridge +126.9 cm
- Tower +109.6 cm

In Fig.2a the raw time-series from the Bridge is shown. In Fig. 2b the upper plot shows the original time-series and sub-semidiurnal oscillations. In the lower plot these oscillations have been removed to reveal the semi-diurnal trend. In Figs. 3a and 3b the corresponding data from the Tower are shown.

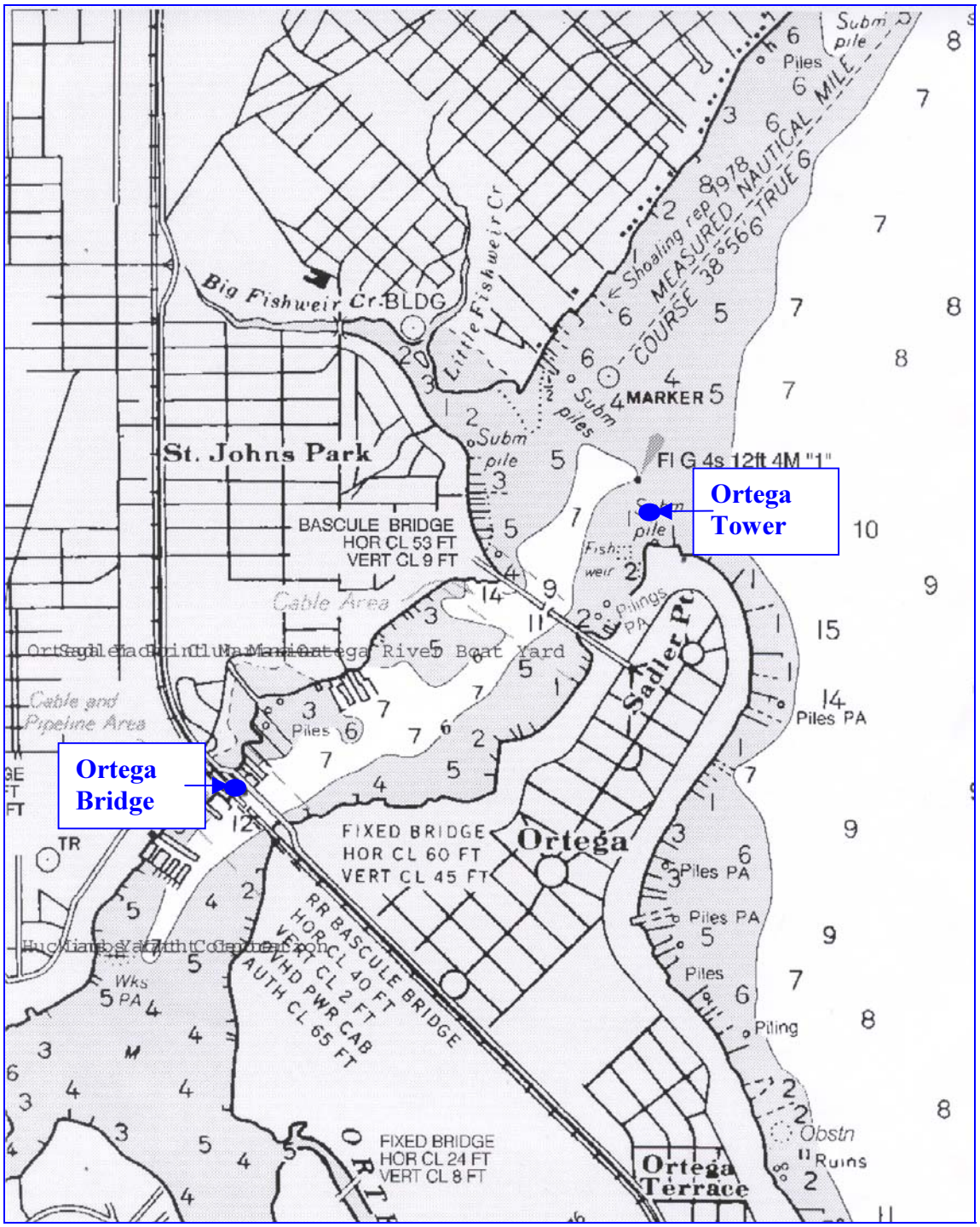

Figure 1. Locations of Ortega Bridge and Ortega Tower data collection sites.

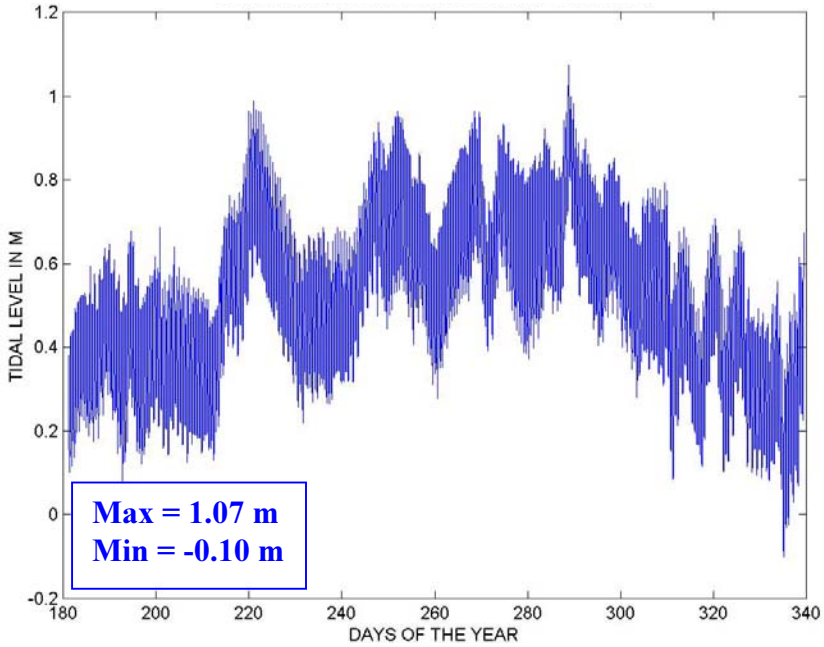

Figure 2a. Tide level time-series at Ortega Bridge: Days 180-340.

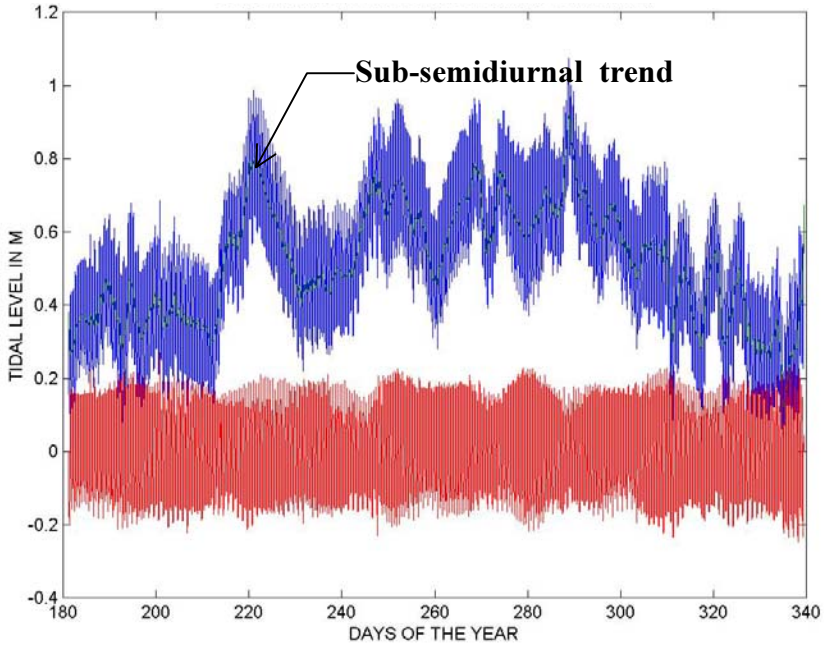

Figure 2b. Tide level time-series at Ortega Bridge: Upper plot shows the original time-series and sub-semidiurnal oscillations. In the lower plot these oscillations have been removed.

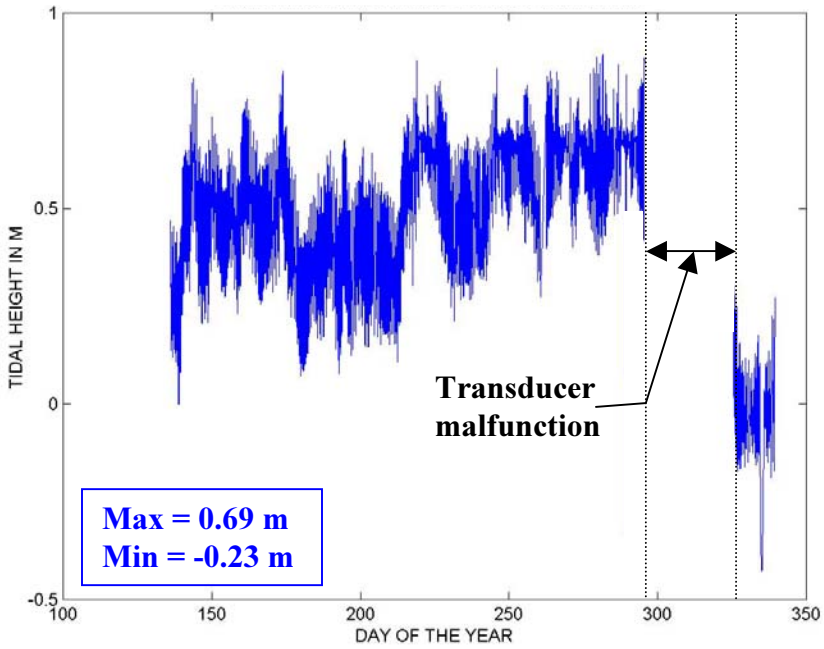

Figure 3a. Tide level time-series at Ortega Tower; Days 140-340.

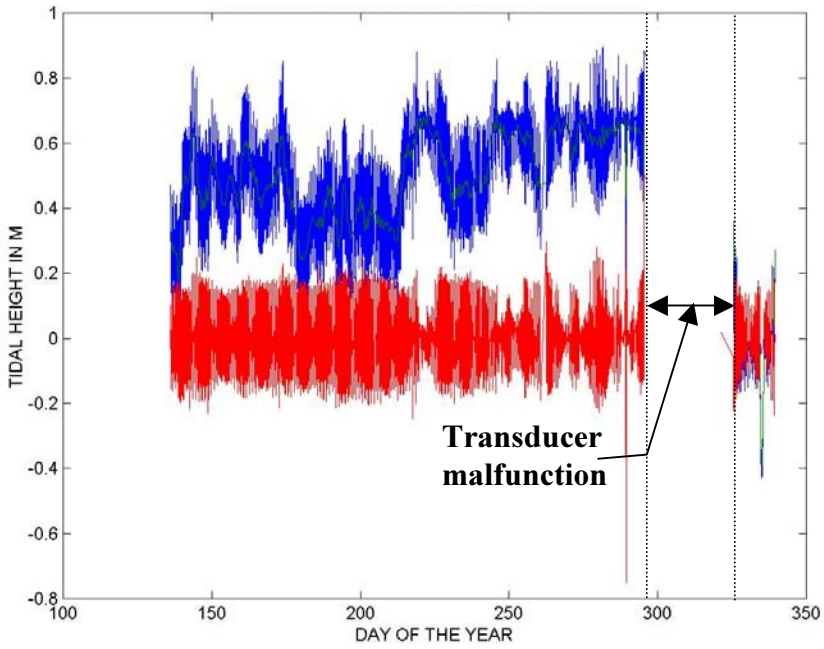

Figure 3b. Tide level time-series at Ortega Tower: Upper plot shows the original time-series and sub-semidiurnal oscillations. In the lower plot these oscillations have been removed.

3. CURRENT

Depth-mean current *magnitude* time-series from the Tower for days 220-240 is shown in Fig. 4, and an example of the direction plot (for days 218-268) is given in Fig. 5. The shift in the angle variability starting with day 240 is believed to be due to a reorientation of the transducer. Current magnitudes for days 264-276 and 326-339 are given in Figs. 6 and 7, respectively.

4. WAVES

Data on the significant wave height time-series from the Bridge site are shown in Fig. 8a for days 264-276. The data show strong diurnal variation of height, possibly due to the corresponding shifts in the wind magnitude and direction. The corresponding modal period data are given in Fig. 8b. The wave heights (maximum 0.15 m) and periods (maximum 2.8 s) are both consistent with the wind speeds and fetches in the St. Johns River main-stem.

5. TOTAL SUSPENDED SOLIDS

Depth-mean TSS concentration time-series for days 220-240, 264-276 and 326-339 are shown in Figs. 9, 10 and 11, respectively. Table 1 provides the maximum, mean and minimum values for each block. These indicate substantial block to block variability. Data from the first block (days 220-240) may also have been affected by bio-fouling of the OBS sensors. In general, however, it appears that TSS concentration in the area is not merely dependent on the local currents, but also on the supply of suspended matter from the main-stem.

Table 1 TSS concentration data summary

Day block	Maximum TSS concentration (mg/L)	Mean TSS concentration (mg/L)	Minimum TSS concentration (mg/L)
220-240	56	42	32
264-276	32	12	6
326-339	86	46	32

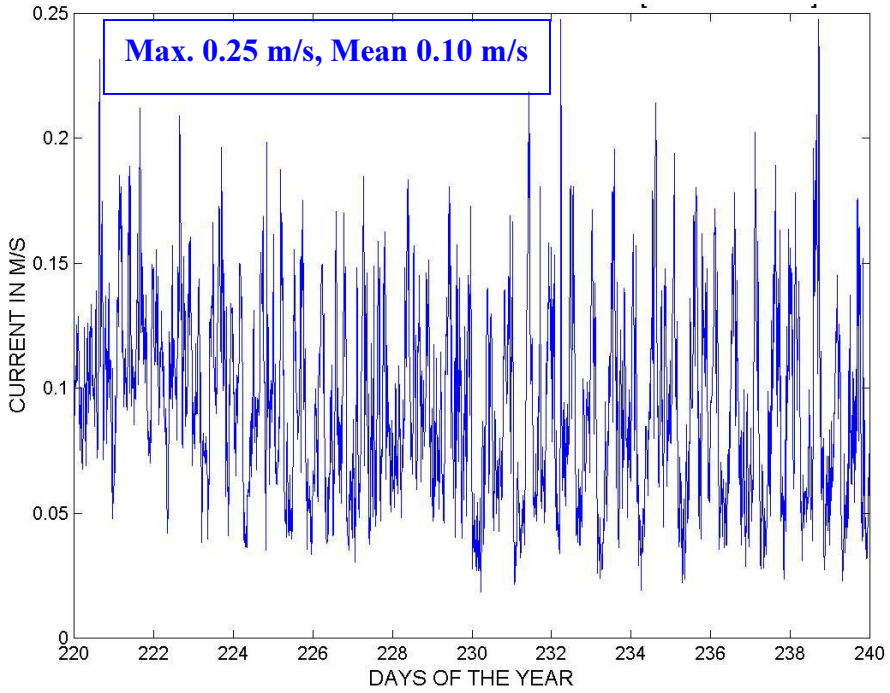

Figure 4. Ortega Tower depth-mean current magnitude time-series: Days 220-240.

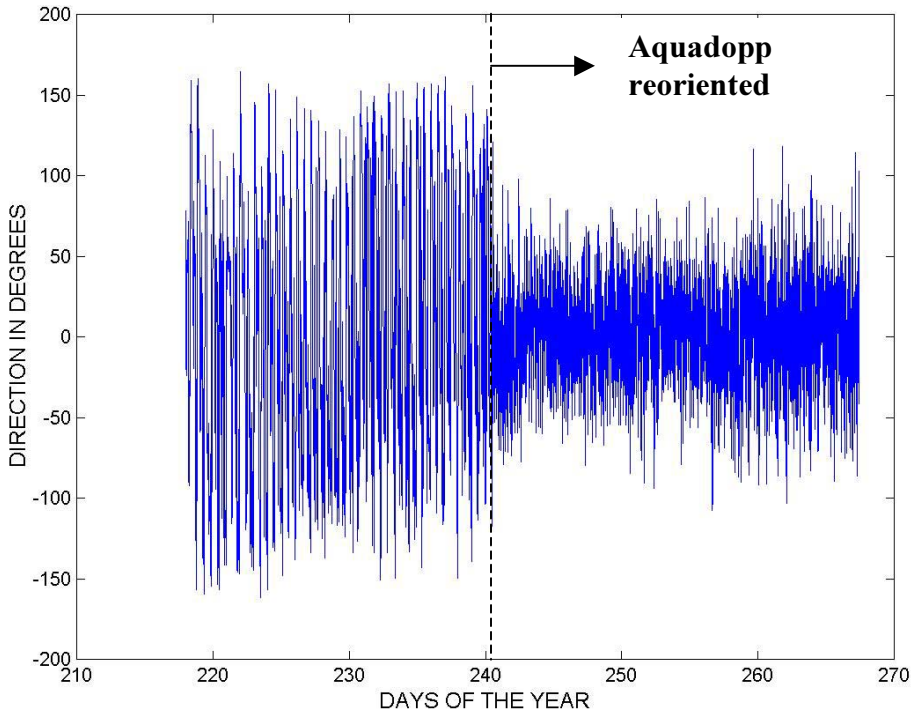

Figure 5. Ortega Tower depth-mean current direction time-series: Days 218-268.

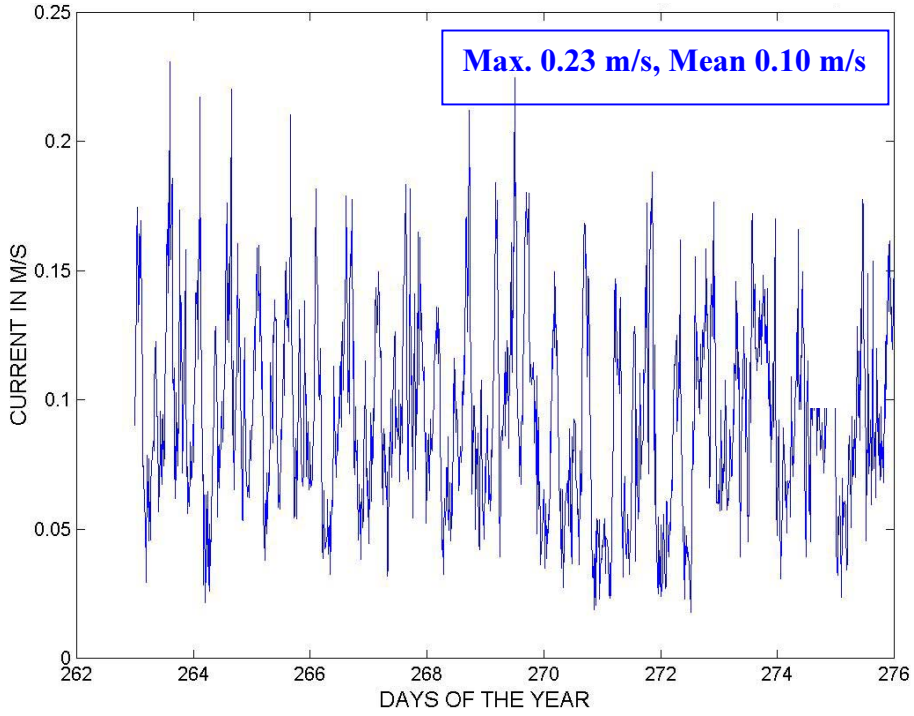

Figure 6. Ortega Tower depth-mean current magnitude time-series: Days 264-276.

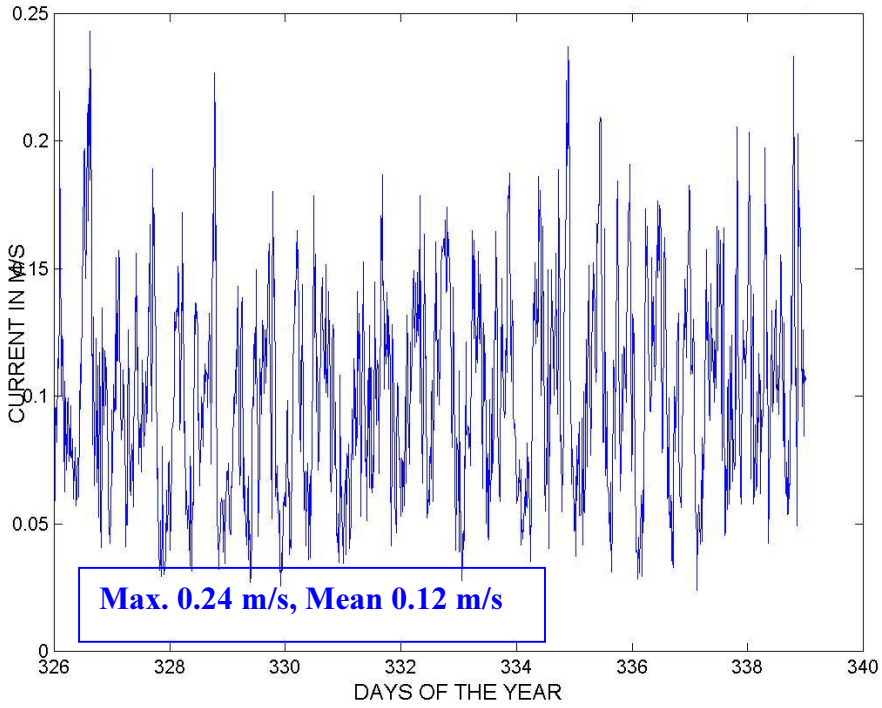

Figure 7. Ortega Tower depth-mean current magnitude time-series: Days 326-339.

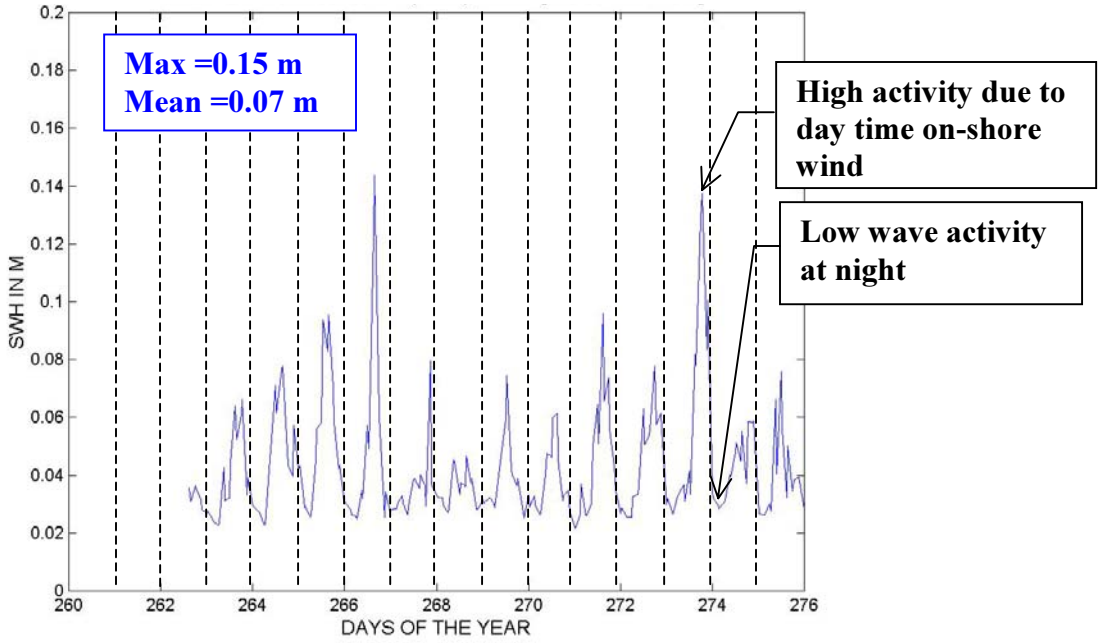

Figure 8a. Ortega Bridge significant wave height time-series: Days 264-276.

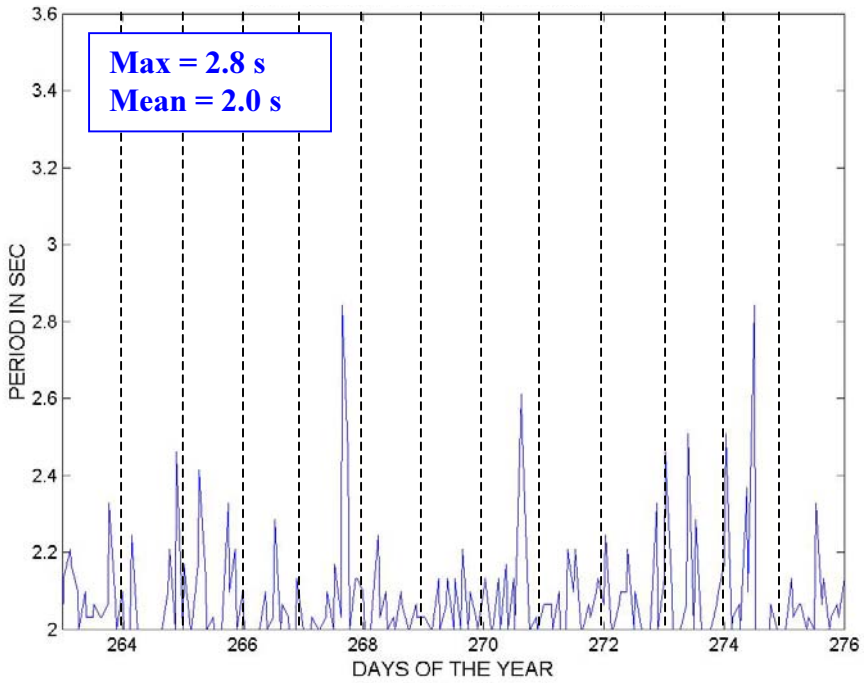

Figure 8b. Ortega river wave period time-series: Days 264-276.

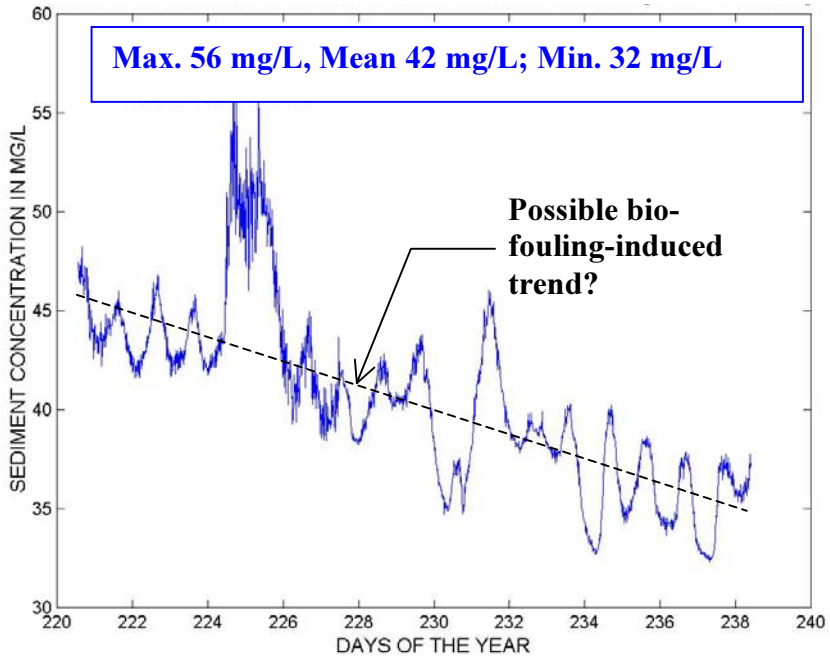

Figure 9. Ortega Tower depth-mean TSS concentration time-series: Days 220-240.

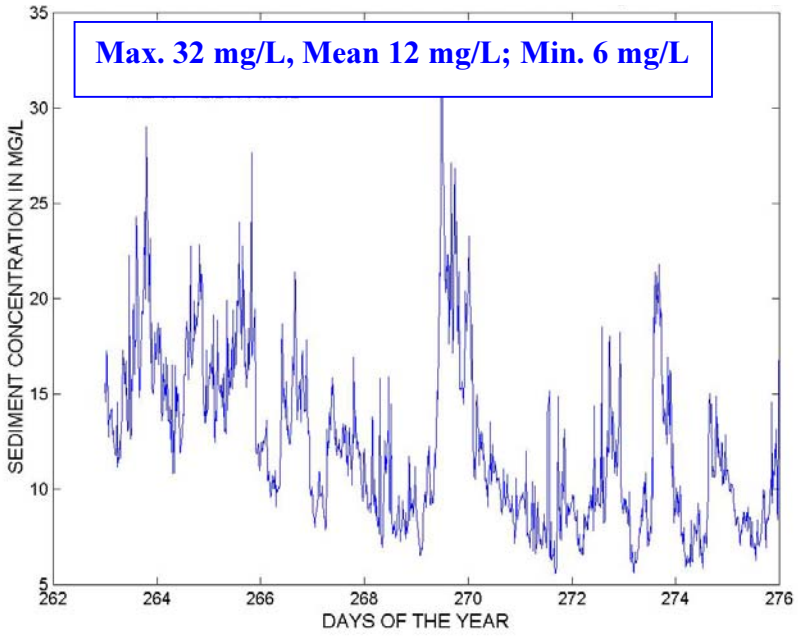

Figure 10. Ortega Tower depth-mean TSS concentration time-series: Days 264-276.

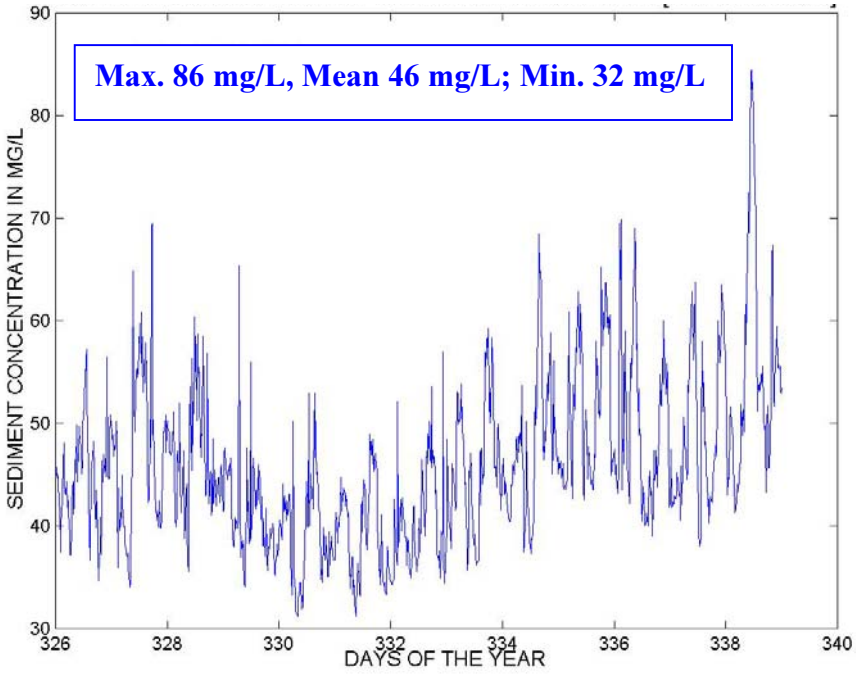

Figure 11. Ortega Tower depth-mean TSS concentration time-series: Days 326-339.

6. CURRENT-TSS CORRELATIONS

After a careful examination of the depth-mean current and TSS data, the current-TSS correlations shown in Figs. 12, 13 and 14 were obtained for the blocks identified in the captions. Two observations are immediately obvious:

1) TSS concentration shows a weak but consistent correlation with tidal current amplitude, and
2) The effect of St Johns River main-stem as a sediment source is very strong. This is especially evident from the intercepts of the best-fit lines with the zero current axis. The value of the corresponding TSS concentration for the three blocks is 36, 6 and 29 mg/L, which represent the block-mean ambient turbidity levels at the site.

In Fig. 14 the data from the three blocks are combined after removing the corresponding ambient concentrations. The resulting best-fit line reflects, very approximately, the effect of local tidal current on TSS.

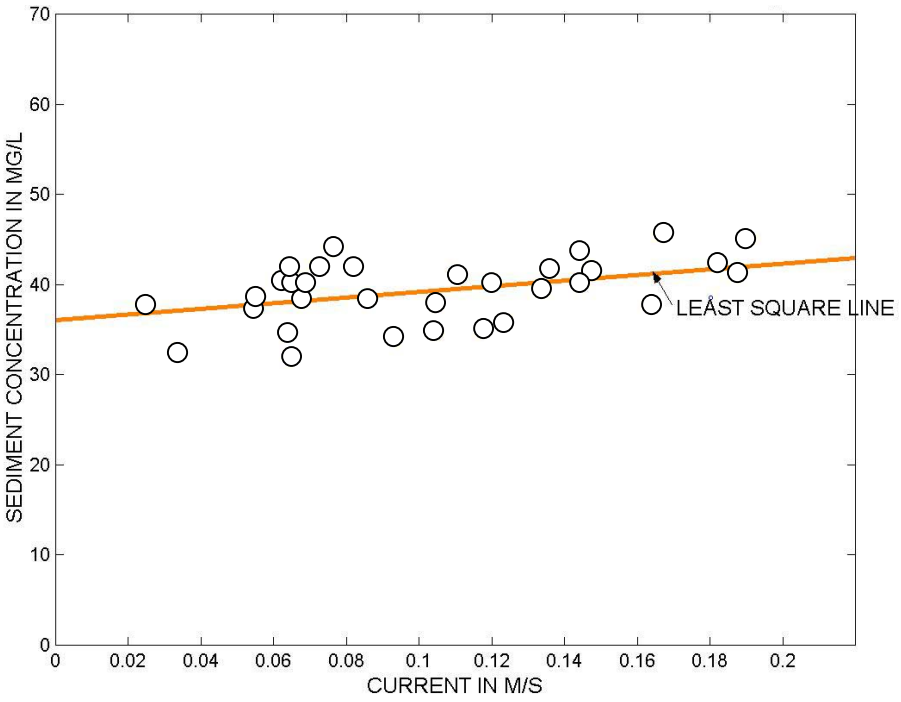

Figure 12. Ortega Tower Current-TSS correlation: Days 220-240.

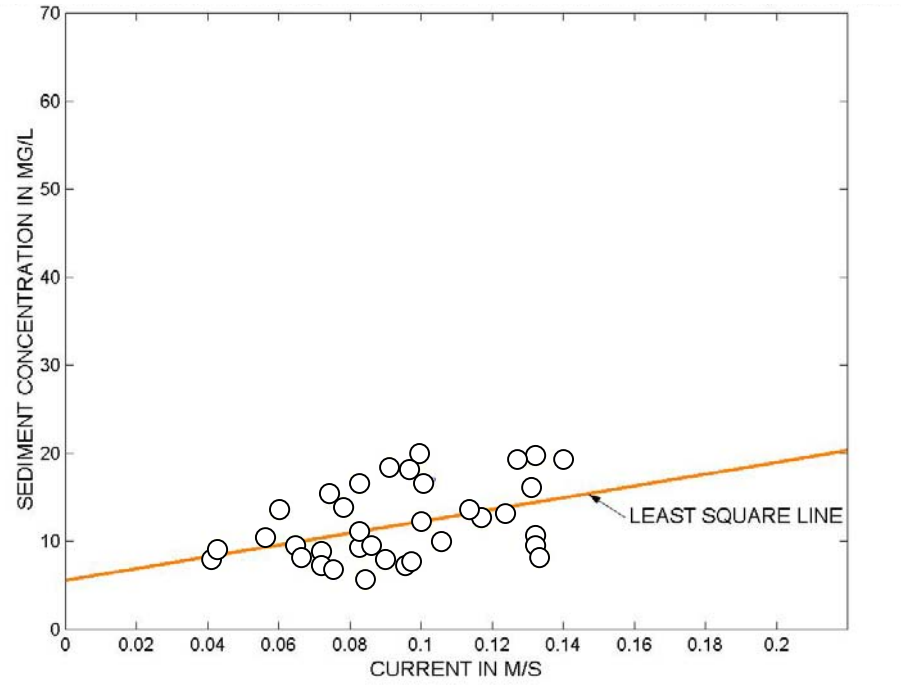

Figure 13. Ortega Tower Current-TSS correlation: Days 264-276.

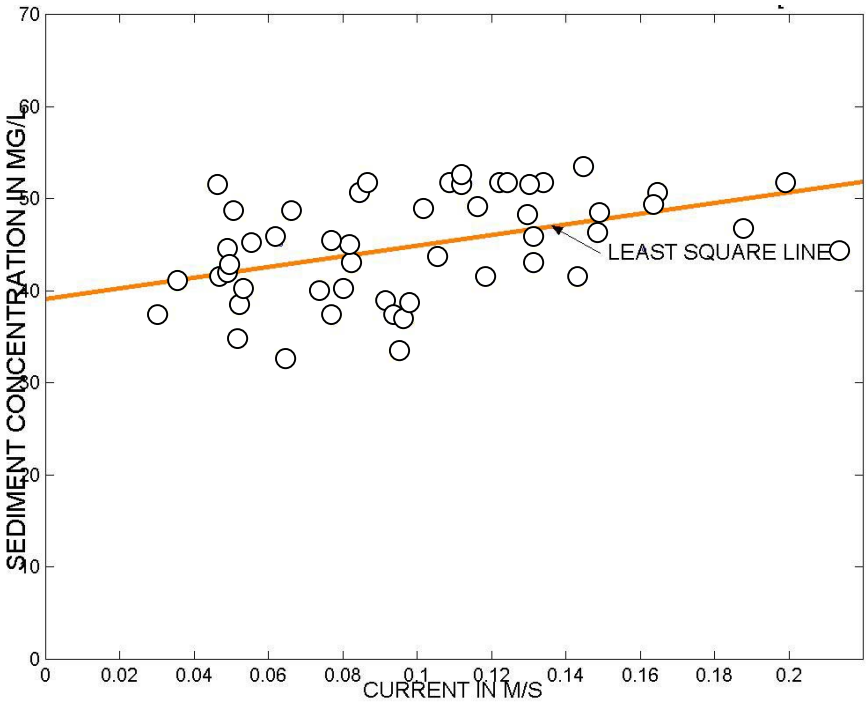

Figure 14. Ortega Tower Current-TSS correlation: Days 326-339.

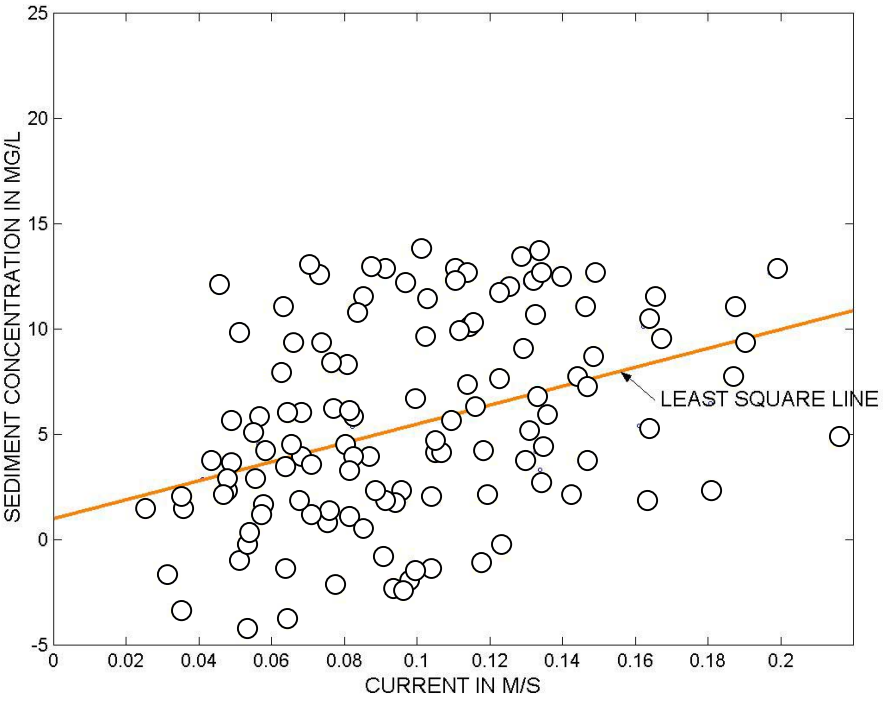

Figure 15. Ortega Tower Current-TSS correlation: Cumulative.